U.S. DEPARTMENT OF COMMERCE
National Technical Information Service

PB-274 029

Proceedings of the 2nd Stationary Source Combustion Symposium, Held at New Orleans, Louisiana, on August 29-September 1, 1977. Volume IV. Fundamental Combustion Research

Industrial Environmental Research Lab, Research Triangle Pk, N C

Jul 77

PB 274 029

EPA

[illegible]

EPA-600/7-77-073d
July 1977

PROCEEDINGS OF THE SECOND STATIONARY SOURCE COMBUSTION SYMPOSIUM

Volume IV. Fundamental Combustion Research

Interagency
Energy-Environment
Research and Development
Program Report

REPRODUCED BY
NATIONAL TECHNICAL
INFORMATION SERVICE
U. S. DEPARTMENT OF COMMERCE
SPRINGFIELD, VA. 22161

. . . RESEARCH REPORTING SERIES

Research reports of the Office of Research and Development, U.S. Environmental Protection Agency, have been grouped into seven series. These seven broad categories were established to facilitate further development and application of environmental technology. Elimination of traditional grouping was consciously planned to foster technology transfer and a maximum interface in related fields. The seven series are:

1. Environmental Health Effects Research
2. Environmental Protection Technology
3. Ecological Research
4. Environmental Monitoring
5. Socioeconomic Environmental Studies
6. Scientific and Technical Assessment Reports (STAR)
7. Interagency Energy-Environment Research and Development

This report has been assigned to the INTERAGENCY ENERGY-ENVIRONMENT RESEARCH AND DEVELOPMENT series. Reports in this series result from the effort funded under the 17-agency Federal Energy/Environment Research and Development Program. These studies relate to EPA's mission to protect the public health and welfare from adverse effects of pollutants associated with energy systems. The goal of the Program is to assure the rapid development of domestic energy supplies in an environmentally--compatible manner by providing the necessary environmental data and control technology. Investigations include analyses of the transport of energy-related pollutants and their health and ecological effects; assessments of, and development of, control technologies for energy systems; and integrated assessments of a wide range of energy-related environmental issues.

REVIEW NOTICE

This report has been reviewed by the participating Federal Agencies, and approved for publication. Approval does not signify that the contents necessarily reflect the views and policies of the Government, nor does mention of trade names or commercial products constitute endorsement or recommendation for use.

This document is available to the public through the National Technical Information Service, Springfield, Virginia 22161.

TECHNICAL REPORT DATA

(Please read Instructions on the reverse before completing)

1. REPORT NO. EPA-600/7-77-073d

2.

3. RECIPIENT'S ACCESSION NO. PB274029

4. TITLE AND SUBTITLE PROCEEDINGS OF THE SECOND STATIONARY SOURCE COMBUSTION SYMPOSIUM Volume IV. Fundamental Combustion Research

5. REPORT DATE July 1977

6. PERFORMING ORGANIZATION CODE

7. AUTHOR(S) Symposium Chairman J.S. Bowen, Vice-Chairman R.E. Hall

8. PERFORMING ORGANIZATION REPORT NO.

9. PERFORMING ORGANIZATION NAME AND ADDRESS NA

10. PROGRAM ELEMENT NO. EHE624

11. CONTRACT/GRANT NO. NA (Inhouse)

12. SPONSORING AGENCY NAME AND ADDRESS
EPA, Office of Research and Development
Industrial Environmental Research Laboratory
Research Triangle Park, NC 27711

13. TYPE OF REPORT AND PERIOD COVERED Proceedings; 8/29-10/1/77

14. SPONSORING AGENCY CODE EPA/600/13

15. SUPPLEMENTARY NOTES IERL-RTP project officer for these proceedings is R.E. Hall, Mail Drop 65, 919/541-2477.

16. ABSTRACT The proceedings document the 50 presentations made during the Second Stationary Source Combustion Symposium held in New Orleans, LA, August 29-September 1, 1977. Sponsored by the Combustion Research Branch of EPA's Industrial Environmental Research Laboratory--RTP, the symposium dealt with subjects relating both to developing improved combustion technology for the reduction of air pollutant emissions from stationary sources, and to improving equipment efficiency. The symposium was divided into six parts, and the proceedings were issued in five volumes: Volume I--Small Industrial, Commercial, and Residential Systems; Volume II--Utility and Large Industrial Boilers; Volume III--Stationary Engine, Industrial Process Combustion Systems, and Advanced Processes; Volume IV--Fundamental Combustion Research; and Volume V--Addendum. The symposium was intended to provide contractor, industrial, and Government representatives with the latest information on EPA inhouse and contract combustion research projects related to pollution control, with emphasis on reducing nitrogen oxides while controlling other emissions and improving efficiency.

17. KEY WORDS AND DOCUMENT ANALYSIS

a. DESCRIPTORS	b. IDENTIFIERS/OPEN ENDED TERMS	c. COSATI Field/Group		
Air Pollution, Combustion, Field Tests	Air Pollution Control	13B	21B	14B
Combustion Control, Coal, Oils	Stationary Sources		21D	11H
Natural Gas, Nitrogen Oxides, Carbon	Combustion Modification		07B	
Carbon Monoxide, Hydrocarbons, Boilers	Unburned Hydrocarbons		07C	13A
Pulverized Fuels, Fossil Fuels, Utilities	Fundamental Research			
Gas Turbines, Efficiency	Fuel Nitrogen	13G	14A	
	Burner Tests			

18. DISTRIBUTION STATEMENT Unlimited

19. SECURITY CLASS *(This Report)* Unclassified

20. SECURITY CLASS *(This page)* Unclassified

21. NO. OF PAGES 336

22. PRICE PC A15 mF A01

EPA-600/7-77-073d
July 1977

PROCEEDINGS OF THE SECOND STATIONARY SOURCE COMBUSTION SYMPOSIUM

Volume IV. Fundamental Combustion Research

Symposium Chairman Joshua S. Bowen
Vice-Chairman Robert E. Hall

Environmental Protection Agency
Office of Research and Development
Industrial Environmental Research Laboratory
Research Triangle Park, North Carolina 27711

Program Element No. EHE624

Prepared for

U.S. ENVIRONMENTAL PROTECTION AGENCY
Office of Research and Development
Washington, D.C. 20460

i (a)

PREFACE

These proceedings document the more than 50 presentations and discussions of the Second Symposium on Stationary Source Combustion held August 29 - September 1, 1977 at the Marriott Hotel in New Orleans, Louisiana. Sponsored by the Combustion Research Branch of the EPA's Industrial Environmental Research Laboratory-Research Triangle Park, the symposium presented the results of recent research in the areas of combustion processes, fuel properties, burner and furnace design, combustion modification, and emission control technology.

Dr. Joshua S. Bowen, Chief, Combustion Research Branch, was Symposium Chairman; Robert E. Hall, Combustion Research Branch, was Symposium Vice-Chairman and Project Officer. The Welcoming Address was delivered by Dr. John K. Burchard, Director of IERL-RTP; the Opening Address was delivered by Robert P. Hangebrauck, Director, Energy Assessment and Control Division, IERL-RTP; and Dr. Howard B. Mason, Program Manager NO_x Environmental Assessment Program, Acurex Corporation, delivered the Keynote Paper.

The symposium consisted of six sessions:

Session I: **Small Industrial, Commercial and Residential Systems**
Robert E. Hall, Session Chairman

Session II: **Utility and Large Industrial Boilers**
David G. Lachapelle, Session Chairman

Session III: **Special Topics**
David G. Lachapelle, Session Chairman

Session IV: **Stationary Engine and Industrial Process Combustion Systems**
John H. Wasser, Session Chairman

Session V: **Advanced Processes**
G. Blair Martin, Session Chairman

Session VI: **Fundamental Combustion Research**
W. Steven Lanier, Session Chairman

TABLE OF CONTENTS
- SESSION VI: FUNDAMENTAL COMBUSTION RESEARCH -

Page

"Fundamental Combustion Research Applied to Pollution Control," T. J. Tyson, M. P. Heap 3

"Chemical Reactions in the Conversion of Fuel Nitrogen to NO_x: Fuel Pyrolysis Studies," A. E. Axworthy, V. H. Dayan 39

"Fate of Fuel Nitrogen During Pyrolysis and Oxidation," Y. H. Song, J. M. Beer, A. F. Sarofim 79

"Interactions Between Sulfur Oxides and Nitrogen Oxides in Combustion Processes," J. O. L. Wendt, T. L. Corley, J. T. Morcomb . . . 101

"Chemical Reactions in the Conversion of Fuel Nitrogen to NO_x: Low-Pressure Flat-Flame Burner Studies," D. R. Kahn, A. E. Axworthy 139

"Formation of Soot and Polycyclic Aromatic Hydrocarbons in Combustion Systems -- Development of a Molecular Beam Mass Spectrometer," J. D. Bittner 183

"Investigation of NO_x, Nitrate and Sulfate Production in Laboratory Flames," D. J. Seery, M. F. Zabielski, L. G. Dodge 209

"Influence of Aerodynamic Phenomena on Pollutant Formation in Combustion: Phase II -- Liquid Fuels," L. J. Spadaccini, J. B. McVey, J. B. Kennedy, F. K. Owen, C. T. Bowman, A. Vranos, A. S. Kesten 235

"Two-Dimensional or Axially Symmetric Modeling of Combusting Flow," H. McDonald, R. C. Buggeln 283

"PRemixed One-Dimensional Flame (PROF) Code Development and Application," J. T. Kelly, R. M. Kendall 311

SESSION VI:

FUNDAMENTAL COMBUSTION RESEARCH

W. STEVEN LANIER
CHAIRMAN

FUNDAMENTAL COMBUSTION RESEARCH APPLIED TO POLLUTION CONTROL

An Overview

By:

T. J. Tyson and M. P. Heap
Energy and Environmental Research Corporation
Santa Ana, California 92705

ABSTRACT

The development of NO_x control techniques by modification of the combustion process in a timely and cost-effective manner is enhanced if there is a basic understanding of the phenomena associated with NO_x formation in stationary combustors. This paper describes the initial planning phase of a program designed to synthesize combustion research activities in one subcontractor-orientated program. The program has been planned to provide support to the various technology development programs being supported by the CRB. In this sense it can be more properly described as an applied research program since it only attacks problems in a manner necessary to provide information to develop control techniques.

The program addresses two time scales. Information will be generated in the two to four year time frame to feed into technology development programs which are essentially directed toward conventional designs. The majority of the effort will be associated with this time scale, however, a non-negligable effort will be expended on more long-term research associated with radical combustor redesign to achieve very low emission levels.

The program concentrates upon the generation and control of nitrogen oxides and primary related pollutants produced during the combustion of nitrogen-containing fuels (coal and residual oil) since these are the primary source of nitrogen oxides. The scientific stragegy associated with setting the initial program objectives and the definition of the areas of research to be conducted in-house and by other organizations under subcontract are discussed in the paper.

Preceding page blank

SECTION 1

INTRODUCTION

In February 1977 the U.S. Environmental Protection Agency awarded a 70,000 man-hour level-of-effort contract to the Energy and Environmental Research Corporation to assume the major responsibility for managing and conducting its fundamental combustion research efforts. The "Fundamental Combustion Research Applied to Pollution Control" (FCR) program objectives are to provide a focused program of basic engineering research designed to:

- Provide the EPA/CRB technology development programs with the necessary understanding of basic combustion behavior required to achieve the minimization of NO_x from stationary sources;
- Provide guidance and mathematical tools required to effectively utilize this body of information in the development of NO_x control techniques; and
- Assure that critical information will be generated within a time frame consistent with the technology development programs.

The words "focused" and "engineering" research are directed at the important issue of relevance. The program will be focused on well-defined priority target areas and the research effort will be directed towards engineering solutions to specific problems. Developing the "necessary understanding" requires that relevant issues be isolated so that the program can be disengaged from studies of irrelevant or nonproblem aspects of the physics and chemistry of combustion.

Several factors need consideration if the information generated by the FCR program is to be utilized effectively. Primary amongst these is the provision of a strong linkage between the understanding of basic behavior and the control of NO_x in practical combustion devices. A unification and generalization of the laboratory observations is required if this linkage

Preceding page blank

is to be achieved. Mathematical modeling is an important component of the FCR program as it provides a formalism whereby this generalization and linkage can be developed. Modeling allows a systematic exploration of the implications of the basic understanding with regard to NO_x control. Effective utilization also requires effective transfer of FCR-generated technology into the CRB Technology Development (TD) programs. Thus, close coupling of the FCR and TD programs is an important factor in the development of FCR.

The final objective listed above relates to the important question of when FCR results must be attained. Many judgement factors enter during the resolution of this question. Obviously inputs to specific CRB Technology Development programs must occur at a time consistent with the schedules of these programs. In general this implies that FCR results must be generated and transferred within a two-to-four year time period. The demands imposed by such a short time frame strongly influences the nature of the research to be undertaken.

To date the majority of the effort expended under FCR has centered around the detailed planning of the program elements and in preparation of work scopes for upcoming subcontracts. It is the intent of this paper to present the results of this initial planning process in the hope that by describing the constraints around which these planning activities proceeded, the potential subcontractors will obtain a better feeling for the thrust of the FCR program, and how they might contribute to fulfilling its objectives.

The motivation for the FCR program stems directly from EPA's stated goal to establish the technology base necessary for maximum reduction of NO_x emissions from stationary sources. In the course of generating an overall EPA strategy to achieve maximum NO_x reduction it has become evident how difficult it is to exploit or transfer a successful control technique developed under one condition to other situations. The lack of a mechanistic understanding of the dominant phenomena prevents a generalization of the observations made during the course of a technology development program. Application of the results to other scales, fuels, device types, and operating regions often becomes impossible.

The use of detailed measurements obtained from pilot scale combustors during the development period to provide the required understanding of controlling mechanisms is a sometimes successful but is more often an unrewarding task. The difficulty lies in the complexity of coupling between dominant mechanisms within a practical combustion device. Controlling mechanisms are not easily identified or characterized under such conditions.

The above factors make the evolution of successful NO_x control techniques exclusively through pilot scale development a costly and lengthy trial and error process. Taken together they provide strong motivation for an FCR program which focuses on defining the dominant mechanics and providing process models which will allow generalization and exploitation of pilot scale results. Further stimulus for a substantial FCR element within the overall EPA program is the recognition that through fundamental understanding it is possible to systematically establish the lower bounds on NO_x emissions that are theoretically attainable within the engineering constraints imposed on a particular device. A knowledge of these lower bounds will provide a much needed yardstick with which to judge the development of low emissions systems and to guide their further development.

The organization of the program is shown in Figure 1. As noted in the middle box planning, review, and redirection functions are carried out by EER staff and staff consultants in conjunction with the EPA Project Officer. The organization is shown in three distinct tiers. The upper tier indicates the various groups outside of EER will provide input to the planning function of the FCR program. Potential subcontractors (their tier) are encouraged to provide critical comment on the FCR program as well as to make available information on their own capabilities and areas in which they are interested in performing research under FCR. The CRB staff, of course, provides the necessary insight into the various technology development programs and is the primary recipient of technology developed under FCR. Coordination will be sought between FCR activities and related ocmbustion research activities within the DOD and DOE, the energy industry, and university laboratories. In addition to EER's staff considerable use of consultants will be made who have recognized expertise in areas of critical importance to the program. In certain circumstances these consultants will also be used as proposal reviewers.

Although not shown in Figure 1, the MIT Energy Laboratory has a special role in the program that distinguishes it from other subcontractors. The Energy Laboratory will be under contract during the entire course of the FCR program providing EER with support in the following areas:

- Program Planning and Review
- Program Management
- Technology Evaluation
- Coordination with other CRB Fundamental Research Activities
- Engineering Analysis
- Exploratory Laboratory Investigations to Provide Definition and Guidance of Subcontractor Tasks
- Technology Transfer

The fourth item above is in recognition of the important fact that several of the CRB Technology Development programs have a fundamental research component. In addition the CRB sponsors grant type programs at a number of universities. Hence participation in the coordination of these activities becomes an important FCR function. Engineering analysis is a significant part of the EER in-house effort. This will include development and application of data analysis techniques, codes designed for numerical experiments, modeling of specific mechanistic behavior, and modular modeling which links together relatively simple models in such a manner as to allow analysis of practical combustion systems.

SECTION 2

PLANNING STRATEGY

Having established the general objectives of the FCR program it is necessary to make these concrete in terms of specific engineering research tasks. The flow diagram shown in Figure 2 outlines the strategy through which this will be achieved. This section discusses the general aspect of the strategy outlined in Figure 2 and the anticipated products resulting from the implimentation of such an approach. Presented later in this paper are specifics regarding the initial planning effort and the definition of an initial program of research which has resulted from this effort.

Information from a variety of sources including the CRB Technology Development programs and the NO_x Environmental Assessment program have been used to establish priorities by device type, size, and fuel, and the time frame in which research results must be generated if they are to be effectively utilized. These studies clearly show that near and intermediate-term requirements will necessarily lead to research focused on retrofit concepts in which the combustion device type cannot undergo drastic changes in design concept. Longer time frame objectives, on the other hand, will allow the research effort to take on a more wide ranging character associated with the possibilities of entirely new combustion system concepts. With these priorities it is possible to define the general flame characteristics associated with the combustion devices and fuels which have the highest priority.

At this point the strategy takes on a more scientific character. Given flame types, what course of research should be pursued to yield the necessary understanding required to achieve EPA's goals for the reduction of NO_x emissions? The answer to this question rests first on the identification of the significant physical and chemical phenomena which dictate the behavior of the flame type under consideration. As defined, "significant" implies phenomena whose alteration will yield a 1st order effect on NO_x or related pollutant emissions.

In order to establish the "significance" of the various phenomena an attempt must be made to answer a number of related questions.

- To what degree are the phenomena controllable through changes in device design parameters?
- Can "cause and effect" history be established which links significant phenomena and provides insight into control methods?
- When do the phenomena occur in the overall process (early, late, intermediate, continuously)?
- What is time constant of the phenomena in comparison to other process time constants?
- If the process rapidly equilibrates how does the equilibrated behavior depend upon process boundary conditions?
- If the process rapidly goes to slowly varying nonequilibrium state how does that state depend on process boundary conditions?
- To what extent are processes coupled?

Answers to these questions not only provide the necessary insight as to what phenomena are important but also provide guidance as to the depth of understanding required for FCR purposes. For example, in examining processes with short-time constants in comparison to other significant phenomena the details of the process path are of little interest. Only the end-point equilibrated behavior as it is affected by the process environment (boundary conditions) is of concern. Consider the coal particle heat-up process. If all other processes in the systems such as rapid devolatilization are slower than this process then only the equilibrated final temperature of the particle is of interest. Under certain circumstances processes which fall into this category might be: turbulence lag, particle ballistics, prompt fuel nitrogen chemistry, and energy release kinetics.

A systematic search for the answers to these questions will lead to the identification of important gaps in current understanding and will provide guidance in the definition of experimental and theoretical tasks to close these gaps.

TECHNOLOGY ASSESSMENTS

In order to identify and characterize significant topics worthy of FCR support there will be continual assessments of the current state-of-understanding in the following areas:

- Gas phase chemical kinetics and soot formation mechanics
- Physics and chemistry of solid and liquid fuel combustion
- Physics of transport phenomena
- Measurement technology
- Mathematical modeling

These assessments will form the basis of a series of special reports setting forth the reasons for supporting particular research programs, and assessing the value of the results of these programs. The intent is to critically review past and present experimental and theoretical investigations and to undertake simple limit-case analyses and numerical experiments which will aid the assessments. The primary motivation for the measurement and modeling areas is to assure that adequate measurement and data analysis techniques are available for all experimental programs sponsored under the FCR project. The product of the assessments, in addition to the identification of gaps, will be to generalize and quantify the information in a form suitable for use in process models.

EXPERIMENTAL AND THEORETICAL STUDIES

With the gaps in understanding of significant phenomena delineated, the core of the FCR program becomes the set of experimental and theoretical studies designed to fill these gaps. The common thread running through these programs are the requirements to:

- Establish how and what basic information will be extracted from experimental data or theoretical study.

- Show strong linkage between phenomenological behavior in experiments or theoretical study and the behavior in practical combustion systems.

- Establish effectiveness of measurement techniques.
- Define how basic information obtained from investigation will be used to achieve ends of program.

ESTABLISHMENT OF LOWER BOUNDS ON NO_X EMISSIONS

A key element in the FCR strategy is the search for lower bounds set on NO_x emissions under various limiting situations and constraints. For example, is it possible to establish the lower bounds on NO_x set by the gas phase chemistry for a particular type of device with its engineering constraints on heat transfer, exit temperature, size, etc.? Such a lower bound study would assume idealized and optimum time-phasing for fuel/air contacting and heat transfer under the imposed constraints. In a similar manner is it possible to establish the lower bounds on NO_x set by fundamental constraints associated with solid and liquid fuel combustion? The value of such studies would be substantial. Not only would they provide a yardstick by which to measure the effectiveness of control schemes but they would provide strong guidance in the development of control techniques.

The search for lower bounds will encompass both physical and numerical experiments. These experiments will investigate numerous limiting situations involving

- Controlled heat and mass transfer reactors
- Sequential, parallel, and feedback staging
- Fuel staging
- Natural staging in turbulent diffusion flames.

THE ROLE OF MATHEMATICAL MODELING IN FCR STRATEGY

Mathematical modeling will play a strong role in the FCR program in the following wide ranging areas:

- Data analysis
- Limit-case studies
- Modular modeling of complex systems
- Relatively simple modeling of complex fluid mechanical behavior

Data analysis capability will be required for all experimental programs to extract the maximum amount of mechanistic information implied by the data. For example, a pulverized coal-stirred reactor experiment would necessarily be complimented with a two-phase stirred reactor code. Measurements of gas and solid phase characteristics could then be used in conjunction with the code to establish the detailed particle mechanics of devolatilization and fuel nitrogen evolution and speciation. Data analysis techniques will include sensitivity studies and inverse methods. Sensitivity studies will allow the determination of phenomenological parameters which have the greatest influence on the observables. Inverse methods allow the data to be used as independent input variables while the mechanistic parameters becomes the calculated dependent variables. The values deduced for the mechanistic parameters would then be checked for plausibility.

The limit-case studies in which certain phenomena are assumed to dominate the process while other phenomena become suppressed are particularly useful in numerical experiments designed to examine the implications of specific phenomenological behavior. The analysis might be as simple as that of the limiting situation of intense backmixing such that the system become perfectly stirred. On the other hand the analysis might be as complex as a two-phase turbulent diffusion flame in the limiting case of no backmixing or recirculation zones. In any event, a common feature of the limit-cases under consideration is that they are all amenable to straightforward numerical analysis using well-known fast and accurate techniques. In conjunction with experiments designed to meet the same limiting assumptions, these codes become data analysis tools to extract basic mechanistic behavior. Once the imbedded physics and chemistry has been modified to be consistent with observations in analogous physical experiments, the models can be effectively used in numerical experiments and as tools in the search for the lower bounds on NO_x emission.

Modular modelling implies the modelling of a complex system using a collection of limit-case elements linked together by means of empirical knowledge of the exchange of heat and mass between these elements. The combustor is divided into zones which have a distinct limit-case character, e.g., recirculation zones, free shear layers, co-axial turbulent diffusion zones, regions where fuel droplets are transported ballistically, etc. In the simplest case the model might consist of a collection of stirred and plug flow reactors connected in series. More complex cases could include feedback (upstream influence) paths and diffusion flame elements. The zone sizes and linkage between zones would in general be estimated through the application of relatively simple fluid mechanical models in conjunction with empirical observations from the specific device type under examination. Stimulus-response experiments would be particularly useful in this regard. In these techniques inert and chemically active tracers are injected at various points within the system and their presence is measured at other points. From such measurements considerable information on macro- and and micro-scale mixing patterns, mass and heat transfer rates, and distribution of residence times can be obtained.

The motivation for semi-empirical modular modeling stems from our inability to mechanistically describe and couple all of the phenomenon present in a complex system in a single unified mathematical model. This is primarily a consequence of two factors — our poor understanding of turbulent transport in complex systems and inadequate numerical techniques. Neither of these conditions is likely to change during the critical time period of the FCR program.

Relatively simple fluid mechanical models will be sought which can describe in a gross fashion certain important fuel/air contacting characteristics of flames. For example, the near field behavior of swirl stabilized flames defies description through a complete mathematical solution of the conservation laws of physics and chemistry. However, a gross fluid mechanical description may be possible which links influential system parameters with characteristics such as shear layer scales and strengths, recirculation zone sizes, ballistic behavior of fuel droplets, etc. If such models can lead to a rough ability to scale observed phenomena then they will have served an important function. Insight to the scaling behavior of complex systems is the single most important objective of predictive modeling.

FCR PRODUCTS

Referring again to Figure 2 it is appropriate to summarize at this point the products that will be generated by the FCR program.

- Identification and characterization of dominant phenomena which significantly effect NO_x and related pollutant emissions.
- Quantification and generalization of results through intuitive or qualitative models, empirical correlations, mathematical models for prediction and scaling.
- Determination of degree to which critical mechanisms can be controlled and insight as to how this control might be achieved.
- Establishment of lower bounds on NO_x emissions set by various physical and chemical factors.
- Direct input to "technology development" programs through review of results from fundamental viewpoint, guidance in design of experiments, and new control concept suggestions.

In addition to the above outputs which related specifically to the objectives of the EPA programs, the FCR program will generate information and tools of general use in the development of combustion devices.

SECTION 3

INITIAL PROGRAM OF RESEARCH

This section reviews the initial effort in applying the planning guidelines outlined in Section 2.

INITIAL PRIMARY OBJECTIVE

A study of stationary combustors indicates that flame types which contribute significantly to the total NO_x generated by these devices can be characterized as follows:

	Dominant Flame Characteristic	Significant Exceptions
•	Transport is turbulent and radiative	
•	Fuel/air contacting is by diffusion and particle penetration	Flame propagation in spark-ignited I.C. engines
•	Flames are large - typically occurring in industrial/utility equipment with characteristic dimension of the energy release zone on the order of feet to tens of feet	Flames in domestic and small commercial furnaces; gas turbines
•	Residual oil and coal are the principal sources of emissions due to high nitrogen content and the difficulties associated with simultaneous NO_x and particulate control	Alternate fuels, natural gas

• The time-mean motion is in steady-state	Reciprocating I.C. engine
• Pressure is atmospheric	I.C. Engines, supercharged boilers
• Flames are confined by cold walls to which the flame radiates	Process furnaces

The primary initial objective follows directly from these observations. The FCR program will focus on the control of NO_x and primary related pollutants generated by large confined one-atmosphere turbulent diffusion flames fueled with pulverized coal or residual oil and radiating to cold walls. Such flames account for 60 percent of all stationary NO_x emissions.

Two time frames must be considered for the application of control technology to this type of equipment which have implications for the FCR program. In the short-term, control strategy will be associated with existing technology and will involve simple system changes such as burner redesign. Thus results must be forthcoming in the two-to-four year time period if they are to have a significant impact upon technology development programs. Results from this same period will also be applicable to long-term NO_x control strategy since they will help to define the expected limits of control that are achievable through the application of existing technology and will form a basis for the development of long-term control technology based upon the design of radical new combustion systems.

SECONDARY OBJECTIVES

A group of secondary objectives have also been identified and are categorized by device/fuel type as follows:

- Large furnaces fired with coal-derived fuels
- Stoker-fired equipment
- Combined cycle and gas turbine combustor fired with residual oil and coal-derived fuels
- Catalytic combustors firing high nitrogen fuels

- Fluid mechanics and kinetics of selective NO_x reduction devices
- Reciprocating internal combustion engines

Stoker-fired boilers receive prominance because they represent the most probable use of coal for systems raising steam at 250,000 lb/hr or less. Combined cycles with their potential for 50 percent efficiency necessarily demand attention. Selective NO_x reduction may be economically attractive in applications where existing technology is incapable of reaching the necessary level of control, and hence, deserves attention especially with regard to the fluid mechanics of adequately mixing the reducing agent and the NO_x-laden combustion products.

Although these areas will not immediately receive direct FCR attention much of the research focused on large turbulent diffusion flames is not device-specific and is applicable to several of these categories. An understanding of pulverized coal combustion provides insight into suspension phase burning in a spreader stoker. The chemical kinetics of fuel nitrogen conversion is generally applicable.

PRELIMINARY TECHNOLOGY ASSESSMENTS

Preliminary technology assessments have been undertaken in order to structure an initial program of research. Some of the conclusions of these assessments are briefly presented below.

Gas Phase Kinetics

A review is currently in progress of the state-of-understanding of the chemical kinetics of NO_x formation and destruction in flames. With regard to fuel nitrogen chemistry, although considerable data and speculation exist as to the pertinent chemistry, there is a clear need for more reactor experiments. Questions need to be resolved regarding the existence of a common stable intermediate nitrogen compound regardless of the nature of the fuel nitrogen. Does such a compound occur very early in the conversion process and hence obviate the need to study the details of "prompt" chemistry? What dictates the extend of fuel nitrogen conversion to this stable intermediate? Can kinetics studies be concentrated upon the long time constant process by which the stable intermediate is converted to NO or N_2.

In examining existing flat flame and stirred reactor data two difficulties arise. First the uncertainty in the measurements due to probe and molecular beam skimmer effects in flat flames and unmixedness and temperature instrumentation in stirred reactors can give rise to a substantial degree of uncertainty in conclusions drawn from the data. Second, considerable difficulty arises in analyzing the data. For example, in flat flames if interest extends to the behavior within the flame front then a knowledge of low temperature kinetics associated with the upstream portion of the flame may be required to examine the high temperature kinetics of interest. Further, if the degree of rapid conversion of fuel nitrogen to a stable intermediate is process-dependent then the existence of a lean zone in an overall rich flat flame makes it difficult to draw general conclusions regarding this process in furnace-type flames. Stirred reactor data analysis requires careful attention to the sensitivity of species concentrations to reaction rates in order to extract basic mechanistic information. Valid sensitivity analyses are accurate only for small variations in rate constants and hence, the process of analysis becomes an iterative one.

There is a clear need for more well-instrumented reactor experiments designed to cover a wide range of residence times, temperatures, stoichiometries, fuel types and fuel nitrogen dopants. The effect of higher C/H ratio fuels needs special attention since the speciation of hydrocarbon radicals as a function of time may influence both the formation of nitrogen intermediates as well as the long time conversion of these intermediates to NO or N_2.

Extending these reactor experiments in a search for the lower bound on NO_x emissions set by the chemistry needs to be done and will become an important part of the FCR program. Such experiments will involve a variety of staging conditions both sequential and parallel to give control over the time-phasing of mass and heat transfer. Additional gas phase kinetics areas which are not well-understood and will receive attention under FCR are:

- SO_x/NO_x interaction
- Soot formation
- Soot/NO_x formation

PHYSICS AND CHEMISTRY OF TWO-PHASE FLOW

The most apparent gap in experimental evidence concerning pollutant formation is pulverized coal and heavy oil combustion is in the area of laboratory reactors which simulate combustion conditions representative of specific regions within furnace-type flames. Reactor experiments should be designed such that the fluid mechanics of fuel/air contacting is sufficently simple ensuring that the results are amenable to analysis. Stirred and plug flow reactors and co-axial turbulent diffusion flames with well-controlled ignition regions are representative of such experiments. They are both analyzable and can be made representative of important furnace-like conditions such as stoichiometry, temperature, particle heat-up times, radiation intensity, residence time, turbulence level, transport behavior, etc. Reactor experiments provide the opportunity not only to obtain global process characteristics of the reactor as an entity but also allow the definition of specific phenomenological behavior relating to oil droplet and coal particle combustion. Understanding the mechanics of devolatilization and vaporization, fuel nitrogen conversion processes, and particulate formulation should be considerably enhanced as a consequence of these experiments.

Figure 3 is a schematic illustration of spray combustion reactor experiments. It illustrates the type of coupled phenomena which can be explored in a well-controlled analyzable experiment. The limiting situations shown are representative of different combustion regimes within a real system and yet are amenable to relatively straightforward analysis. Liquid fuel combustion has the unique feature of ballistic penetration of fuel into the combustion system due to high droplet momentum. This provides the potential for greatly enhanced fuel/air contacting rates. Key to this behavior are the relative vaporization, dynamical equilibration, and turbulent transport times. Before dynamical equilibration or vaporization take place transport can be by ballistics or turbulence or both. Following vaporization or velocity equilibration transport is, of course, only by turbulence. Well-controlled reactor experiments can explore these limits. The sketch at the bottom of Figure 3 simulates the conditions existing in a shear layer surrounding the stabilizing recirculation zone of a swirl or bluff body burner. The simulation approximates an injection system designed to place the fuel into the shear region.

The above does not negate the value of single particle or controlled multi-particle experiments provided a strong linkage can be made between the results of such investigations and the critical behavior of practical combustors. For example, the effect of liquid fuel and coal properties on NO_x and particulate formation may be further illuminated by continued detailed investigations of pyrolysis and combustion with independent control of heat-up rates, gas phase composition, and particle spacing.

MATHEMATICAL MODELING

The numerical analysis problems associated with Navier-Stokes modeling of complex flame behavior are:

1. Significant diffusion-type errors are associated with attempts to gain numerical stability.
2. Near-equilibrium behavior (e.g., turbulence, particle dynamics, particle heat-up, chemical kinetics) can lead to severe numerical stability problems.
3. Adequate flow field definition in regions of large gradients (e.g., shear layers, energy release zones) requires a high density of grid points.

In general, the resolution of these problems leads to prohibitively long computation times. Problems associated with near-equilibrium behavior can be eliminated through reformualtion of the mathematical description such that when any short-time-constant process closely approaches its equilibrium state that process is in fact redefined as equilibrated.

New numerical techniques which have the potential to resolve the problems listed above are the subject of much research in applied mathematics. "Flux-Correcting" methods show considerable promise for step-wise correction of the numerically-induced diffusive flux associated with stable integration. "Adaptive" grid control methods must be developed in which the grid-point density is locally adapted as a function of gradient intensity. Other research related to "finite Element" techniques in which local integration is performed across finite elements imbedded within the flow field may eventually prove to be the most satisfactory approach.

Adequate Navier-Stokes solution techniques will not be forthcoming in the time frame of the primary FCR objectives. Long-term (10 year) FCR objectives, however, may dictate that the program should attempt to influence the direction of research in numerical methods. To this end, consideration is being given to supporting a task to define a sensible long-term program of research in numerical methods suitable to FCR needs. The results of such an effort would then be used to influence the actions of other government sponsors.

With regard to mathematical modeling the FCR program will concentrate on developing adequate data analysis and modular modeling codes. The primary thrust of the FCR modeling element will be directed toward the development of adequate data analysis and module modeling codes. The numerical techniques required for such codes are proven standard methods and will not require further development.

TRANSPORT PHENOMENA AND FLUID MECHANICS

The principal unresolved issues related to transport phenomena in furnace-type combustors are:

1. Nature of complex transport phenomena in near-field dominated flames.
2. Turbulence-kinetics coupling due to segregation.
3. Nature of macroscale transport in long turbulent diffusion flames.
4. Participation of liquid or solid phase in turbulent transport.
5. Turbulence lag phenomena.
6. Radiation transport — effect on gas and condensed phase temperatures.

The first issue constitutes perhaps the largest gap in our understanding of significant transport and flow field behavior. To elaborate on this we note that large furnace flames can be broadly classified into two groups of very different character:

- Near-field dominated — typified by present-day wall-fired furnaces in which fuel processing, flame holding, energy release, and quenching are intimately coupled in an intense region near to and dominated by the burner.

- Far-field dominated — typified by corner-fired boilers in which stabilization is achieved through flame-flame impingement or through hot product recirculation on a scale of the furnace size.

These classifications aid in making our primary objective more concrete from the standpoint of defining the flame characteristics of interest. It is the fluid mechanics of near-field dominated flames that is the concern of the first issue raised above, and more work is required to bring our understanding of such flow fields to the necessary level. Attempts at gaining this understanding through solutions to the full Navier-Stokes equations have failed due to inadequate knowledge of physics and mathematics. What knowledge we do have of turbulent transport is relegated primarily to simple classical flow fields such as free shear layers, boundary layers, and coaxial jets. A well-designed experimental and theoretical effort will be undertaken to explore the basic fluid mechanical characteristics of burner-dominated flames. Initially an engineering approach using empiricism and relatively simple fluid mechanical modeling will be pursued.

The objectives of the investigation will be to link the basic fluid mechanical behavior and fuel particle mechanics with controllable design parameters. Flame types which are potentially attractive for NO_x control must receive emphasis. The study should examine the fluid mechanical consequences of energy release patterns associated with several distinct fuel distributions and recirculation zone characteristics. Included would be: (1) injecting most of the fuel at high momentum down the centerline through a stabilizing "donut" vortex pair; (2) depositing most of the fuel at low momentum into a central torroidal vortex; and (3) placing a portion of the fuel into the intense shear layer region surrounding a central vortex. These fuel distributions are illustrated schematically in Figure 4. Individually and in combination such fuel injection and recirculation configurations are representative of the several hypothesis regarding NO_x control. For example, placing coal in a hot, rich, long residence time recirculation zone may allow most of the fuel nitrogen to be driven out of the fuel prior to char burnout and into a near equilibrium gas phase state which would minimize overall conversion to NO_x. Injecting fuel down the centerline, with just sufficient burner or combustion chamber-induced recirculation for flame stability, represents an attempt to shield the fuel region from oxidative species. Hot combustion products mix with the fuel jet providing a hot, long residence time environment while the flame prevents the penetration of oxidizing species into the rich fuel zone. Placing fuel into the vortex boundary shear zone leads to intense combustion with high NO_x concentrations. A potential control scheme would embody parallel staging wherein a portion of the fuel is burned in the shear layer yielding high NO_x and a portion is burned under conditions yielding high XN compounds. Brought together in the proper manner the possibility exists of the NO_x being reduced by the XN giving rise to a low final NO_x level.

The main point of this discussion of flame characteristics is to emphasize the need for sufficient understanding to allow manipulation of flame behavior in very specific ways. Some questions follow which underscore the type of understanding required. How is a central or torroidal-pair vortex generated which has a specific size, residence time, and shear layer strength? How do these quantities scale? How can fuel be ballistically inserted into specific regions of this flow field? How does the energy release distribution effect flow patterns? How are burner parameters such as divergence geometry, radial profile of swirl and axial velocities, and fuel injection characteristics related to the significant flame properties?

The pressure field is an important fluid mechanical variable which can be used as an intermediate link between burner parameters and velocity field characteristics. Stagnation conditions and attendent adverse axial pressure gradients required to induce recirculation can be achieved in a variety of ways. These include confined flows with sudden area expansion, the presence of a bluff trailing edge body, coaxial mixing between streams with large velocity ratios, and swirling flows subjected to sudden area expansion. A "donut" vortex pair can be generated by a combination of swirl and high centerline axial velocity. Figure 5 illustrates these basic methods of inducing recirculation. The required experimental and theoretical investigations should provide an understanding of such flow fields, especially swirl stabilized flows, including the turbulent and ballistic mixing of fuel and combustion air, and the effect of energy release on the basic flow configurations. Integral techniques offer one promising theoretical approach. Stimulus-response methods should be investigated as an aid in the experimental program.

The remaining issues requiring investigation that are listed at the beginning of this section pertain to both near and far-field dominated flames. The significance of turbulent-kinetics coupling rests on the question of whether long life time coherent structures (eddies) exist in furnace-type flames. If a large eddy remains stable for periods comparable to molecular diffusion times across the internal lamina of the eddy then significant segregation effects can be present. Both theoretical and experimental programs are contemplated to explore these questions. An adequate description of macroscale transport in long coaxial diffusion flames rests again on the degree of coherent structure, and hence segregation, existing in furnace-type flames. Substantial overlap of time-mean concentrations of fuel and air on the centerline of such flames is the primary indicator of significant segregation.

Turbulence lag refers to a state of turbulence which is not wholly dependent on the local kinematics of the flow but rather shows a persistence of turbulent structure generated at an earlier time. That is the turbulence "lags" its equilibrium state which is dictated by the local flow kinematics. The important question again is whether such behavior is characteristics of furnace-type flows. The answer rests on determining the relative time constants for turbulence equilibration and the streamwise changes in the time-mean flow. Plausibility arguments and numerical experiments suggest that furnace-type flows are equilibrated but the issue needs further clarification.

INITIAL SUBCONTRACTOR AND EER TASKS

Following the preliminary technology assessments and identification of gaps in the understanding of significant phenomenon an initial program of subcontractor-oriented research tasks has been set forth. Initial procurements are contemplated in the following areas.

1. Stirred reactor and plug flow investigation of the gas phase chemistry of fuel nitrogen conversion, soot formation, and SO_x/NO_x interation.
2. Pulverized coal combustion reactor studies — stirred, plug flow, controlled mixing.
3. Residual oil combustion reactor studies — stirred, plug flow, controlled spray combustion.
4. Experimental investigation of the basic fluid mechanical characteristics of residual oil burners as they relate to fuel nitrogen conversion.
5. Evaluation of NO_x sampling measurement techniques and development of standard procedures.
6. Theoretical investigation of the basic fluid mechanical behavior of near-field burner-dominated flames as it pertains to energy release and fuel nitrogen conversion.
7. Theoretical investigation of the fluid mechanics of coherent structure turbulent diffusion flames as it pertains to energy release and fuel ntirogen conversion.
8. Experimental search for the lower bound of fuel nitrogen conversion in gaseous systems.
9. Application of laser holography to determine behavior of coal particles during heat up and devolatilization.

In addition, consideration for initial subcontracts is being given to:

1. Liquid fuel pyrolysis studies — linkage of fuel properties to combustion behavior and fuel nitrogen conversion.
2. Residual oil droplet burning experiments — linkage between combustion environment, droplet-droplet interaction and tendency to produce particulates.
3. Experiments designed to investigate the presence of long life time coherent structure in furnace-type flames.

In-house EER efforts under the FCR program are presently concentrated on the development of data analysis and modular modeling codes as follows:

1. Stirred Reactor Sensitivity Analysis — predicts influence of rate constant changes on species concentrations.
2. Inverse Flat Flame Analysis – generates rate constants consistent with observed species distributions.
3. Two-Phase Stirred Reactor Code for arbitrary distribution of input particle size.
4. Gaseous Diffusion Flame Code modified to account for confinement and the effect of segregation on overall flame properties.
5. Modular Modeling Code extended to allow for parallel staging.
6. Two-Phase Turbulent Diffusion Flame Code.
7. Initiation of a task to develop a simple fluid mechanical model for scaling of near-field burner behavior.

In addition there are several FCR-related tasks at EER under the sponsorship of other CRB Technology Development programs. These include:

1. Chemical reaction screening for the $CH_4/FN/SO_x/Air$ system.
2. Flat flame data analysis.
3. Reactor and diffusion flame studies of fuel nitrogen conversion in oil, coal, and low Btu gas combustion.

The initial MIT Energy Laboratory effort in addition to the general role of participating in the planning and review functions includes the following specific tasks:

1. Participation in technology assessment of gas phase and heterogeneous chemical kinetics of fuel nitrogen conversion.
2. Participation in developing a sound scientific strategy by which the problems of significance can be distinguished from the non-problems.
3. Development of a methodology whereby NO_x lower bound estimates can be made under different sets of constraints.

Figure 6 illustrates the output expected from the initial set of tasks described in this section. The gas phase kinetic information in conjunction with the various codes allows a description of NO formation in a variety of simple reactors and laminar flames for which the transport physics is well-understood. Armed with this information a systematic search, both experimental and theoretical, can be undertaken for lower bound estimates. Moving down the figure more information pertaining to transport and two-phase behavior is generated and used for NO prediction in generally more complex situations. Although coal flames appear at the bottom it should not be implied that they are necessarily the most difficult to describe. For example, a long turbulent coal flame may act much like a fuel-staged gaseous diffusion flame followed by an essentially premixed two-phase char burnout. In principle, this situation is less complex than burner-dominated heavy oil combustion.

SUMMARY

A three-year program of fundamental combustion research is underway which is focused on the control of NO_x and primary related pollutants from stationary sources.

The initial emphasis has been placed on the combustion of pulverized coal and heavy residual oil in large boilers. Initial planning and technology assessments have been completed. These have led to the definition of initial subcontractor tasks and EER and MIT Energy Laboratory in-house tasks. The initial program of research is weighted heavily toward coal and oil reactor experiments which, in a controlled manner, simulate different regions and limit situations within practical combustors.

The program is conservative with a high probability of success in generating useful information for design and development of low emission combustors within a short time period. This confidence stems in large part from the program of fundamental research sponsored by the CRB over the last seven years. The results of these investigations have provided the insight which allows the delineation of significant phenomena and the formulation of a directed program of research.

ACKNOWLEDGEMENTS

The formulation of the FCR program plan has been a team effort and includes contributions from amny sources. The authors would like to express their appreciation to all those organizations who invited us to visit their laboratories to discuss the program. These discussions were most helpful and gave us an understanding of many research programs which are planned or are underway, and which will impact FCR. We would like to thank the staff of the CRB for their interest and their thoughts on the support expected from fundamental research activities in other program areas. We are particularly indebted to Professors Gerstein of USC, Samuelson of U.C. Irvine and Wendt of U. of Arizona for their help in defining critical problem areas in the various scientific disciplines involved in pollutant control. We would also like to thank Professors Beér, Langwell, Louis and Sarofim of M.I.T. for their helpful comments in reviewing the initial plan.

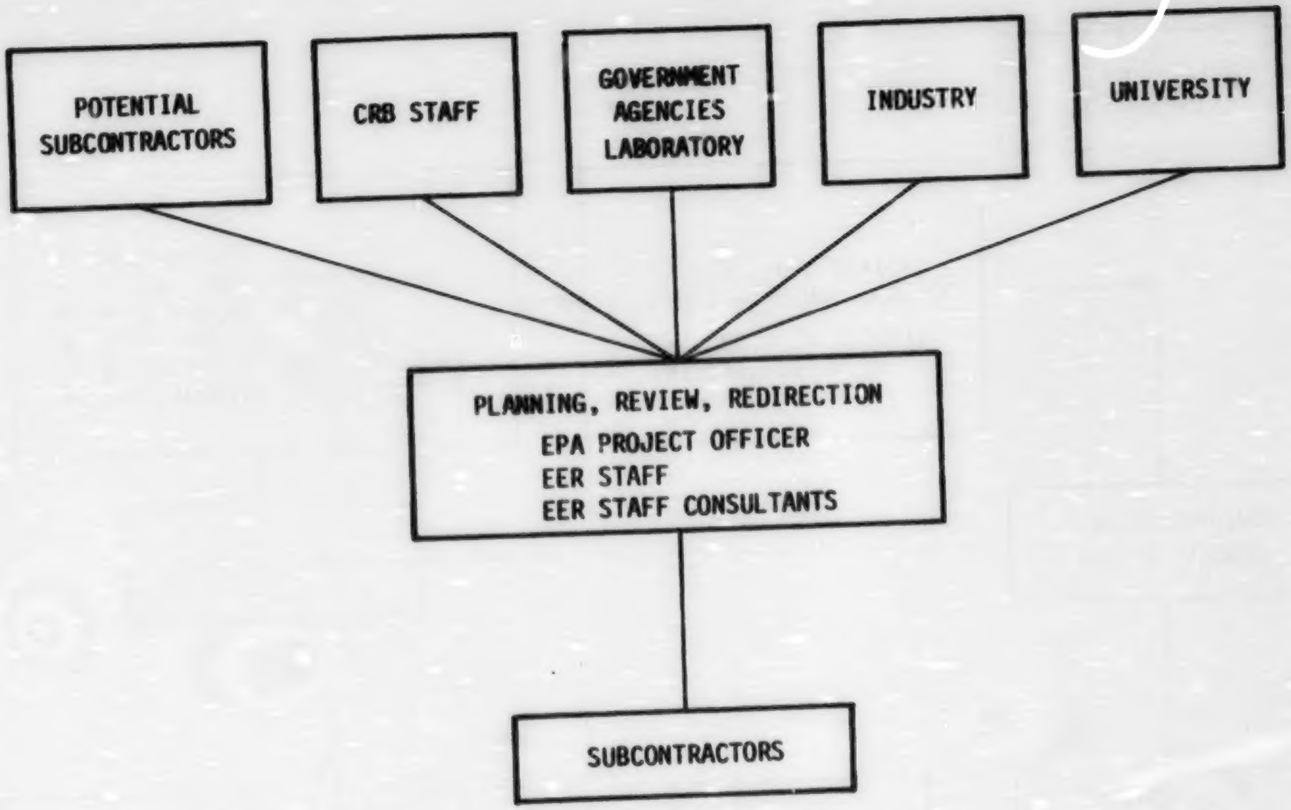
POTENTIAL SUBCONTRACTORS
CRB STAFF
GOVERNMENT AGENCIES LABORATORY
INDUSTRY
UNIVERSITY
PLANNING, REVIEW, REDIRECTION
EPA PROJECT OFFICER
EER STAFF
EER STAFF CONSULTANTS
SUBCONTRACTORS

Figure 1. Program Organization

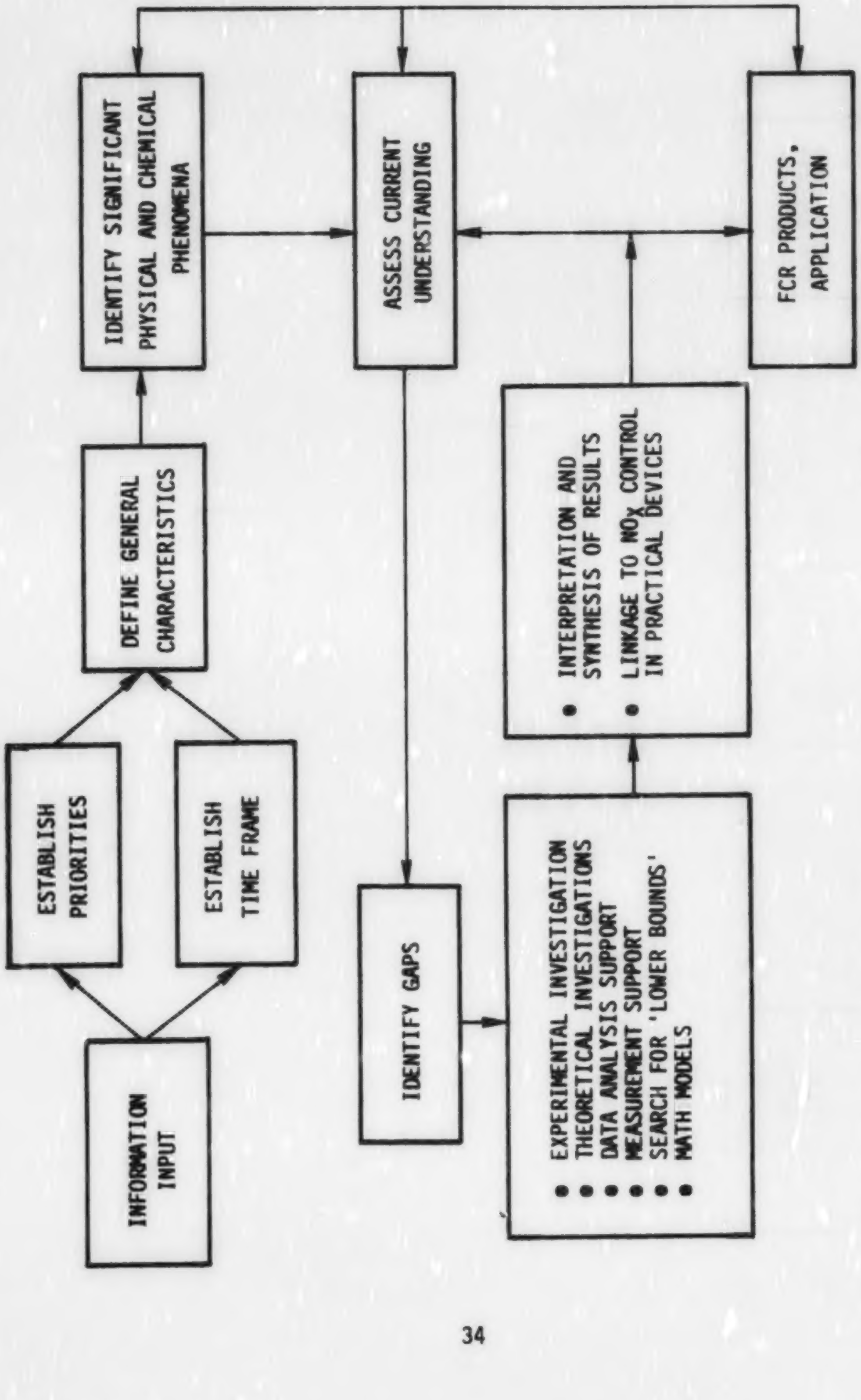
INFORMATION INPUT
ESTABLISH PRIORITIES
ESTABLISH TIME FRAME
DEFINE GENERAL CHARACTERISTICS
IDENTIFY SIGNIFICANT PHYSICAL AND CHEMICAL PHENOMENA
ASSESS CURRENT UNDERSTANDING
FCR PRODUCTS, APPLICATION
IDENTIFY GAPS
• EXPERIMENTAL INVESTIGATION
• THEORETICAL INVESTIGATIONS
• DATA ANALYSIS SUPPORT
• MEASUREMENT SUPPORT
• SEARCH FOR 'LOWER BOUNDS'
• MATH MODELS
• INTERPRETATION AND SYNTHESIS OF RESULTS
• LINKAGE TO NO$_X$ CONTROL IN PRACTICAL DEVICES

Figure 2. FCR Planning Strategy — Flow Chart

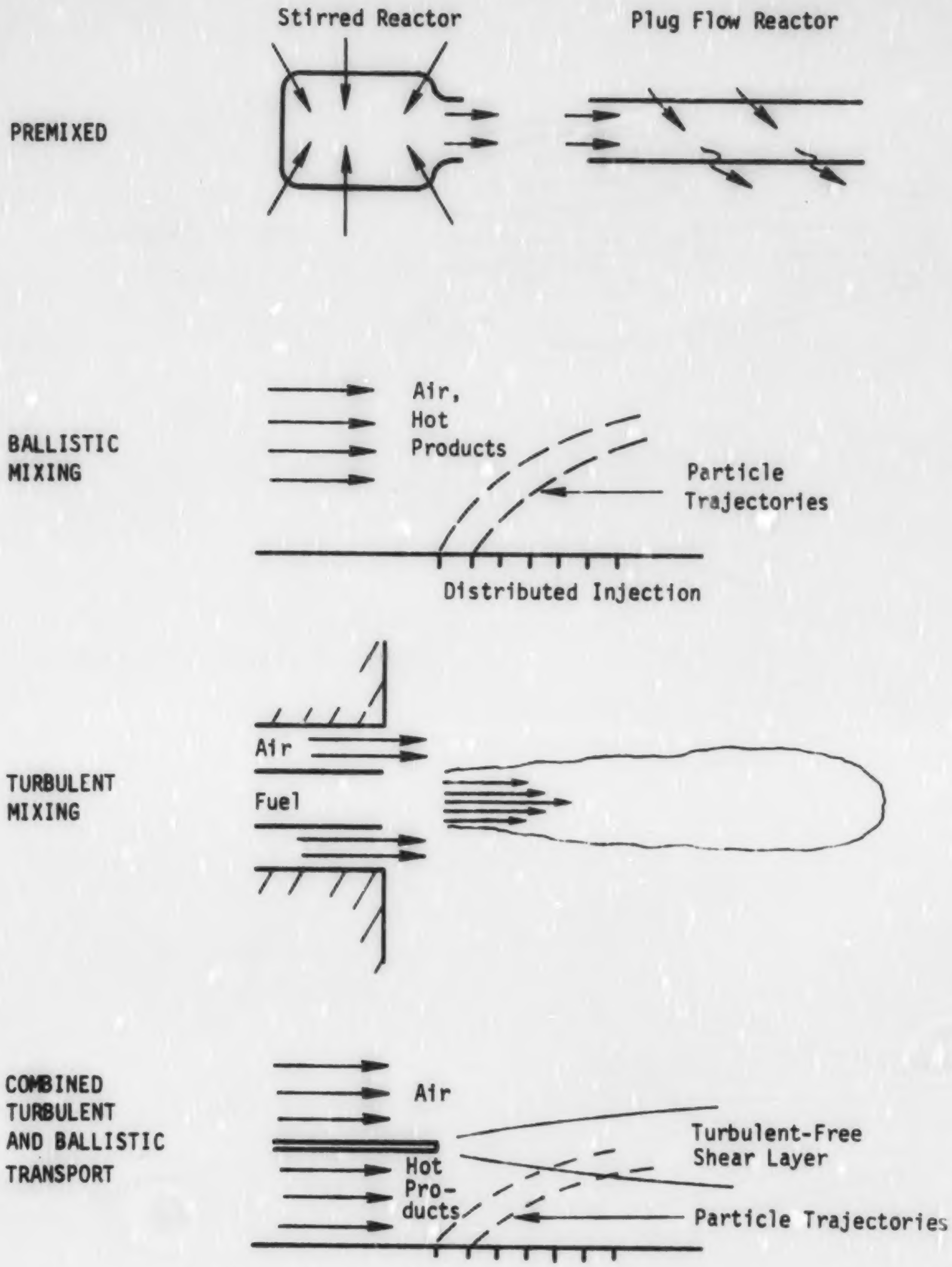
Stirred Reactor
Plug Flow Reactor
PREMIXED
BALLISTIC MIXING
Air, Hot Products
Particle Trajectories
Distributed Injection
TURBULENT MIXING
Air
Fuel
COMBINED TURBULENT AND BALLISTIC TRANSPORT
Air
Hot Products
Turbulent-Free Shear Layer
Particle Trajectories

Figure 3. Schematic Spray Combustion Experiments

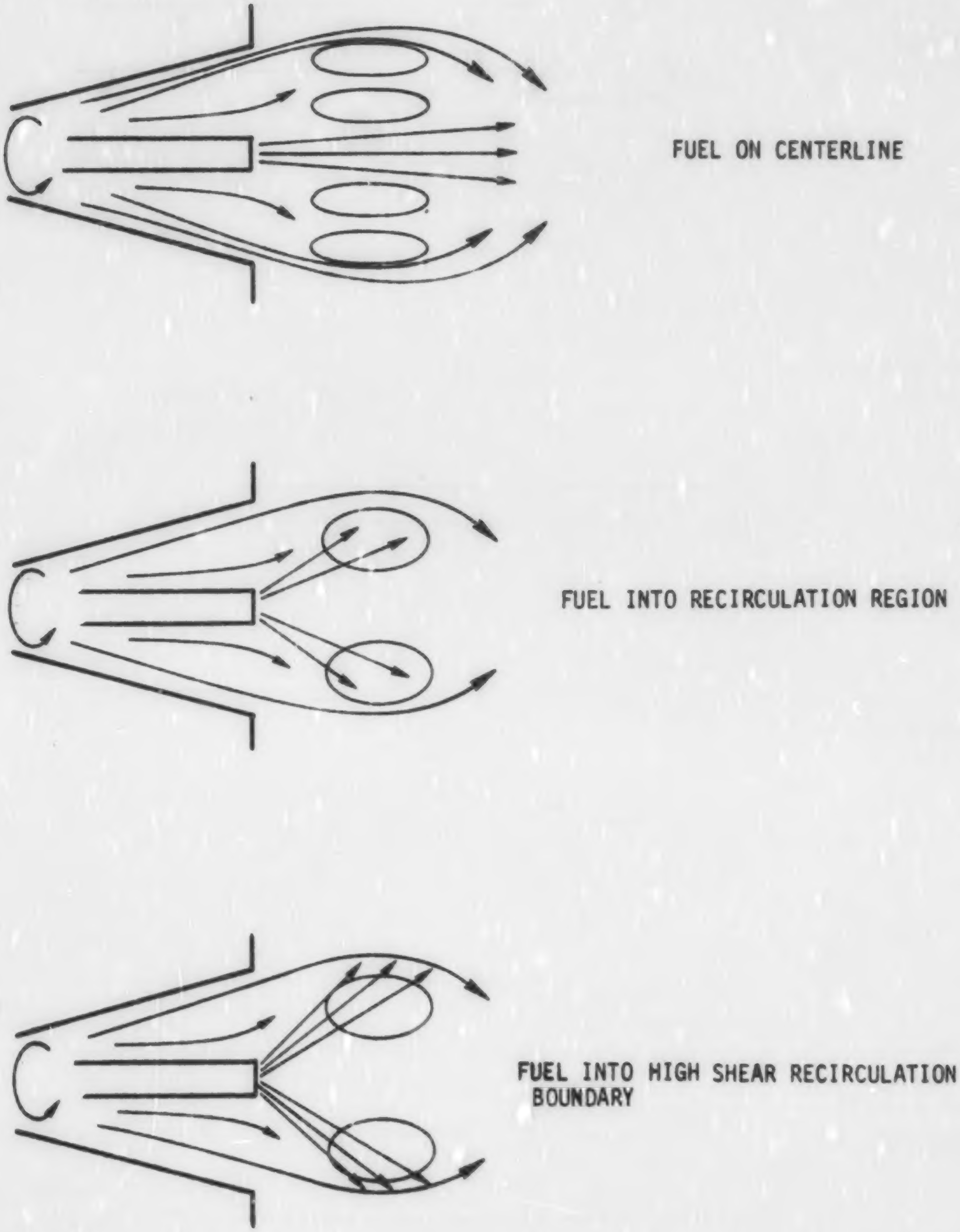
FUEL ON CENTERLINE
FUEL INTO RECIRCULATION REGION
FUEL INTO HIGH SHEAR RECIRCULATION BOUNDARY

Figure 4. Schematic of Several Fuel Distributions with Divergent-Swirl Induced Recirculation

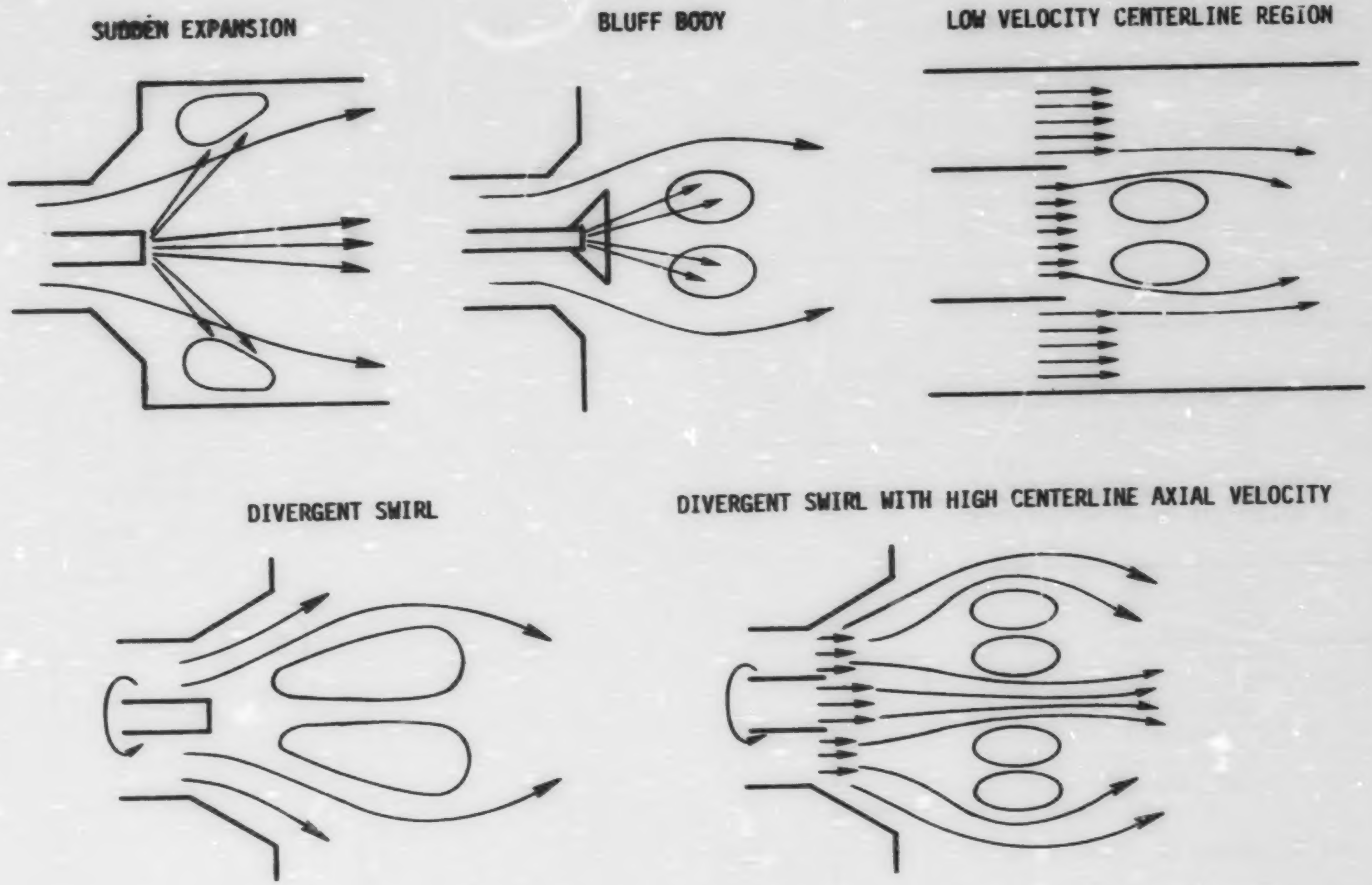
SUDDEN EXPANSION
BLUFF BODY
LOW VELOCITY CENTERLINE REGION
DIVERGENT SWIRL
DIVERGENT SWIRL WITH HIGH CENTERLINE AXIAL VELOCITY

Figure 5. Schematic of Various Methods of Inducing Recirculation

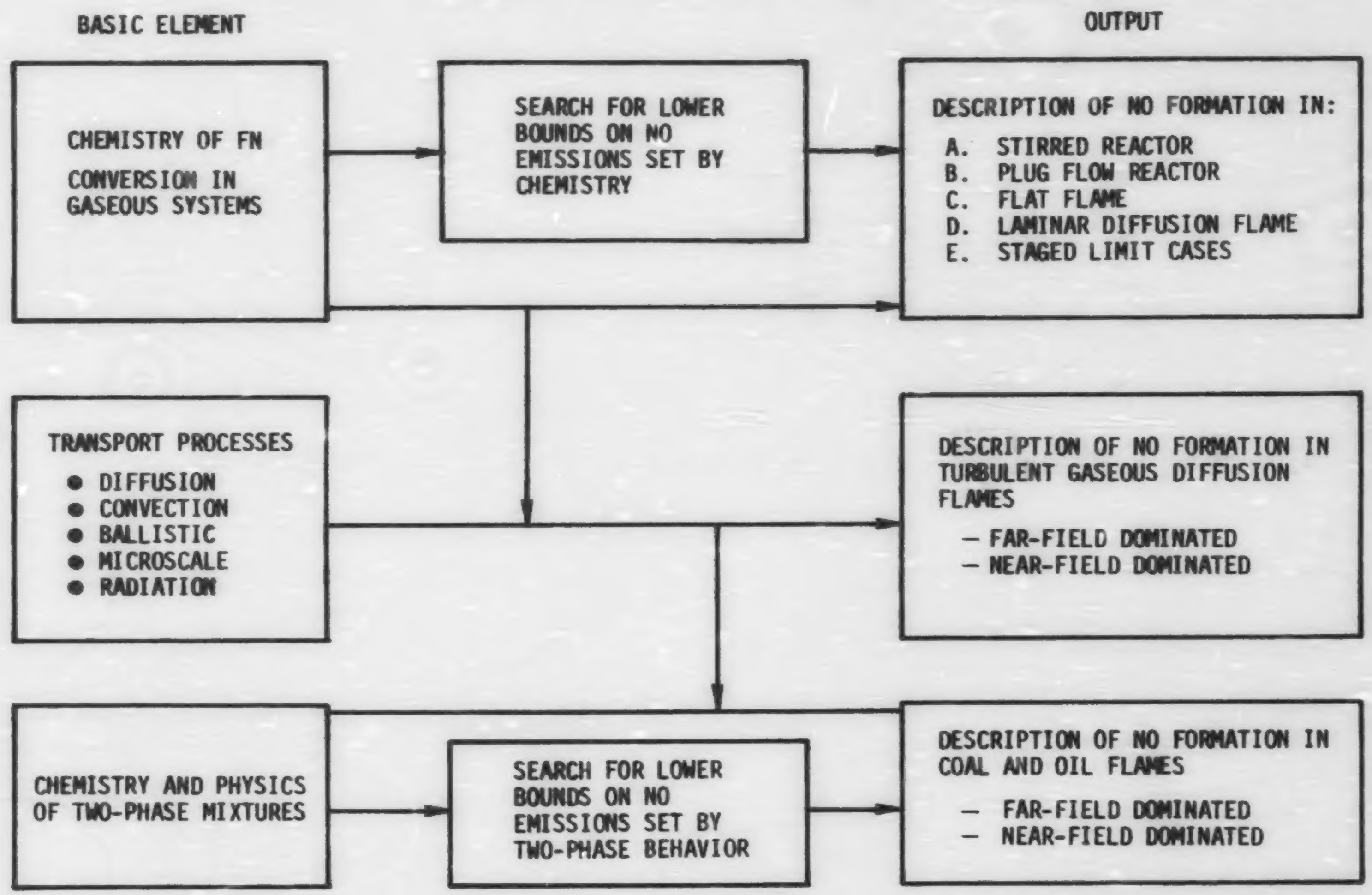
BASIC ELEMENT
OUTPUT
CHEMISTRY OF FN
CONVERSION IN GASEOUS SYSTEMS
SEARCH FOR LOWER BOUNDS ON NO EMISSIONS SET BY CHEMISTRY
DESCRIPTION OF NO FORMATION IN:
A. STIRRED REACTOR
B. PLUG FLOW REACTOR
C. FLAT FLAME
D. LAMINAR DIFFUSION FLAME
E. STAGED LIMIT CASES
TRANSPORT PROCESSES
● DIFFUSION
● CONVECTION
● BALLISTIC
● MICROSCALE
● RADIATION
DESCRIPTION OF NO FORMATION IN TURBULENT GASEOUS DIFFUSION FLAMES
— FAR-FIELD DOMINATED
— NEAR-FIELD DOMINATED
CHEMISTRY AND PHYSICS OF TWO-PHASE MIXTURES
SEARCH FOR LOWER BOUNDS ON NO EMISSIONS SET BY TWO-PHASE BEHAVIOR
DESCRIPTION OF NO FORMATION IN COAL AND OIL FLAMES
— FAR-FIELD DOMINATED
— NEAR-FIELD DOMINATED

Figure 6. Flow Diagram Illustrating Path to FCR Output for Initial Plan

CHEMICAL REACTIONS IN THE CONVERSION OF FUEL NITROGEN TO NO_x: FUEL PYROLYSIS STUDIES

By:

A. E. Axworthy and V. H. Dayan
Rockwell International/Rocketdyne Division
Canoga Park, California 91304

ABSTRACT

The objective of this study is to investigate the types of "preflame" reactions fuel nitrogen compounds can undergo. The inert pyrolysis study was extended to include additional coals and alternate liquid fuels. At 1100 C, the HCN yield (% fuel nitrogen recovered as HCN) ranged from 23 to 44% for seven No. 6 fuel oils and from 24 to 30% for six coals. A COED char yielded less than 2% HCN, while a liquefied (catalytic) coal yielded 51% HCN and two hydrotreated shale oils produced 60 and 69% HCN, respectively.

A two-stage pyrolysis reactor was developed in which volatile nitrogen compounds are evolved from fuels in the first stage and subsequently react under conditions that can be quite different. The two-stage experiments demonstrated that nearly all of the HCN forms from the secondary reactions of volatile nitrogen compounds and little forms in the initial pyrolysis process. When the first-stage temperature is decreased from 1100 to 750 C, while maintaining the second stage at 1100 C, the HCN yield from a fuel oil decreases by one-fourth. For a similar experiment with three coals and the first stage at 600 C, the HCN yields are one-third to three-fourths those obtained with both stages at 1100 C. It is postulated that more nitrogen remains in the char at the lower temperature.

In addition, a study was carried out on the oxidative pyrolysis and oxidation of the model fuel nitrogen compounds pyridine and benzonitrile. The major nitrogen-containing products from both model compounds are mainly HCN and NH_3 at lower temperatures (~720 C) and are N_2, N_2O, and NO at higher temperatures (~760 C). With both model compounds, the maximum N_2O yield exceeds 45% (at about 770 C).

Preceding page blank

INTRODUCTION

An experimental and analytical program is being conducted to investigate the chemical processes involved in the conversion of fuel-bound nitrogen to NO_x in combustion. The results obtained during the first phase of this study, performed under EPA Contract 68-02-0635, have been reported previously (Ref. 1 through 3). The study is continuing and the additional results obtained to date from pyrolysis and oxidation experiments are reported herein (Ref. 4). The objective of this task of the program was to investigate the types of preflame reactions that volatile fuel nitrogen species can undergo during pyrolysis and before reaching the flamefront.

Since the previous symposium, model fuel nitrogen compounds have been pyrolyzed in an oxidative atmosphere, and oils and coals have been pyrolyzed with emphasis on inert conditions. A two-stage reactor was developed in which the secondary reactions of the nitrogen-containing volatiles formed in the initial pyrolysis process could be studied independently.

BACKGROUND

In the previous pyrolysis studies, that were conducted during the first phase of this program (Ref. 1 through 3), fossil fuels and model nitrogen compounds were pyrolyzed in an inert atmosphere (helium) in small quartz flow reactors. HCN was the major volatile nitrogen compound formed in all cases, indicating that HCN probably forms from nitrogen-containing fuels during the initial, pre-flame stages of combustion and may be the principal intermediate in the formation of fuel nitric oxide.

MODEL COMPOUND PYROLYSIS (INERT)

Model compound vapors, diluted to a concentration of 3% in helium, were passed through a quartz capillary reactor at temperatures between 900 and 1100 C with a nominal residence time in the heated zone of 1 second. Samples of the model compound liquid, 0.2 μl in size, were vaporized into the preheated carrier gas stream before it entered the reactor.

Preceding page blank

Under these inert pyrolysis conditions, HCN and a carbonaceous residue are the major nitrogen-containing products derived from pyridine and benzonitrile, the two model compounds that were studied in detail. The fraction of the organic nitrogen that is converted to HCN rather than being contained in the residue increases with temperature. The HCN yields from benzonitrile and pyridine at 960 C are 49 and 40%, respectively. At 1100 C, however, the HCN yield from benzonitrile is 82%, and all of the pyridine-N is converted to HCN. No molecular nitrogen and only minor amounts of ammonia form from the inert pyrolysis of the model fuel nitrogen compounds. At the lower temperature, pyridine forms a few percent of benzonitrile, quinoline, and acrylonitrile.

Based on the kinetic parameters obtained from the pyrolysis of the model fuel nitrogen compounds, it was established that even in the absence of oxygen the organic nitrogen compounds present in fossil fuels should decompose in fractions of a millisecond at a temperature around 1700 K. It was postulated, therefore, that when a diffusion flame surrounds a coal particle or oil droplet the volatile fuel-nitrogen compounds will be mostly converted to HCN before reaching the flame-front.

FOSSIL FUEL PYROLYSIS (INERT)

Two bituminous coals and six No. 6 fuel oils were rapidly heated in a quartz reactor to either 950 or 1100 C. The volatile pyrolysis products formed were carried through the reactor in a helium stream, and the nitrogen containing species were measured. The fuel samples, 1 to 2 milligrams in size, were placed in a minature quartz boat that was moved very quickly into the preheated reactor. The residence time of the volatile products in the heated zone was about 1 second.

The fraction of organic fuel nitrogen that was converted to HCN under these conditions ranged from 15 to 25% at 950 C and from 23 to 42% at 1100 C (Ref. 1 through 3). In each case, the amount of HCN formed at 950 C was about six-tenths of that formed at 1100 C. Wilmington crude oil yielded 30% HCN at 950 C and 50% at 1100 C.

The NH_3 and N_2 formed in these fossil fuel experiments were measured together (after converting any NH_3 to N_2). The total amount of NH_3 plus N_2 formed from the fuel oils (measured as N_2) was nearly independent of the nitrogen content of the oil and of the temperature, and ranged from 0.5 to 0.8 micrograms of N_2 per milligram of oil. Because these values are only slightly greater than the solubility of N_2 in oils, it appears that the amounts of NH_3 and N_2 formed under these inert pyrolysis conditions are quite small. One of the coals yielded slightly more N_2 plus NH_3 (1.1 ±0.1 micrograms per milligram), but this was equivalent to only 9% of the fuel-N. It was established, therefore, that NH_3 and N_2 are only minor products of the rapid, high-temperature inert pyrolysis of fosssil fuels. This would be predicted from the model compound results.

It was assumed that the remainder of the fuel nitrogen was contained in the char and in the carbonaceous residue that formed on the reactor wall from the volatiles. Since it has been demonstrated (Ref. 5) that much of the fuel nitrogen in coals is nonvolatile at these temperatures and would remain in the char, the amounts of HCN formed at 1100 C may represent nearly all of the "volatile" organic nitrogen contained in these fuels. It was not possible to distinguish in these experiments between HCN formed in the primary pyrolysis process and that formed from the secondary reactions of the volatile nitrogen species. The model compound results suggested that most of the measured HCN may have formed downstream of the sample boat from the secondary reactions of the volatiles.

EXPERIMENTAL

The experimental procedures employed in this phase of the pyrolysis study are similar to those developed previously (Ref. 1 through 3). The model compound experiments were again carried out in a reactor that was simply a heated section of 2-mm ID quartz capillary, but the carrier gas was changed to a 3:1 O_2-He mixture so that the oxidative processes could be investigated.

Shown schematically in Fig. 1 are the single-stage fuel reactor, used in the previous study (Ref. 1 through 3), and a two-stage reactor developed and used in the present investigation. In both reactors, the volatiles formed from the pyrolysis of the fuel sample in the quartz boat (that can be moved rapidly into the preheated reactor) flow through a 2-cc volume downstream microreactor in which secondary reactions can occur. In the single-stage reactor, the quartz boat and the microreactor are at the same temperature and the carrier gas is of the same composition at each of these points. With the two-stage reactor, however, the temperatures at the stop position of the boat and at the microreactor can differ by as much as 500 C, and oxygen can be introduced into the microreactor only. Thus the fuel can be pyrolyzed in helium at a given temperature and the volatiles formed can be reacted downstream at a different temperature in either an inert or oxidizing atmosphere.

Only the two-temperature-zone feature of this reactor has been employed in the experiments conducted thus far, i.e., O_2 has not yet been added to the second stage. A study of the oxidation of the volatile fuel nitrogen species in the second stage only is planned. It has been demonstrated in the inert pyrolysis experiments that operation of the two-stage reactor with both stages at the same temperature gives, as expected, results nearly equivalent to those obtained in the single-stage reactor. Therefore, for simplicity, such single-temperature experiments will be referred to as single-stage experiments in this paper.

The remaining experimental details will be described in the following sections where the results from each type of pyrolysis experiment are presented and discussed.

INERT PYROLYSIS OF FOSSIL FUELS
(SINGLE STAGE)

Additional fossil fuels have been pyrolyzed in helium under the single-stage condition (where both the primary and secondary reactions take place at the same temperature) and the amount of HCN formed has been determined. The reactor was again operated at atmospheric pressure, the only change in the procedure being to increase the helium flowrate from 20 to 40 cc (STP)/min so that shorter residence times could be investigated (~0.7 second). It was established that at 1100 C the HCN yield is independent of flowrate over this range. The volatile nitrogen compounds apparently react completely even at the shorter residence time. This is in agreement with the results of the previous model compound experiments.

HCN YIELDS FROM OILS AT 1100 C (SINGLE STAGE)

Listed at the top of Table I are the HCN yields obtained at 1100 C from four additional oils. Also listed for comparison are selected results from the previous study. A No. 6 fuel oil containing 0.71% nitrogen gave an HCN yield of 44.5%.

This is the largest percentage yield that has been obtained from a petroleum-based No. 6 fuel oil but is less than the 50% HCN yield obtained from Wilmington Crude Oil (Table I). The HCN yield from this No. 6 fuel oil amounts to 6.1 μgm HCN per mg of oil (or 6.1 gms of HCN per kilogram), which is about the same as was formed from both a No. 6 fuel oil (obtained mainly from California crudes) that contained twice as much fuel nitrogen and from Wilmington Crude Oil.

A sample of liquefied coal prepared by the Synthoil process was pyrolyzed under these same inert conditions at 1100 C. This oil, which contained 1.3% nitrogen, produced twice as much as HCN as any oil that has been tested. The amount of HCN produced was 12.8 μgm/mg, which represents an HCN yield of 51.0%.

Two hydrotreated shale oils gave large HCN percentage yields of 60 and 70%, respectively, under these conditions, but the amounts of HCN produced were only 3.1 and 2.4 μgm/mg because of the low nitrogen contents of these treated oils. The first of these oils (C in Table I) was a treated full boiling range shale oil that contained 0.27% N and 0.04 S. The raw oil before treatment contained 2.05% N and 0.57% S. The second oil (D) was a treated middle distillate that contained 0.18% N and 0.04% S after treatment and 1.60% N and 0.57% S before.

These limited results with a liquefied coal and two treated shale oils suggest that the fuel nitrogen compounds in these oils form HCN more readily during rapid inert pyrolysis than do those in No. 6 petroleum-based fuel oils. This also suggests that these alterante fuels may show a greater extent of conversion of NO_x to fuel nitrogen during combustion with excess air.

EFFECT OF TEMPERATURE ON HCN YIELDS (SINGLE STAGE)

The HCN yield from the No. 6 fuel oil that was listed at the top of Table I was measured at the three temperatures 750, 950, and 1100 C. These results are plotted on linear scales in Fig. 2A and in the Arrhenius form in Fig. 2B. Under these single-stage conditions, the HCN yield drops from 46% at 1100 C to 4% at 750 C. The decrease in the HCN yield of a factor of 2 between 1100 and 950 C is in the range observed for other fuels in the single-stage experiments.

The Arrhenius plot shows a slight curvature, but the average apparent activation energy for HCN formation is 19 kcal/mole over this temperature range. This apparent activation energy may result from a combination of the temperature dependencies of the following effects: (1) the fraction of fuel-N that remains in the residue, (2) the fraction of the volatile fuel nitrogen species that decomposes before exiting the reactor, (3) the formation of HCN from the fuel-N species that do react, and (4) the inclusion of nitrogen in the carbonaceous residue that forms from the volatiles. It will be shown in a later section that the results of two-stage reactor experiments with this fuel oil indicate that the amount of nonvolatile nitrogen that remains in the residue, effect (1) above, does not change appreciably over this temperature range.

HCN YIELDS FROM COALS AT 1100 C (SINGLE STAGE)

The HCN yields obtained from the inert pyrolysis of three coals at 1100 C are listed at the top of Table II. The results from the two coals studied previously are also for comparison. All five of these coals gave HCN yields in the range of 24 to 30%. The amount of HCN produced ranged from 3 μgm/mg to 8.5.

INERT PYROLYSIS OF FOSSIL FUELS
(TWO STAGE)

The production of HCN in the inert pyrolysis of fossil fuels was investigated using the two-stage reactor described in the Experimental section of this paper. The fuels were pyrolyzed in helium at one temperature and the volatile products formed were passed through a 2-cc microreactor held at a different temperature. The objective of this study was to determine what fraction of the HCN produced is formed from the secondary reactions of the volatile species that form in the primary pyrolysis process. The previous model compound results had indicated that these volatile nitrogen compounds should convert almost completely to HCN when pyrolyzed in helium at 1100 C.

It was suggested (Ref. 2) that most of the HCN is formed in secondary reactions of the volatiles rather than in the initial fuel vaporization/pyrolysis process. If this is the case, the HCN yield should increase with the temperature at which the volatiles react and be fairly independent of the vaporization temperature--particulary for oils where the amount of nitrogen left in the residue is expected to be nearly independent of temperature. In the present two-stage experiments, the effect on the HCN yield of varying the temperature of each stage independently was investigated.

TWO-STAGE INERT PYROLYSIS OF A NO. 6 FUEL OIL

The No. 6 fuel oil listed at the top of Table I (Oil A) was employed in this series of experiments. The first stage of the two-stage reactor (Fig. 1) was constructed of 2-mm ID quartz capillary tubing and had a volume of only 0.25 cc. The second stage, which was also quartz capillary tubing, contained the 2-cc microreactor in which the volatiles had sufficient residence time to react. The oil samples were nominally 1.8 mg in size; this amount of oil should form about 0.8 cc of hydrogen during pyrolysis (calculated at 950 C). Therefore, the residence time of the volatiles in the first stage will be even less than 10% of the second-stage residence time and the microreactor volume is required to prevent the hydrogen formed from expelling the volatiles from the heated zone before they can react.

Duplicate experiments were conducted at each of the nine temperature combinations that can be obtained by setting each stage at 750, 950, or 1100 C. The HCN yields obtained are listed in Table III.

Experiments With First Stage at 950 or 750 C

Plotted in Fig. 3A and 3B are the HCN yields obtained in experiments in which the first stage was at 950 or 750 C. The yields are plotted as a function of second-stage temperature to demonstrate the amount of HCN that was formed in the second stage. If all of the HCN should form in the first stage, the HCN yield would be independent of the second-stage temperature. This is definitely not the case.

The yields shown in Fig. 3 are dependent on the first-stage temperature only in the case where the second stage is at 750 C. Under this condition, increasing the first-stage temperature from 750 to 950 C increases the HCN yield from 4 to 14%. This demonstrates that in all of the experiments in which the first stage is at 950 C, from 10 to 14% (absolute) of the HCN yield is formed in the first stage. When the first stage is at 750 C, however, this amount of fuel nitrogen is vaporized in a form that can be converted to HCN in the second stage if the second-stage temperature is 950 C or greater. This causes the two curves in Fig. 3 to coincide at the higher second-stage temperatures. According to this interpretation of the data in Fig. 3, the amounts of HCN formed in each stage under these six conditions are:

750 C/750 C	750 C/950 C	750 C/1100 C
0 to 4%/0 to 4%	0 to 4%/0 to 4%	0 to 4%/34 to 38%

950 C/750 C	950 C/950 C	950 C/1100 C
10 to 14%/0 to 4%	10 to 14%/10 to 14%	10 to 14%/27 to 31%

With the second stage at 1100 C, therefore, two-thirds or more of the HCN forms from reaction of volatiles in the second stage. The HCN that forms in the first stage at 950 C may also from from reaction of volatiles before they exit the first stage. Thus, most or all of the observed HCN is formed from the reactions of volatile fuel-nitrogen species in the second stage.

Experiments With First Stage at 1100 C

Plotted in Fig. 4 are the HCN yields from the six experiments in which the first stage was heated to 1100 C. Under this condition, the yield is much less dependent on the temperature of the second stage and an HCN yield of 35% is obtained even with the second stage at 750 C. This indicates that 31 to 35% of the HCN is formed in the first stage when it is at 1100 C. Thus the amounts of HCN formed in each stage are:

1100 C/750 C	1100 C/950 C	1100 C/1100 C
31 to 35%/0 to 4%	31 to 35%/7 to 11%	31 to 35%/11 to 15%

The most likely explanation for the results obtained with the first stage at 1100 C is that the pyrolysis rate of the volatile nitrogen species becomes so high that about three-quarters of the volatile nitrogen species react in the first stage during the short time they are flowing through this portion of the two-stage reactor. Although the HCN yield has a rather low temperature coefficient (apparent activation energy) of about 19 kcal/mole (Fig. 2B), the rate of pyrolysis of the volatile species should have an activation energy on the order of 70 kcal/mole as does pyridine decomposition (Ref. 2). The rate of a reaction with an activation energy this large will increase by a factor of 280 between 750 and 950 C and by another factor of 23 between 950 and 1100 C. It is not surprising, therefore, that the formation of much of the HCN from the volatile nitrogen species should occur in the first stage of the reactor at 1100 C. Some of this reaction may occur in the first stage even at 950 C.

Conclusions From Two-Stage Experiments With a No. 6 Fuel Oil

These results establish that most or possibly all of the HCN formed in the inert pyrolysis of this fuel oil forms from the secondary pyrolysis of volatile nitrogen species formed or released in the initial vaporization/pyrolysis process. Similar two-stage experiments were conducted with coals to investigate if the effect of the first-stage temperature on the amount or type of volatile nitrogen species formed is more important with a solid fuel.

TWO-STAGE INERT PYROLYSIS OF COALS

The two-stage results obtained with a Pittsburgh No. 8 coal (coal No. I in Table II) are summarized in Table IV. Holding the second stage at its maximum temperature of 1100 C, to convert as much of the volatile nitrogen species to HCN as possible, results in HCN yields of about 23% whether the first stage is at 1100 or 750 C. This indicates that the nitrogen species present in this coal that are convertible to HCN are moderately volatile. In fact, lowering the first-stage temperature to 600 C only decreases the HCN yield by about one-fourth. When the second-stage temperature is lowered to 750 C, with the first stage at 750 C also to drive off most of the volatile nitrogen (last line of Table IV), the HCN yield is only 7%. This demonstrates that at least 70% of the maximum amount of HCN formed from this coal is formed in the second stage.

Two additional coals and a COED char were pyrolyzed with the first stage at 600 C and the second stage at 1100 C to determine the yield of HCN from each. These results are listed in Table V. The bituminous coals, No. V and No. VI, which were studied under the previous program, produced only about 12% HCN under this condition and, as expected, the COED char yielded very little HCN. In the singe-stage reactor, coals No. V and No. VI had produced 30.0 and 24.4% HCN, respectively, at 1100 C (last column of Table V). Therefore, they produce only about one-third and one-half as much HCN with the first stage at 600 C while the Pittsburgh No. 8 coal (No. I) gives about 75% as much HCN at 600 C as at 1100 C. This suggests that there are considerable differences in the types of nitrogen species in these coals.

INERT PYROLYSIS OF OILS DOPED WITH MODEL COMPOUNDS

Single-stage inert pyrolysis experiments were conducted at 1100 C with two low-nitrogen-content oils that had been "doped" with benzonitrile or quinoline to bring their nitrogen contents to about 2%. The purpose was to determine if any species formed in the pyrolysis of those oils interact with the nitrogen species in some manner that affects the amount of HCN that is formed from the model compounds. Pyridine was too volatile for such experiments so the less-volatile model compounds were used.

The results of these pyrolysis experiments are listed in Table VI. Each result is based on the average of two or three experiments and it can be seen that the reproducibility was quite good. The undoped No. 6 fuel oil gave an HCN yield of 40.7%, which is slightly greater than the yield of 37.0% that was obtained in the previous study (Table I). In calculating the results of the experiments in which this oil was used, it was assumed that the conversion of fuel-N to HCN was 40.7%.

When benzonitrile was added to a No. 2 diesel fuel (also sold as No. 2 heating oil), an HCN yield of 80.6% was obtained. This is about the same as the 82% yield obtained previously from benzonitrile alone at 1100 C in the model compound apparatus. When benzonitrile was added to a No. 6 fuel oil, the HCN yield decreased by 15%, indicating a small interaction with the fuel products.

Quinoline gave the same yield of HCN, 63%, when added to either oil. The HCN yield from quinoline alone was not measured in the model compound apparatus but quinoline would be expected to give a somewhat lower yield because it forms larger amounts of carbonaceous residue (Ref. 2).

The results obtained with the doped oils under these conditions do not indicate any major interaction between the nitrogen compounds and the oil substrate. Because of differences between the molecular weights, however, some of the model compound may pyrolyze before the oil does, thereby masking a part of any interaction that does occur.

OXIDATIVE PYROLYSIS AND OXIDATION OF MODEL FUEL NITROGEN COMPOUNDS

A study was conducted of oxidative pyrolysis and oxidation of pyridine and benzonitrile. The major goal was to identify and measure the nitrogen-containing products of oxidative pyrolysis to determine what nitrogen intermediates may be important in the conversion of fuel nitrogen to NO_x in combustion. The model compound vapor was flowed continuously through the reactor and an excess of O_2 was employed so that its concentration would remain essentially constant even at complete reaction.

The experimental conditions and a schematic of the apparatus are presented in Fig. 5A and 5B, respectively. In each experiment a 3:1 O_2-He mixture was passed continuously through a quartz capillary reactor (2-mm ID) at atmospheric pressure and a flowrate of 40 cc/min (measured at room temperature). The gas entering the reactor contained 10 torr of model compound vapor in most experiments and 1 torr in others. The reactor effluent passed through a heated line (~200 C) to a 5-cc loop in a heated Carle gas sampling valve from which samples were diverted periodically to gas chromatographs, or through an aqueous bubbler system to collect the HCN or NH_3 for colorimetric analysis (Ref. 2).

Conditions for gas chromatographic analyses of the product gas stream were as follows:

Gas Constituent	Column	Temperature	Detector
Unreacted model compound and organic products	Chromosorb 103	Temperature programmed (60 to 240 C)	Flame ionization
N_2 and CO	Molecular sieve 5A	Ambient temperature	Thermal conductivity
N_2O and CO_2	Molecular sieve 5A	Isothermal 160 C	Thermal conductivity
$(CN)_2$	Poropak Q	120 C	Thermal conductivity

In addition to the gas chromatographic analyses, the amount of NO_x formed was evaluated by flowing the reactor effluent directly into a TECO chemiluminescence NO_x analyzer (with sample-flow-control capillary removed). A needle valve was placed between the reactor and the CA so that atmospheric pressure could be maintained in the reactor. NO_2 also was measured by placing Saltzman's reagent in the bubbler. However, calibration with an NO_2 in N_2 standard indicated that the amounts of NO_2 measured (by either method) may have been much less than that actually formed. Apparently, the NO_2 reacts with moisture on the walls of the system downstream of the reactor.

EFFECT OF TEMPERATURE AND CONCENTRATION ON OXIDATIVE PYROLYSIS RATES

Shown in Fig. 6 are the amounts of pyridine and benzonitrile remaining unreacted as a function of temperature. Benzonitrile is much more stable than pyridine under the conditions of oxidative pyrolysis investigated. Reducing the reactant concentrations by a factor of 10 had only a small effect on the fraction reacted at a given temperature. This is in contrast to the inert pyrolysis results (Fig. 29 of Ref. 2) where a decrease in the pyridine concentration by an order of magnitude increased the 50% decomposition temperature by 60 C. Measurements were not made with the higher concentration of benzonitrile below 720 C because a residue formed at the lower temperatures, which resulted in the eventual plugging of the system downstream of the reactor. A similar residue formed from pyridine but not to as great an extent.

PRODUCTS FROM PYRIDINE AT HIGHER CONCENTRATION

The yields of nitrogen-containing products from the oxidative pyrolysis of pyridine are plotted in Fig. 7A as a function of temperature, and the carbon product yields are shown in Fig. 7B. The unreated pyridine curve from Fig. 6 is reproduced on each of these plots for reference. The upper curves in Fig. 7A and 7B demonstrate that, within experimental error, all the nitrogen and carbon present in the pyridine is recovered in the volatile products above about 750 C. At lower temperatures, the recoveries decrease with both the nitrogen and carbon recoveries being about 80% at 720 C. This indicates that the C/N molar ratio in the nonvolatile products is about 5 as it is in pyridine itself.

At temperatures below 720 C, HCN is the major volatile nitrogen-containing product from pyridine (Fig. 7A), but NH_3 is also formed in appreciable quantities. This is in contrast to the results obtained in the previous inert pyrolysis study wherein NH_3 was formed in only very minor amounts. N_2O was found to be an appreciable oxidation product of pyridine, starting at 710 C, and the yield increased to 45% at about 770 C. Molecular nitrogen, which was not formed in the inert pyrolysis of pyridine, does not form at 710 C, but its yield increases rapidly at slightly higher temperatures (in the same region where the yields of HCN and NH_3 decrease rapidly). The yields of NO and NO_2 from pyridine, shown in the following table, were quite small under these conditions (i.e., at the higher pyridine concentration), reaching maximum values at 900 C:

Temperature, C	Yield, %	
	NO	NO_2
710	0.7	0.05
749	0.5	0.1
900	3	0.7

At 720 C, equal amounts of CO and CO_2 are formed from pyridine (Fig. 7B). As the reactor temperature is increased, the CO yield decreases rapidly while the CO_2 increases even more rapidly. It is likely that the CO_2 forms at the higher temperatures via the homogeneous oxidation of CO (i.e., through the reaction $CO + OH = CO_2 + H$). Extrapolating the high-temperature rate expression derived from the post-flame gas results of Sobolev (Ref. 6), gives the following predicted half-lives under our conditions (assuming that the mole fraction of H_2O is 0.03):

Temperature, C	550	600	650	700	750
CO Half-Life, second	0.9	0.4	0.2	0.07	0.04

The residence time of the carrier gas in the heated zone of the reactor under these conditions (1 atm, 40 cc/min, and 700 C) can be calculated from the upper curve in Fig. 28 of Ref. 2 for which the residence time was 0.6 second. Correcting the residence time for the differences in temperature, pressure, and flowrate gives 0.4 second for the present conditions. Therefore, Sobolev's rate expression predicts that one-half of the CO should oxidize homogeneously at 600 C, compared with the observed temperature of about 720 C. This is fair agreement, considering that Sobolev's rate expression was obtained in the temperature range of 1600 to 2100 C and Dryer et al. (Ref. 7) have demonstrated that the CO + OH reaction does not have a simple Arrhenius temperature dependence. Also, the H_2O concentration has not been measured in our experiments.

PRODUCTS FROM PYRIDINE AT LOWER CONCENTRATION

The NO and NO_2 percentage yields (Fig. 8) were considerably higher when the pyridine concentration in the reactor feed was lowered by an order of magnitude. No other product measurements were carried out under these conditions because the sample sizes were quite small.

PRODUCTS FROM BENZONITRILE AT HIGHER CONCENTRATIONS

The products from the oxidative pyrolysis of benzonitrile are plotted in Fig. 9A and 9B. As with pyridine, nearly all the carbon is recovered in the volatile products above 750 C. Nitrogen recovery is approximately quantitative at 750 C, but drops off to about 80% at higher temperatures. At 722 C, where only 42% of the benzonitrile reacts, the recoveries of carbon and nitrogen (based on the reacted benzonitrile only) are 43 and 49%, respectively. This indicates that the C/N ratio in the nonvolatile products, which apparently form in a 45% yield at this temperature, is the same as in benzonitrile (i.e., a molar ratio of 7), suggesting that some type of "oxidative polymerization" takes place at the lower reaction temperatures.

Comparing Fig. 7A and 9A, it can be seen that the nitrogen products from benzonitrile and pyridine are quite similar. The major differences are that with benzonitrile the N_2O yield drops off to only 15% at the higher temperatures, and NO forms in 20% yield while NO was only a minor product from pyridine (at the higher concentration being discussed in this section). By coincidence, each of the four products (HCN, NH_3, N_2O, and N_2) are produced in about 25% yield from benzonitrile at 740 C. The maximum NH_3 yield is about the same (~25%) from each of the two model compounds. However, the maximum HCN yield was only 25% from benzonitrile, compared with 40% from pyridine.

In both Fig. 7A and 9A, the N_2 yield increases abruptly from nearly zero at 720 C to about 53% at 750 C. The N_2 yield from pyridine continues to increase at higher temperatures; for benzonitrile, however, the N_2 yield decreases to 45%. Although the N_2O yield from both pyridine and benzonitrile reaches the same maximum (about 47%), the N_2O curves are quite different in shape. Benzonitrile forms no N_2O at 720 C, whereas pyridine forms about 15%. The N_2O yield from pyridene only decreases slightly from its maximum value as the temperature is increased, but the N_2O yield from benzonitrile drops to about 15% at temperatures above 800 C. For reasons that are not apparent, the total nitrogen species balance from benzonitrile also falls off at the higher temperatures, i.e., the increase in NO yield is not large enough to account for the decreased yields of N_2O and N_2.

The NO_2 yield from benzonitrile was low, reaching about 2% above 800 C. One possible explanation for the low nitrogen recovery from benzonitrile between 800 and 900 C would be that 20% or more NO_2 was actually formed, in this region, but most of it was lost before reaching the TECO CA. Some of the NO_2 calibration experiments indicate that one mode of NO_2 loss, probably reaction with moisture on the wall, results in the formation of one-half mole of NO per mole NO_2 reacted. Thus, if 40% NO_2 formed from benzonitrile at the higher temperatures and reacted in this manner, this would account for the 20% yield of NO and the 20% of nitrogen that is missing.

Comparing Fig. 7B and 9B, the CO_2 and CO yield curves are quite similar. The CO_2 first approaches its maximum at about 760 C in both cases and the CO "burns out" at only a slightly higher temperature in the pyridine experiments than in the benzonitrile experiments.

PRODUCTS FROM BENZONITRILE AT LOWER CONCENTRATION

The NO and NO_2 yields from the oxidative pyrolysis of benzonitrile at the lower concentration are plotted in Fig. 10. These results are similar to those obtained in the lower concentration pyridine experiments. It is noteworthy that of the four conditions studied (two model compounds at two concentrations) only pyridine at the higher concentration (Fig. 7A) did not produce about 20% NO at 900 C. An explanation for this is not apparent.

DISCUSSION OF MODEL COMPOUND OXIDATIVE PYROLYSIS RESULTS

It can be seen from Fig. 7A and 9A that HCN, which is a major product of inert pyrolysis, is also formed in appreciable yields in oxidative pyrolysis. Ammonia, on the other hand, is a major product of oxidative pyrolysis even though it was not important under inert pyrolysis conditions. It is not possible to establish from the available data if the change in product composition as the reactor temperature is increased results from a change in the primary products of oxidative pyrolysis or from secondary reactions of the primary products before they exit the reactor. Experiments are in progress to investigate the possible secondary reactions.

If secondary reactions are controlling the product distributions at the higher temperatures, the differences between the products from pyridine and benzonitrile must result mainly from the secondary reactions of the low-volatility products that are formed from the model compounds in the initial pyrolysis process. At temperatures below about 750 C, much of this material exits the reactor, leading to incomplete carbon and nitrogen balances and to the formation of deposits at the reactor exit and in the sampling valve. At higher temperatures, all of this low-volatility material reacts before exiting the reactor (at least in the case of pyridine) and may, therefore, affect the product distribution.

OXIDATIVE PYROLYSIS OF FUEL OILS
(SINGLE STAGE)

The planned two-stage fuel oxidative pyrolysis experiments should be the most informative because only the volatiles that form in the initial (inert) pyrolysis process will encounter an oxidative atmosphere. Preliminary oxidative pyrolysis experiments were carried out, however, with two No. 6 fuel oils under single-stage conditions where both the fuel sample and the products were in contact with an oxidative atmosphere.

The conditions were those used previously in the inert fuel pyrolysis studies, except that lower temperatures were employed and oxygen was present in the carrier gas system. It should be noted that under these single-stage conditions all the sample eventually reacts and, unlike inert pyrolysis, no residue is left in the quartz boat. The products measured include both those formed from the oxidation of the volatile portion of the oil and those formed in the heterogeneous oxidation of the char. In some of the experiments, the boat was removed from the reactor after approximately one-half of the sample had reacted to determine how much of the HCN formed in the later stages of reaction. Listed in Table VII are the nominal reaction times and yields of HCN and NH_3 obtained in the experiments in which the sample was allowed to react to completion.

Experiments in addition to those in which the products were measured were carried out to determine the time for the entire sample to react. This was done by removing the boat periodically from the heated zone for inspection. At 700 C with only O_2 flowing, the sample flared up and the light reflected in such a way that the flame was visible outside of the furnace. With 20% O_2 in helium, the time for complete reaction of a 1.3-mg sample of Oil-A increased from 8 seconds at 700 C to about 8 minutes at 500 C (Table VII). Oil-C reacted substantially slower under the same conditions. The oil samples would initially be present as a drop at one point in the boat. Shortly after the samples were heated, they flowed to cover the interior surface of the boat and then formed a char that gradually reacted.

The HCN yields increased with decreasing temperature (Table VII). The maximum yield of HCN was obtained at 500 C where the reaction rate is quite slow and the reaction is almost certainly heterogeneous. It is possible that at the higher furance temperatures, self-heating of the sample surface increases the temperatures to the point where part of the HCN formed undergoes oxidative pyrolysis. Calibration samples of HCN passed through this fuel reactor underwent only 15% reaction in 100% O_2 at 700 C. Therefore, the surface temperature of the sample would have to have been well in excess of 700 C for any HCN to have been lost once it was formed. The maximum yield of HCN from Oil-A under these oxidative conditions was 23%, while Oil-G produced only about two-thirds of this HCN yield.

Under conditions where the maximum HCN yield was obtained and the rate was the slowest, 500 C, it was found that about one-half of the HCN formed from Oil-A during the first 3-1/2 minutes of reaction and about one-half during the final 3-1/2 minutes. In a similar experiment at 600 C, 72% of the HCN formed during the first 20 seconds of reaction and 28% formed during the remaining 20 seconds of reaction.

NH_3 measurements were made only with Oil-A at 650 and 500 C (Table VII). The ammonia yields were 11.5 and 13.5%, respectively. One-microliter samples of pyridine also were passed through the fuel reactor under these conditions and the amount of NH_3 formed was measured (Table VIII). Practically no NH_3 formed below 700 C, indicating that pyridine-type fuel nitrogen compounds will not react homogeneously under these conditions. At 700 C, a 12% yield of NH_3 was obtained from pyridine, but this decreased to 2.3% when the oxygen concentration was increased. The decrease in NH_3 may result from oxidation of the NH_3 that formed before it exited the reactor. Only minor amounts of NO and NO_2 were formed under these conditions (Table VII).

The measurement of the inorganic nitrogen species formed is more difficult in the fuel oxidation experiments than when a helium atmosphere is employed. If the fuel contains sufficient sulfur, the sulfite ion formed interferes with measurement of HCN by the barbituric acid colorimetric method. It was found, however, that a reduction in the temperature of the Na_2CO_3 trapping solution to 0 C negates this interference. To measure NO by the Saltzman procedure, it must be concentrated in O_2 so that it will oxidize to NO_2. A procedure was developed in which the NO present in the product stream is trapped on a stainless-steel surface at-196 C. This procedure is satisfactory at the 2-μgm level of NO. N_2 and N_2O must be trapped out of the carrier gas stream and transferred to a helium carrier gas stream. The feasibility of a procedure involving trapping N_2 and N_2O on molecular sieve 13X at -80 and 30 C, respectively, has been established but must be tested at the μgm level.

SUMMARY AND CONCLUSIONS

The objective of this study was to investigate the types of preflame reactions that volatile fuel nitrogen species can undergo during pyrolysis and before reaching the flameout. The inert pyrolysis studies were extended to include the use of a two-stage reactor, and the oxidative pyrolysis of model fuel nitrogen compounds was studied in detail.

The single-stage inert pyrolysis of coals and No. 6 fuel oils gave HCN yields at 1100 C ranging from 24 to 44%. A liquefied coal produced 51% HCN, and the HCN yields from two hydrotreated shale oils were 60 and 70%, respectively. Based on these limited results, the nitrogen compounds in the alternate fuels appear to form HCN more readily during rapid inert pyrolysis than do typical No. 6 fuel oils. The HCN yield from a No. 6 fuel oil gave an apparent activation energy of 19 kcal/mole between 750 and 1100 C. Since this temperature coefficient results from the differences between the activation energies of three individual processes the activation energy for the overall chemical reaction that forms HCN may be much larger.

Production of HCN in the inert pyrolysis of a No. 6 fuel oil was studied in a two-stage reactor. The oil was pyrolyzed at one temperature and the volatile products formed reacted further in a second-stage that could be maintained at a different temperature. These experiments established that most or possibly all of the HCN formed in the inert pyrolysis of this fuel oil forms from secondary pyrolysis of the volatile nitrogen species. With the first-stage temperature at 750 C, for example, increasing the second-stage temperature from 750 to 1100 C increased the HCN yield from 4 to 38%.

The two-stage inert pyrolysis of three bituminus coals showed a much larger effect of first-stage temperature than was the case with the No. 6 fuel oil. Holding the second stage at 1100 C to convert as much of the volatile nitrogen species to HCN as possible, while reducing the first-stage temperature from 1100 to 600 C, resulted in decreases in the HCN yields from these three coals of one-fourth, one-half, and two-thirds, respectively. These differences may result from differences in the amount of nitrogen that remains in the residue, and suggests that there are considerable differences in the types of fuel nitrogen species in these coals.

The inert pyrolysis at 1100 C of oils doped with the model compounds benzonitrile and quinoline gave about the same HCN yields as did the neat model compounds. This indicates that there is no major interaction between the nitrogen compounds and the oil substrate under these conditions.

The oxidative pyrolysis of the model fuel nitrogen compounds pyridine and benzonitrile was investigated in a quartz flow reactor. HCN was also a major product under these conditions and NH_3, which did not form to any appreciable extent in inert pyrolysis, was a significant product of oxidative pyrolysis. Quite surprisingly, N_2O formed in a 45% yield from each of these model compounds at about 760 C. These oxidative pyrolysis results indicate that, NH_3 and N_2O in addition to HCN, may be important intermediates in the formation of fuel NO_x in combustion.

ACKNOWLEDGEMENT

This study was sponsored by the U. S. Environmental Protection Agency under Contract No. 68-02-1886, with G. Blair Martin as the Project Officer.

REFERENCES

1. Axworthy, A. E., G. R. Schneider, and V. H. Dayan, "Chemical Reactions in the Conversion of Fuel Nitrogen to NO_x, "Proceedings of the (First) Stationary Source Combustion Symposium, September 1975, Vol. I, Fundamental Research, EPA-600/2-76-152a, Rockwell International, Rocketdyne Division, Canoga Park, California, June 1976.

2. Axworthy, A. E. et al, Chemistry of Fuel Nitrogen Conversion to Nitrogen Oxides in Combustion, EPA-600/2-76-039, EPA Contract No. 68-02-0635, February 1976.

3. Axworthy, A. E., V. H. Dayan, and G. B. Martin, "Reactions of Fuel Nitrogen Compounds under Conditions of Inert Pyrolysis," FUEL (accepted for publication).

4. The results of the flat-flame burner study that is also being carried out under this program will be reported at this meeting by Dr. Daniel Kahn.

5. Pohl, J. H., and A. F. Sarofim, 16th Symposium (International) on Combustion, 1976.

6. Sobolev, G. F., Seventh Symposium (International) on Combustion, p. 386, 1958.

7. Dryer, F., D. Naegeli, and I. Glassman, Combustion and Flame, 17, 270, 1971.

TABLE I. HCN YIELDS FROM INERT PYROLYSIS OF OILS AT 1100 C[a]

Oil	% N	% S	µgm HCN per mg of oil	HCN yield, %
A. No. 6 Fuel Oil[b]	0.71		6.1	44.5 ±0.3
B. Liquefied Coal (SYNTHOIL)	1.3		12.8	51.0 ±0.3
C. Treated Shale Oil[c] (Full Boiling Range)	0.27	0.04	3.1	60.0 ±1.3
D. Treated Shale Oil[c] (Middle Distillate)	0.18	0.04	2.4	69.5 ±2.5
E. No. 6 Fuel Oil[c,f] (Mainly California Crudes)	1.41	1.6	6.31	23.2
F. Wilmington Crude Oil[d,f]	0.63	1.6	6.06	49.8
G. No. 6 Fuel Oil[b,f]	0.38	0.3	2.58	35.2
H. No. 6 Fuel Oil[e,f]	0.22	0.9	1.56	37.0

[a] Single-Stage Reactor, 40 cc/min helium carrier gas

[b] Supplied by Ultrasystems Corporation

[c] Supplied by Gulf Research and Development Company

[d] Supplied by U.S. Bureau of Mines, Laramie, Wyoming

[e] Supplied by EPA (IERL-RTP)

[f] Results from Table 17 of Ref. 2 for comparison, 20 cc/min helium flowrate

TABLE II. HCN YIELDS FROM INERT PYROLYSIS OF COALS AT 1100 C[a]

Coal		% N[b]	μgm HCN/mg	HCN yield, %
I.	Pittsburg No. 8[c]	1.2	5.5	23.6 ±1.5
II.	Montana Lignite-A (hvA-b)[d]	0.61	2.8	23.8 ±1.6
III.	Montana Coal[c]	0.93	4.8	26.8 ±0.3
IV.	COED Char[g,h]	0.99	0.3	1.7 ±0.1
V.	Bituminous Coal[e,g]	1.17	6.8	30.0
VI.	Bituminous Coal[f,g]	1.8	8.5	24.5

[a] Single-Stage Reactor, 40 cc/min helium carrier gas

[b] As-received basis

[c] Supplied by Aerotherm/Acurex

[d] Supplied by MIT

[e] Supplied by EPA (IERL-RTP)

[f] Supplied by International Flame Research Foundation

[g] Results from Ref. 2 for comparison, 20 cc/min

[h] Supplied by D. Pershing, University of Arizona

TABLE III. HCN YIELDS FROM THE TWO-STAGE PYROLYSIS OF A NO. 6 FUEL OIL[a]

(Atmospheric Pressure, Helium at 40 cc/min)

First-Stage Temperature, C	Second-Stage Temperature, C 1100	950	750
	HCN Yield, %		
1100	46.2 ±1.9	41.9 ±1.3	34.8 ±0.8
950	40.8 ±1.2	23.5 ±0.7	13.6 ±1.7
750	38.5 ±2.0	23.7 ±0.4	4.4 ±0.7

[a] Oil A in Table I.

TABLE IV. RESULTS OF TWO-STAGE INERT PYROLYSIS OF A PITTSBURGH NO. 8 SEAM COAL (1.2%-N)[a]

Temperature, C		
First Stage	Second Stage	HCN Yield, %
1108	1100	23.6 ±1.5
745	1098	22.6 ±0.3
600	1100	17.6 ±1.3
747	749	7.2 ±0.7

[a] Coal I in Table II

TABLE V. TWO-STAGE PYROLYSIS OF COALS
(Low-Temperature First Stage)

	Temperature, C		HCN Yield, %	
Coal[a]	First Stage	Second Stage	Two Stage	Single Stage[b]
I. Pittsburgh No. 8[c] (1.2%-N)	600	1100	17.6 ±1.3	23.6
V. Bituminous (1.17%-N)	598	1099	11.0 ±1.0	30.0
VI. Bituminous (1.8%-N)	600	1098	12.7 ±0.7	24.5
IV. COED Char (0.99%-N)	604	1097	1.8	1.7

[a] See Table II

[b] From Table II for comparison

[c] From Table IV for comparison

TABLE VI. INERT PYROLYSIS OF DOPED OILS AT 1100 C

(Single Stage, 20 cc/min Helium)

Oil	Additive (% by weight)	% Fuel-N	% Additive-N	% Additive-N to HCN
No. 6 Fuel Oil-H[c]	None	0.22	--	40.7 ±0.2[a]
No. 2 Diesel	Benzonitrile (12.74%)	0.03	1.73	80.6 ±1.1[b]
No. 6 Fuel Oil-H	Benzonitrile (15.34%)	0.22	2.08	68.7 ±1.2[b]
No. 2 Diesel	Quinoline (19.29%)	0.03	2.09	63.0 ±0.6[b]
No. 6 Fuel Oil-H	Quinoline (19.03%)	0.22	2.06	63.2 ±0.4[b]

[a] Yield of HCN from Fuel-N (no additive in this oil sample)

[b] Assuming Fuel-N gives 40.7% yield of HCN

[c] See Table I

TABLE VII. FUEL OIL OXIDATIVE PYROLYSIS - RESULTS

(Single Stage, 1 atm, 40 cc/min)

	No. 6 Fuel Oil-A[a] (0.71% N)			No. 6 Fuel Oil-G[a] (0.38% N)		Pyridine (17.7% N)
		Yield, %				
Condition	Reaction Time[b]	HCN	NH_3	Reaction Time[b]	HCN Yield, %	NH_3 Yield, %
700 C, 100% O_2	1 second	6.0 10.6 7.2				2.3
700 C, 20% O_2	8 seconds	6.2 3.9		12 seconds		12.1
650 C, 20% O_2	16 seconds	10.0	11.2 12.1			0.45
600 C, 20% O_2	40 seconds	12.1 12.4		75 seconds	7.1 7.4	
500 C, 20% O_2	7 to 8 minutes	23.4 22.7 23.9	13.2 14.2	12 minutes	16.7 15.9	0.14

[a] See Table I

[b] For 1.3 mg sample

[c] The yields of NO and NO_2 were less than 1 and 5%, respectively, at these conditions

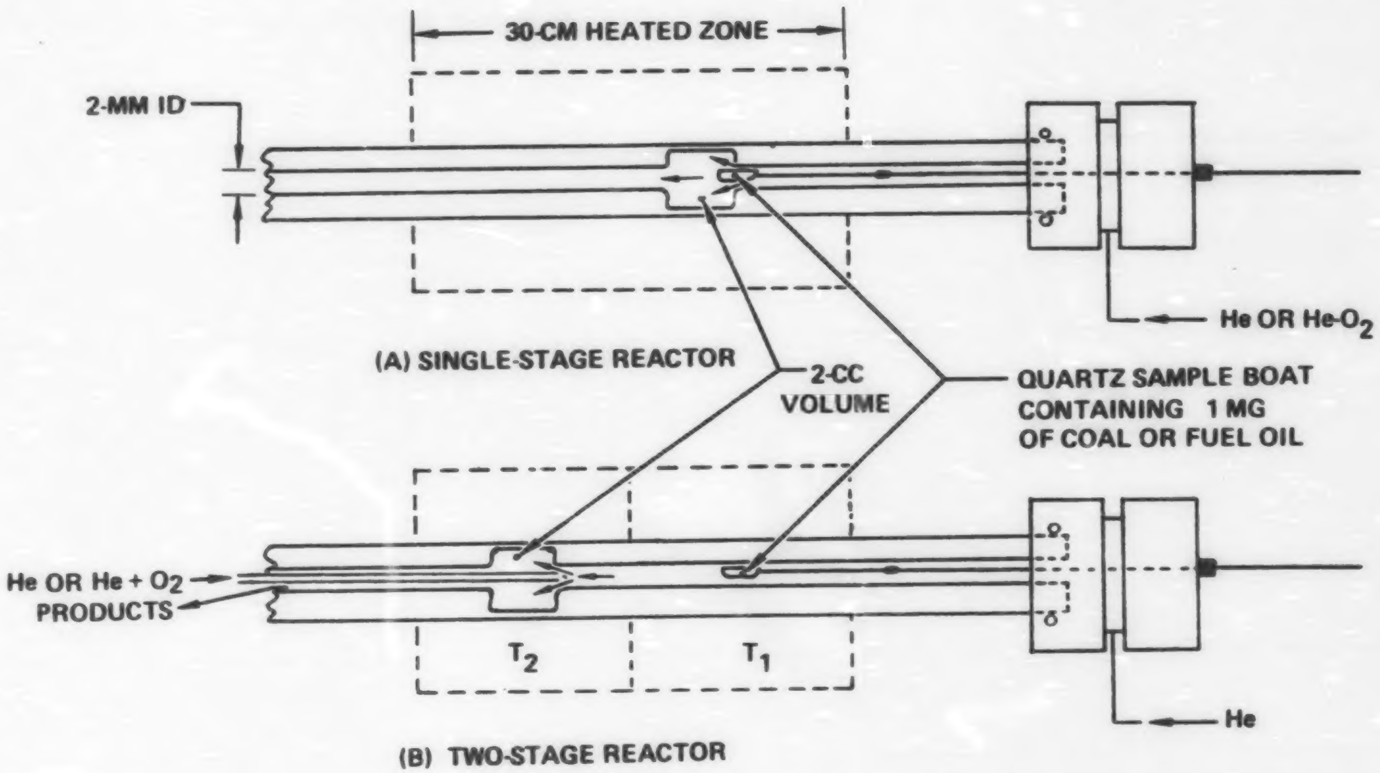
30-CM HEATED ZONE
2-MM ID
He OR He-O_2
(A) SINGLE-STAGE REACTOR
2-CC VOLUME
QUARTZ SAMPLE BOAT CONTAINING 1 MG OF COAL OR FUEL OIL
He OR He + O_2
PRODUCTS
T_2
T_1
He
(B) TWO-STAGE REACTOR

Figure 1. Quartz Fuel Pyrolysis Apparatus (Vertical Scale is Greatly Expanded for Clarity)

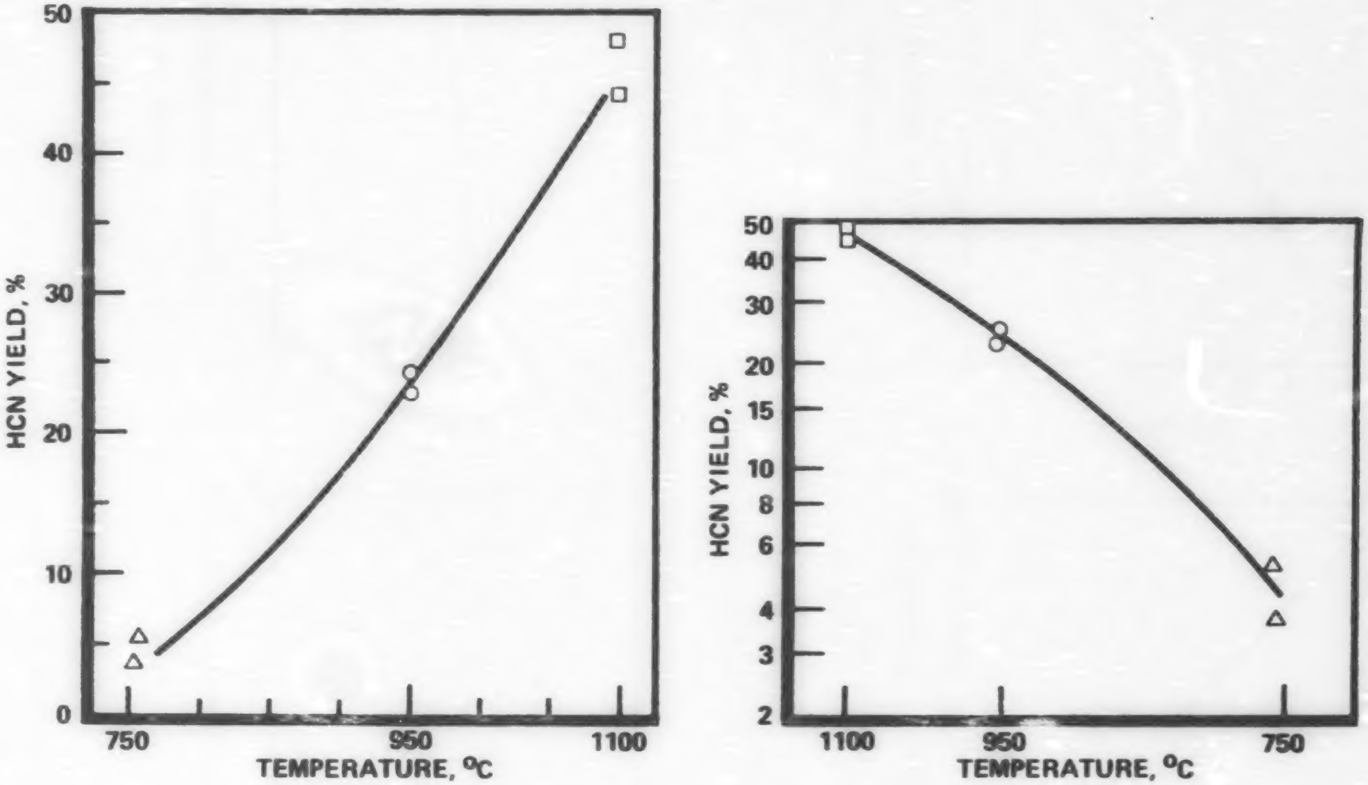

A. LINEAR PLOT

B. ARRHENIUS PLOT

Figure 2. HCN Yield vs Temperature in Single-Stage Inert Pyrolysis of a No. 6 Fuel Oil

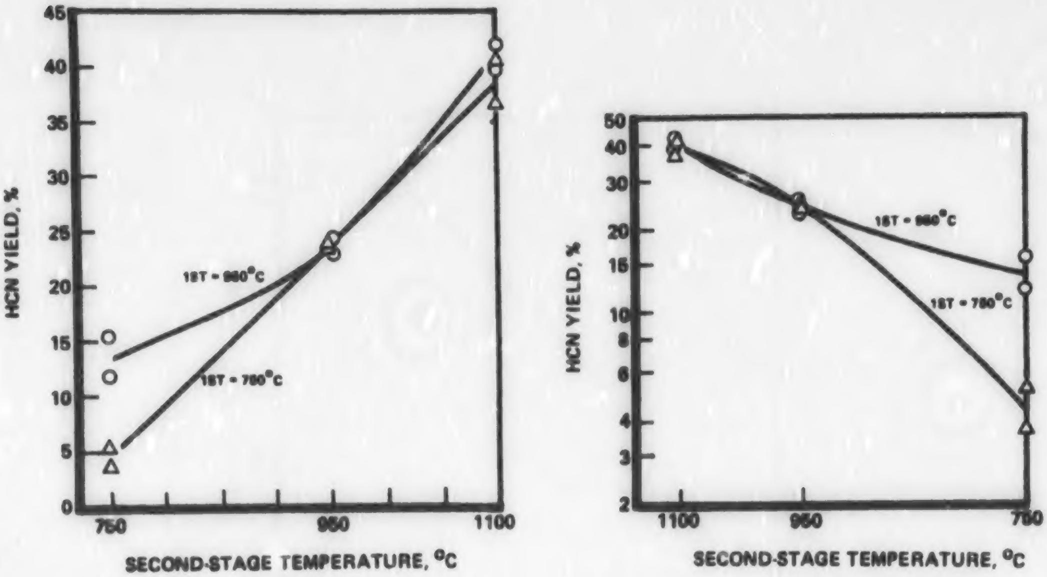

A. LINEAR PLOT

B. ARRHENIUS PLOT

Figure 3. Two-Stage Inert Pyrolysis of a No. 6 Fuel Oil

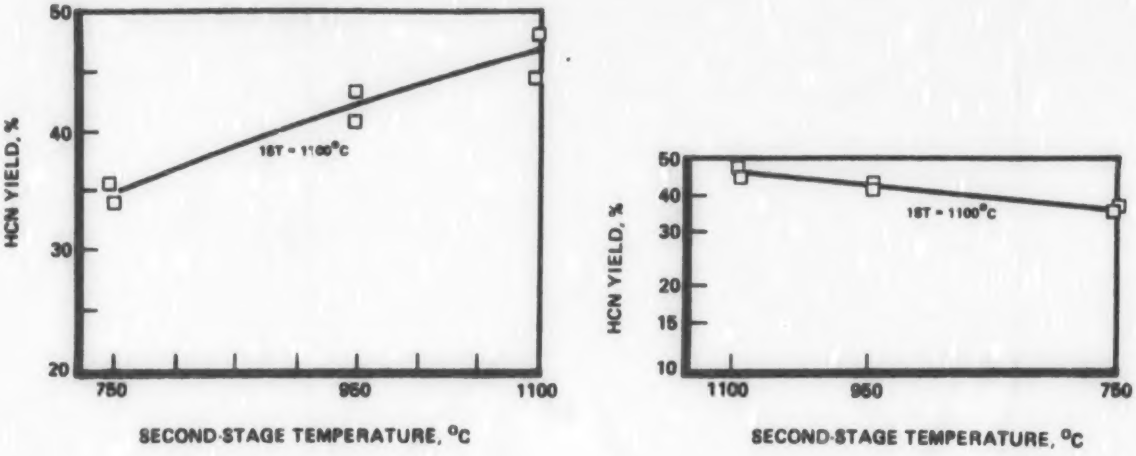

A. LINEAR PLOT

B. ARRHENIUS PLOT

Figure 4. Two-Stage Inert Pyrolysis of a No. 6 Fuel Oil
With First Stage at 1100 C

- 2-MM ID QUARTZ REACTOR
- 40 CC/MIN OF 75% O_2 - 25% He CARRIER GAS
- ATMOSPHERIC PRESSURE
- CONTINUOUS FLOW OF SAMPLE VAPOR
  - 1.4 MOLE PERCENT IN MOST EXPERIMENTS
  - 0.14 MOLE PERCENT IN SOME
- MEASURED UNREACTED COMPOUND, ORGANIC PRODUCTS, HCN, NH_3, NO, NO_2, N_2O, CO, CO_2, AND $(CN)_2$

A. CONDITIONS

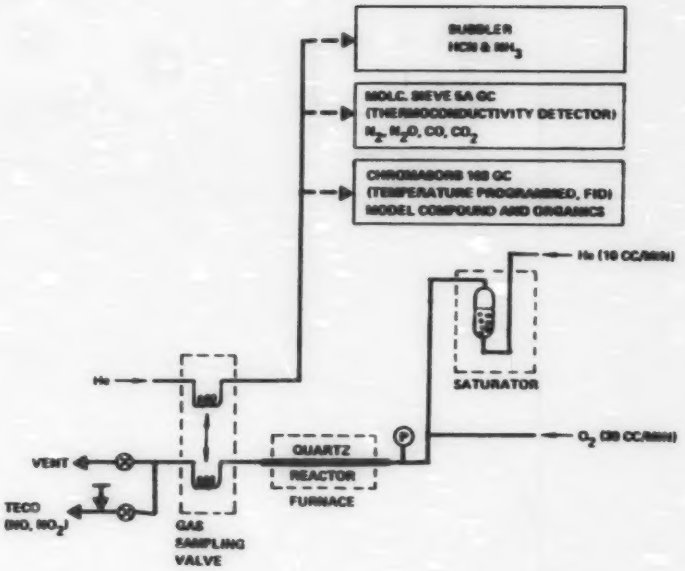
BUBBLER
HCN & NH_3
MOLC. SIEVE 5A GC
(THERMOCONDUCTIVITY DETECTOR)
N_2, N_2O, CO, CO_2
CHROMASORB 103 GC
(TEMPERATURE PROGRAMMED, FID)
MODEL COMPOUND AND ORGANICS
He (10 CC/MIN)
SATURATOR
He
P
O_2 (30 CC/MIN)
QUARTZ
REACTOR
FURNACE
VENT
TECO
(NO, NO_2)
GAS
SAMPLING
VALVE

B. APPARATUS

Figure 5. Model Compound Oxidative Pyrolysis

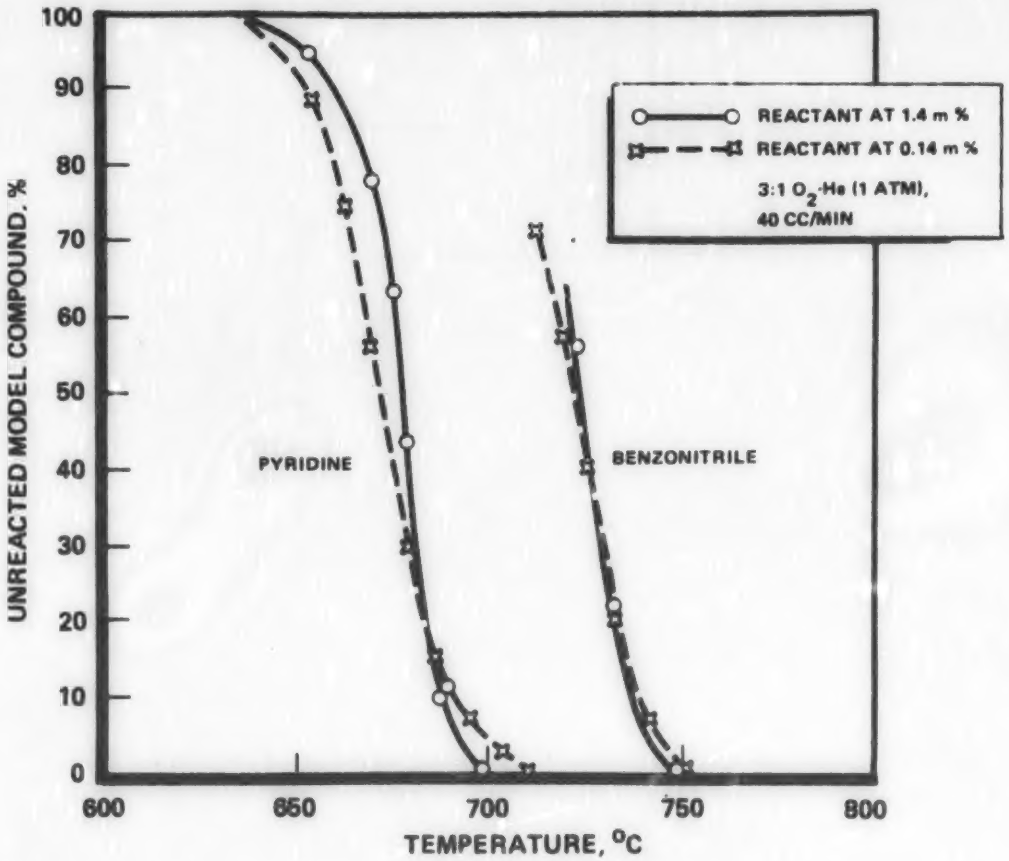

Figure 6. Extent of Reaction as a Function of Temperature and Model Compound Concentration

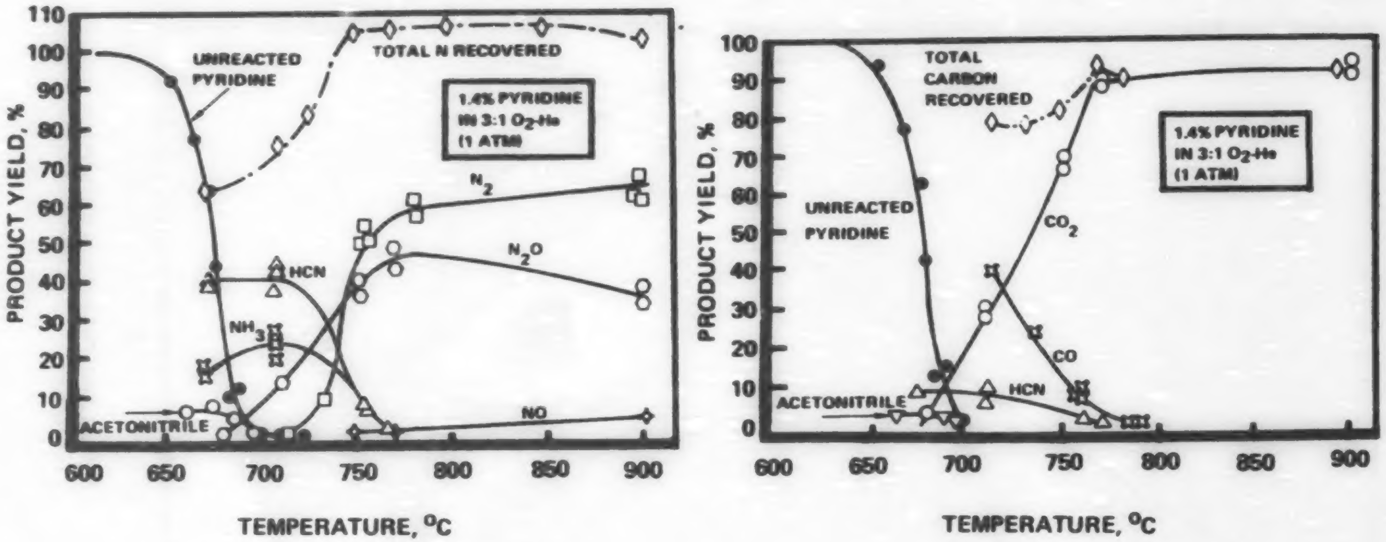

A. NITROGEN-CONTAINING PRODUCTS

B. CARBON-CONTAINING PRODUCTS

Figure 7. Products From Oxidative Pyrolysis of Pyridine
(Yields Based on Reacted Pyridine)

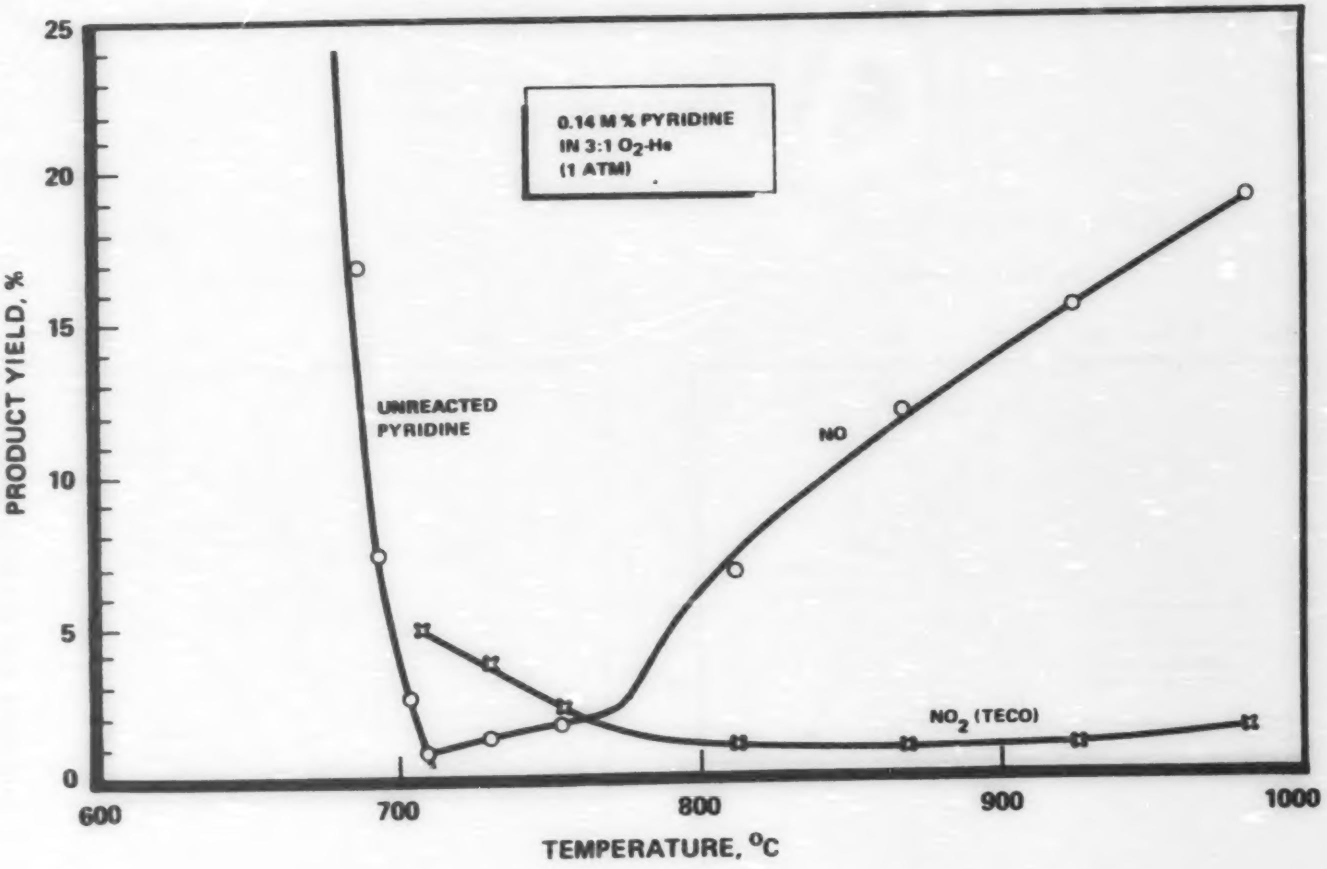

Figure 8. NO and NO_2 Yields From Pyridine (Lower Concentration Experiments)

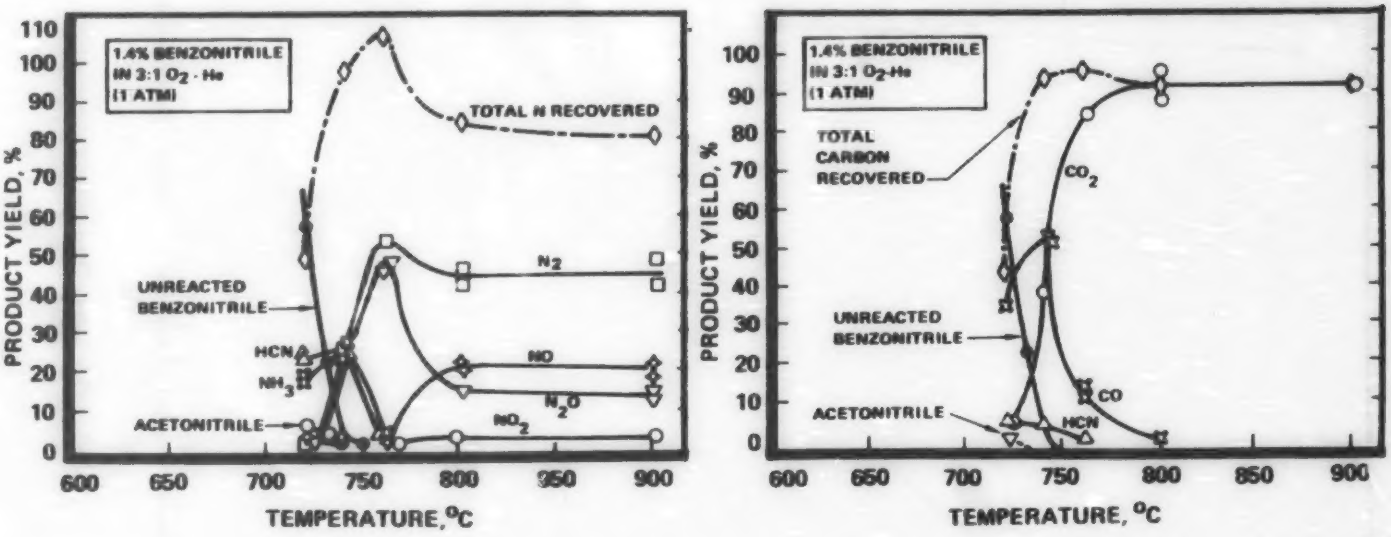

A. NITROGEN-CONTAINING PRODUCTS

B. CARBON-CONTAINING PRODUCTS

Figure 9. Products From Oxidative Pyrolysis of Benzonitrile
(Yields Based on Reacted Benzonitrile)

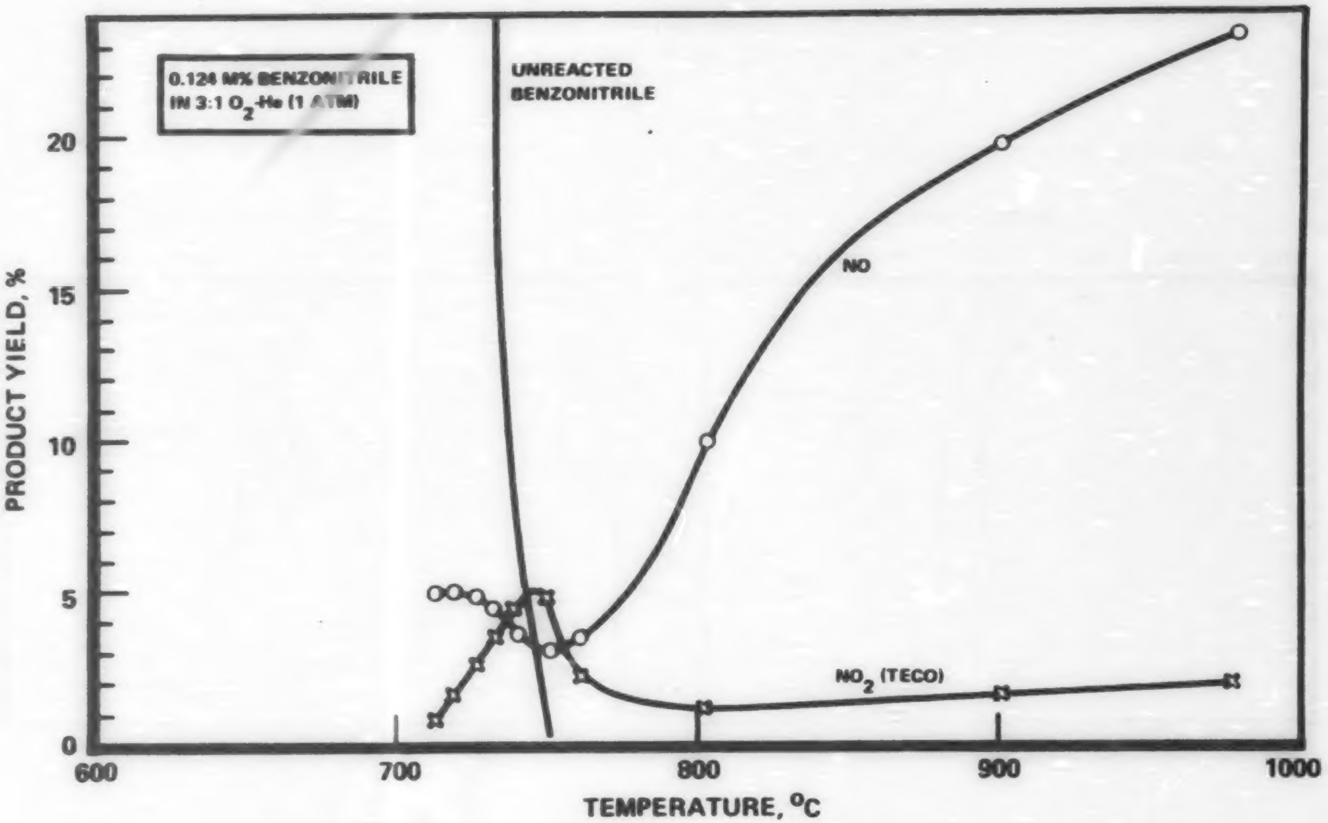

Figure 10. NO and NO_2 Yields From Benzonitrile (Lower Concentration Experiments)

FATE OF FUEL NITROGEN DURING PYROLYSIS AND OXIDATION

By:

Y. H. Song, J. M. Beer and A. F. Sarofim
Massachusetts Institute of Technology
Cambridge, Massachusetts 02139

SUMMARY

Regulation of nitric oxide emissions by modification of coal combustion processes requires a better understanding of the mechanism of fuel nitrogen conversion to nitrogen oxides. To this end, the fate of coal nitrogen in both inert and oxidizing atmospheres has been studied in a laboratory furnace at temperature levels and for time intervals of interest in pulverized coal combustors.

Data on the overall conversion of coal-nitrogen into nitrogen oxides obtained at several different temperatures are reported. Oxidation experiments were carried out with both coal and char to enable the respective contributions of coal volatiles and char to the emissions of nitrogen oxides to be determined. The char used in the oxidation studies was prepared by pyrolysis of coal at the temperature and residence time of the corresponding oxidation experiments. The conversion to nitric oxide of char-nitrogen was lower than that of coal-nitrogen. The yields of nitric oxide from both coal- and char-oxidation were found to decrease monotonically with increasing fuel/oxygen ratios. Results also show that the conversion of fuel nitrogen to nitrogen oxides decreases slightly with increasing temperature.

Rates of oxidation of char and char nitrogen were determined at temperatures of 1250 to 1750 K and oxygen partial pressures of 0.2 and 0.4 atmosphere. The char in these latter studies was produced by pyrolyzing coal particles at 1750 K during a residence time of one second. The variation of nitrogen/carbon ratio of the char samples with time suggests that oxidation and pyrolysis of the char nitrogen occur simultaneously.

Preceding page blank

INTRODUCTION

In staged combustion, the conversion of fuel nitrogen to nitrogen oxides is reduced by delaying the addition of the oxygen required to complete the combustion until after the fuel nitrogen has reacted (1,2). In this manner the fuel nitrogen oxidation occurs under fuel rich conditions which favor the formation molecular nitrogen. For coal the problem is complicated by the fact that the release of fuel nitrogen is relatively slow and is a strong function of temperature (3,4). In order to provide an understanding of the effect of this slow release of fuel nitrogen on nitric oxide emissions from coal combustors and to guide the further developments of control strategies, the fate of coal nitrogen during pyrolysis and oxidation has been studied under well controlled conditions in a laboratory furnace. The study has included the determination of the effect of fuel/air equivalence ratio and temperature on nitric oxide emissions under simulated combustion conditions, the identification of the contributions of the char and volatiles to the total emission, and time-resolved measurements of coal pyrolysis and char oxidation in order to provide data on the kinetics of these processes.

Results on the pyrolysis kinetics and some of the oxidation experiments have been reported previously (4,5,6). In this paper, data on the effect of temperature on the contribution of volatiles and char to NO_x emission and on the rate of oxidation of char nitrogen are presented.

EXPERIMENTAL

A schematic of the experimental apparatus is shown in Fig. 1. It consists of an Astro Model 1000A electrically heated furnace with an alumina muffle tube. A preheated inert or oxidizing gas stream is fed to the working section of the furnace through a honeycomb straightener. The coal or char is injected along

Preceding page blank

the axis, and the products are withdrawn through a water-cooled probe the position of which could be suitably adjusted to vary residence time. The reactions are quenched by injection of argon at the mouth of the probe and the solid products are collected in a sintered bronze filter. The equipment can also be operated in a "free-fall" mode where the probe is removed and a water-cooled section added to the bottom of the furnace. In this mode of operation, particles are allowed to fall through the cooled section onto a bronze disk collector at the bottom of the furnace. For the production of char for use in oxidation experiments, a minor modification is made to the free-fall mode of operation to permit the collection of the char in a flask. The maximum residence time in the hot zone of the furnace is about one second. Details of the apparatus are provided in Refs. 4 and 7.

The properties of the coals and chars used are summarized in Table I.

RESULTS

1. Conversion of Coal Nitrogen to Nitric Oxide

The percentages of the nitrogen in a Montana lignite that are converted to nitric oxide for a hot zone residence time of one second as a function of fuel/air ratio are shown in Figs. 2 and 3 for furnace temperatures of 1250 K and 1750 K, respectively. The coal particles used have a nominal size of 38 to 44 microns. Also shown at the top of the figures are the total solid weight loss (on a dry-ash-free basis) and, in the middle, the fraction of the original coal nitrogen retained by any unburned char. Oxidation experiments were also carried out on char in order to identify the separate contributions to the nitric oxide emissions of the volatiles and char. The char used in the oxidation studies was prepared by pyrolysis of the coal at the temperature and residence time corresponding to those of the oxidation experiments. Results of char-nitrogen conversions at 1250 K and 1750 K are presented in Figs. 4 and 5. As can be seen from Figs. 2 to 5, the conversion to nitric oxide of char-nitrogen was lower than the corresponding values for coal-nitrogen while both coal- and char-nitrogen conversion to nitric oxide were found to decrease monotonically with increasing fuel/oxygen equivalence ratios. In both cases of coal and char oxidations, the percentages of solid weight loss decreased and the percentages of the nitrogen retained in the unburned char increased as the equivalence ratio increased. The effect of temperature on fuel nitrogen oxidation is small and the effect may be masked by day-to-day variations in operating conditions. In order to critically test the effect of temperature on the conversion of coal-nitrogen to nitric oxide, a series of experiments were conducted in which the fuel/oxygen ratios were fixed and the furnace temperature was varied. The data in Fig. 6 were obtained for a Montana sub-bituminous coal in this manner. The nitric oxide yields were essentially the same at 1250 K and 1500 K while they decreased by about 20 to 25 percent as the temperature was increased from 1500 to 1750 K. This is consistent with results shown in Figs. 2 and 3. Comparison of the data in Fig. 6 with those in Figs. 2 and 3 show very little differences even though differenc coals are involved. This is consistent with the findings of Pershing (8) and results previously obtained in this laboratory.

2. Kinetics of Char Oxidation

Time-resolved measurements of char-nitrogen oxidation were made by the rapid quenching of samples taken at different distances from the char injector. The char in these latter studies was produced by pyrolyzing lignite particles at 1750 K for a residence time of one second. The char produced was then size-graded to select particles in the 38 to 44 micron size range for further oxidation experiments. Oxidation experiments were carried out at temperatures of 1250 K, 1500 K, and 1750 K, and oxygen partial pressures of 0.2 atm and 0.4 atm. The weight loss of char particles as a function of distance between the feeder and the collector is presented in Fig. 7. Selected char samples were sent to Galbraith Laboratory, Inc. of Knoxville, Tennessee for elemental analyses. The variation of nitrogen/carbon ratio, expressed in terms of the percentage of the original N/C ratio in the char, is presented as a function of distance from the feeder in Fig. 8. The nitrogen/carbon ratios were found to decrease with increasing temperatures and/or with decreasing oxygen partial pressures. At high oxygen pressures and low temperatures, the nitrogen/carbon ratio remains constant at its initial value.

DISCUSSION

1. Conversion of Coal Nitrogen to Nitric Oxide

A simplified scheme that represents the fate of the fuel nitrogen during combustion of coal has been suggested previously(4,5,6), and is summarized below:

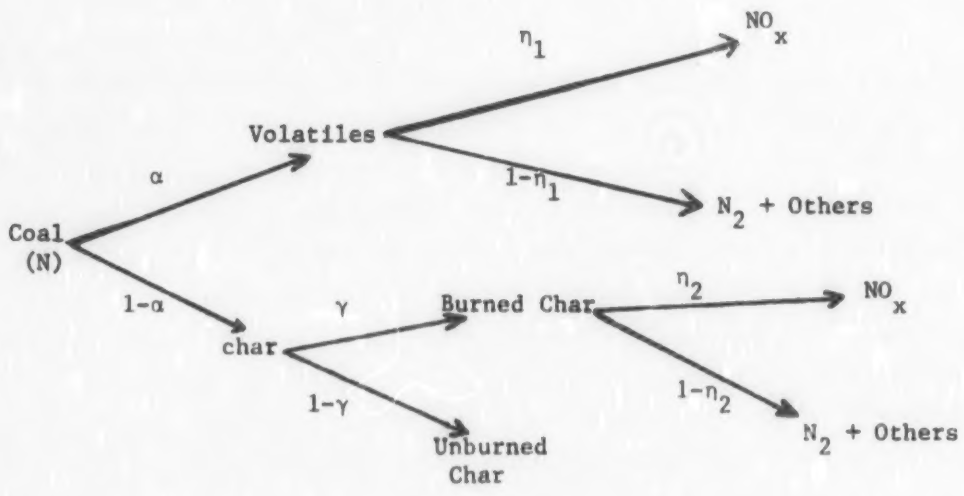

By a first order approximation which assumes that the volatile-nitrogen conversion to nitric oxide and char-nitrogen conversion are independent, the overall conversion η^* of coal-nitrogen to nitric oxide

$$\underset{\substack{\text{overall}\\ \text{conversion}\\ \text{to NO}_x}}{\eta^*} = \underset{\substack{\text{volatile}\\ \text{contri-}\\ \text{bution}}}{\alpha\eta_1} + \underset{\substack{\text{char}\\ \text{contribution}}}{(1-\alpha)\,\gamma\eta_2}$$

where

α = fraction of the coal-N that is released as volatiles

$1-\alpha$ = fraction of the coal-N that is retained in the char

γ = fraction of the char-N that is consumed

$\gamma\eta_2$ = fraction of the char-N that is converted to NO_x

η_1 = fraction of the volatile-N that is converted to NO_x

The values of $1-\alpha$ have been found to be 0.75 at a temperature of 1250 K and 0.27 at 1750 K, in good agreement with the values previously reported by Pohl (4,6). The values of η^* are reported as functions of fuel/oxygen equivalence ratio in Figs. 2 and 3 and the values of $\gamma\eta_2$ in Figs. 4 and 5. The values of η_1, the volatile-nitrogen conversion efficiency, and $\frac{\alpha\eta_1}{\eta^*}$, the percentage of the volatile-nitrogen contribution to nitric oxide, can now be derived from the above information. The results of this derivation for temperatures of 1750 K and 1250 K, are shown in Fig. 9. The efficiency of conversion to nitric oxide of volatile nitrogen and the contribution to the total emissions of the volatile nitrogen were found to decrease monotonically with increasing fuel equivalence ratios. As expected, the contribution to nitric oxide by the volatiles increases with temperature. The conversion to nitric oxide of the volatile nitrogen, however, decreases with increasing temperature. These two effects tend to compensate and partially explain the small dependence on temperature of the conversion of coal nitrogen. In this study, a small net decrease is observed. In a separate study, Pershing (8) has found practically no effect of temperature on the conversion of fuel nitrogen to nitric oxide. The present results suggest that it is optimal to operate the first stage of a combustor at high temperatures since this will favor the completion of the devolatilization under fuel-rich conditions.

2. Kinetics of Char Oxidation

Figs. 2 and 3 demonstrate that with increasing fuel equivalence ratios, the percent conversion of coal nitrogen to nitric oxide decreases. Under the same fuel-rich conditions, however, an increasing amount of the coal nitrogen may escape the first stage of the combustor with the unburned char. The main objective of the study of the kinetics of oxidation of char was to establish the residence time requirements for completing the combustion of the char and to determine the fate of the char-nitrogen during oxidation. The data in Figs. 7 and 8 are plotted as a function of distance. For determining kinetic parameters, residence time measurements are necessary. Such measurements were made by Kobayashi (7), who used essentially the same system and showed that the average particle velocity may be approximated by 1.4 times the average main gas velocity. For the interpretation of results of the present study, distances were converted to residence times, using Kobayashi's approximation. The results with times reported in milliseconds are summarized below:

Temperature, K \ Distance, inch	3	4	5	6	7
1250	256	340	427	512	599
1500	213	283	356	426	500
1750	183	243	305	365	428

It has been previously shown (4) that during coal pyrolysis the carbon loss appears to become asymptotic at times exceeding 100 milliseonds at 1750 K, the temperature used to produce the char in this study, but that nitrogn release continues for longer times. The rationalization of the results was that while carbon is present in relatively stable compounds in the char, no comparable stabilized nitrogen structures are formed; consequently, char-nitrogen continues to be released until it is completely eliminated from char. Therefore, when a char particle is oxidized, the nitrogen loss will be due to both devolatilization and oxidation, but the carbon loss will be exclusively due to oxidation.

Assuming the fuel nitrogen is uniformly distributed throughout the char, the oxidation rate of the nitrogen should therefore equal the product of the oxidation rate of the carbon and the mole ratio of the fuel nitrogen to carbon in the char (9). Since the pyrolysis loss and oxidation loss of char-nitrogen are additive, the consumption rate of char-nitrogen can be written as

$$\left\{\begin{array}{l}\text{total consumption-rate}\\ \text{of char-nitrogen}\end{array}\right\} = \left(\begin{array}{l}\text{consumption-rate of}\\ \text{char-nitrogen due}\\ \text{to pyrolysis}\end{array}\right) + \left(\begin{array}{l}\text{consumption-rate of}\\ \text{char-nitrogen due}\\ \text{to oxidation}\end{array}\right)$$

or

$$\frac{dN}{dt} = \left(\frac{\partial N}{\partial t}\right)_{\text{pyrolysis}} + \left(\frac{\partial N}{\partial t}\right)_{\text{oxidation}}$$

since

$$\frac{dC}{dt} = \left(\frac{dC}{dt}\right)_{\text{oxidation}}$$

therefore,

$$\frac{dN}{dt} = \left(\frac{\partial N}{\partial t}\right)_{\text{pyrolysis}} + \left(\frac{dC}{dt}\right)_{\text{oxidation}} \cdot \left(\frac{N}{C}\right)_{\text{following pyrolysis}}$$

This model indicates that for low oxygen pressure and high temperature char oxidation, the nitrogen to carbon ratio in the char will decrease as a function of reaction time. As the oxygen pressure increases and temperature decreases, the oxidation process tends to compensate the depreciation of nitrogen/carbon ratio due to pyrolysis and keeps this ratio more or less constant during the course of the combustion process. The experimental findings support this conclusion. The data will be used to derive kinetic parameters for the oxidation and pyrolysis of the char nitrogen. The experiments were carried out with large excess of oxygen so as to maintain a constant oxygen partial pressure and thus facilitate interpretation of the results. The basic kinetic parameters derived from the data can then be used to analyze char burnout under the varying oxygen concentrations that will be encountered in practical combustors.

CONCLUSIONS

The data on coal and char oxidation show that the devolatilized nitrogen compounds account for the major fraction of the nitric oxide produced from coal nitrogen at high temperatures and low fuel/air ratios, but that the char nitrogen contribution cannot be neglected. Increasing temperature increases the volatile contribution but decreases the efficiency with which it is converted to NO_x. For the combustor in this study, there is a net decrease in emissions with increases in temperature above 1500 K, suggesting that NO_x emissions can be reduced by increases in both the temperature and the fuel/air ratio in the first stage of a staged combustor. Oxidation experiments on chars support the view that there is no selectivity between nitrogen and carbon loss during oxidation but that the char nitrogen may undergo pyrolysis in parallel with the oxidation. The time-resolved measurements may be used to infer kinetic data needed to size the first stage of a staged combustor.

ACKNOWLEDGEMENT

The authors wish to thank Dr. John H. Pohl and Dr. Joel M. Levy for valuable discussions, and Mr. Gerald Mandel and Mr. Anthony J. Modestino for their technical assistance. The work was supported by the EPA under grant number R-803242.

REFERENCES

1. Pershing, D.W., Martin, G.B. and Berkau, E.E., Influence of Design Variables on the Production of Thermal and Fuel NO from Residual Oil and Coal Combustion, A.I.Ch.E. Symposium Series No. 148, 71 (1975).
2. Armento, W.J. and Sage, W.L., Effect of Design and Operation Variables on NO_x Formation in Coal Fired Furnaces: Status Report, A.I.Ch.E. Symposium Series No. 148, 71 (1975).
3. Axworthy, A.E., Chemistry and Kinetics of Fuel Nitrogen Conversion to Nitric Oxide, A.I.Ch.E. Symposium Series No. 148, 71 (1975).
4. Pohl, J.H., Fate of Coal Nitrogen, Sc.D. Thesis, M.I.T. (1976).
5. Pohl, J.H. and Sarofim, A.F., Fate of Coal Nitrogen During Pyrolysis and Oxidation, paper presented at EPA Symposium on Stationary Source Combustion, Atlanta, GA (1975).
6. Pohl, J.H. and Sarofim, A.F., Devolatilization and Oxidation of Coal Nitrogen, paper presented at Sixteenth International Symposium on Combustion, Cambridge, Mass. (1976).
7. Kobayashi, H., Devolatilization of Pulverized Coal, Ph.D. Thesis, M.I.T. (1976).
8. Pershing, D.W., Nitrogen Oxide Formation in Pulverized Coal Flames, Ph.D. Thesis, University of Arizona (1976).
9. Wendt, J.O.L. and Schulze, O.E., On the Fate of Fuel Nitrogen During Coal Char Combustion, A.I.Ch.E. Journal, 22, 102 (1976).

TABLE I. CHARACTERIZATION OF COALS AND CHARS

		Proximate Analysis A.R. Wt%			Ultimate Analysis A.R. Wt%				
Type	Specification	VM	H_2O	Ash	C	H	N	S	O (by Diff.)
Montana Lignite-A	Savage	36.20	13.60	7.80	54.40	4.96	0.88	0.84	17.42
Montana Sub-bituminous**	Powder River Region	35.16	21.23	9.34	53.26	3.35	0.87	0.78	11.17
1250 K Lignite Char		NM*	4.20	12.08	66.94	2.09	1.02	0.56	13.11
1750 K Lignite Char		NM	2.02	18.03	76.42	0.69	0.55	1.06	1.23
1750 K Lignite Char***		NM	2.10	19.00	76.11	0.36	0.58	1.11	0.74

*NM = Not Measured

**Supplied by Aerotherm Division of Acurex Corporation

***Used in time resolved measurements.

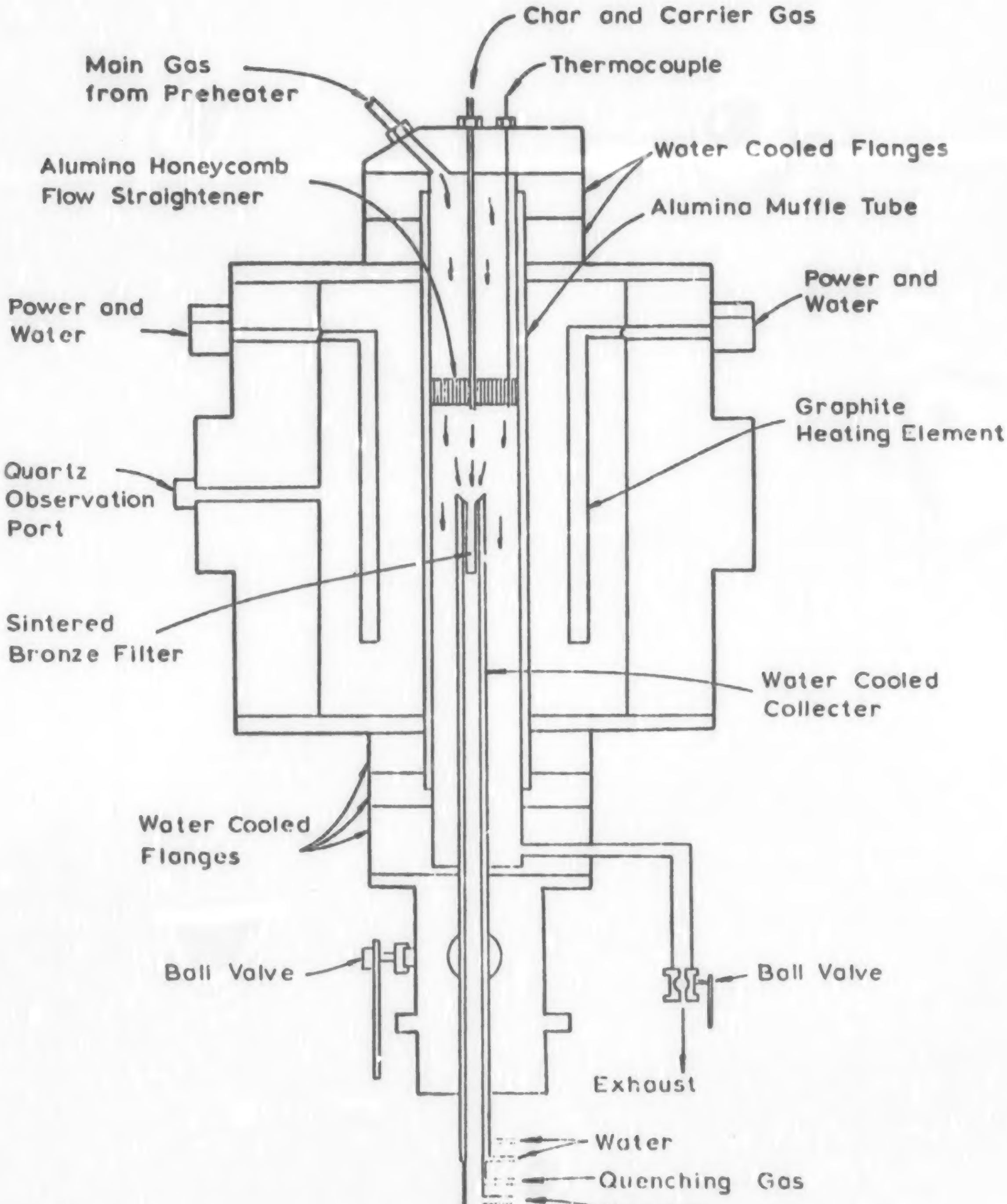
Char and Carrier Gas
Main Gas from Preheater
Thermocouple
Water Cooled Flanges
Alumina Honeycomb Flow Straightener
Alumina Muffle Tube
Power and Water
Power and Water
Graphite Heating Element
Quartz Observation Port
Sintered Bronze Filter
Water Cooled Collecter
Water Cooled Flanges
Ball Valve
Ball Valve
Exhaust
Water
Quenching Gas
Vacuum

Figure 1. Schematic of Experimental Furnace

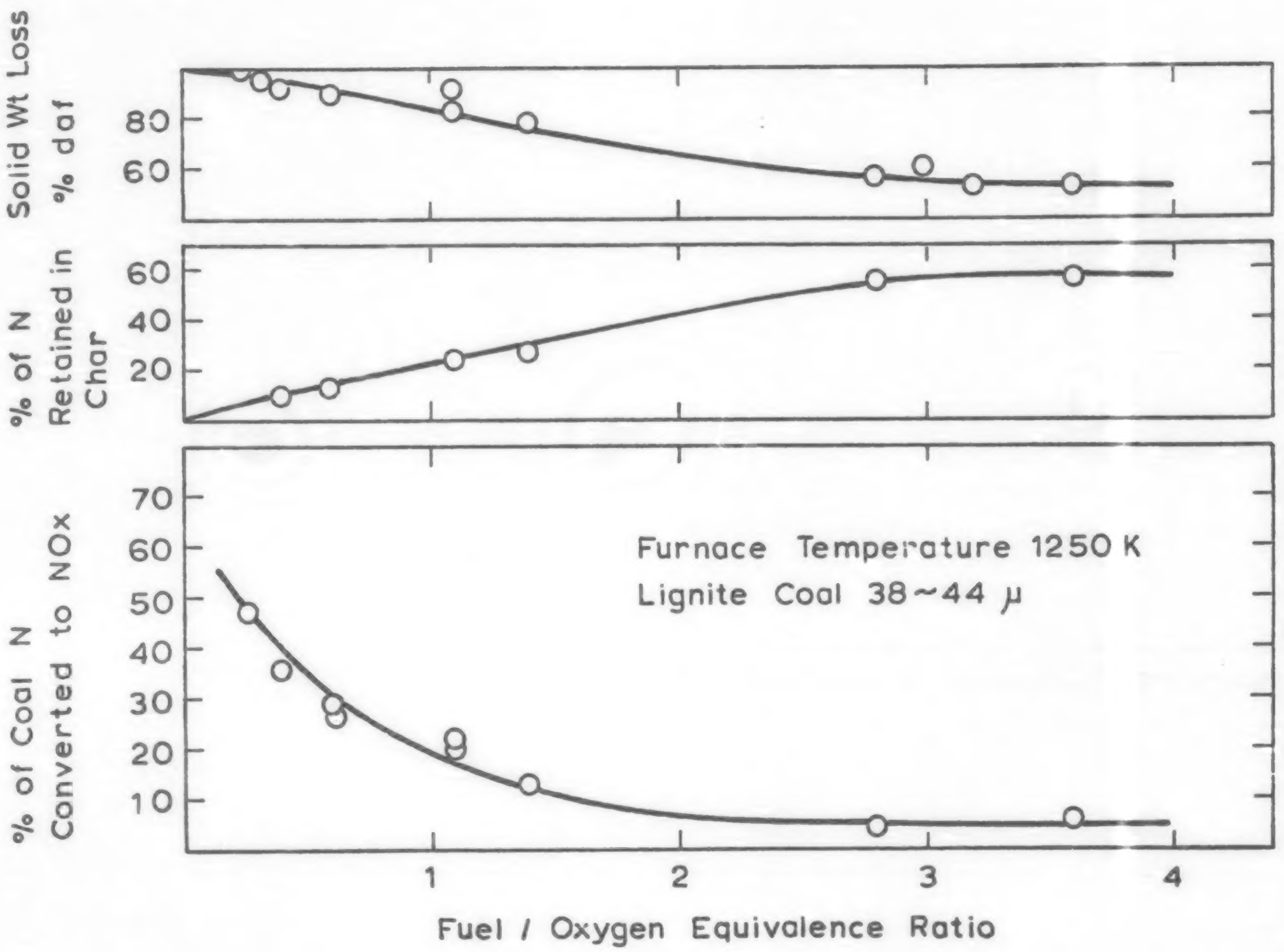

Figure 2. Fate of Fuel Nitrogen During Oxidation: Conversion to Nitric Oxide (Bottom), Retention by Unburned Char (Middle), and Combustion Efficiency Defined by Solid Weight Loss (Top). Montana Lignite at 1250 K.

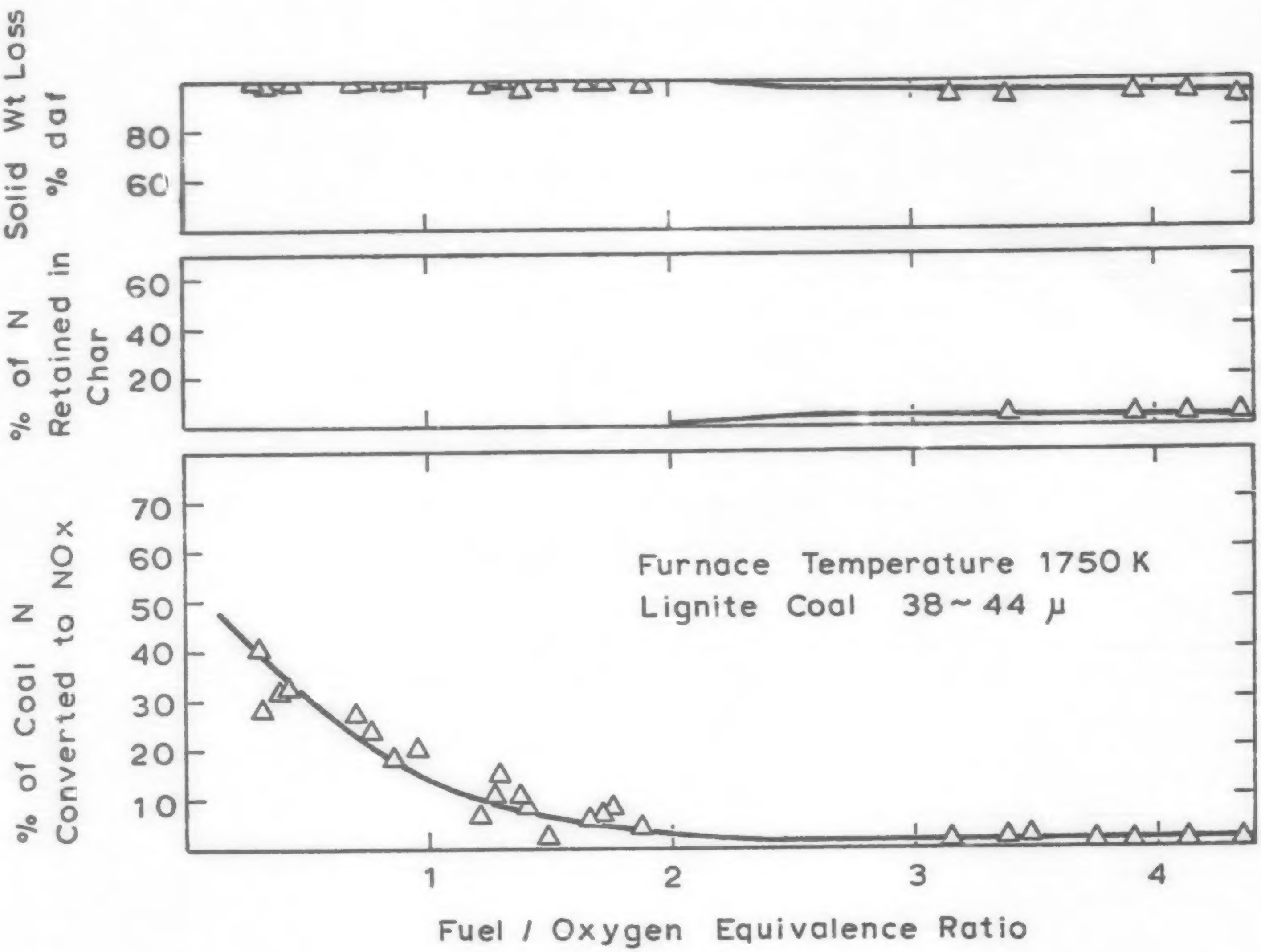

Figure 3. Fate of Fuel Nitrogen During Oxidation: Conversion to Nitric Oxide (Bottom), Retention by Unburned Char (Middle), and Combustion Efficiency Defined by Solid Weight Loss (Top). Montana Lignite at 1750 K.

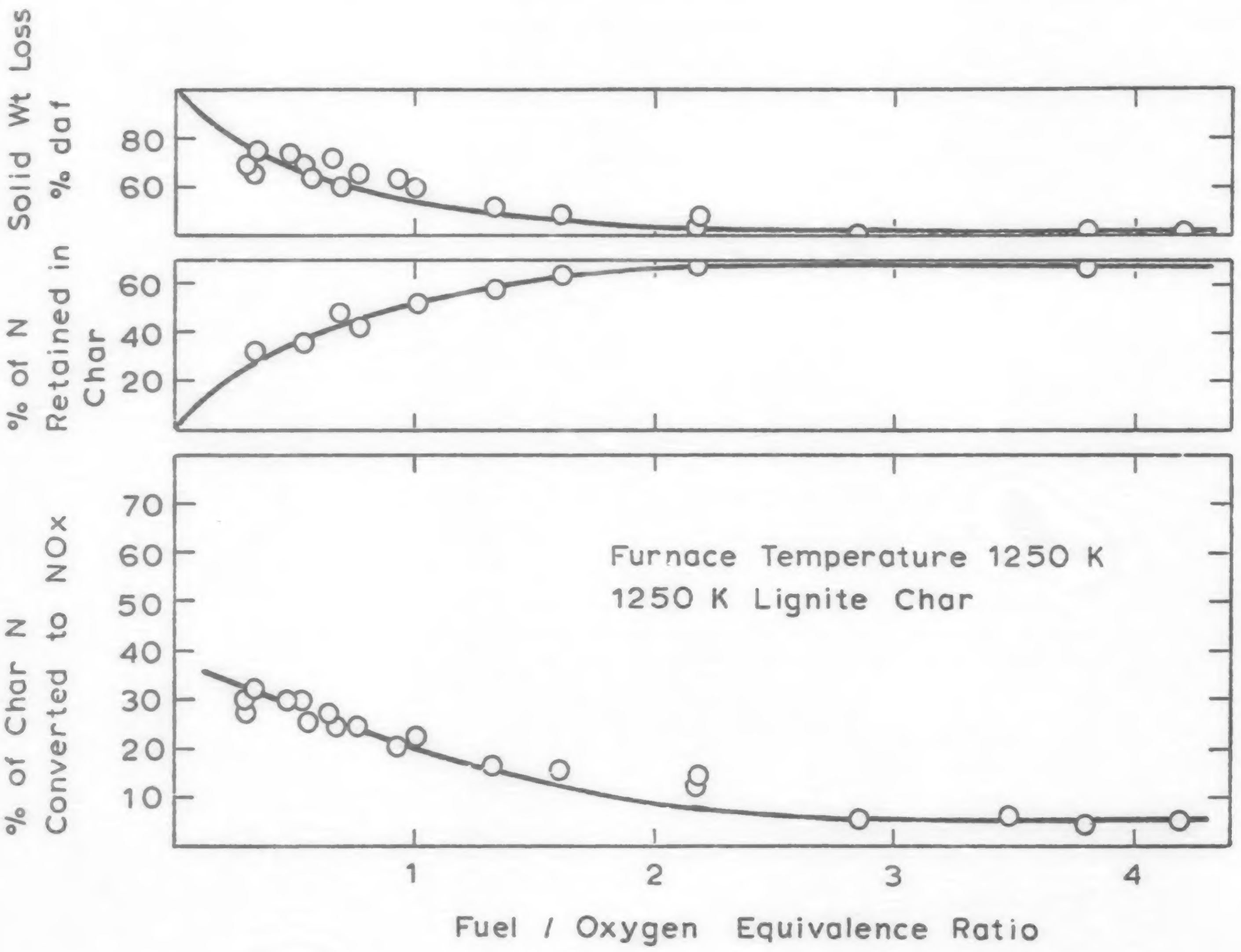

Figure 4. Fate of Char Nitrogen During Oxidation: Conversion to Nitric Oxide (Bottom), Retention by Unburned Char (Middle), and Combustion Efficiency (Top). Char from Montana Lignite Pyrolyzed and Oxidized at 1250 K.

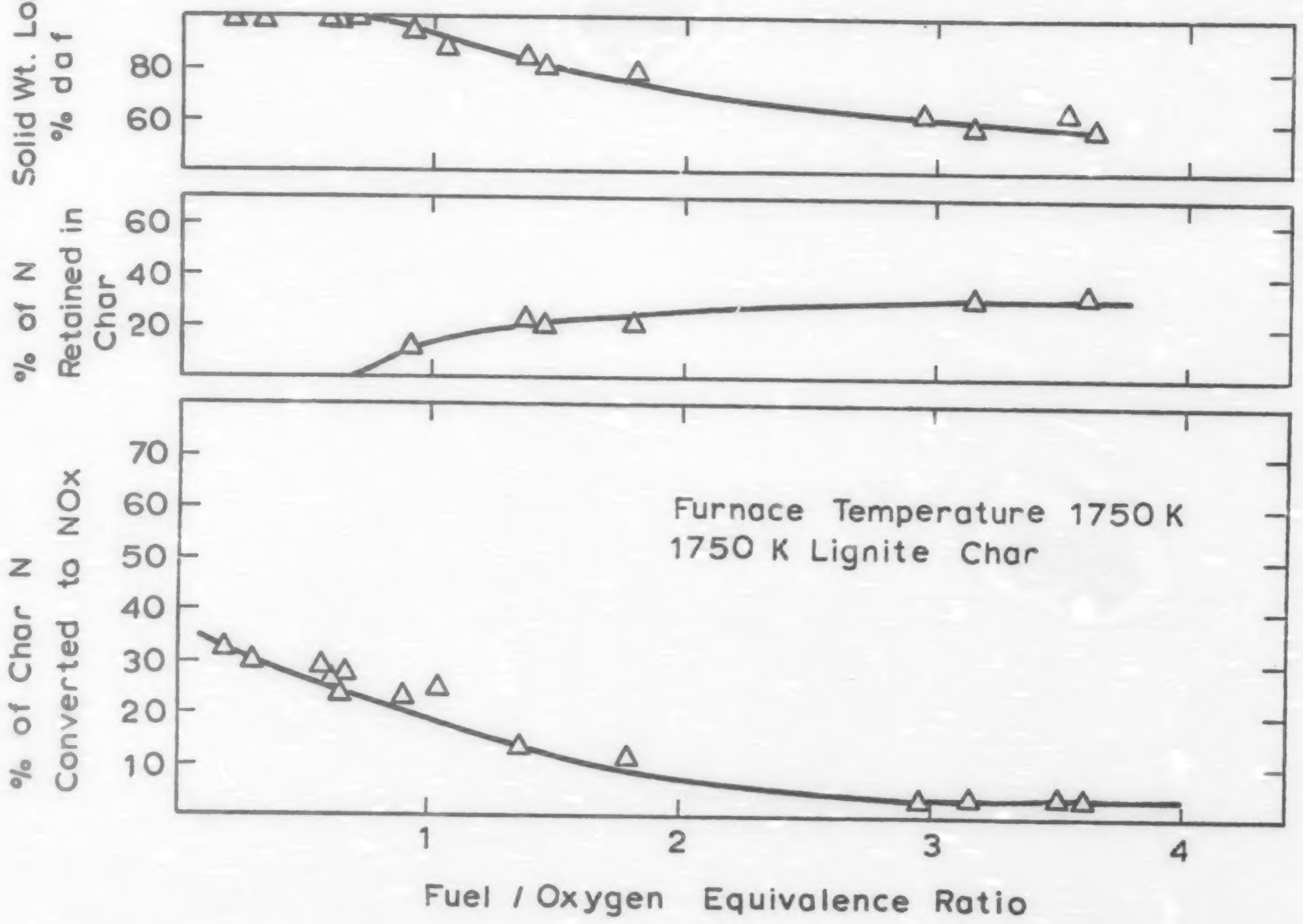

Figure 5. Fate of Char Nitrogen During Oxidation: Conversion to Nitric Oxide (Bottom), Retention by Unburned Char (Middle), and Combustion Efficiency (Top). Char from Montana Lignite Pyrolyzed and Oxidized at 1750 K.

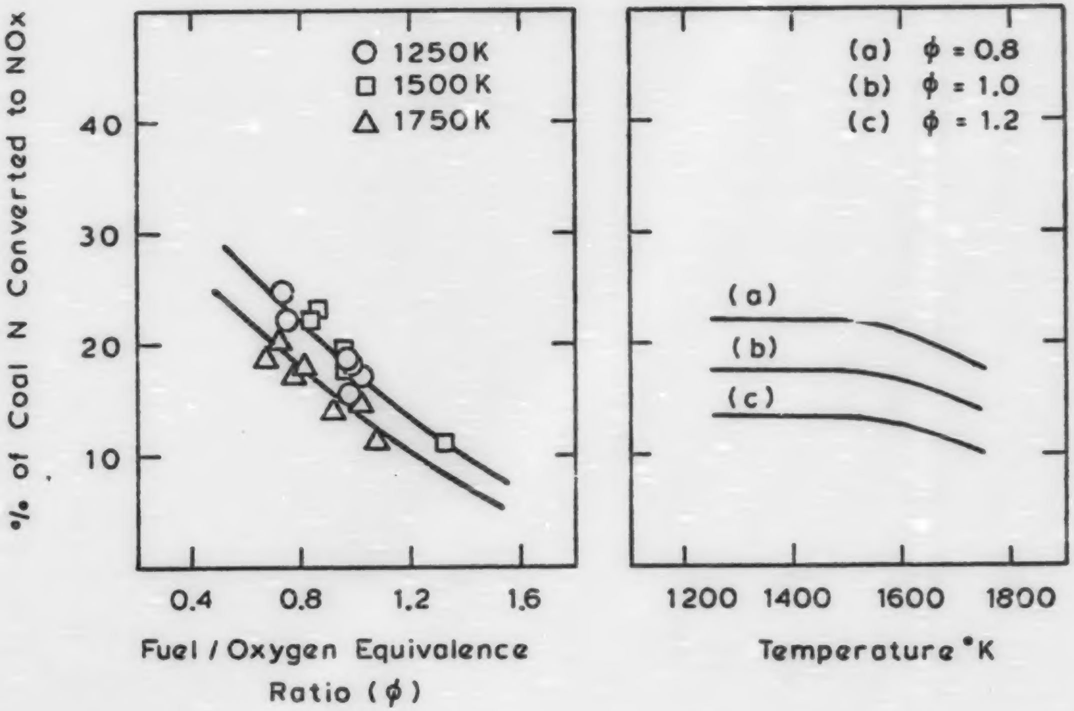

Figure 6. Effect of Temperature on Conversion of Coal Nitrogen to Nitric Oxide. Montana Sub-bituminous Coal.

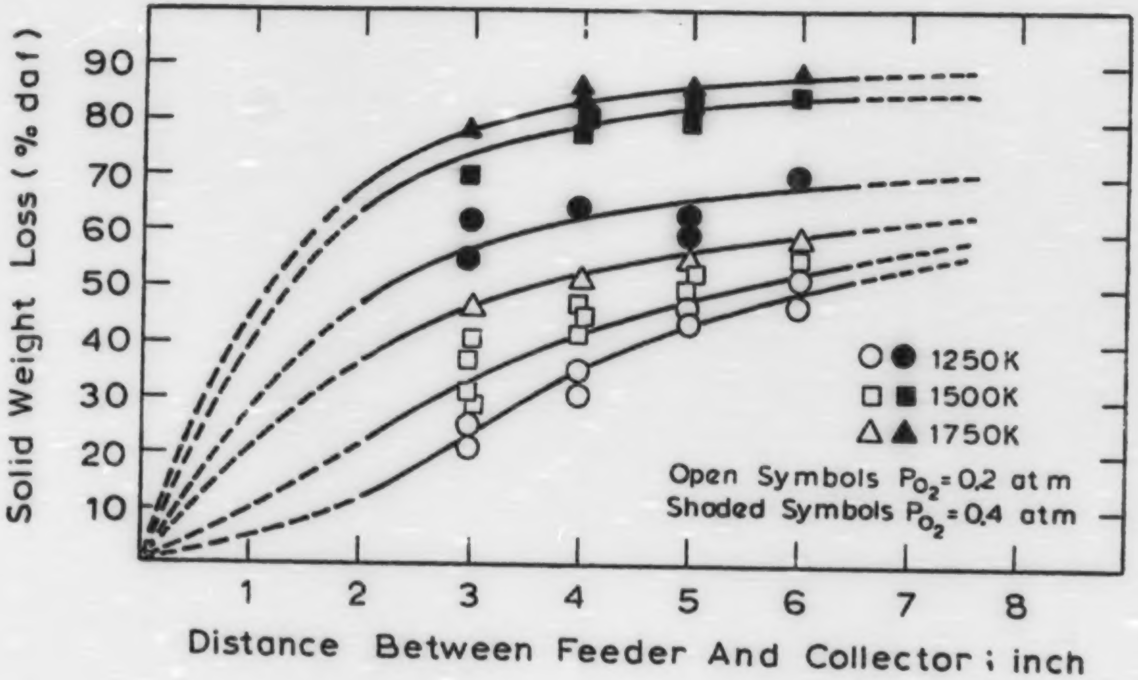

Figure 7. Weight Loss of Char Prepared from a Montana Lignite as a Function of Distance to the Collector During Oxidation.

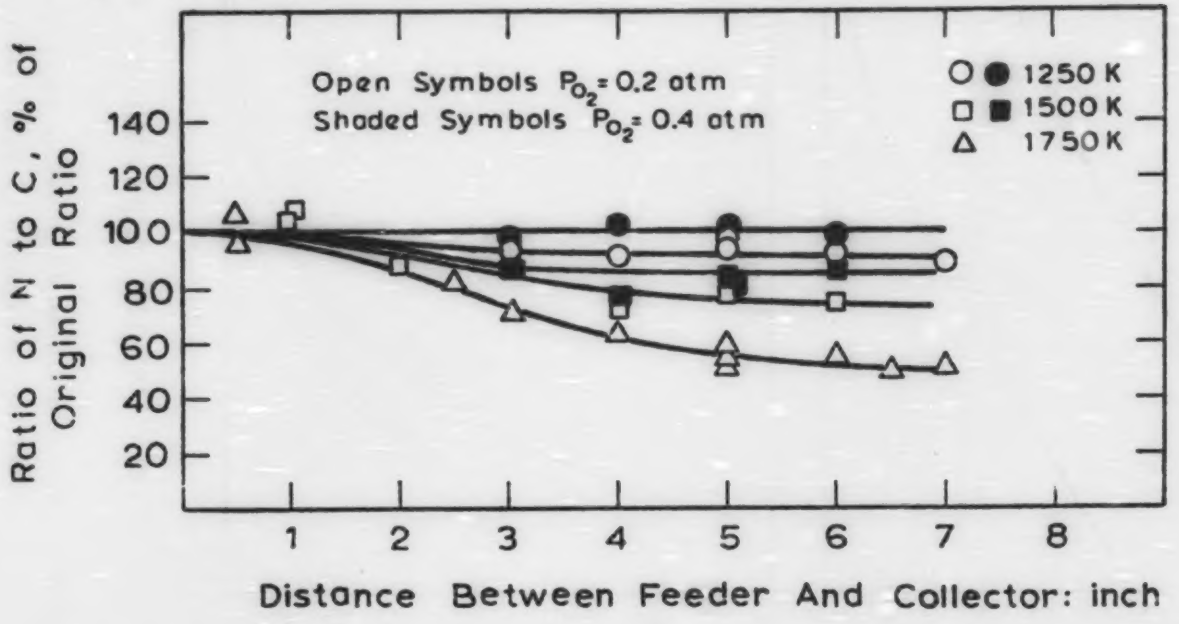

Figure 8. Nitrogen/Carbon Ratio as Percentage of that in the Original Char as a Function of Distance to the Collector During Oxidation.

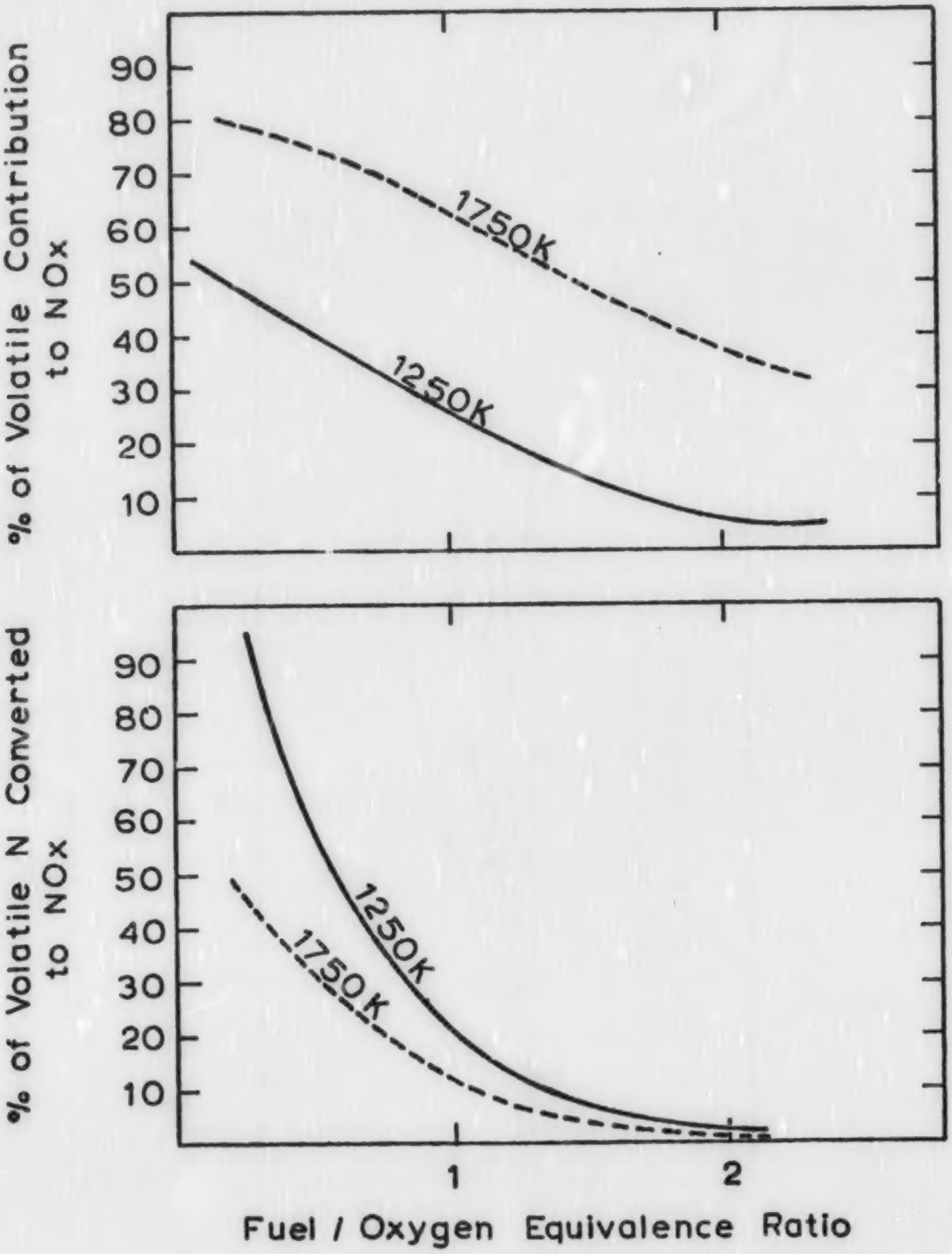

Figure 9. Contribution of Volatiles to NO_x Emission: Total NO_x Contributed by Volatiles (Top), and Conversion of Volatiles to NO_x (Bottom).

INTERACTIONS BETWEEN SULFUR OXIDES
AND
NITROGEN OXIDES IN COMBUSTION PROCESSES

By:

J. O. L. Wendt, T. L. Corley, and J. T. Morcomb
University of Arizona
Tucscon, Arizona 85721

ABSTRACT

Turbulent diffusion flame studies on gas and oil show that the presence of fuel sulfur could either inhibit, enhance or have no effect on both thermal and fuel NO_x, depending on flame aerodynamics and air preheat. Laboratory flat flames studies showed that under fuel rich conditions, the presence of fuel sulfur could have a radical effect on fuel NO formation mechanisms. Both enhancement and apparent inhibition of fuel NO were observed, depending on the stoichiometric ratio, and the residence time at which the measurement was made. The results can be interpreted in the light of current theories on fuel NO formation mechanisms.

Preceding page blank

INTRODUCTION

Chemically bound nitrogen in fossil fuel has been shown to be an important contributor to nitrogen oxide emissions from combustion processes. Recent research has focussed on mechanisms governing the oxidation of fuel nitrogen to fuel NO (Morely, 1976; Haynes, 1977), in the hope that the insight and understanding gained, thereby, will lead to development of new combustion modifications for NO_x control. However, many fuels containing chemically bound nitrogen also contain sulfur, in various amounts. Indeed, in so far as pulverized coal is concerned, a wide variation in sulfur content is possible, even from coals with similar nitrogen contents. The question can, therefore, be posed whether the sulfur content of a fuel is likely to have a major influence on the resulting NO_x emissions and specifically whether the presence of fuel sulfur will cause major changes in mechanisms of fuel NO formation. Furthermore, since there exists a wide variety of possible combustion conditions and combustion modifications, it is to be expected that the potential importance of SO_x/NO_x interactions depends not only on the fuel quality, but also on the conditions under which the fuel is burned.

This project was divided into two phases. Phase 1 consisted of screening experiments on turbulent diffusion flames. The purpose of this phase was to determine whether fuel sulfur had an important effect on NO_x emissions in practical combustion systems. Phase 2

Preceding page blank

continued the investigation of SO_x/NO_x interactions, but in a premixed flat flame environment. The purpose of this phase was to determine in more detail the conditions under which these interactions occurred. Results in Phase 2 would help generalize the data obtained in Phase 1 and would help determine how to relate premixed combustion data to the environment controlling pollutant formation in turbulent diffusion flames.

Although oxidation of chemically bound sulfur in the fuel can result in significant sulfur oxide emissions, there is little or no data concerning the pertinent mechanisms involved. The combustion of H_2S has been studied extensively (Levy and Merryman, 1965; Merryman and Levy, 1967; Sachyan, Gershezon, and Nalbandyan, 1967). There is good agreement on the mechanisms involved in forming SO_2 from H_2S, and on the sulfur species present at different stages of the combustion process. The limited data available on combustion of organic sulfur compounds indicate the presence of sulfur species identified in the combustion of H_2S (Cullis and Mulcahey, 1972). Due to the general lack of data, it would appear necessary to treat bound sulfur in the fuel as if it were H_2S to analyze the possible interactions with NO formation. Furthermore, there is evidence (Cullis and Mulcahey, 1972) that sulfur species are equilibrated under fuel rich conditions. Intermediate products are SO, S and SH. Addition of SO_2 to a fuel to simulate sulfur, will produce a distribution of intermediates not very different from those produced using H_2S, especially in the post primary reaction zone.

The possibility of interactions between sulfur and nitrogen oxides at low temperatures is not new (Wendt and Sternling, 1973). This interaction results in the catalysis, by NO, of the oxidation of SO_2 to SO_3. At higher temperatures, typical of combustion conditions, free radicals are produced in super-equilibrium concentrations. Since free radicals are important in NO formation, and since it has been shown (Durie, Johnson, and Smith, 1971) that sulfur dioxide is an effective catalyst in reducing super-equilibrium free radical concentrations, it is reasonable to expect that sulfur dioxide, and possibly other fuel sulfur compounds, inhibit the formation of NO in flames. Indeed, Wendt and Ekman (1975) found that the addition of high levels of SO_2 or H_2S to premixed, flat, methane-air flames inhibited thermal NO formation significantly. The inhibition effect was attributed to the catalysis of super-equilibrium oxygen atom recombination reactions by SO_2, and was in evidence for both prompt NO and post flame NO. DeSoete (1975) on the other hand, found that low levels of sulfur could enhance "prompt NO" formation in rich hydrocarbon flames. It should be noted that here flame temperatures were in excess of $2100^{o}K$. DeSoete attributed the observed enhancement to mechanisms involving CH, N_2, HCN, SO_2, that is, to interactions between fuel sulfur and the Fenimore (1971) mechanism for prompt NO. Clearly, some discrepancies between Wendt's data and DeSoete's data still remain to be resolved.

DeSoete (1975) also, consistently found that fuel sulfur enhanced fuel nitrogen (NH_3, NO) conversion in argon/hydrocarbon/oxygen flames under fuel rich conditions. At a stoichiometric ratio of 0.6 at flame temperatures of $2220^{\circ}K$ he found that 250ppm H_2S in the inlet mixture led to an increase of 70% in NO emissions. Under fuel lean conditions, a slight inhibition was observed. Indications from preliminary but incomplete studies conducted by Wendt and Ekmann (1975) on fuel sulfur interactions with fuel NO formation were that, although the effect is not significant under fuel-lean conditions, it may, under fuel rich conditions, have a marked influence on the rate at which fuel NO is formed.

The unanswered questions addressed in this paper are: 1) Does fuel sulfur influence fuel and thermal NO emissions in turbulent diffusion flames? 2) What is the nature and extent of fuel sulfur/fuel nitrogen interactions in premixed flat flames? Furthermore, the applicable conditions to be examined in the premixed flat flame experiments were determined by inferences drawn from the turbulent diffusion flame data. In this sense, the pilot scale experimentation guided the more fundamental laboratory scale research, which is the converse of normal procedure. It should be noted that one essential difference between turbulent diffusion flames and premixed flames is that any fuel additive does not immediately come into contact with oxygen in the former, while it does in the latter.

TURBULENT DIFFUSION FLAMES

Experimental Combustor

Swirling turbulent diffusion flames were supported on a small scale 80,000 Btu/hr burner in a 6" ID diameter combustor. Hardware details can be found elsewhere (Pershing and Wendt, 1977, Pershing, 1976). It is important to note that by proper adjustment of fuel and air velocities, of volume fraction of secondary air given tangential momentum (hereafter denoted by % swirl), and of injector hole angle, it was possible to sustain a wide variety of flame types, ranging from axial Type I flames, with little primary recirculation, to Type II and Type III flames with increasing intensity of primary recirculation. The gas injector utilized allowed poorly mixed turbulent diffusion flames (Type I) to be supported when gas flowed through an axial port, but also supported more intensely mixed compact turbulent diffusion flames (Type II) when the gas flowed through radial ports. The total area of the six holes for the radial case is equivalent to the area of the single hole axial case. The oil injector used for doped distillate oil was water cooled and utilized standard pressure atomizing Monarch nozzles rated at 0.5gph at 100p.s.i. Most tests were conducted with a 30^{o}R solid cone nozzle. Additives could be bled into the fuel stream (gas and oil), or into the air stream without changing total flow rate. Further details can be found elsewhere (Corley 1976). The sampling and analytical system provided continuous monitoring of NO, NO_2, CO, CO_2, O_2 and SO_2 and has been described elsewhere (Pershing and Wendt, 1977). Suffice it to say that SO_2 was shown not to significantly interfere with the chemiluminescent NO readings. The diesel oil utilized contained 0.3% wt. sulfur and 147ppm wt. nitrogen, while the natural gas was rated at 1064 Btu/scf and contained merely 0.07 grains/100scf sulfur. Additives used were, for the natural gas studies, SO_2 and NH_3; for the distillate oil studies, thiophene (C_4H_4S) and pyridine (C_5H_5N).

SO_x/Thermal NO Interactions

Fig. 1 shows results for natural gas and the radial injector at zero secondary air preheat. This flame could be classified as Type II and was highly mixed. SO_2 was injected first into the fuel only, and then into the air only. In each case, fuel sulfur inhibited thermal NO_x, and it made very little difference whether the additive was injected into the fuel or air. This is consistent with the premixed flame data of Wendt and Ekmann (1975), and indicates that a) superequilibrium free radical concentrations are important for this type flame, and b) mixing is rapid in so far as SO_2/thermal NO_x reactions are concerned. At 440°F, secondary air preheat (Fig. 2) results show essentially the same, with the exception that mixing does now become important at low excess air values, because there the inhibition was less with the sulfur in the fuel than in the air. One might also deduce that the Fenimore prompt NO mechanism was not of paramount importance for this flame, since DeSoete's enhancement, thereof, was not observed.

Data for the axial injector (Type I flame) show that at low air preheat values (Fig. 3), SO_2 added to the air has a larger inhibitory effect then when added to the fuel. Clearly, mixing now controls the importance of SO_x/NO_x interactions.

Local sulfur concentrations will be higher on the fuel lean side or fuel rich side of the reaction zone, depending on whether SO_2 is injected in the air or fuel. Therefore, one can conclude for this type flame, that inhibition of thermal NO_x (probably through reduction of superequilibrium oxygen atoms) occurs on the fuel lean side of the local reaction zone.

At high air preheat (Fig. 4) the situation is different, in that, although inhibition is observed when SO_2 is injected into the air, an enhancement is observed when SO_2 is injected into the fuel. Since flame temperatures are now high, this would indicate that the Fenimore prompt NO/SO_x interactions first observed by DeSoete are of paramount importance in the axial flames. The practical importance of Figs. 1 and 4 is that fuel sulfur will inhibit Thermal NO_x from Type II and Type III flames, but will enhance Thermal NO_x from Type I flames.

It is of interest to note that only an inhibition of Thermal NO_x was observed when 3.8% wt. S (as thiophene) was added to distillate oil, both for low and high air preheat values. In these cases, however, Type II flames were stabilized, allowing rapid mixing.

Fuel NO - Fuel Sulfur Interactions

The addition of thiophene to a pyridine-distillate oil fuel mixture was used to investigate the effect of fuel sulfur on fuel NO emissions. For the majority of studies conducted, the fuel sulfur level was 2.05 wt. % S, corresponding to about 1100ppm SO_2 in the exhaust for complete conversion; the fuel nitrogen level was .78 wt. % N, corresponding to approximately 960ppm NO in the flue for complete conversion. These levels are representative of fuel nitrogen contents of low-grade crudes or residual oils.

The oil firing rate was about 70,000 Btu/hr. The fuel was mechanically atomized after passing through a water-cooled injector. The same injector was used for all studies although the nozzle was changed before each study. The flames produced were short, bushy, and luminous (Type II). These flames were attached to the nozzle about ½" above the orifice of the nozzle. For the majority of studies, 30°R solid cone nozzles were used.

To insure that the observed effects on fuel NO were due to the presence of fuel sulfur, and not to other transients introduced by the addition of thiophene, efforts were made to ascertain that all other conditions remained constant. First, it was shown that addition of benzene to a quinolene doped distillate oil did not affect fuel NO emissions. Since thiophene is itself a fuel and changes in the stoichiometric air requirements would be expected when it was introduced into the pyridine-oil fuel mixture, the following procedure was, therefore, employed in these studies:

1. Baseline thermal NO data were taken over the excess air range of interest without the presence of pyridine.
2. Pyridine was added to the fuel and excess air conditions were varied over the range of interest.
3. Thiophene was added to the pyridine-oil mixture and NO measurements were made over a range of excess air conditions.
4. Thiophene addition was stopped and NO measurements were again taken for the pyridine-oil mixture at selected excess air conditions.
5. Finally, pyridine addition to the oil was stopped, and thermal NO readings were taken to compare with the original baseline data.

The most important problem encountered in the studies conducted with #2 diesel oil was coke formation on the oil nozzles. The severity of coke formation increased with air preheat, decreasing excess air conditions, and when fuel nitrogen was present. A reduction in coking was observed when thiophene was added to the pyridine-oil mixture.

Since the presence of SO_2 or H_2S in premixed and diffusion flames has been found to reduce carbon formation (Cullis and Mulcahey, 1972), this is not unexpected.

Fig. 5 shows results of 2.05% sulfur addition to a distillate oil containing 0.78% chemically bound nitrogen. No effect was observed. Fig. 6, however, shows that at high secondary air preheat values, fuel sulfur enhanced fuel NO conversion. It is important to note, however, that not only had the combustion temperature increased, but the baseline (0% S) fuel NO had decreased, indicating a decrease in mixing intensity and the persistence of more fuel rich regions. The observed enhancement of 40% due to sulfur might be due to either of these effects. Subsequent experiments in which SO_2 was added in the air showed that sulfur had to penetrate into fuel rich regions in which some fuel NO_x was being formed, before enhancement of fuel nitrogen conversion could be observed.

Indications were, therefore, that enhancement of fuel nitrogen oxidation by fuel sulfur in turbulent diffusion flames would occur under poorly mixed (or Type 1) flame configurations and at high air preheats. Experiments were performed with natural gas doped with ammonia, using the axial injector. This gave a Type I flame, and results (Fig. 7) clearly show a significant enhancement (40%) of fuel NO emissions when SO_2 was added to fuel. Some enhancement was also observed when SO_2 was added to the air.

PREMIXED FLAT FLAMES

The turbulent diffusion flame results described above indicated that fuel NO_x/SO_x interactions were important primarily in a fuel rich combustion region. Furthermore, DeSoete's work indicated that enhancement could occur only under fuel rich conditions. Therefore, in our premixed flat flame studies, we focussed on fuel NO/fuel sulfur interactions under fuel rich conditions and attempted to address the following critical questions:

1) What is the relationship between local stoichiometry and temperature for the observed enhancement to occur?
2) To what extent does the presence of fuel sulfur radically change fuel nitrogen oxidation mechanisms?
3) Does the importance of these interactions under fuel rich conditions indicate that fuel sulfur will have a major influence on staged combustion configurations for fuel NO_x abatement from pulverized coal.

Experimental Burner

The premixed flat flame burner was similar to that utilized by Axworthy et. al. (1976). It was nominally 5cm I.D. and allowed a flat flame to be stabilized over a coarse stainless steel screen (10 x 10 mesh, 0.028" wire). The burner was enclosed by a 15cm I.D., 60cm high quartz chimney, the inside surfaces of which were purged with nitrogen in order to prevent soot deposition. Details can be found elsewhere (Morcomb, 1977). Temperature measurements were made using the sodium D-line reversal technique, with experimentally obtained corrections for the glass chimney surfaces. Flows of major (O_2, CH_4, Ar) and minor species (C_2N_2, SO_2, H_2S) were controlled and metered with sonic orifices, rotameters and laminar flow elements where appropriate.

Sampling was accomplished through both uncooled and cooled quartz probes. NO_x analysis was by chemiluminescence and a Molybdenum converter. Teflon lines were used throughout. We were concerned about reactions occurring at room temperature in the sampling line. Special experiments, including some in which SO_2 in the sample line was removed at various points, showed that our NO measurements were not due to an interference between sulfur and any potential NO_x forming species between the probe and the analyzer. Both the hot and cooled probes withdrew the sample through a 1.5mm orifice, allowing a normal sampling rate of 1.3 liters/min. Special tests on the hot quartz probe showed that when soot, previously exposed to SO_2, was present, the baseline (no sulfur) NO was lowered by 7ppm, compared to results from the cooled probe. The cooled probe did not allow the build up of soot, and changing sampling rates by a factor of five did not change "exhaust" ppm NO measured, both in the presence and absence of sulfur. The cooled probe, however, caused the peak flame temperature of 1953^{o}K to drop 30^{o}K when it was in the immediate vicinity. This interference became negligible 2cm away from the probe. Most of the results reported below are with the cooled probe, except as noted.

A chart recorder was used to observe transients and baseline reproducibility. Changing or cleaning the porous disk and screen on the burner had no effect on results.

Results:

Figs. 8 through 12 show the effects of various fuel sulfur levels on fuel NO profiles at various stoichiometries. The total dry and wet molar flow rates of the burned gas were calculated assuming chemical equilibrium in the fuel rich mixtures. Residence times and ppm NO corresponding to 100% conversion of fuel nitrogen were calculated using these molar flow rates. In general, the sulfur additive ranged from 0.2 through 3.8 mole percent of the fuel; the nitrogen contents were 0.2 and 1.0 mole percent nitrogen in the fuel. Specific details for each condition investigated can be found in the figures and figure captions. The major species were argon, methane and oxygen. In all cases, there was no evidence of NO_2, either with or without sulfur present, although it should be cautioned that long term exposure to CO can affect the performance of the Molybdenum converter.

At a stoichiometric ratio of 0.46 ($\Phi = 2.17$) sulfur greater than 0.2 mole percent in fuel had a large qualitative and quantitative effect on the entire fuel NO profile (Fig. 8). Open symbols denote data taken with the cooled probe, shaded symbols are those taken with the hot probe. The baseline fuel NO rose quickly to a constant 10ppm. Addition of 3.8 mole percent sulfur dioxide to the fuel prompted a rapid increase of fuel NO with a peak of 130ppm occurring downstream of the luminous zone of the flame. This high value decayed slowly to 40ppm over a residence time greater than 0.1 seconds. Although sulfur does act as a combustion inhibitor, the position of the luminous zone of the flame varied only slightly within a few millimeters of the grid. However, it is important to note that with sulfur present, NO is destroyed by a slow reaction at low temperatures (less than 1600°K). This does not occur in the absence of sulfur. The fact that the baseline NO does not change over the same distance indicates that along the centerline dilution is not significant.

Clearly, at very fuel rich conditions, the presence of sulfur compounds has a marked influence on fuel NO formation mechanisms.

Fig. 9 shows results of a similar experiment but with H_2S added as the fuel sulfur additive. Qualitatively similar profiles were obtained as with SO_2, but comparison of this figure with Fig. 8 indicates a less extreme effect. It should be noted that H_2S addition does lower the stoichiometric ratio, thus, tending to lower fuel nitrogen conversions. This is in contrast to DeSoete's results which showed H_2S to have a larger effect on prompt NO than did SO_2. However, our results indicate that it is sulfur, rather than the initial form of sulfur, which is responsible for the large effect observed.

Fig. 10 shows results at a stoichiometric ratio of 0.61 (Φ = 1.64). Again, sulfur (as SO_2) added to the fuel radically changed fuel NO mechanisms. The peak now occurred closer to the luminous zone in the flame, and a steady NO consumption brings the NO profile below the baseline case. In this case, whether fuel sulfur inhibits or enhances NO depends entirely on where the measurement is taken. It should be noted that temperatures in Fig. 10 were significantly hotter than at the richer case. Also, here H_2S addition had a similar effect as did SO_2.

At higher stoichiometric ratios, sulfur has less of an effect (Fig. 11; SR = 0.68), although the salient features observed before are present, i.e. sulfur compounds cause a rise followed by a steady decline in fuel NO.

Results for a fuel nitrogen content of 1 mole percent and a stoichiometric ratio of 0.46, are shown in Fig. 12. These data should be compared to those in Fig. 8. The results are essentially analogous. One important difference is that at the higher nitrogen content, a significant reduction in baseline NO, without sulfur, was observed close to the flame front. With sulfur, the NO profile again formed a high peak followed by a slow decay.

Discussion

Previous work (Haynes, 1976), has indicated that the route to NO from fuel nitrogen occurs through HCN, NCO and NH_x. Under fuel rich conditions, SO_2 is reduced to SO, H_2S, and SH, and these species may well interact with NH_x to change the distribution among NH, NH_2 species. There exists evidence (Lyon and Longwell, 1976, Wendt et. al., 1973) that NH_3 or its derivatives, will reduce NO at moderately low temperatures. Note that at very low stoichiometric ratios, the equilibrium NH_3 concentration is greater than the equilibrium NO. It might be conjectured, therefore, that reduced sulfur species directly change the NH_x profiles in a flame, so that the NH_x species responsible for NO reduction persists far beyond the flame zone, thus, accounting for the steady NO reduction. This conjecture might also explain why the early NO peaks are so high. In the flame zone, the sulfur has delayed the formation of the NO reducing species (Fenimore, 1976) until the post flame region is reached.

That the presence of sulfur allows NO profiles to decay sometimes below the baseline case is not surprising, since equilibrium NO values at SR= 0.61 are well below 1ppm. In fact, given that sulfur promotes this slow decay, it is not surprising that it can allow measured values to be above or below the baseline values. It is hard to rationalize that the slow NO reduction observed results from reactions with CH (Myerson, 1975) or other hydrocarbon fragments, since one would not expect them to persist so far from the reaction zone.

Our results differ from those of DeSoete (1975), in that he did not observe NO reduction prompted by sulfur, although he did observe significant enhancement of NH_3 conversion due to the presence of H_2S. However, measurements made in this work were over much longer residence times, and they involved both higher nitrogen and sulfur levels, and lower flame temperatures. Furthermore, DeSoete's experiments on the role of sulfur utilized NH_3 and NO as nitrogenous additives, while this work utilized C_2N_2. The nitrogen species involved may be important when sulfur is present.

It is interesting to note that the NO profiles measured here in the presence of sulfur, are qualitatively similar to NO profiles in fuel rich pulverized coal combustion (Pershing et. al., 1977), while the profiles without sulfur are not. The presence of sulfur in coal may have a significant effect on NO abatement by staged combustion, since one would expect sulfur levels in the volatiles to be high.

CONCLUSIONS

The presence of fuel sulfur can increase thermal NO emissions from poorly mixed Type I flames, but decrease thermal NO emissions from well mixed flames. Furthermore, fuel sulfur has a first order influence on mechanisms governing the oxidation of fuel nitrogen under fuel rich conditions. This can manifest itself in a significant increase in NO_x emissions when a fuel containing chemically bound nitrogen is burned with sulfur in an axial diffusion flame. Fuel oils containing both nitrogen and sulfur are likely to give higher NO emissions than those containing little sulfur, especially at high temperatures.

Increased emphasis on NO_x abatement of dirty fuels through fuel rich and staged combustion would appear to dictate that fuel nitrogen oxidation mechanisms in the presence of sulfur should be investigated. The data reported herein lend support to the hypothesis that the staged combustion of dirty fuels containing sulfur may be less effective than that of fuels of low sulfur content, although this may depend on the first stage stoichiometric ratios and residence times involved. Clearly, fuel sulfur and fuel nitrogen interactions are of first order importance for many practical combustion systems.

ACKNOWLEDGEMENTS

The authors would like to express their appreciation to David W. Pershing and Edward M. Morcomb, without whose help, some of the data reported herein would not have been obtained. We would also like to thank Michael P. Heap and W. S. Lanier for their valuable technical input to this project.

LITERATURE CITED

Axworthy, A. E., G. R. Schneider, M. D. Shuman and V. H. Dayan "Chemistry of Fuel Nitrogen Conversion to Nitrogen Oxides in Combustion", EPTS Report EPA-600/2-76-039, February, 1976.

Corley, T. L., "Fuel Sulfur Effects on NO_x Formation in Turbulent Diffusion Flames", M.S. Thesis, University of Arizona, Department of Chemical Engineering, December, 1976.

Cullis, C. F. and M. F. R. Mulcahey, "The Kinetics of Combustion of Gaseous Sulfur Compounds", Comb. Flame, 18 (1972).

DeSoete, G., "La Formation des Exyde D'Azote Dans La Zone d'Oxydation des Flammes d'Hydrocarbures", Institut Francais du Pétrole, Final Report No. 23309, June, 1975. Ruiell Malmaison, France.

Durie, R. A., G. M. Johnson, and M. Y. Smith, "The Effect of Sulfur Dioxide on Hydrogen-Atom Recombination in the Burnt Gas of Premixed Fuel-Rich Propane-Oxygen-Nitrogen Flames", Comb. Flame, 17 (1971).

Fenimore, C. P., "Formation of Nitric Oxide in Premixed Hydrocarbon Flames", Thirteenth Symposium (International) on Combustion, The Combustion Institute, Pittsburgh, Pennsylvania (1971).

Fenimore, C. P., "Reactions of Fuel-Nitrogen in Rich Flame Gases", Comb. Flame 26, 249 (1976).

Haynes, B. S., "Reactions of Ammonia and Nitric Oxide in the Burnt Gases of Fuel-Rich Hydrocarbon-Air Flames", Comb. Flame, 28, 81 (1977).

Levy, A. and E. L. Merryman, "The Microstructure of Hydrogen Sulfide Flames", Comb. Flame, 9 (1965).

Lyon, R. K. and J. P. Longwell, "Selective, Non-Catalytic Reduction of NO_x by NH_3", The Proceedings of the NO_x Technology Seminar, EPRI Special Report EPRI SR-39, February, 1976.

Merryman, E. L. and A. Levy, "Kinetics of Sulfur-Oxide Formation in Flames. II Low Pressure H_2S Flames", J. Air Poll. Control Assoc., 17 (1967).

Morley, C., "The Formation and Destruction of Hydrogen Cyanide from Atmospheric and Fuel Nitrogen in Rich Atmospheric-Pressure Flames", Comb. Flame, 27, 187 (1976).

Morcomb, T. J., "Interactions Between Fuel Sulfur and Fuel NO_x Formation Mechanisms", M.S. Thesis, University of Arizona, Department of Chemical Engineering, December, 1977.

Myerson, A. L., "The Reduction of Nitric Oxide in Simulated Combustion Effluents by Hydrocarbon-Oxygen Mixtures", Fifteenth Symposium (International) on Combustion, p. 1085, The Combustion Institute, Pittsburgh, Pennsylvania (1975).

Pershing, D. W., "Nitrogen Oxide Formation in Pulverized Coal Flames", PhD. Dissertation, University of Arizona, Department of Chemical Engineering, August, 1976.

Pershing, D. W. and J. O. L. Wendt, "Pulverized Coal Combustion: The Influence of Flame Temperature and Coal Composition on Thermal and Fuel NO_x", Sixteenth Symposium (International) on Combustion. The Combustion Institute, Pittsburgh, Pennsylvania (1977).

Pershing, D. W., J. W. Lee and J. O. L. Wendt, "Fate of Coal Nitrogen Under Fuel Rich and Staged Combustion Conditions", Paper to be presented at 70th Annual AIChE Meeting, New York, November, 1977.

Sachyan, G. A., Y. M. Gershenzon, and A. B. Nalbandyan, "Multistage Nature of Combustion in Dilute Hydrogen Sulfide Flames", Dokl. Aked. Nauk SSSR, 175 (1967), [English version, 175 (1967)].

Wendt, J. O. L. and C. V. Sternling, "Catalysis of SO_2 Oxidation by Nitrogen Oxides", Comb. Flame, 21 (1973).

Wendt, J. O. L., C. V. Sternling and M. A. Matovich, "Reduction of Sulfur Trioxide and Nitrogen Oxides by Secondary Fuel Injection", Fourteenth Symposium (International) on Combustion, p. 897, The Combustion Institute, Pittsburgh, Pennsylvania (1973).

Wendt, J. O. L. and J. M. Ekmann, "Effect of Fuel Sulfur Species on Nitrogen Oxide Emissions from Premixed Flames", Comb. Flame 25 (1975).

Wendt, J. O. L. and J. M. Ekmann, "Effect of Fuel Sulfur on NO_x Emissions from Premixed Flames", EPTS Report EPA-600/2-75-075, October, 1975.

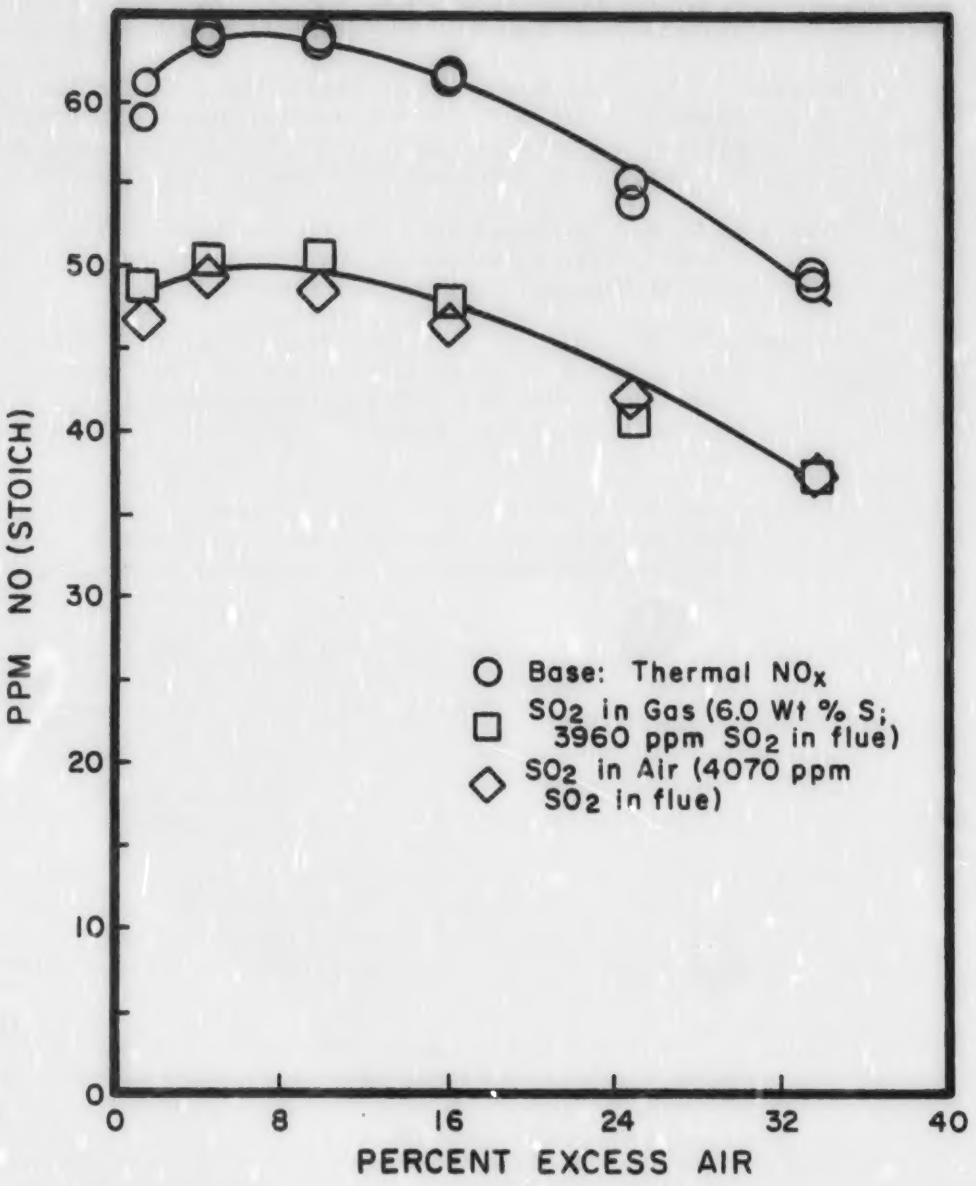

Figure 1: Turbulent Diffusion Flames: Natural Gas/Radial Injector, Effect of SO_2 on Thermal NO (38% Swirl; 100°F Air Preheat)

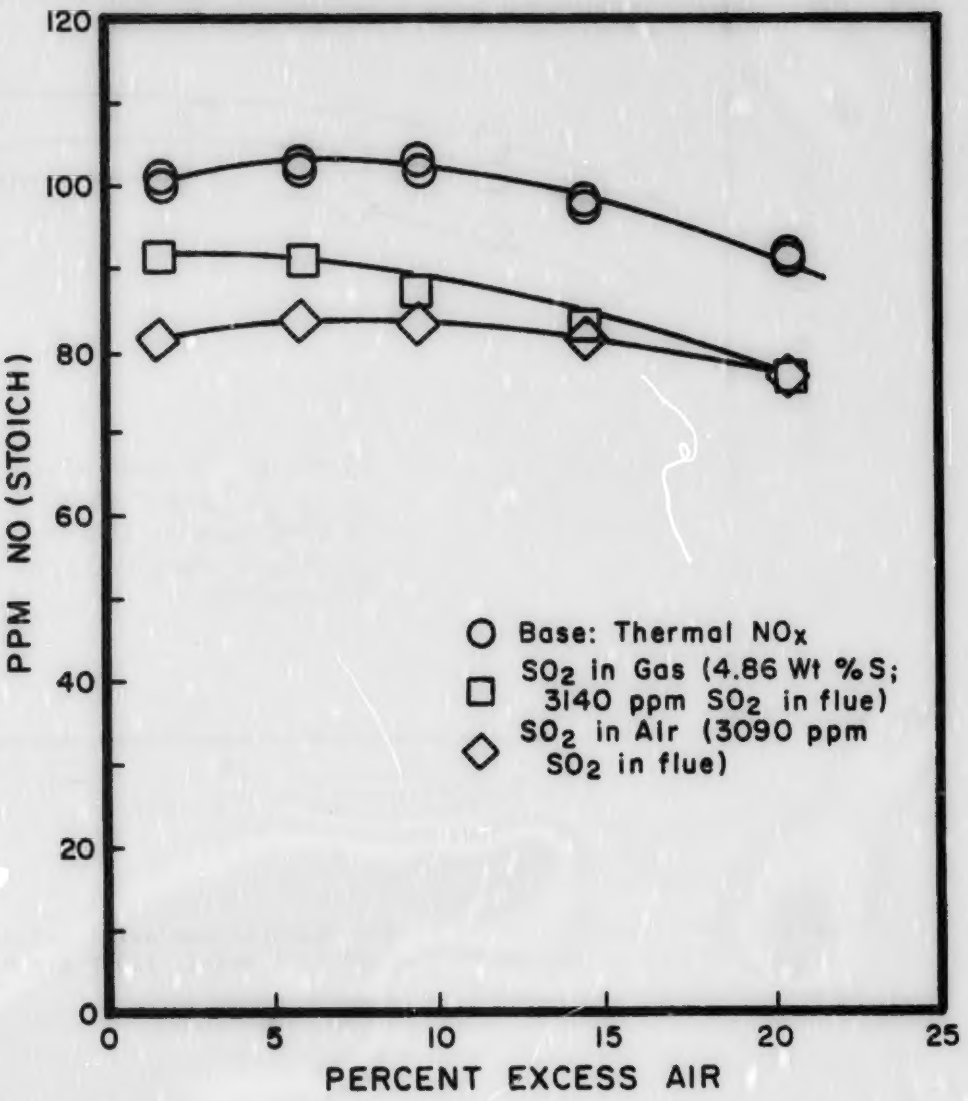

Figure 2: Turbulent Diffusion Flames: Natural Gas/Radial Injector, Effect of SO_2 at High Air Preheat (42% Swirl; 440°F Air Preheat)

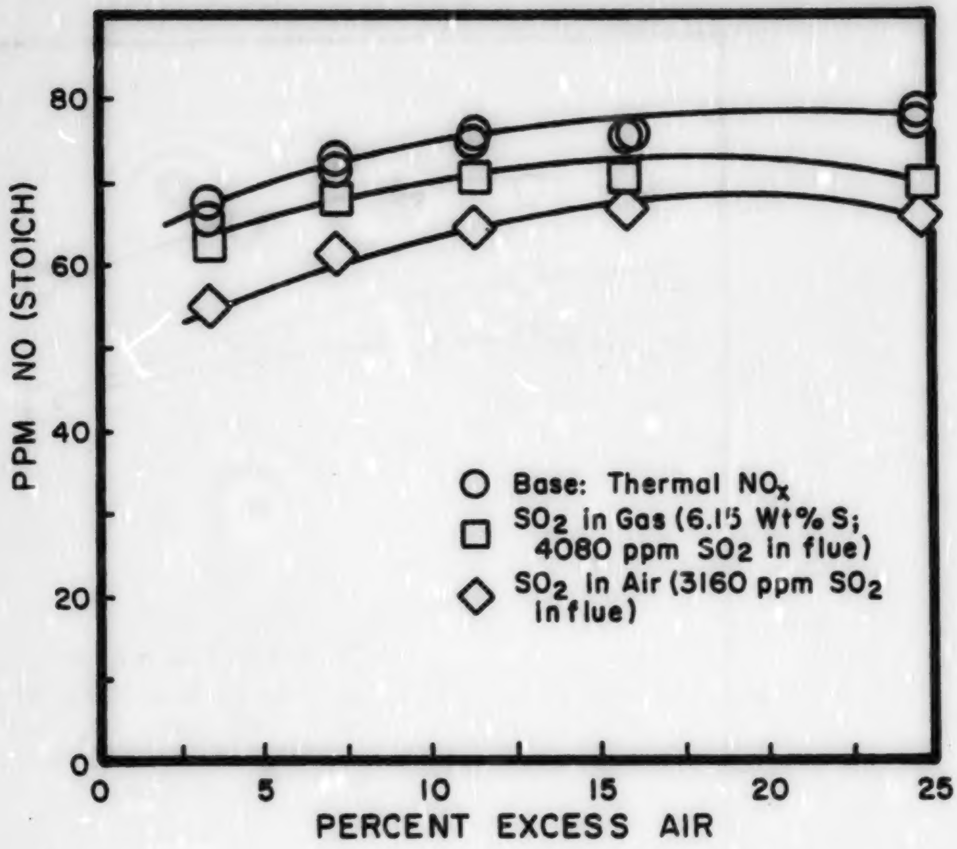

Figure 3: Turbulent Diffusion Flames: Natural Gas/Axial Injector, Effect of SO_2 on Thermal NO (37% Swirl; 120°F Air Preheat)

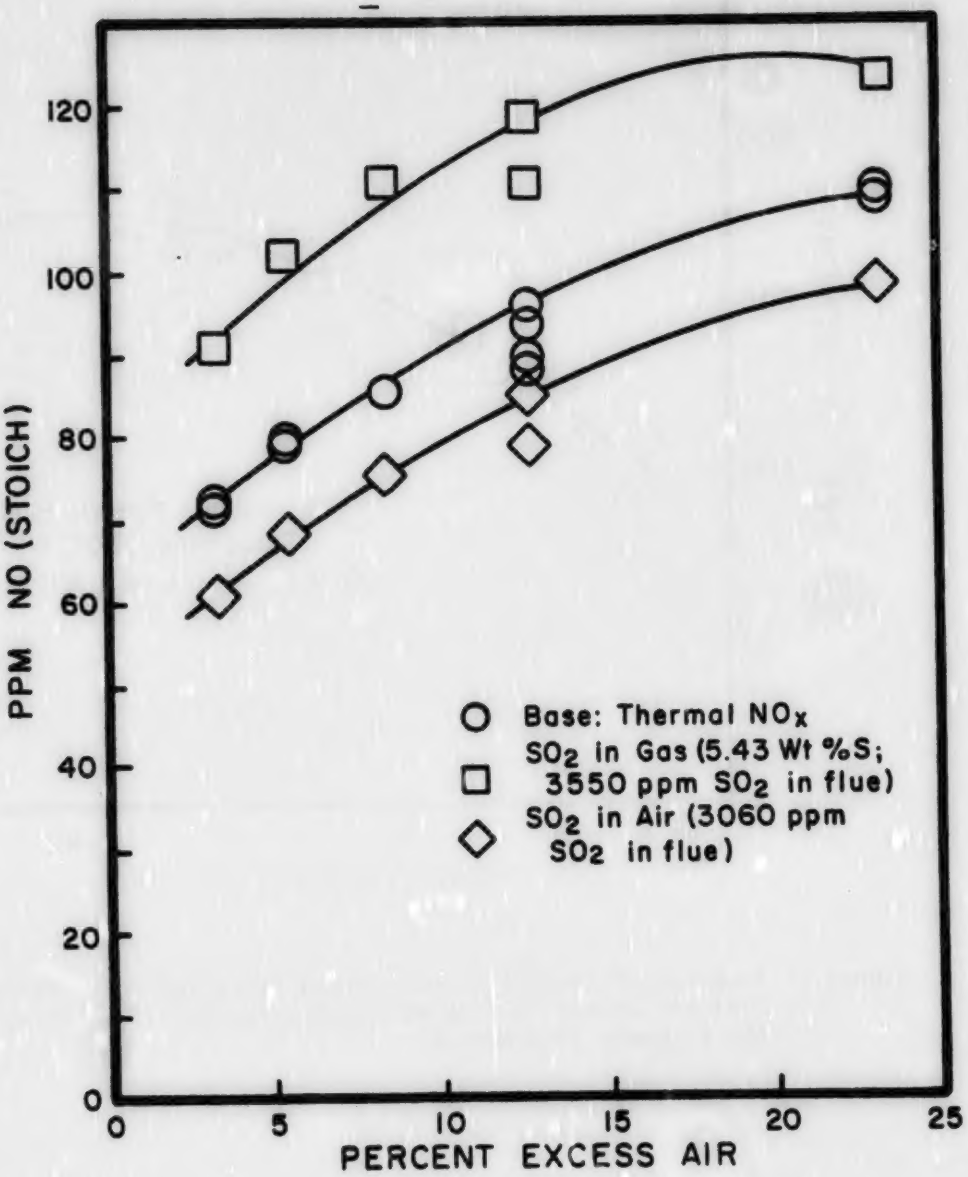

Figure 4: Turbulent Diffusion Flames: Natural Gas/Axial Injector, Effect of SO_2 on Thermal NO at High Air Preheat (40% Swirl; 440°F Air Preheat)

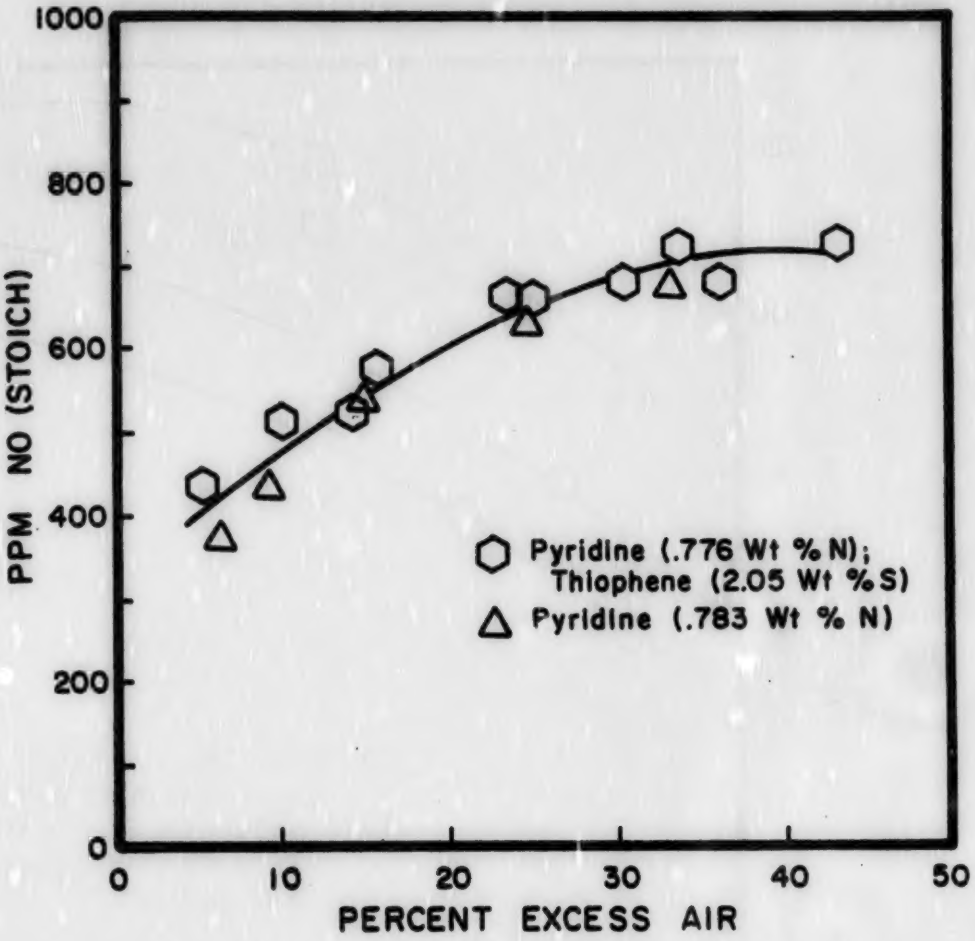

Figure 5: Turbulent Diffusion Flames: Doped Distillate Oil, Thiophene Does Not Affect Fuel NO at Low Air Preheat (43% Swirl; 100°F Air Preheat; 30°R Nozzle)

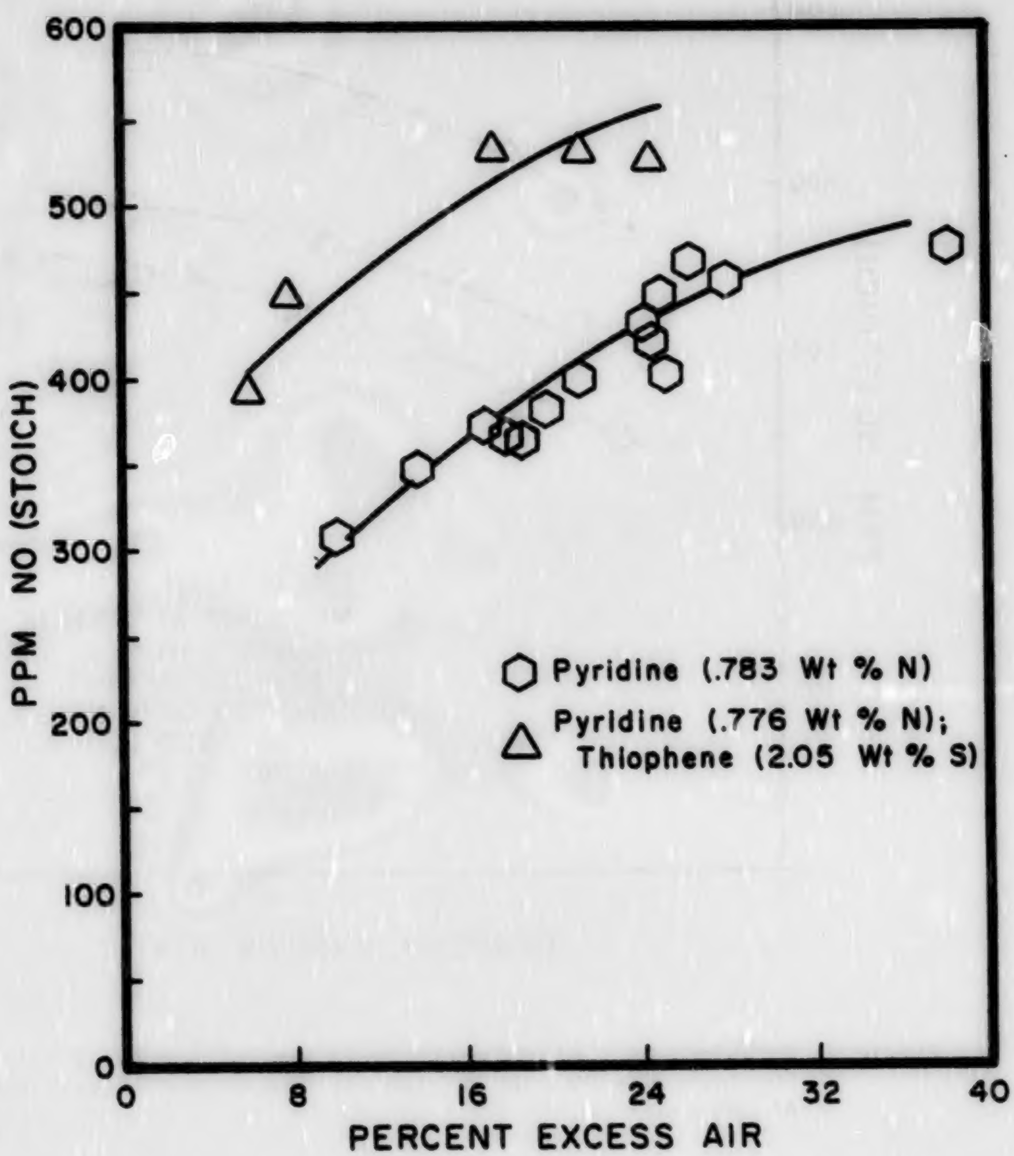

Figure 6: Turbulent Diffusion Flames: Doped Distillate Oil, Thiophene Increases Fuel NO at High Air Preheat (40% Swirl; 310°F Air Preheat, 30°R Nozzle)

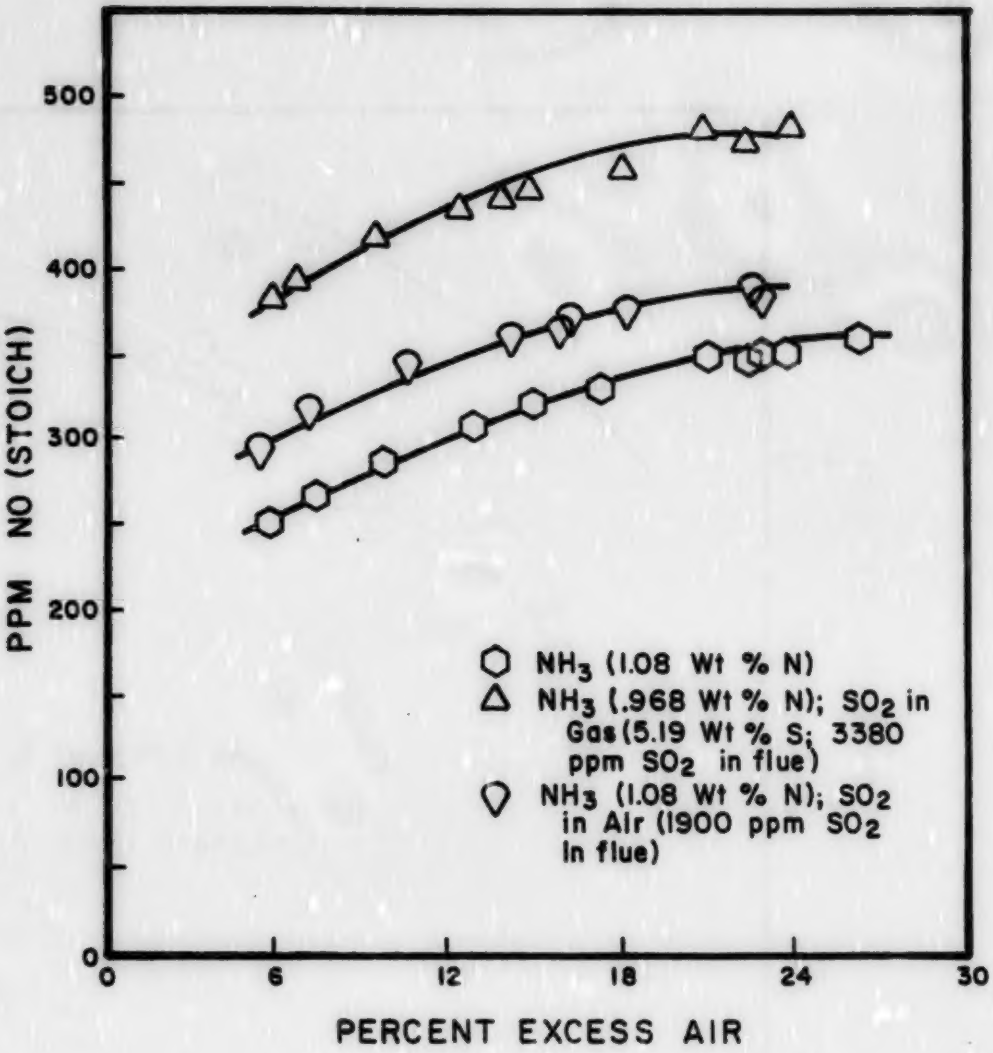

Figure 7: Turbulent Diffusion Flames: Doped Natural Gas/Axial Injector SO_2 Increases Fuel NO at High Air Preheat (44% Swirl; 430°F Air Preheat)

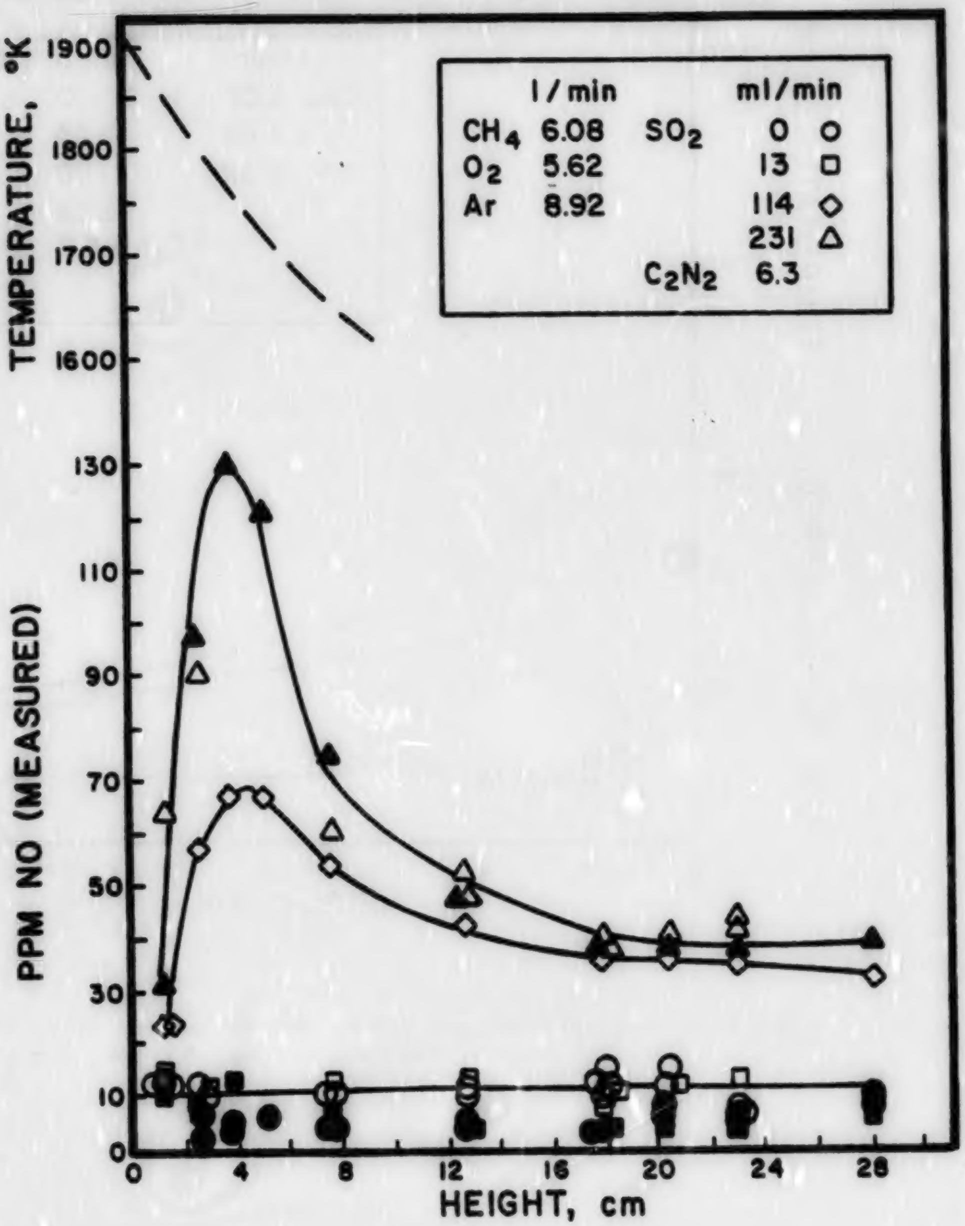

Figure 8: Laminar Premixed Flame: Stoichiometric Ratio 0.46 (0.21% fuel N, 100% conversion ≈ 553 ppm, 1cm ≈ 7.67 ms at 1900°K)

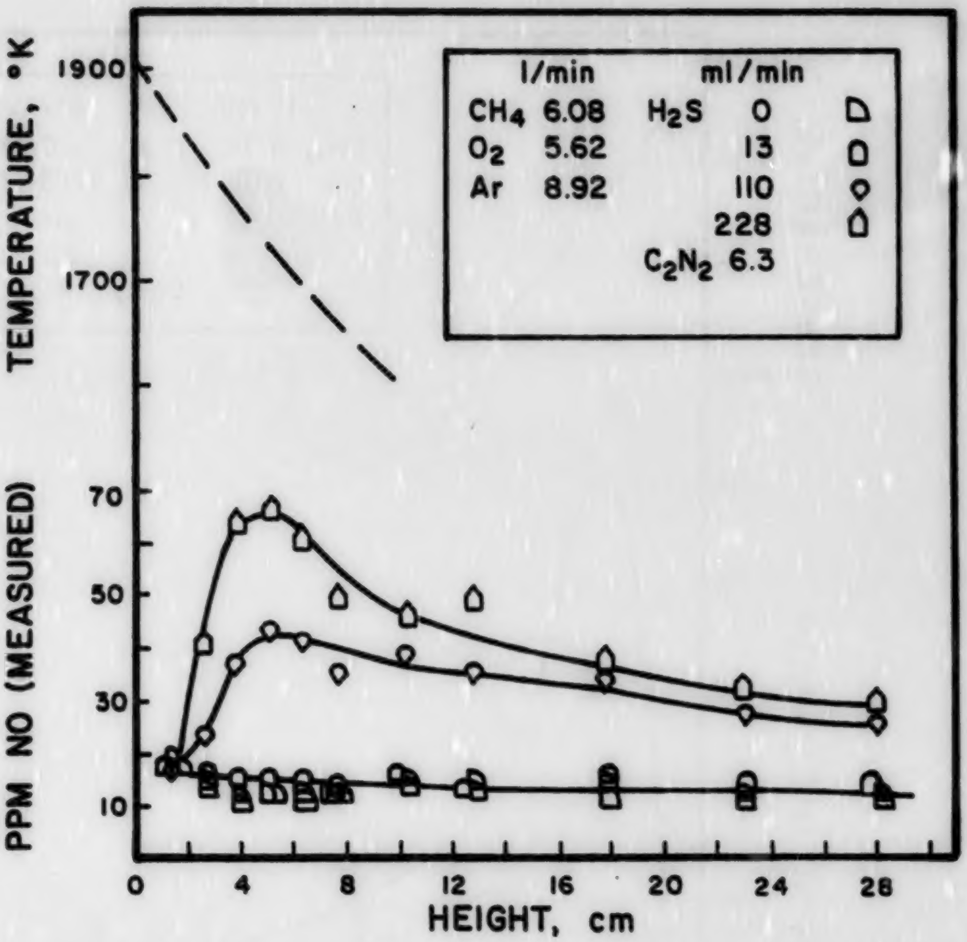

Figure 9: Laminar Premixed Flame: Stoichiometric Ratio 0.46 (0.21% fuel N, 100% conversion ≈ 553 ppm, 1cm ≈ 7.67 ms at 1900°K)

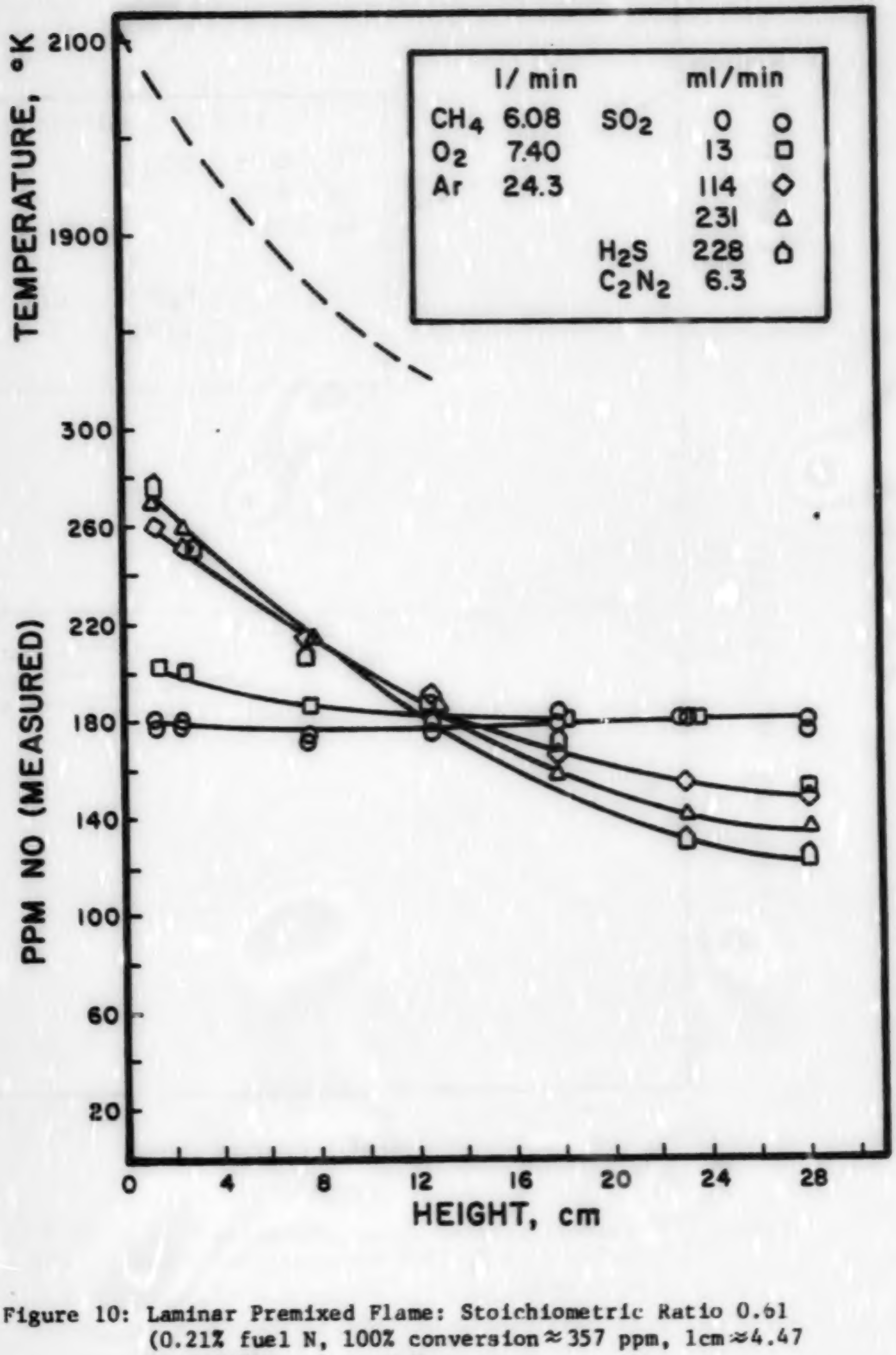

Figure 10: Laminar Premixed Flame: Stoichiometric Ratio 0.61 (0.21% fuel N, 100% conversion ≈ 357 ppm, 1cm ≈ 4.47 at 2100°K)

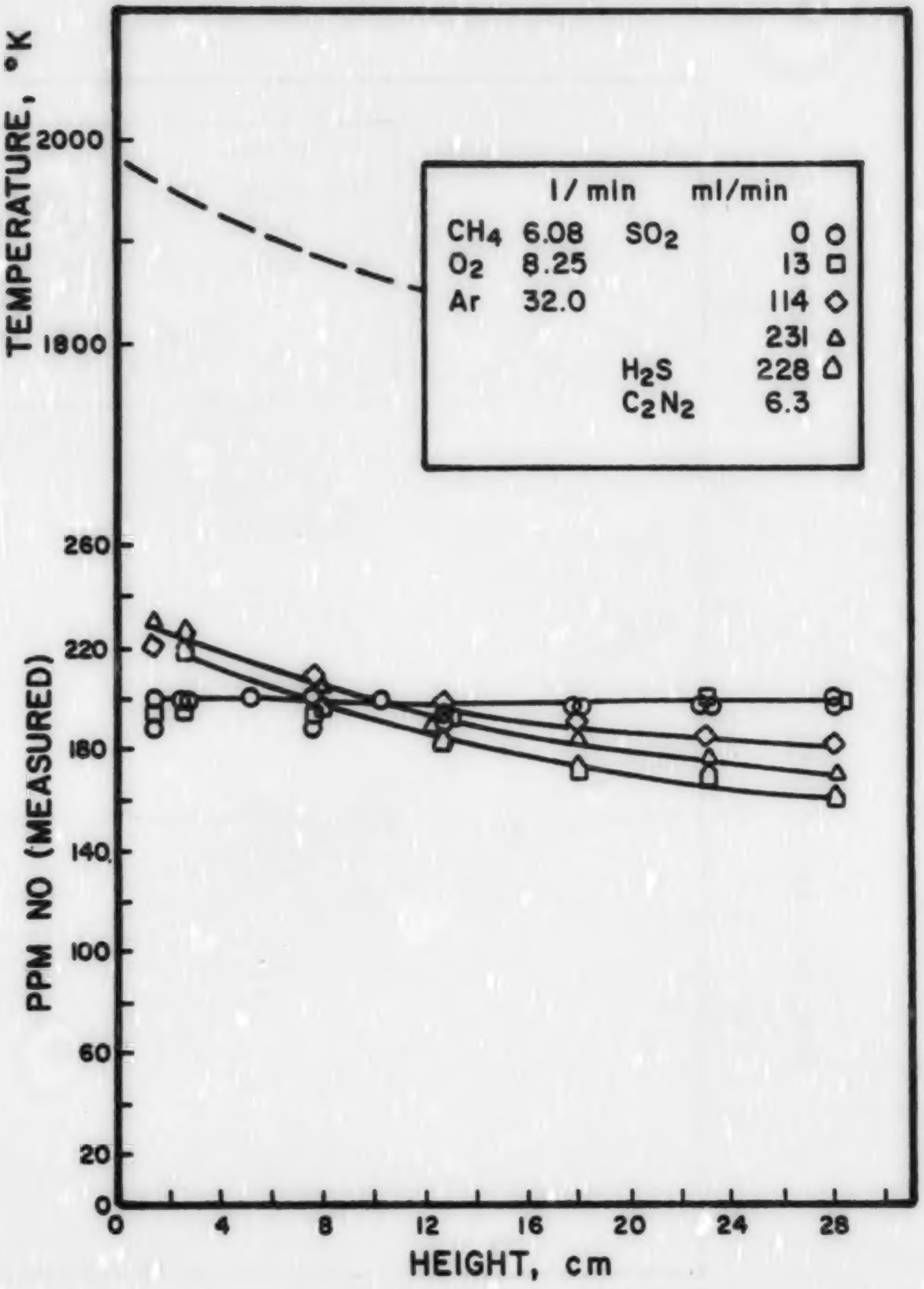

Figure 11: Laminar Premixed Flame: Stoichiometric Ratio 0.68 (0.21% fuel N, 100% conversion ≈ 300 ppm, 1cm ≈ 4.47 at 1980°K)

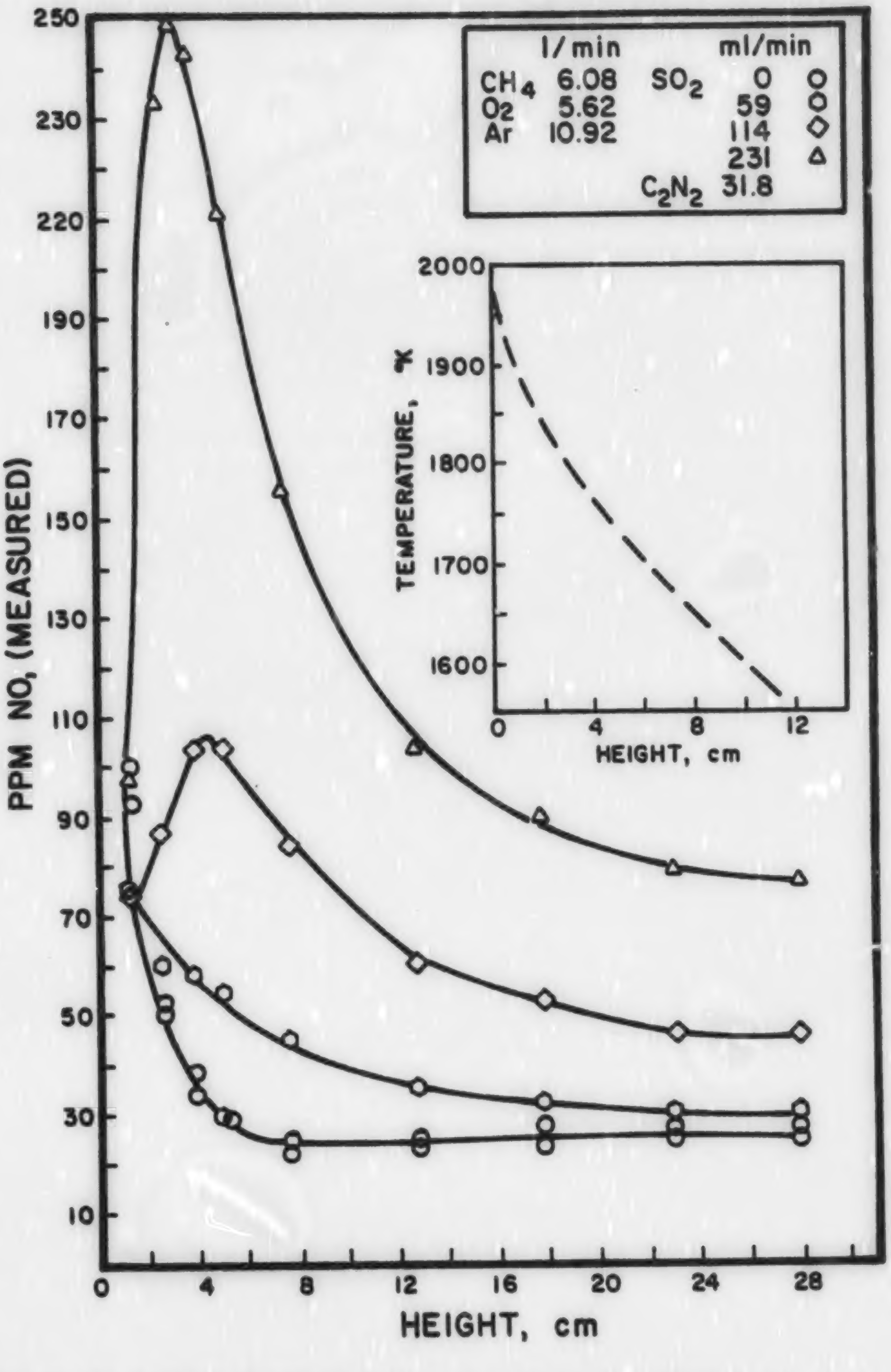

Figure 12: Laminar Premixed Flame: Stoichiometric Ratio 0.46 (1.05% fuel N, 100% conversion ≈ 2793 ppm, 1cm ≈ 7.40 ms at 1970°K)

CHEMICAL REACTIONS IN THE CONVERSION OF FUEL NITROGEN TO NO_x: LOW-PRESSURE FLAT-FLAME BURNER STUDIES

By:

D. R. Kahn and A. E. Axworthy
Rockwell International/Rocketdyne Division
Canoga Park, California 91304

Preceding page blank

ABSTRACT

The objective of this study is to use a low-pressure, premixed, flat-flame burner as a tool for investigating the mechanism and kinetics of the chemical reactions that are involved in the formation of NO_x in the combustion of fossil fuels or alternate fuels derived from fossil fuels. A detailed probing study of a CH_4-O_2-N_2 flame at 0.1 atm was conducted with the addition of 50 ppm of NH_3 or HCN to the feed gas. These additives were used to simulate the expected products of preflame reactions of the fuel nitrogen species that are contained in coals and residual fuel oils (mainly heterocyclic aromatic compounds). An experimental procedure was developed that permitted NO, NO_2, NH_3, and HCN to be measured independently below, in, and above a low-pressure flame.

The methane flame experiments were carried out under fuel-rich ($\phi = 1.5$) and fuel-lean ($\phi = 0.8$) conditions at a diluent ratio of 0.7 with and without the addition of NH_3 or HCN. The formation of "thermal" NO_x from N_2 (via both the Zeldovich and "prompt" paths) was compared directly with the formation of "fuel" NO_x from the added NH_3 or HCN. In all cases, thermal (prompt) NO and fuel NO formed very rapidly at approximately the same location just above the top of the luminous zone, and the amounts formed were approximately additive. In fuel-rich flames, both prompt NO and fuel NO appeared to form almost exclusively via HCN as an intermediate.

In a similar study of NO_x formation in the fuel-rich flame of a simulated low-Btu fuel (a mixture of hydrogen and carbon monoxide), NO formed from added NH_3 in high yield but more than one-half of this NO was consumed just above the luminous zone. Only 20% of added NO was consumed in the absence of added NH_3.

Preceding page blank

INTRODUCTION

This work is part of an experimental and analytical research program which is being conducted to provide information on fuel decomposition and flame reactions required for the development of a complete understanding of the chemical phenomena involved in the conversion of fuel-nitrogen to NO_x. The program extends the fuel pyrolysis and flame studies previously carried out in this laboratory (Ref. 1 and 2). Task 1 consists of experimental studies of the types of chemical reactions fuel nitrogen species can undergo as the fuel decomposes in the early (preflame) stages of combustion. Low-pressure, flat-flame burner studies are being conducted under Task 2 to investigate the mechanism and kinetics involved in the conversion of fuel-nitrogen intermediates (such as NH_3 and HCN) to NO_x in the combustion of fossil fuels or alternate fuels derived from fossil fuels. Under Task 3, the combustion data for the conversion of fuel nitrogen to NO_x are being analyzed in terms of the chemical mechanisms and physical processes involved.

The present paper summarizes recent effort completed under Task 2, Combustion Kinetics. Following a description of the flat-flame burner apparatus and a brief discussion of the pertinent experimental techniques, the results obtained in two series of detailed flame probing studies will be presented. The first study involved the comparison of "fuel" NO_x and "thermal" NO_x formation in the CH_4-O_2-N_2 flame system (0.1 atm) at fuel-rich (equivalence ratio, ϕ, of 1.5) and fuel-lean ($\phi = 0.8$) conditions using NH_3 and HCN as additives. The second study is concerned with fuel NO_x formation in a simulated low-Btu gas flame system of H_2, CO, O_2, and Ar (0.066 atm) at fuel-rich conditions ($\phi = 1.4$) to which NH_3 or NO has been added.

DESCRIPTION OF THE EXPERIMENTAL APPARATUS

The design of the flat-flame burner employed in the combustion kinetics experiments is depicted in Fig. 1, and a schematic of the overall burner system is shown in Fig. 2A.

The water-cooled, stainless-steel burner is 5.72 cm in diameter, and can be positioned vertically with a precision of better than 0.01 mm with a

Preceding page blank

micrometer-driven translation stage. A stainless-steel sintered porous plate 3.2 mm (1/8 inch) thick cemented in a recess at the burner exit furnishes a flat velocity profile across the port. An 8-mesh, stainless-steel screen spot-welded to the top of the burner port serves as a flame holder. The burner and igniter are enclosed in a Pyrex glass chamber so that a pressure of 0.1 atm or less can be maintained to spread the flame and permit more detailed probing.

An uncooled quartz microprobe is used to remove gas samples from the flame reaction zone along the centerline of the burner. The reacting gases are quenched aerodynamically by expanding them from the reaction chamber pressure (50 to 76 torr) to about 1 torr. The microprobe was constructed from 9 mm quartz tubing drawn to a very small-diameter tip containing the sonic sampling orifice. The diameter of the sonic orifice was between 75 and 100 microns, while a taper of approximately 30 degrees was used to ensure minimum flow disturbance occurring upstream of the probe as a result of gas sampling (Ref. 3).

Temperature measurements were performed along the centerline of the flame with a 3-mil Pt/Pt-10% Rh thermocouple coated with a 2- to 3-micron thick layer of Al_2O_3 using a high-vacuum sputtering technique. The thermocouple probe itself consisted of 10-mil thermocouple wire support arms of Pt and Pt-10% Rh strung through a two-hole alumina tube held in place with Sauereisen cement.

The inlet feed gases CH_4 or H_2/CO, O_2, and N_2 or Ar are metered with critical flow orifices. The flow system is similar to that reported by Anderson and Friedman (Ref. 4). The fuel-nitrogen additives (NH_3, HCN, and NO), and the purge gas flowing along the annular region of the burner chamber, are metered with Brooks flowmeters.

GAS ANALYSIS PROCEDURES

Gas samples withdrawn from the flame are analyzed for the mole fraction of stable species using two different techniques--mass spectrometry and chemiluminescent analysis. The major stable species (CH_4, CO, CO_2, O_2, H_2, N_2, or Ar) are measured by mass spectrometry using a batch gas-sampling procedure.

An on-line sampling technique using a Thermo Electron Corp. (TECO) Model 10A chemiluminescent analyzer (CA) enables the nitrogen species NO, NO_2, NH_3, and HCN to be determined by converting them to NO (as described later). The CA was modified to operate with on-line sampling by bypassing its capillary flow metering system and using the sonic sampling orifice at the tip of the quartz microprobe to regulate the gas sample flow to the CA reaction chamber. The pressure in the CA reactor with no sample feed was reduced to 0.8 torr by lowering the ozone feed rate. With sample feed, the CA reactor pressure is maintained between 0.9 to 1.1 torr, depending on the diluent chosen and other flow conditions. Under the conditions employed, the photon emission rate is directly proportional to the product of the NO concentration and the sample flowrate. Over the range of sample feed rates employed, the CA reaction chamber pressure remains nearly constant. Because the sample flowrate is small, the composition of the sample does not have an appreciable effect on the sensitivity of the CA.

Contained within the TECO CA is a stainless-steel catalytic converter for converting NO_2, NH_3, and HCN to NO. A small flow of O_2 is added to the sample just before it enters the TECO CA. This added O_2 is used in all experiments in which fuel-rich conditions are employed. The purpose of the O_2 is to ensure that the gas sample is overall oxidizing in composition to prevent catalytic removal of NO in the stainless-steel converter. A modular molybdenum catalytic NO-NO_x converter unit (and a temperature regulator) also manufactured by TECO is used to convert only NO_2 to NO. At 800 C under overall oxidizing conditions, the conversion of $NH_3 \rightarrow NO$ in the stainless-steel converter is 100% over the full range of concentrations employed in these studies (0 to 2800 ppm NH_3). The conversion efficiency for HCN → NO at these same conditions is dependent on the HCN concentration, decreasing from 100 to approximately 80% for the range 80 to 2500 ppm.

Since the system of catalytic converters only permitted the sum of NH_3 and HCN to be determined, a selective chemical trapping agent (Cosorb, manufactured by Mallinckrodt) can be introduced into the gas sampling line upstream of the catalytic converters to remove HCN quantitatively while allowing the NH_3 to pass through the absorbent bed. The Cosorb solid reagent also removes NO_2 quantitatively and removes a minor amount of NO.

The procedure used to uniquely determine the concentrations of NO, NO_2, NH_3, and HCN in the sample that is flowing continuously from the probe is shown schematically in Fig. 2B. The sample (at a pressure of 1 torr) is passed through each of the four paths shown, and the concentration of NO in the gas reaching the reaction chamber of the CA is measured in each case. Individual species are obtained from the appropriate differences in the amount of NO measured. The amount of NO in the sample is determined first without the use of either converter or the chemical trap, path (1). In path (2), the moly converter converts only NO_2 to NO, and the amount of NO measured is equal to (NO) + (NO_2) in the sample. The stainless-steel converter converts all of these nitrogen species to NO, so the (NO) from path (4) is equal to (NO) + (NO_2) + (NH_3) + E(HCN) in the sample where E is the efficiency of HCN conversion in this converter. In path (3), the HCN and NO_2 are removed in the chemical trap before the sample passes through this converter, giving a measure of (NO) + (NH_3) in the sample. The species concentrations are essentially calculated from these four measurements by solving four equations with four unknowns. It should be noted that any nitrogen-containing free radicals present in the flame gases as they enter the sampling probe will be measured also if they form NH_3 or HCN in the probe. If they form N_2 they will not be measured.

CH_4-O_2-N_2 FLAME STUDIES: FUEL-RICH FLAMES

The purpose of this series of experiments with a CH_4-O_2-N_2 flame was to investigate the mechanism and rate of thermal NO_x formation under fuel-rich conditions and to compare directly thermal and fuel NO_x formation under identical conditions. Three detailed probing experiments (No.'s 2, 3, and 6) were carried out at an equivalence ratio (ϕ) of 1.5, a diluent ratio (DR)* of 0.7, a total pressure (P_T) of 76 torr, and an inlet gas feed rate ($\overline{F}_T$) of 7520 cm^3/min (STP). The reactants in experiment 2 contained no additive and, therefore, all of the

---

*The diluent ratio is defined as

$$DR \equiv \frac{\text{Diluent}/O_2}{(N_2/O_2)_{air}}$$

NO formed from N_2 or from species formed from N_2. In experiments 3 and 6, 50 ppm NH_3 and 50 ppm HCN, respectively, were added to investigate the interactions, if any, between the reactions that form thermal NO and those that form fuel NO.

The temperature profile measured along the axis of the burner (corrected for radiation) from experiment No. 2 is shown in Fig. 3A, and is typical of all the temperature profiles obtained under these fuel-rich conditions. The temperature rises rapidly below and through the luminous zone region, reaches a maximum just above the luminous zone, and thereafter decreases gradually which axial distance. This almost linear decrease beyond the maximum temperature point is attributed mainly to flame radiation losses*, although some gradual mixing of the outer, cooler purge gas with the inner core of hot combustion gas may occur far above the flame front. In these three fuel-rich experiments, the luminous zone extended between about 3.5 and 5.5 mm above the top of the burner, with the maximum temperature of about 2000 K occurring at 7.6 mm.

In experiment No. 3, the mole fractions of the major reactant and product species (CH_4, O_2, H_2, CO, CO_2, N_2, and H_2O) were determined as a function of distance above the burner using mass spectrometry. The mass spectrometric analysis determines the concentrations of the species CH_4, O_2, H_2, and CO_2 relative to the sum of CO + N_2. The CO and N_2 cannot be measured separately in a low-resolution mass spectrometer because they have the same molecular weight, and masses of the lower-molecular-weight fragments formed are not unique in these two species. The partial pressure of water vapor also cannot be measured accurately because of its affinity for surfaces. The CO concentrations were set equal to the amount required to balance the C/N ratio of each sample to the C/N ratio in the reactants, while the concentration of H_2O in each sample was adjusted to balance the H/N ratio to that of the reactants. The major species mole fraction profiles for the fuel-rich flame, calculated using this procedure, are plotted in Fig. 3B.

The calculated H_2O concentration are not shown in Fig. 3B; the H_2O begins to increase just above 3 mm and levels off at 19 mole percent at about 5.5 mm. The theoretical final concentration of H_2O is 20.5%, indicating that the H_2

---

*Calculations are being carried out to verify this assumption.

balance is quite good. The predicted equilibrium concentrations of CO and CO_2 at this temperature are 10.5 and 4.9%, respectively. This is in fair agreement with the measured values at 8 mm of 8.5 and 5.7% (Fig. 3B).

The concentrations of O_2 and CH_4 measured in an unburned sample of reactants are plotted at the left side of Fig. 3B (X = 0). These are in good agreement with the metered concentrations denoted as O_2^o and CH_4^o.

Because H_2 diffuses so rapidly, its concentration profile is quite flat. It can be seen that H_2 formed in the flame front diffuses upstream toward and possibly through the screen flame holder. The H_2 concentration is nearly 4% at the first data point which is only 0.6 mm above the top of the screen (the screen extends from 0 to 1.1 mm on the assigned distance scale). This is in agreement with the predictions of preliminary kinetic-diffusion flame model calculations that have been carried out.

A plot of the species flux provides more information since it takes into consideration the diffusion of each species and gives a more precise indication of the exact location at which species are forming and disappearing. Following the one-dimensional flow model presented in Ref. 1 and 2, measuring the slopes of the mole fraction profiles at selected points and knowing the gas temperature profile enabled the molar flux profiles to be calculated. It can be seen from Fig. 3C that the CH_4 and O_2 react in the luminous zone, as expected, and that the CO and H_2 also form in this region. The slowest reaction involving the major species is the oxidation of CO to CO_2.

THERMAL NO FORMATION IN FUEL-RICH CH_4-O_2-N_2 FLAME

The NO mole fraction profile measured in experiment 2 is plotted in Fig. 4A. This fuel-rich methane flame contained no additive. Little NO is present in the luminous zone, and the maximum NO mole fraction of about 50 ppm is not reached until beyond 30 mm above the burner where the temperature has dropped more than 100 degrees from its maximum value. Also plotted in Fig. 4A are the calculated equilibrium NO values for these conditions. Fenimore (Ref. 5) had obtained a correlation in ethylene flames that indicated that the amount of prompt NO formed in very rich flames was approximately equal to the amount of

NO that would form at chemical equilibrium. Since our NO profile does not have the shape obtained by Fenimore, it is not possible to separate prompt NO, but the total NO is greater than the equilibrium NO. The calculated equilibrium NO is fairly temperature sensitive under these conditions, doubling every 68 degrees. Thus, if the measured temperatures were low by 70 degrees for some reason, the measured NO would not exceed the equilibrium values. Even if the measured temperatures were in error by this amount (which is unlikely), the fact that the NO profile continues to increase in the region where the temperature is decreasing establishes that our NO yield is not limited by chemical equilibrium.

Plotted in Fig. 4B on an expanded distance scale are the measured mole fractions of HCN, NO, and NO_2. The HCN, formed in this flame from the reaction of N_2, reaches a maximum mole fraction of 35 ppm just above the top of the luminous zone.

Using the temperature profile and the mole fraction plots for NO, NO_2, and HCN, the molar flux profile for each of the fuel nitrogen species was calculated. The NO and HCN flux profiles are plotted in Fig. 4C and on an expanded distance scale in Fig. 5D where they are compared with the results of experiment 3 that will be discussed later. As shown in Fig. 4C and 5D, most of the NO forms well above the luminous zone where the HCN is disappearing. Less than 20% of the NO has formed at the point of maximum temperature where the HCN flux has reached its maximum. The maximum HCN flux is 75% of the maximum NO flux. More than one-half of the HCN appears to form in the luminous zone.

The fact that the maximum measured HCN flux is only 75% of the maximum NO flux does not preclude the possibility that all of the NO forms via an HCN intermediate under these conditions. The reason for this is that HCN is probably being both formed and consumed in some regions of the flame. If the 10 to 20% of the NO that forms below the point of maximum HCN flux forms from HCN, this amount of HCN will not contribute to the maximum HCN flux. Likewise, any HCN that is formed after this maximum is reached will not contribute to the maximum value. At the point of maximum HCN flux, the rates of HCN formation and consumption are equal. It is unlikely, therefore, that HCN only forms below the point where this maximum occurs and is only consumed above this point. The decrease in the

HCN flux between 7 and 19 mm is about 90% of the increase in the NO flux in that region, and some HCN undoubtedly forms in that region also. The rate of NO formation at 12.5 mm is 83% of the rate of HCN decay, suggesting that HCN is the principal intermediate in that region.

The NO_2 flux profile is not plotted but, as expected from the NO_2 mole fractions in Fig. 4B, the flux increases from zero at 4.5 mm to a maximum of 1×10^{-9} at 5.6 mm and then decays rapidly.

Discussion of Results: "Prompt" NO Formation

Fenimore (Ref. 5) observed that in fuel-rich hydrocarbon-air flames at 1 atm a rapid transient formation of NO occurs in the "primary reaction zone" followed by the slower formation of additional NO in the post-flame gases. He termed the initial rapidly formed NO "prompt NO" and, since the slow rate observed in the post-flame gases agreed with that predicted by the well-known Zeldovich mechanism ($O + N_2 = NO + N$, etc.), concluded that prompt NO forms by some other mechanism. He proposed reactions such as:

$$CH + N_2 = HCN + N \tag{1}$$

$$C_2 + N_2 = CN + CN \tag{2}$$

Bauer (in the discussion at the end of Ref. 5) cited data that indicates that attack on N_2 by C_1 and C_3 are more likely reaction paths.

Sarofim and Pohl (Ref. 6) studied NO formation in premixed methane-air flames at equivalence ratios (ϕ) from 0.89 to 1.15. They found that the peak rates of NO formation in the "flame zone" were 1 to 2 orders of magnitude greater than in the post-flame zone. They claim that even the peak rates they observed are in agreement with Zeldovich kinetics when the free radical concentrations are derived from the concentration of stable species by use of partial-equilibrium assumptions for the fast-flame reactions. Unfortunately, they did not carry their study to more fuel-rich conditions. In the discussion at the end of Ref. 6, Eberius pointed out that the prompt NO effect is greater at $\phi = 1.32$, and that he observed HCN at the ppm level under these conditions.

Iverach et al. (Ref. 7) showed that in ethylene-air flames, for example, the Zeldovich mechanism could not reasonably account for the rapid early rate of NO formation above an equivalence ratio of about 1.15 (cf. Fig. 8 of Ref. 7).

Their results at $\phi = 1.4$ would require the oxygen atom concentration to be about 3000 times its equilibrium value.

Perhaps the strongest evidence that much of the NO forms via a non-Zeldovich mechanism in fuel-rich premixed flames are the recent observations that considerable HCN forms as a measurable intermediate under these conditions. Bachmaier et al. (Ref. 8) found that in their propane-air flame at $\phi = 1.1$ HCN reaches a concentration of 12 ppm about 5 mm above the burner, and then reacts completely. The yield of prompt (and total) NO is 60 ppm. At $\phi = 1.5$, however, the measured HCN reaches 23 ppm at 15 mm and remains unchanged to the last measurement point at 45 mm, while the amount of NO formed is less than 10 ppm under this condition. Haynes et al. (Ref. 9) measured up to 250 ppm HCN in acetylene-air flames at $\phi = 1.95$, but obtained less than 3 ppm HCN from their methane flames. Morley (Ref. 10) found that HCN formed from N_2 in the reaction zone of rich hydrocarbon flames, the amount being roughly proportional to the N_2 concentration but not very dependent on the type of fuel (CH_4, C_2H_4, or C_2H_2) or on the temperature (between 2000 and 2560 K). The amount of HCN formed was strongly dependent upon equivalence ratio and increased as the flame became richer. The thermal HCN subsequently reacted completely within the flame, in part to NO. At an equivalence ratio of 1.58 in an atmospheric-pressure CH_4-air flame at 2560 K, Morley obtained a peak HCN mole fraction of 71 ppm with a resultant prompt NO formation of 102 ppm, i.e., $[HCN]_{max}/[NO]_{prompt} = 0.70$. This ratio is identical to that obtained in experiment 2 of this study: $[HCN]_{max}/[NO]_{max} = 35/50 = 0.70$.

The thermal NO flux profile obtained in experiment 2 (Fig. 4C) can be used to determine accurately the maximum rate of NO formation in this fuel-rich flame, and a comparison can be made to the rate predicted by the Zeldovich mechanism at these same flame conditions. Ignoring the slight surge of NO at the top of the luminous zone (Fig. 5D), the maximum rate of NO formation occurs between 6 and 9 mm on the assigned distance scale and has a value of 1.5×10^{-8} mol/cm^3-sec. The temperature is 1991 K in this region. The mole fraction of N_2 is 0.54, while the calculated equilibrium oxygen atom mole fraction is 4.0×10^{-6}. Using Baulch's rate expression (Ref. 11) of

$$k = 7.6 \times 10^{13} \exp(-38{,}000/T), \ \text{cm}^3/\text{mol-sec}$$

for the reaction $O + N_2 \rightarrow NO + N$, then

$$d(NO)/dt = 2k\ (O)(N_2) = 6.2 \times 10^{-13}\ \text{mol/cm}^3\text{-sec}$$

Although the NO flux curve in Fig. 4C does not have the typical prompt NO shape, it is indeed "prompt" NO since the maximum rate of formation exceeds the predicted Zeldovich rate (assuming equilibrium O atom) by a factor of 2.4×10^4. The apparent NO decay beyond 35 mm is a result of the gas temperature dropping rapidly beyond the point of maximum temperature, and some mixing of purge gas into the central flame region beyond 30 mm above the burner.

NH_3 ADDITION TO A FUEL-RICH CH_4-O_2-N_2 FLAME

Shown in Fig. 5A through 5D are the mole fraction and molar flux profiles for experiment 3 with 50 ppm NH_3 added to the conditions employed in experiment 2. Only a relatively small difference existed between the temperature profiles measured in experiments 2 and 3.

The thermal NO mole fraction curve from experiment 2 is plotted in Fig. 5A for comparison. The addition of 50 ppm NH_3 (0.026 wt % N in fuel) increased the maximum NO mole fraction from 49.2 to 90.5 ppm, indicating an 83% yield of NO from the added NH_3 (assuming that the yields of thermal NO and fuel NO are purely additive). The maximum NO flux (Fig. 5C) increased from 11.0×10^{-9} to 20.0×10^{-9} for an added NH_3 flux of 10.0×10^{-9}. The conversion of NH_3 to NO is, therefore, 90% based on maximum fluxes.

In Fig. 5D the HCN and NO fluxes from experiments 2 and 3 are compared. The HCN flux peaks at the same distance above the burner in each case, and the HCN begins to form rapidly just below the top of the luminous zone in each. It can be seen that the addition of NH_3 at a flux of 10.0×10^{-9} increases the maximum HCN flux by 11×10^{-9}, indicating that most of the NH_3 is converted to HCN under these conditions and the HCN then forms NO.

HCN ADDITION TO A FUEL-RICH CH_4-O_2-N_2 FLAME

In experiment 6, 50 ppm (nominal) HCN (0.026 wt % N in fuel) was added to the conditions used in experiment 2. Thus, the conditions in experiments 6 and 3 were identical except for the substitution of HCN for NH_3 as the fuel nitrogen additive. The temperature profile obtained in this experiment agreed fairly well with that measured in experiment 2, with the position of the luminous zone and the maximum temperature point occurring at virtually the same location. The maximum temperature measured in experiment 6 was 2040 K compared to 1992 K in experiment 2. The two profiles differ by approximately 40 to 50 K over the entire range of the measurement (2.0 to 77.0 mm).

The mole fraction profiles for the fuel-nitrogen species are plotted in Fig. 6A and 6B together with the thermal NO and thermal HCN profile obtained in experiment 2. The addition of 49.8 ppm HCN increased the maximum NO mole fraction from 49.2 to 82.9 ppm indicating a 68% yield of NO from the added HCN. This assumes that the yields of thermal and fuel NO are purely additive. The NO formed well above the luminous zone where the HCN is disappearing.

Note that the measured HCN mole fraction in experiment 6 initially decreases and reaches a minimum of 42.5 ppm at a point (2.6 mm) where the thermal HCN is also very low, then increases to nearly 60 ppm, indicating the formation of "thermal" HCN. Both the fuel and thermal HCN mole fraction profiles have maximum points above the top of the luminous zone and just below the point where the maximum flame temperature is reached. Using the Cosorb solid trapping agent in conjunction with the stainless-steel converter, NH_3 levels of 0.6 to 1.8 ppm were measured below and in the flame front between 1.8 and 5.0 mm. However, it should be pointed out that these values were obtained by taking small differences between two relatively large numbers and, therefore, must be considered only as approximate.

The molar flux profile for NO obtained in experiment 6 is compared in Fig. 6C with the NO profiles obtained in experiments 2 and 3. Similarly, the HCN molar flux profiles are compared in Fig. 6D for the same three experiments. It can be seen that the maximum NO flux increased from 10.9×10^{-9} to 18.4×10^{-9} mol/cm^2-sec for an added HCN flux of 9.9×10^{-9} mol/cm^2-sec. The conversion of HCN to NO is thus 76% based on maximum fluxes. For comparison, the conversion of NH_3 to NO was determined to be 92% based on maximum fluxes in experiment 3. The NO flux profiles obtained in experiments 2, 3, and 6 are all very similar in shape. The maximum rate of NO formation occurs at a point approximately midway between the top of the luminous zone and the location of the maximum gas temperature. The maximum NO flux occurs at about 35 mm downstream, then decreases slightly.

The HCN flux profile in experiment 6 reaches a maximum at 15.5 x 10^{-9} mol/cm^2-sec at 7.0 mm, just below the maximum temperature point, and thereafter decreases, approaching zero at 20.0 mm downstream. It is likely that more than this amount of HCN forms, since undoubtedly some HCN is reacting before the maximum is reached and some forms beyond the maximum. It can be seen in Fig. 6D that, regardless of the form from which the HCN is obtained, the maximum HCN flux occurs at the same location. The thermal and fuel HCN flux curves decay in a similar manner, as might be expected. Note that the maximum rate of HCN disappearance occurs at approximately the same point as the maximum NO formation rate. In experiment 6 at 7.0 mm, $[d(NO)/dt]_{max}$ was found to be 3.1 x 10^{-8} mol/cm^3-sec, while $[-d(HCN)/dt]_{max}$ was determined to be 2.7 x 10^{-8} mol/cm^3-sec.

Discussion of Results: HCN Oxidation

In a recent publication, Morley (Ref. 10) observed that when various nitrogen compounds (NO, NH_3, CH_3CN, and pyridine) are added to fuel-rich atmospheric-pressure hydrocarbon flames, they are converted quantitatively to HCN in the reaction zone regardless of the type of N-additive. He subsequently studied HCN oxidation within flames between 2300 and 2560 K, and found the rate to be consistent with the following reaction being the rate-limiting step:

$$CN + OH \rightarrow NCO + H \quad \text{(Mechanism A)}$$

A rate expression was derived for this reaction:

$$d\ell n(HCN)/dt = k_{18}\ (H_2O)/(H_2) \cdot 6 \times 10^{25} \lambda^2 \exp(-135{,}000/RT)$$

where λ is a factor which takes into account any disequilibrium in the radical concentrations in the flame, and $k_{18} = 1 \times 10^{-10}$ cm^3/mol-sec. Morley's rate data are plotted in the Arrhenius form in Fig. 7 for equivalence ratios of 2.05, 1.8, and 1.56.

Using the rate data obtained in the present experiment 6 at 7.5 mm downstream ($T = 2040$ K), letting $\lambda = 1$ and

$$(H_2O)/(H_2) = [(H_2O)/(H_2)]_{eq.\ at\ 2040\ K} = 2.11,$$

$$[d\ell n(HCN)/dt](H_2)/(H_2O) = 425$$

at $\frac{1}{T} = 4.90 \times 10^{-4}\ K^{-1}$. If a straight line is drawn approximately through Morley's data points in Fig. 7 for $\phi = 1.56$ between 2000 and 2400 K, the data point calculated above for experiment 6 of this work appears to lie very close to this line. It is suggested that the data points from the lower temperature flames lie above the expected trend because of a superequilibrium of radicals ($\lambda > 1$). Morley proposed an alternate mechanism for HCN oxidation, namely

$$O + HCN \rightarrow NCO + H \quad \text{(Mechanism B)}$$

but the predicted rate for this reaction is too slow to explain the experimental results (Fig. 7).

CH_4-O_2-N_2 FLAME STUDIES: FUEL-LEAN FLAMES

The purpose of these experiments (No. 4 and 5) was to investigate the mechanism and rate of thermal NO formation at fuel-lean conditions and to compare directly thermal and fuel NO formation under identical conditions. Both experiments were carried out with a CH_4-O_2-N_2 flame at $\phi = 0.8$, DR = 0.7, $P_T = 76$ torr, and $\overline{F}_T = 7520$ cc/min at STP. The reactants in experiment No. 4 contained no additive and, hence, all of the measured NO formed from N_2. In experiment No. 5, 54 ppm NH_3 on a total volume basis (0.044 wt % N in CH_4) was added to investigate the interactions, if any, between the reactions that form "thermal" and "fuel" NO.

The flame temperature profile obtained in experiment No. 4 is given in Fig. 8A. The luminous zone extended from 1.8 to 3.0 mm above the burner top, while the maximum temperature of 1953 K occurred at 5.2 mm. The temperature profile measured in experiment No. 5 agreed closely with that in experiment No. 4, the maximum temperature being 1940 K also at 5.2 mm. The temperature profiles were strikingly similar in the vicinity of the luminous zone and differed by only about 30 K at 80 mm downstream.

In these CH_4-O_2-N_2 fuel-lean flames, the mole fractions of the major reactant and product species were also determined as a function of axial distance using mass spectrometry. Following the same computational technique described in the previous section, the mole fraction and molar flux profiles were calculated and are shown in Fig. 8B and 8C for CH_4, O_2, H_2, CO, and CO_2.

The concentrations of O_2 and CH_4 in an unburned sample of reactants are plotted at the left side of Fig. 8B, while the metered concentrations are indicated at $X = 0$. The CH_4 values agree fairly well, while the measured O_2 concentration is about 2% higher than the metered value.

The predicted equilibrium concentration of CO and CO_2 at 1935 K are 0.12 and 9.8%, respectively, which is in good agreement with the measured values at 7.0 mm of 0.25 and 9.5% (Fig. 8B). The measured O_2 concentration at this location is 6.2% compared to the predicted value of 4.8%, but this is not unreasonable considering the measured inlet O_2 concentration. The H_2 mole fraction profile again is seen to be relatively flat, but the measured concentration of 0.70% at 7.0 mm is considerably higher than the calculated equilibrium value of 0.055%.

It can be seen from Fig. 8C that most of the CH_4 consumption and about one-half of the O_2 consumption occurs in the luminous zone. H_2 forms near the top of the luminous zone and then reacts just above this region where the CO is forming. The CO oxidation step again appears to be the slowest reaction involving the major species.

THERMAL NO FORMATION IN A FUEL-LEAN CH_4-O_2-N_2 FLAME

The mole fraction and molar flux profiles for NO and NO_2 in experiment 4 are shown in Fig. 9A through 9C and 10C. The maximum NO mole fraction was determined to be 9.3 ppm (at 47 mm) compared to the maximum NO_2 mole fraction of only 2.7 ppm (at 3.0 mm). It can be shown from Fig. 9C that the maximum rate of NO formation occurs just above the top of the luminous zone, and the NO formed in that region diffuses into the luminous zone and is rapidly consumed. The rate of formation becomes nearly constant just beyond the location of the maximum gas temperature, and eventually becomes zero at about 40 to 50 mm downstream. NO_2 appears to be forming in the luminous zone and the maximum rate of NO_2 disappearance coincides with the maximum NO production rate at a point just above the top of the luminous zone. No HCN or NH_3 formed in these experiments.

Discussion of Results: Thermal NO Formation

Table I compares the rate of NO formation (slope of the NO flux profile) measured at three points along the NO flux curve of Fig. 9C with that predicted by the Zeldovich mechanism, assuming equilibrium oxygen atom concentration. The latter is calculated in the manner described earlier using Baulch's rate expression for the reaction $O + N_2 \rightarrow NO + N$. As can be seen from Table I, the measured rate exceeds the predicted Zeldovich rate (assuming equilibrium oxygen atom concentration) by a factor of 4.6×10^3 at the top of the luminous zone, but decreases to only a factor of 27 at 5.15 mm downstream (i.e., 2 mm above top of luminous zone).

Sarofim and Pohl (Ref. 6) have studied NO formation in a premixed methane-air flame (1 atm) at an equivalence ratio of 0.89 (T_{max} = 2000 K), and observed that the NO mole fraction peaked at approximately 10.5 ppm. This is in good agreement with the maximum NO mole fraction of 9.3 ppm obtained in this study at $\phi = 0.8$ (DR = 0.7, T_{max} = 1953 K). They determined that the peak rates of NO formation, which they observed in the "flame zone" are in agreement with Zeldovich kinetics when the free radicals are calculated from the concentration of stable species using the partial-equilibrium assumptions for the fast-flame reactions. Thus, the experimental data and partial equilibrium calculations of Sarofim and Pohl provide a plausible explanation for the differences in measured versus calculated NO formation rates shown in Table I at fuel-lean conditions, i.e., the presence of excess [O] radicals.

NH_3 ADDITION TO A FUEL-LEAN CH_4-O_2-N_2 FLAME

For comparison, the mole fraction and molar flux profiles for experiment 5 are shown in Fig. 10A through 10D together with the thermal NO profiles obtained in experiment 4. The addition of 54.5 ppm NH_3 to the conditions of experiment 4 increased the maximum NO mole fraction from 9.3 to 60.9 ppm, indicating a 95% yield of NO from the added NH_3 assuming that the yields of thermal and fuel NO are purely additive. The maximum NO_2 mole fraction measured in experiment 5 with NH_3 addition is 6.6 ppm at 1.7 mm (Fig. 10B). However, the trend of the data suggests that more than this amount of NO_2 may have formed in the region near the top of the burner.

From Fig. 10C it can be seen that the maximum NO flux increased from 1.86×10^{-9} to 12.14×10^{-9} mol/cm^2-sec for an added NH_3 flux of 10.87×10^{-9} mol/cm^2-sec. The conversion of NH_3 to NO is thus also 95% based on maximum fluxes. As in experiment 4, the maximum rate of NO_2 formation (Fig. 10D) occurs just below the top of the luminous zone, and the NO_2 reacts rapidly just above the top of the luminous zone.

Figure 10D reveals that the maximum rate of NO formation in experiments 4 and 5 occurred at exactly the same location, namely, 3.2 mm above the top of the burner and just above the top of the luminous zone (3.0 mm). This is in the region where both the NH_3 and NO_2 flux profiles are decreasing rapidly. The NH_3 flux begins to decrease abruptly at the bottom of the luminous zone and finally disappears just beyond the point where the NO flux has reached its maximum value (3.5 to 4.0 mm).

H_2-CO-O_2-Ar FLAME STUDIES: FUEL-RICH FLAMES

There is considerable interest in burning low-Btu gas, which has been obtained from coal gasification processes, in commercial power plants. However, these synthetic gases may contain trace quantities of fuel nitrogen species, such as NH_3, which can be converted to NO_x during combustion. Preliminary calculations reported in the literature (Ref. 12 through 14) have shown that proper combustion design can contribute significantly to reduction of NO_x emissions from low-Btu gas systems and that staging of the combustion process has the potential for reducing NO_x emissions by a factor of 3 or 4. Fundamental kinetic data on the conversion of fuel-nitrogen species in a low-Btu gas system, particularly under fuel-rich conditions, would be very useful in developing combustion models for determining optimum conditions for reducing NO_x emissions from low Btu gas power generation systems. To employ a low-pressure, flat-flame burner system to collect such information, the data should be obtained at flame temperatures which correspond approximately to those measured in real combustor configurations when using low-Btu gas derived from a typical coal conversion process.

The basis for the experimental burner conditions subsequently chosen for the present study came from the recent work by Tyson (Ref. 13), who developed a kinetic model for NO_x emissions in a low-Btu gas combustor, validated the model by comparison with experimental data, and applied this information to idealized combustor configurations for two representative combined cycle systems. In one case, for an advanced-technology, high-temperature gas turbine with a waste-heat boiler, the optimum design for an adiabatic gas generator was found to be a rich ($1.33 < \phi < 1.45$) primary reactor section (200-msec residence time) followed by a gradual mixing of the primary products into the dilution air stream. Using the staged system as opposed to an unstaged system resulted in calculated NO_x emissions reduced by a factor of 4.

The fuel composition employed by Tyson in his gas turbine combustor calculations was that of a typical air-blown Lurgi gas and contained 10.1% H_2O, 19.6% H_2, 13.3% CO, 13.3 CO_2, 5.5% CH_4, 37.6% N_2, and 0.4% NH_3. This value for the NH_3 mole fraction was arrived at by assuming a hot-gas removal process for H_2S (1088 K), and was based on the high-temperature cleanup data reported by Robson (Ref. 15). The fuel gas inlet temperature and the air inlet temperature were 1500 and 1000 F, respectively, while the total pressure was maintained at 10 atm.

The H_2/CO ratio chosen in the present work was set at 1.4 to simulate the H_2/CO ratio found in the low-Btu gas derived from the typical air-blown Lurgi process. Argon was selected initially as the diluent to preclude the possibility of thermal NO_x formation and to permit the CO to be measured mass spectrometrically. From Tyson's conclusions, a fuel-rich condition appeared to be the most interesting for these studies, and an equivalence ratio (ϕ) of 1.4 was chosen. From adiabatic flame temperature calculations at $\phi = 1.4$, it was found that a diluent ratio of 1.9 assigned to the simulated low-Btu gas (H_2-CO-O_2-Ar-NH_3) at 0.1 atm would nearly match the adiabatic flame temperature (2150 K) of the Lurgi-air system at 10 atm.

Preliminary screening experiments with the H_2-CO-O_2-Ar flame system revealed that this fuel burns much differently in a low-pressure burner than does methane. To position the luminous zone above the burner so that suitable detailed probing measurements could be made, the total system pressure was reduced to 50 torr, while the total inlet gas feed rate was increased 17% over that employed in the previous CH_4 flame studies to 8750 cc/mm (STP).

Two experiments were conducted to determine the rate and extent of the conversion of fuel nitrogen species added to a simulated low-Btu fuel flame of H_2, CO, O_2, and Ar. NH_3 was added to the flame in experiment 8 at 2740 ppm on a total feed basis, which is equivalent to 4200 ppm on a Lurgi fuel basis. The conditions utilized in experiment 9 were identical to those employed in experiment 8 ($\phi = 1.4$, DR = 1.9, 50 torr, and 8750 cm^3/min), with the exception that 2230 ppm NO was added as the fuel-N species instead of NH_3 to determine how much of the NO, if any, is consumed as it passes through the flame front.

The temperature profile along with the centerline of the burner (corrected for radiation) obtained in experiment 8 is given in Fig. 11A. The luminous zone extended between 3.3 and 8.2 mm above the top of the burner. The maximum flame temperature of 1857 K ($T_{adiabatic} = 2144$ K) was at 12.9 mm. The detailed probing was performed with a 3-mil Al_2O_3-coated Pt/Pt-10% Rh thermocouple. There was evidence that the thermocouple coating was deteriorating and that some catalytic reactivity of the thermocouple was occurring in the region below and through the luminous zone. If the measured temperatures are somewhat high, the net effect would be to place an upper limit on the N-species mole fraction and molar flux profiles. However, the conclusions drawn from the experiment do not appear to be critically dependent on the accuracy of the temperature measurement.

As in the CH_4 flame experiments, the mole fractions of the major reactant and product species were measured as a function of axial distance using mass spectrometry. The data were reduced to yield the mole fraction and molar flux profiles shown in Fig. 11B and 11C for H_2, CO, O_2, and CO_2. In this analysis, CO was determined directly, since no N_2 was fed initially to the burner, and H_2O was calculated as before by balancing the H/Ar ratio to that of the burner feed.

As expected, H_2 reacts at a much faster initial rate than does CO. Above the top of the luminous zone, however, some H_2 appears to reform. If this small increase in the concentration is real and results from the recombination of H atoms, the H atoms present at 9 mm must have reacted with O_2 in the probe rather than recombining to H_2.

Equilibrium calculations indicated that virtually no O_2 should remain in this fuel-rich system at complete reaction. It was not expected that any O_2 would remain unreacted above the luminous zone in the presence of excess H_2. The kinetic-diffusion calculations that are being carried out will establish what the O_2 reaction rate should be in this region.

NH_3 ADDITION TO A FUEL-RICH H_2-CO-O_2-Ar FLAME

The molar flux profiles for NH_3 and NO in experiment 8 are shown in Fig. 12A and 12B. There was no measurable NO_2 or HCN within the detection limits of the analytical system in either experiment. The added NH_3 (2740 ppm total basis) in experiment 8 appears to have completely reacted by just above the bottom of the luminous zone. The location of the maximum NH_3 decay rate corresponds approximately to the point of initial NO formation. The maximum rate of NO formation is 1.58 x 10^{-6} mol/cm^3-sec and occurs at approximately the same point where the NH_3 flux becomes zero. The maximum NO flux of

4.84×10^{-7} mol/cm^2-sec (76% yield) occurs at a point roughly three-fourths of the distance into the luminous zone. Thereafter the NO is consumed, reaching a minimum near the maximum flame temperature location, and then gradually increases and levels off at 70 mm downstream. The flux at this latter location (3.10×10^{-6} mol/cm^2-sec) corresponds to a NO yield of 49%.

The most interesting feature of the N-species profiles can be found in Fig. 12B where the sum of the NH_3 and NO fluxes are plotted versus distance. Note that at 4.0 mm, only 26% of the initial fuel nitrogen is present in a form which can be measured by the chemiluminescent analyzer/converter system (NH_3, NO, NO_2, or HCN). Obviously there is an undertermined radical species which forms in the flame as an intermediate, and which subsequently can react further to yield either NO or N_2 (but presumably forms mostly N_2 in the probe).

NITRIC OXIDE ADDITION TO A FUEL-RICH H_2-CO-O_2-Ar FLAME

Because much of the NO that forms from the added NH_3 is unexpectedly consumed above the luminous zone and then partially reforms, NO was added in the absence of NH_3 to see how much, if any, is consumed above the luminous zone. With 2230 ppm NO (total basis) added instead of the NH_3, the NO flux profile in experiment 9 (Fig. 12A and 12B) remains relatively constant at its initial value up to about 4.5 mm. The initial decrease in NO flux in experiment 9 corresponds to the point in the luminous zone where the NO formation rate in experiment 8 begins to decrease from its maximum value. In both experiments, the NO flux decreases rapidly near the top of the luminous zone. However, the NO flux in experiment 8 decreases significantly more than in 9. Both curves reach a minimum at the same point (approximately 18 mm) just above the maximum temperature location. It would appear that there are additional free radical species present in the experiment with NH_3 addition which can also promote NO depletion. At least one very long-lived nitrogen intermediate must be involved in experiment 8 because the NO flux continues to increase more than 40 mm above the burner (and the NH_3 additive changes the visible color of the flame at even greater distances), whereas in experiment 9 the NO flux begins to decrease above 40 mm.

SUMMARY AND CONCLUSIONS

Low-pressure flat-flame burner experiments provide an excellent tool for studying the types of reactions that are involved in the formation of NO_x during the combustion of fossil fuels or alternate fuels derived from fossil fuels. In CH_4-O_2-N_2 flame studies at fuel-rich conditions ($\phi = 1.5$), thermal (prompt) NO forms from N_2 via a non-Zeldovich mechanism involving HCN as an intermediate species.

At low levels of fuel nitrogen addition (50 ppm), 90 and 76% yields of NO are obtained from added NH_3 and HCN, respectively. Regardless of the additive type, HCN forms as an intermediate in these flames and the maximum HCN molar flux occurs just above the top of the luminous zone, while most of the NO forms well above this region. The data indicate that the yields of thermal and fuel NO are purely additive. The rate of HCN disappearance agrees with recent data published by Morley (Ref. 10) and suggests that NO formation from HCN proceeds through an oxidized intermediate, such as NCO (cf. mechanism in Ref. 1).

In fuel-lean CH_4-O_2-N_2 flames, thermal NO formation in the flame zone appears to be in agreement with Zeldovich kinetics when the concentrations of oxygen and other free radicals are calculated from the concentration of stable species using the partial equilibrium assumptions for the flat-flame reactions. Adding NH_3 at low concentrations (50 ppm) to this flame results in a 95% conversion to NO (based upon maximum fluxes). From these results, the yields of thermal and fuel NO also appear to be additive.

In a simulated low-BTU gas system of H_2-CO-O_2-Ar at fuel-rich conditions ($\phi = 1.4$), adding NH_3 to the flame (2740 ppm) results in a maximum conversion to NO of 76% near the top of the flame front. The NO is rapidly consumed above this point, reaches a minimum just beyond the point of maximum flame temperature, and thereafter begins to increase gradually. Near the bottom of the luminous zone only one-quarter of the initial fuel nitrogen is in a form that can be measured by the chemiluminescent analyzer/catalytic converter system (NH_3, HCN, NO_2, or NO). There is obviously an undertermined radical species that forms in the flame as an intermediate and subsequently reacts to yield either NO or N_2.

Adding NO to a similar flame under identical conditions to determine whether it too would be consumed in the region just above the luminous zone did not result in the same rapid NO decline. Apparently, there are additional free radical species present when NH_3 is added that can promote NO depletion in the region of the flame just above the luminous zone and can also cause the NO flux to increase far above the burner.

ACKNOWLEDGEMENT

This study was sponsored by the U.S. Environmental Protection Agency under Contract No. 68-02-1886 with G. Blair Martin as the Project Officer. The following individuals have contributed to the technical aspects of this program: V. Dayan, L. Grant, M. Heap, G. B. Martin, W. Nurick, D. Seery, G. R. Schneider, B. Tuffly, and T. Tyson.

REFERENCES

1. Axworthy, A.E., G. R. Schneider and V. H. Dayan, "Investigation of the Chemistry of Fuel Nitrogen Conversion to Nitrogen Oxides in Flames - Final Report", EPA-600/2-76-039, February 1976.

2. Axworthy, A. E., G. R. Schneider and V. H. Dayan, "Chemical Reactions in the Conversion of Fuel Nitrogen to NO_x", Proceedings of the Stationary Source Combustion Symposium, Vol. I, pp 185-216, EPA-600/2-76-152a, June 1976.

3. Fristrom, R. M. and A. A. Westenberg, Flame Structure, McGraw-Hill, New York, 1965.

4. Andersen, J. W. and R. Friedman, "An Accurate Gas Metering System for Laminar Flow Studies," Rev. Sci. Instr., 20, 61 (1949).

5. Fenimore, C. P., "Formation of Nitric Oxide in Premixed Hydrocarbon Flames," Thirteenth Symposium (International) on Combustion, The Combustion Institute, Pittsburgh, pp 373-380, 1971.

6. Sarofim, A. F. and J. Pohl, "Kinetics of Nitric Oxide Formation in Premixed Laminar Flames," Fourteenth Symposium (International) on Combustion, The Combustion Institute, Pittsburgh, pp 739-754, 1973.

7. Iverach, D., K. S. Basden and N. Y. Kirov, "Formation of Nitric Oxide in Fuel-Lean and Fuel-Rich Flames," Ibid., p. 767, 1973.

8. Bachmaier, F. et. al., "The Formation of Nitric Oxide and the Detection of HCN in Premixed Hydrocarbon-Air Flames," Comb. Sci. and Tech. 7, pp. 77-84 (1973).

9. Haynes, B. S., D. Iverach and N. Y. Kirov, "The Behavior of Nitrogen Species in Fuel-Rich Hydrocarbon Flames," Fifteenth Symposium (International) on Combustion, The Combustion Institute, Pittsburgh, p. 1103, 1975.

10. Morley, C., "The Formation and Destruction of Hydrogen Cyanide from Atmospheric and Fuel Nitrogen in Rich Atmospheric-Pressure Flames," Combustion and Flame, 27, pp. 113-121 (1977).

11. Baulch, D. L., D. D. Drysdale and D. G. Horne, *Evaluated Kinetic Data for High Temperature Reactions, Vol. 2: Homogeneous Gas Phase Reactions of the H_2-O_2-N_2 System*, Butterworths, London, (1973).

12. Martin, G. B., "NO_x Considerations in Alternate Fuel Combustion," presented at EPA Symposium; *Environmental Aspects of Fuel Conversion Processes*, Hollywood, Florida, December 14-18, 1975.

13. Tyson, T. J., "Chemical and Physical Limitations on Low BTU Gas Combustor NO_x Emissions," presented at EPA Combustion Research Branch Contractors Meeting, MIT, Cambridge, Mass., August 1976.

14. Heap, M. P., T. J. Tyson, J. E. Cichanowicz, R. Gershman, C. J. Kau, G. B. Martin, and W. S. Lanier, "Environmental Aspects of Low BTU Gas Combustion," presented at the *16th Symposium (International) on Combustion*, MIT, Cambridge, Mass., August 1976.

15. Robsen, F. L., and A. J. Giramonti, "The Environmental Impact of Coal-Based Advanced Power Systems" Symposium Proceedings; *Environmental Aspects of Fuel Conversion Technology*, EPA-650/2-74-118, October 1974, pp. 237-257.

TABLE I. COMPARISON OF EXPERIMENTALLY MEASURED (EXPERIMENT NO. 4) VS CALCULATED NO PRODUCTION RATES

	Measured* Gas Temperature, K	Measured** NO Production Rate, mol/cm^3-sec	Calculated*** NO Production Rate, mol/cm^3-sec	$\frac{R_{meas}}{R_{calc}}$
ΔX = 3.0 to 3.2 mm ● At Top of Luminous Zone	1900	1.16×10^{-7}	2.55×10^{-11}	4550
ΔX = 5.15 mm ● Location of Maximum Gas Temperature	1953	1.59×10^{-9}	5.84×10^{-11}	27
ΔX = 8.00 mm ● Constant NO Formation Rate	1935	3.70×10^{-10}	3.66×10^{-11}	10

*Corrected for thermocouple radiation loss
**See Fig. 9
***Assumes equilibrium concentration of [0]

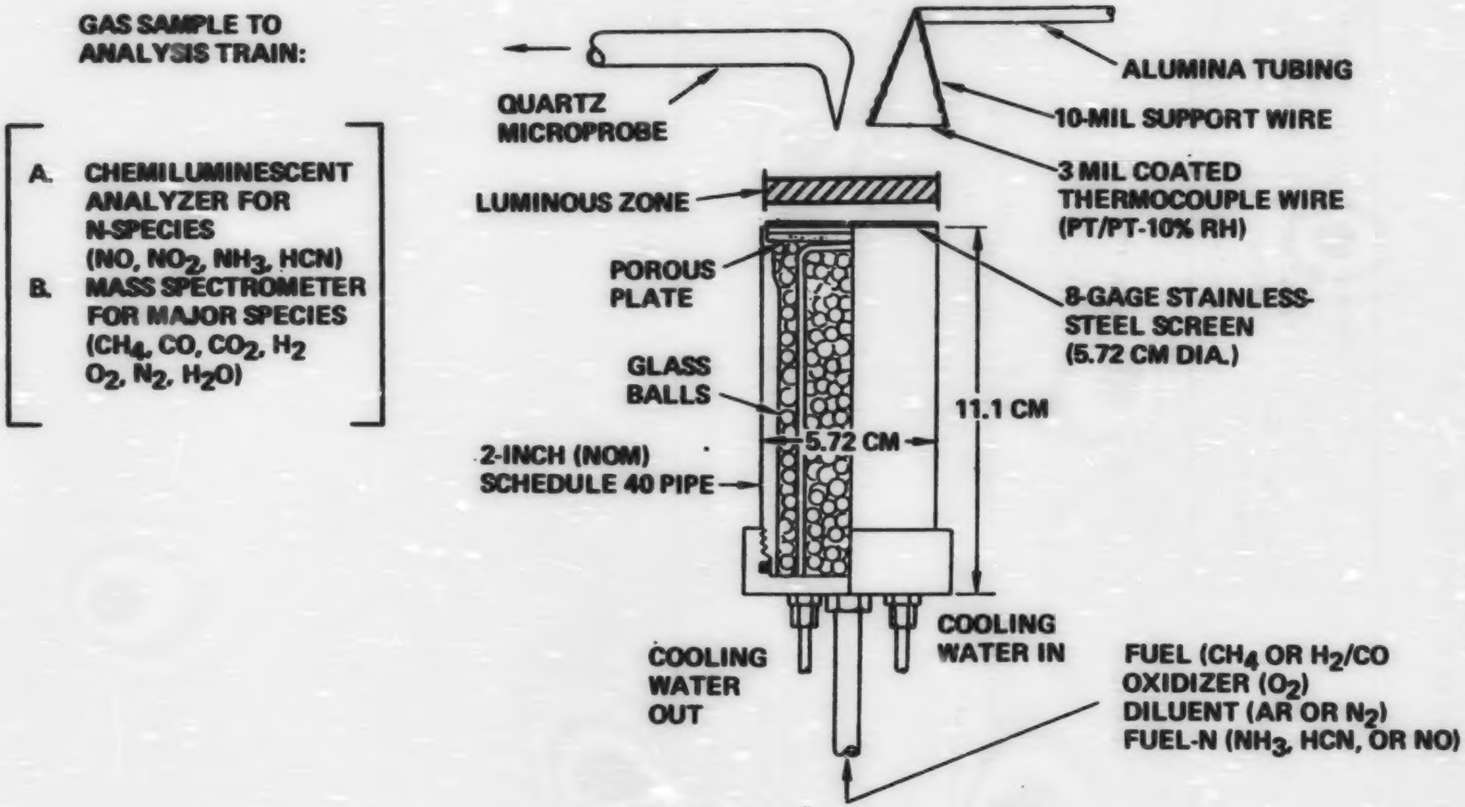
GAS SAMPLE TO
ANALYSIS TRAIN:
A. CHEMILUMINESCENT ANALYZER FOR N-SPECIES (NO, NO_2, NH_3, HCN)
B. MASS SPECTROMETER FOR MAJOR SPECIES (CH_4, CO, CO_2, H_2, O_2, N_2, H_2O)
QUARTZ MICROPROBE
LUMINOUS ZONE
POROUS PLATE
GLASS BALLS
2-INCH (NOM) SCHEDULE 40 PIPE
5.72 CM
11.1 CM
ALUMINA TUBING
10-MIL SUPPORT WIRE
3 MIL COATED THERMOCOUPLE WIRE (PT/PT-10% RH)
8-GAGE STAINLESS-STEEL SCREEN (5.72 CM DIA.)
COOLING WATER OUT
COOLING WATER IN
FUEL (CH_4 OR H_2/CO
OXIDIZER (O_2)
DILUENT (AR OR N_2)
FUEL-N (NH_3, HCN, OR NO)

Figure 1. Design of the Flat-Flame Burner

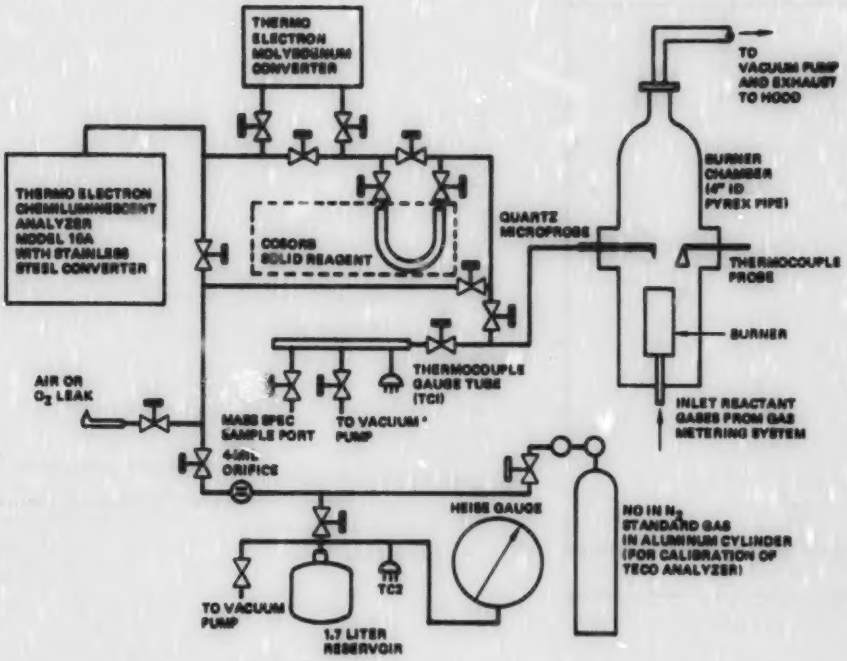
THERMO ELECTRON MOLYBDENUM CONVERTER
TO VACUUM PUMP AND EXHAUST TO HOOD
THERMO ELECTRON CHEMILUMINESCENT ANALYZER MODEL 10A WITH STAINLESS STEEL CONVERTER
BURNER CHAMBER (4" ID PYREX PIPE)
QUARTZ MICROPROBE
COSORB SOLID REAGENT
THERMOCOUPLE PROBE
BURNER
THERMOCOUPLE GAUGE TUBE (TCI)
AIR OR O_2 LEAK
MASS SPEC SAMPLE PORT
TO VACUUM PUMP
INLET REACTANT GASES FROM GAS METERING SYSTEM
4-mil ORIFICE
HEISE GAUGE
NO IN N_2 STANDARD GAS IN ALUMINUM CYLINDER (FOR CALIBRATION OF TECO ANALYZER)
TO VACUUM PUMP
TC2
1.7 LITER RESERVOIR

Figure 2A. Schematic of the Flat-Flame Burner System

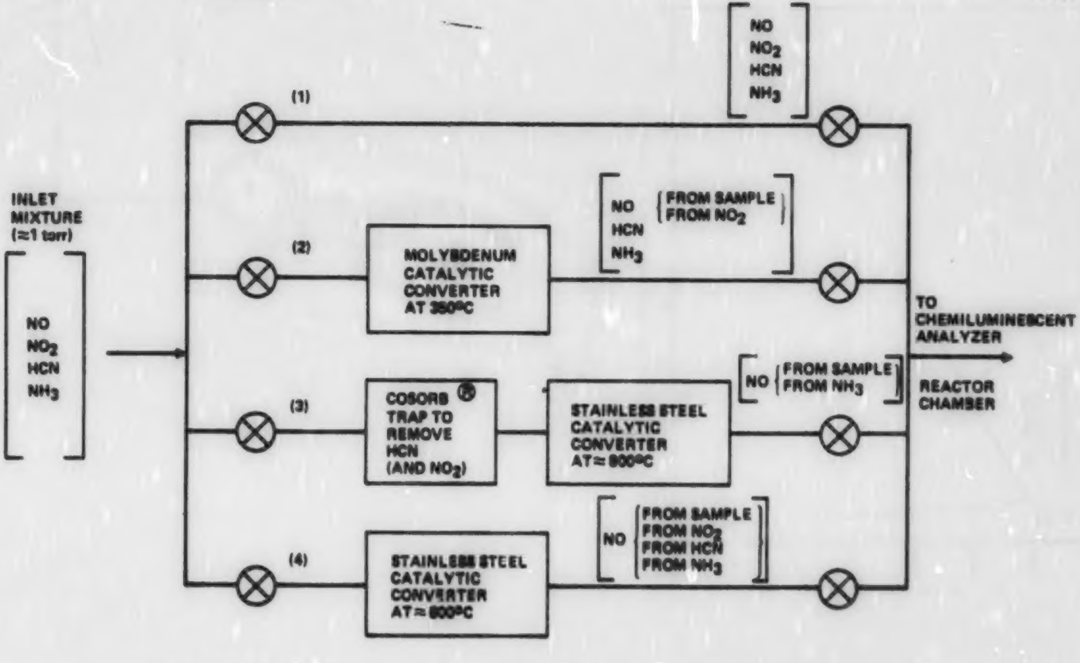
NO
NO_2
HCN
NH_3
(1)
INLET MIXTURE (≈1 torr)
NO
NO_2
HCN
NH_3
(2)
MOLYBDENUM CATALYTIC CONVERTER AT 350°C
NO
HCN
NH_3
FROM SAMPLE
FROM NO_2
TO CHEMILUMINESCENT ANALYZER
REACTOR CHAMBER
(3)
COSORB ® TRAP TO REMOVE HCN (AND NO_2)
STAINLESS STEEL CATALYTIC CONVERTER AT ≈ 800°C
NO
FROM SAMPLE
FROM NH_3
(4)
STAINLESS STEEL CATALYTIC CONVERTER AT ≈ 800°C
NO
FROM SAMPLE
FROM NO_2
FROM HCN
FROM NH_3

Figure 2B. Experimental Scheme for Determination of NO, NO_2, NH_3 and HCN

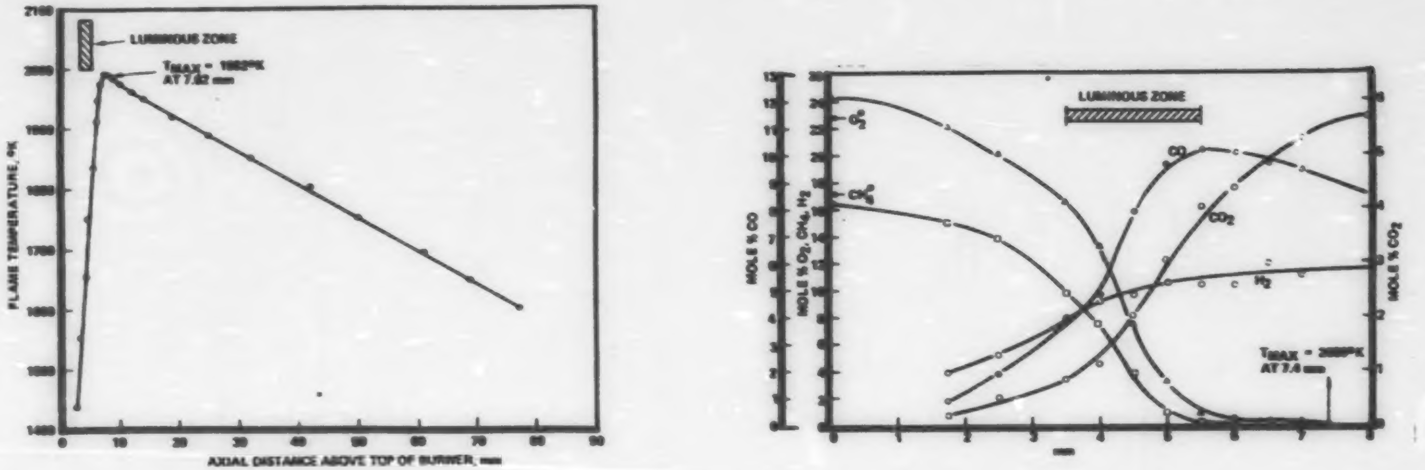

A. FLAME TEMPERATURE VS DISTANCE (EXPT NO. 2)

B. MOLE FRACTION PROFILES OF MAJOR SPECIES (EXPT NO. 3)

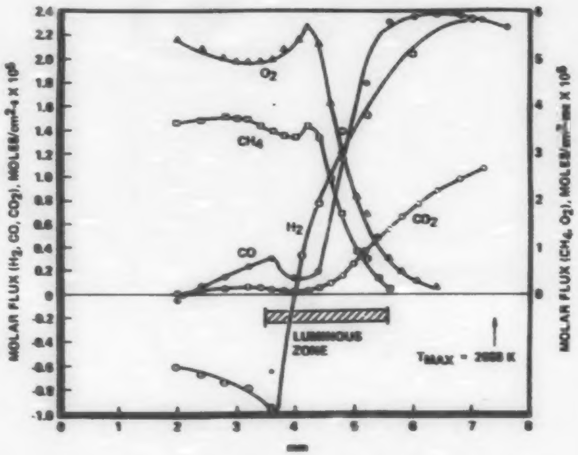

C. MOLAR FLUX PROFILES OF MAJOR SPECIES (EXPT NO. 3)

Figure 3. Fuel-Rich CH_4-O_2-N_2 Flame (ϕ = 1.5, DR = 0.7, P_T = 76 torr, $\overline{F}_T$ = 7520 cc/min at STP)

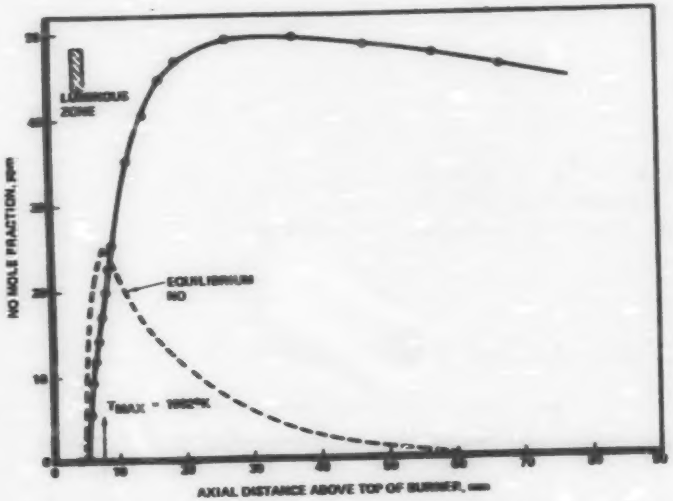

A. NO MOLE FRACTION PROFILE

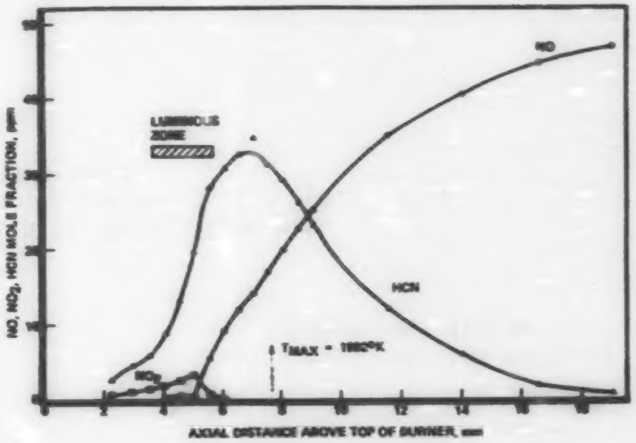

B. N-SPECIES MOLE FRACTION PROFILES

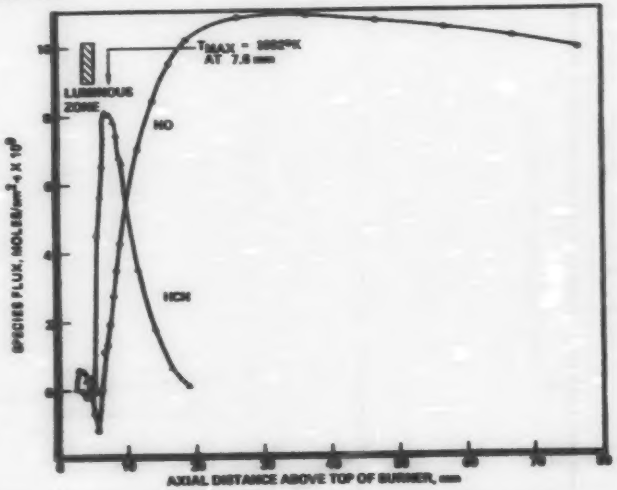

C. N-SPECIES MOLAR FLUX PROFILES

Figure 4. Thermal NO From a Fuel-Rich CH_4-O_2-N_2 Flame - Experiment No. 2
(ϕ = 1.5, DR = 0.7, P_T = 76 torr, $\bar{F}_T$ = 7520 cc/min)

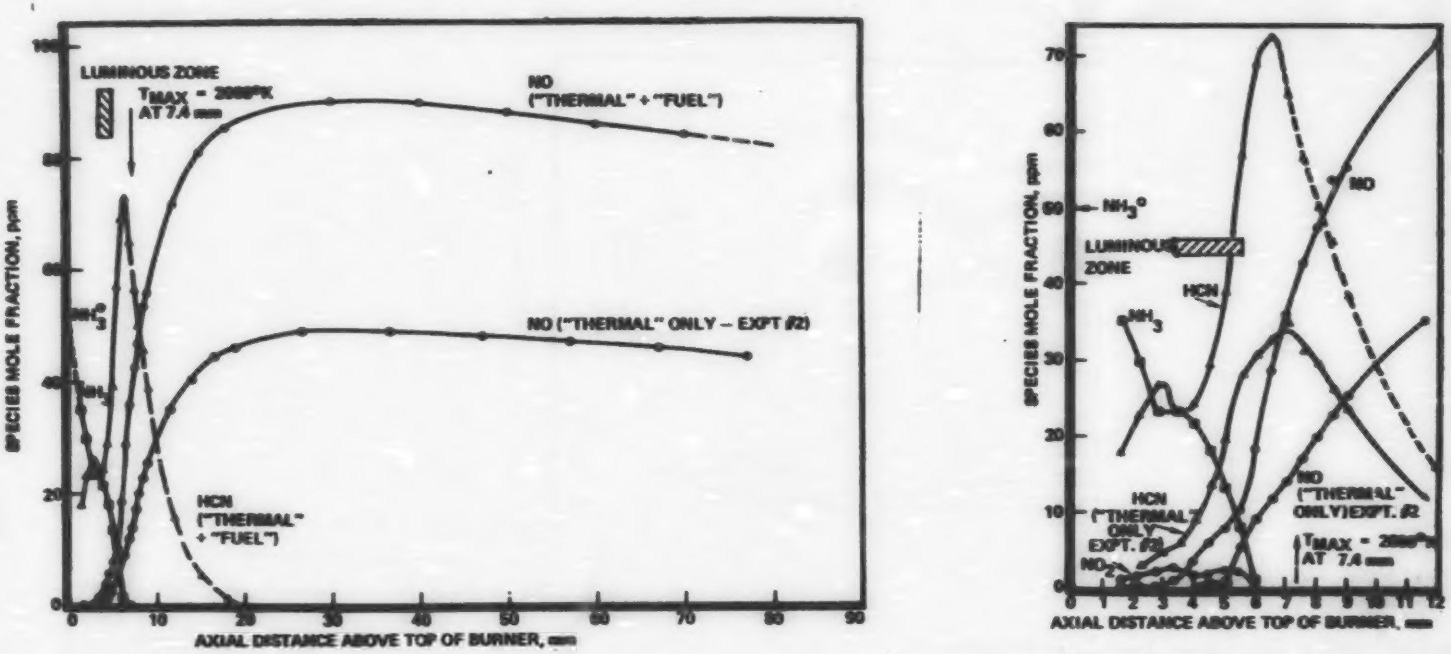

A. N-SPECIES MOLE FRACTION PROFILES

B. N-SPECIES MOLE FRACTION PROFILES IN LUMINOUS ZONE REGION

Figure 5. Thermal and Fuel NO From Fuel-Rich CH_4-O_2-N_2 Flame With 50 ppm NH_3 Added - Experiments No. 2 and No. 3 (ϕ = 1.5, DR = 0.7, P_T = 76 torr, $\bar{F}_T$ = 7520 cc/min)

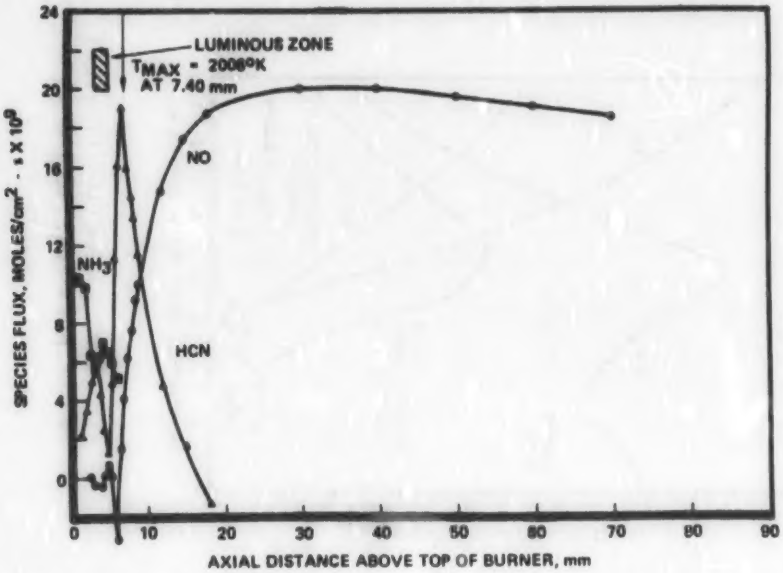

C. N-SPECIES MOLAR FLUX PROFILES

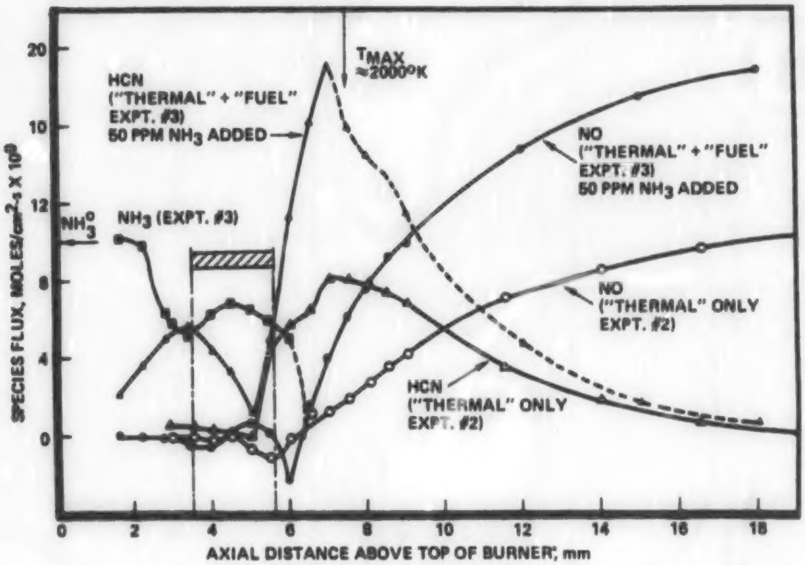

D. COMPARISON OF MOLAR FLUX PROFILES FOR HCN AND NO IN LUMINOUS ZONE REGION

Figure 5. (Concluded)

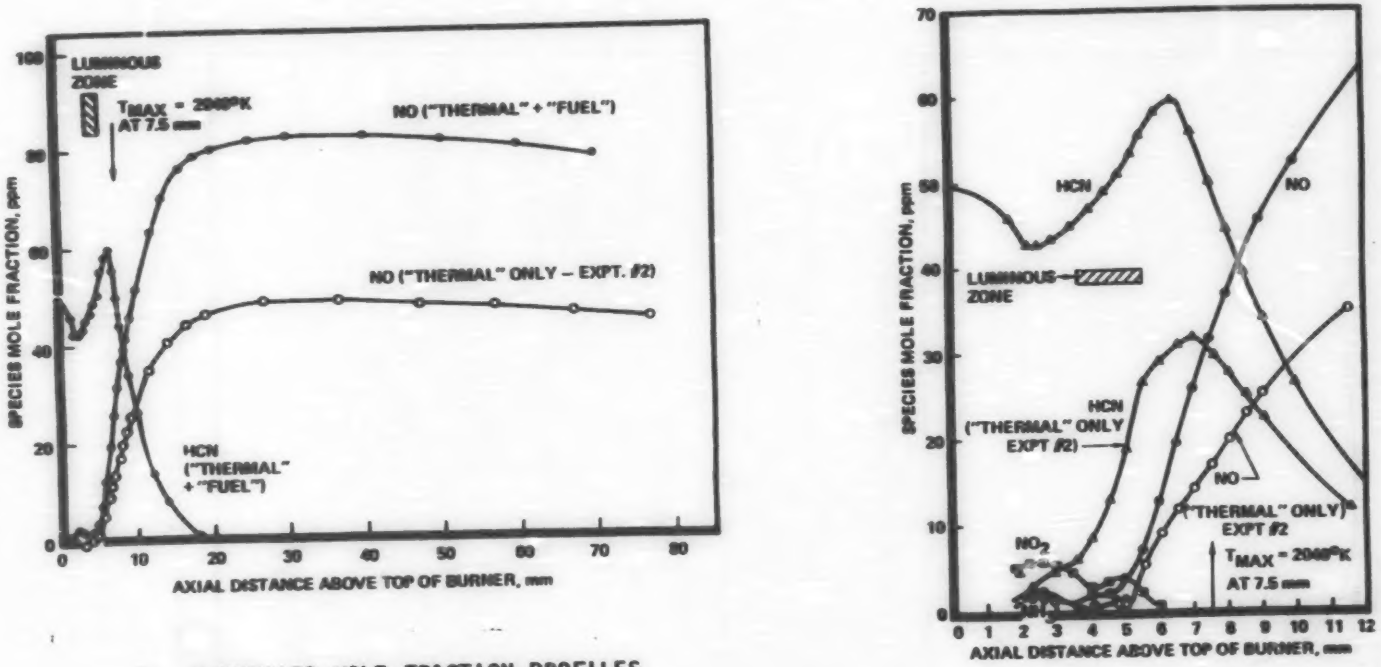

A. N-SPECIES MOLE FRACTION PROFILES

B. N-SPECIES MOLE FRACTION PROFILES IN LUMINOUS ZONE REGION

Figure 6. Thermal and Fuel NO From Fuel-Rich CH_4-O_2-N_2 Flame With 50 ppm HCN Added - Experiments No. 2 and No. 6 (ϕ = 1.5, DR = 0.7, P_T = 76 torr, $\bar{F}_T$ = 7520 cc/min.)

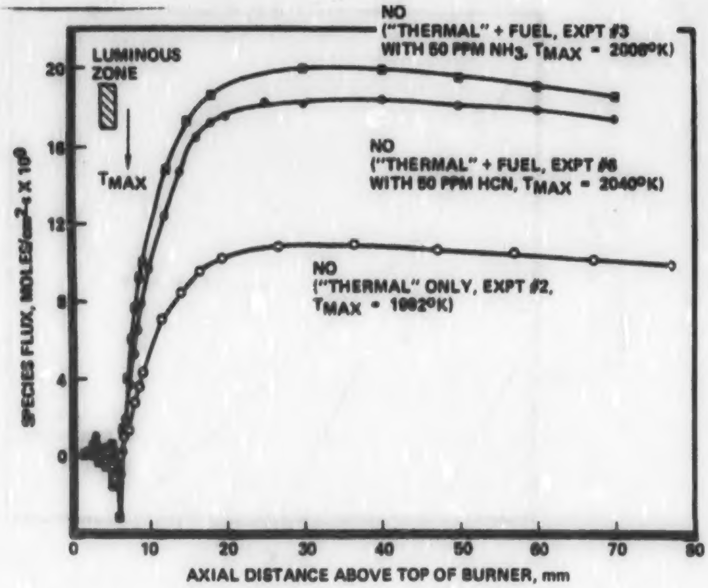

C. COMPARISON OF NO MOLAR FLUX PROFILES FROM EXPERIMENTS NO. 2, 3, and 6

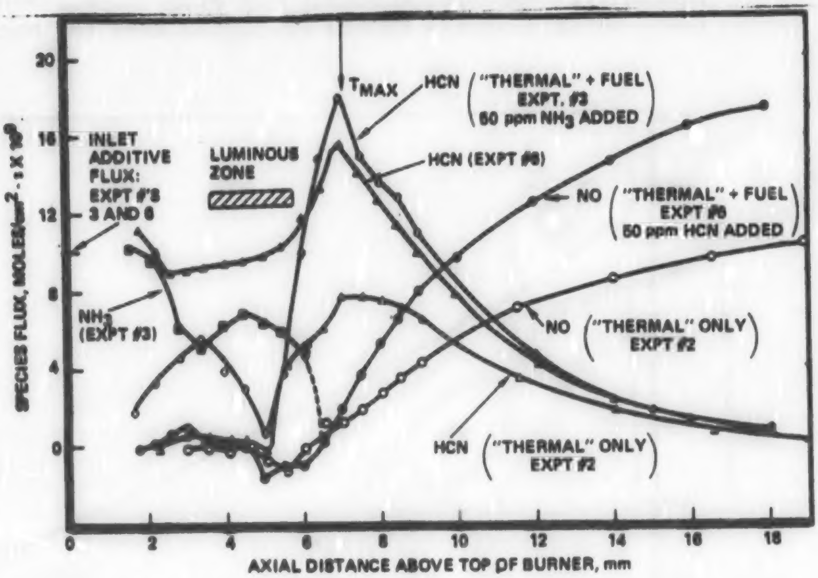

D. COMPARISON OF MOLAR FLUX PROFILES FOR HCN AND NO FROM EXPERIMENTS NO. 2, 3, AND 6 IN LUMINOUS ZONE REGION

Figure 6. (Concluded)

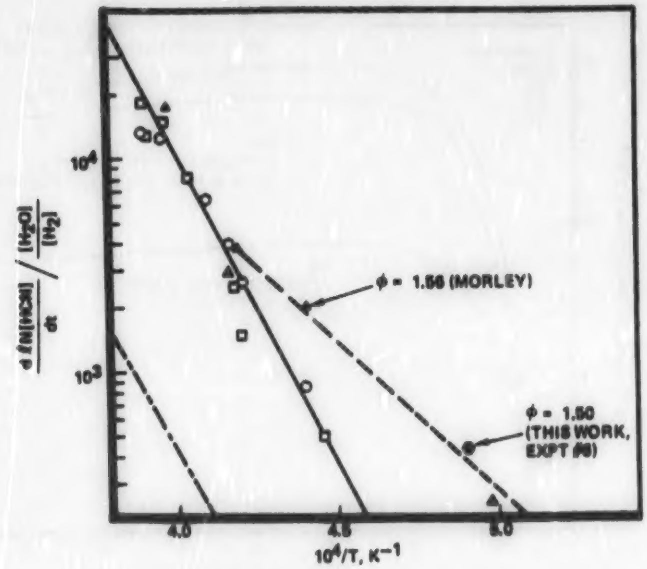

Figure 7. Arrhenius Plot for HCN Oxidation Given by Morley (Ref. 10) Solid Line Corresponds to Mechanism A (136 kcal/mole) for Equivalence Ratios: ○, 2.05; □, 1.8; △, 1.56. Broken Line (— – —) Corresponds to the Predicted Rate for Mechanism B.

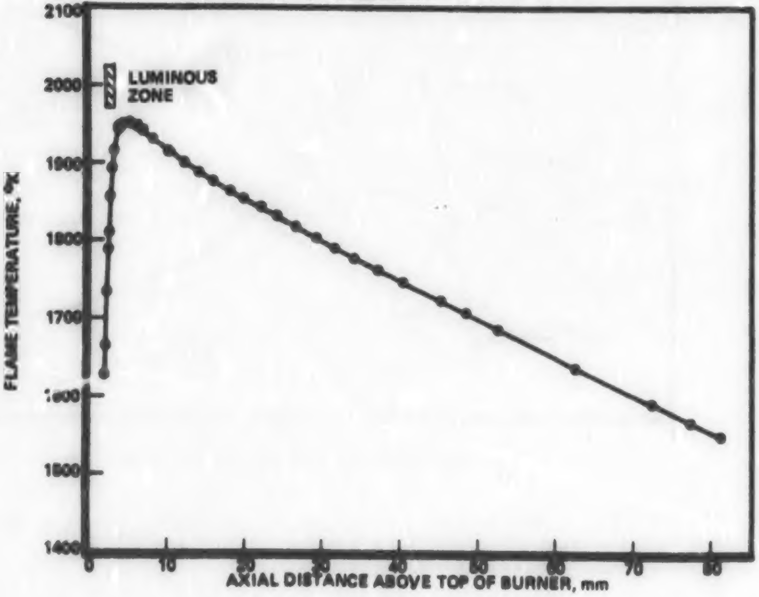

A. FLAME TEMPERATURE VS DISTANCE (EXPT NO. 4)

Figure 8. Fuel-Lean CH_4-O_2-N_2 Flame (ϕ = 0.8, DR = 0.7, P_T = 76 torr, $\overline{F}_T$ = 7520 cc/min at STP)

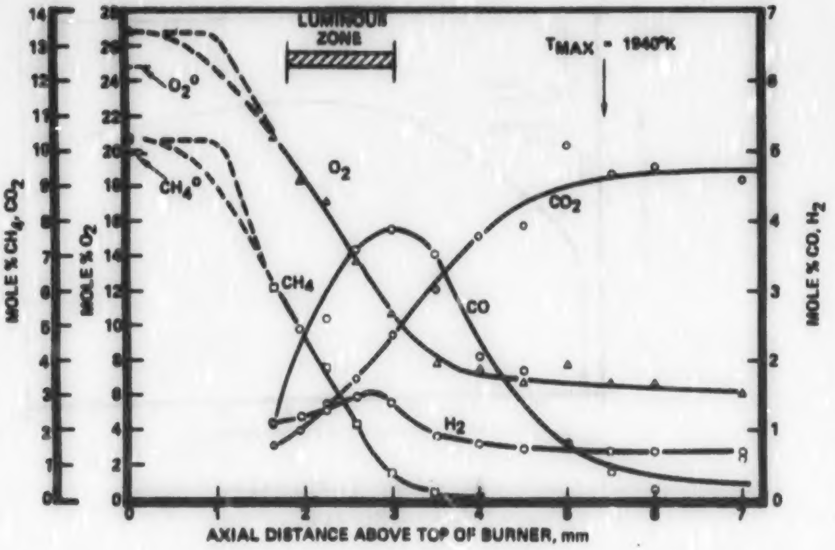

B. MOLE FRACTION PROFILES OF MAJOR SPECIES (EXPT NO. 5)

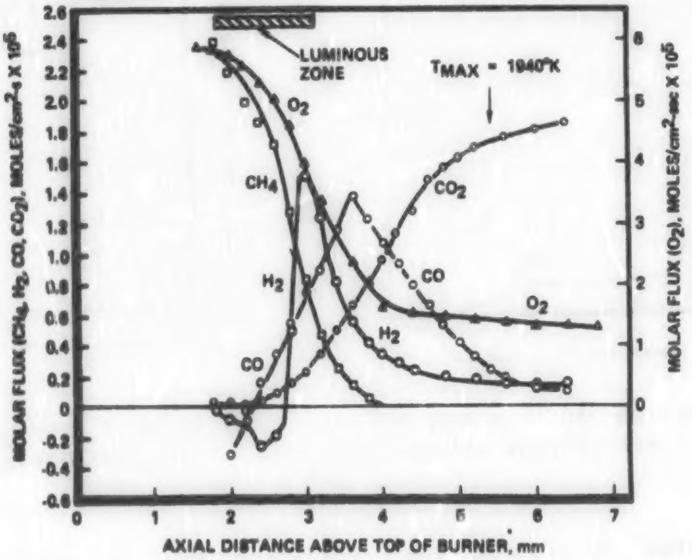

C. MOLAR FLUX PROFILES OF MAJOR SPECIES (EXPT NO. 5)

Figure 8. (Concluded)

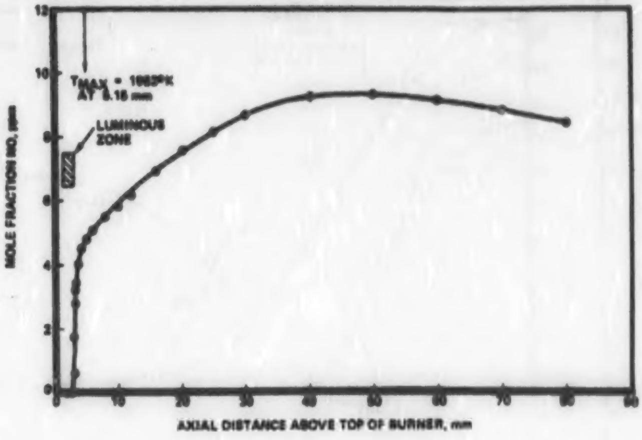

A. NO MOLE FRACTION PROFILE

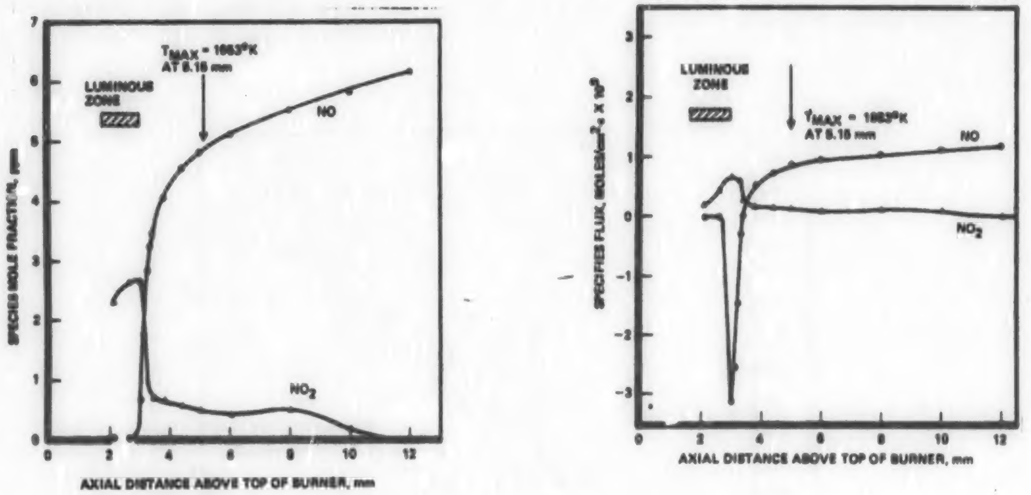

B. MOLE FRACTION PROFILES FOR NO AND NO_2 IN LUMINOUS ZONE REGION

C. MOLAR FLUX PROFILES FOR NO AND NO_2 IN LUMINOUS ZONE REGION

Figure 9. Thermal NO and NO_2 From a Fuel-Lean CH_4-O_2-N_2 Flame--Experiment No. 4 (ϕ = 0.8, DR = 0.7, P_T = 76 torr, $\overline{\overline{F}}_T$ = 7520 cc/min)

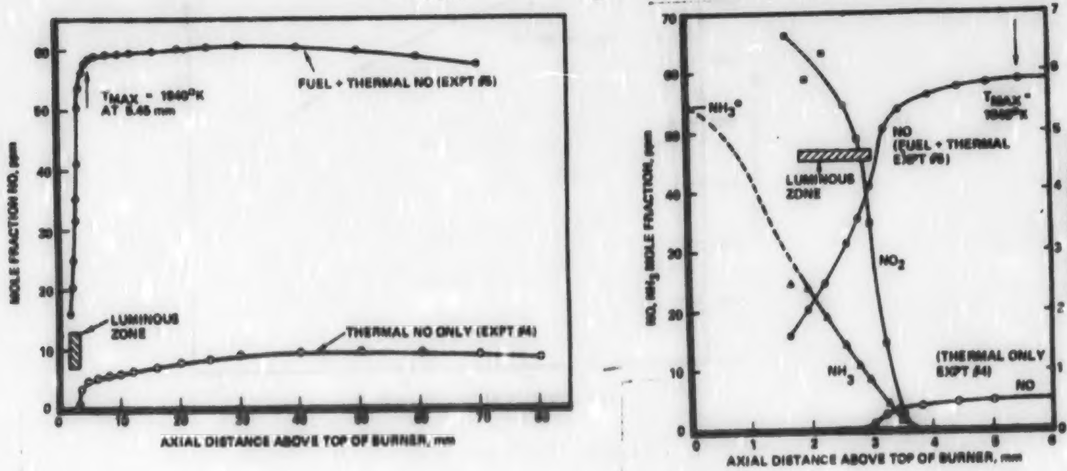

A. COMPARISON OF NO MOLE FRACTION PROFILES

B. N-SPECIES MOLE FRACTION PROFILES IN LUMINOUS ZONE REGION

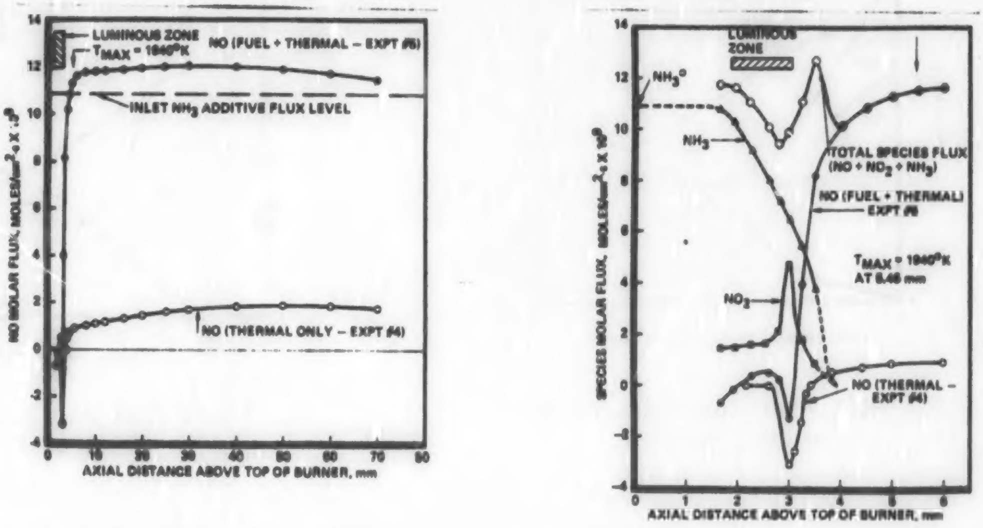

C. COMPARISON OF NO MOLAR FLUX PROFILES

D. N-SPECIES MOLAR FLUX PROFILES IN LUMINOUS ZONE REGION

Figure 10. Thermal and Fuel NO Formation From Fuel-Lean CH_4-O_2-N_2 Flames With 54 ppm NH_3 Added--Experiments No. 4 and No. 5 (ϕ = 0.8, DR = 0.7, P_T = 76 torr, $\overline{F}_T$ = 7520 cc/min)

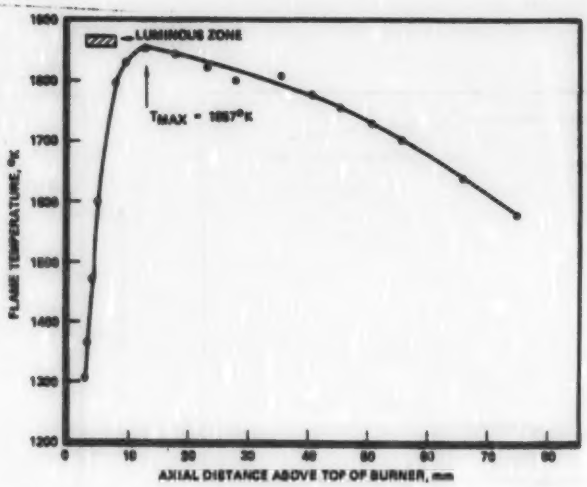

A. FLAME TEMPERATURE VS DISTANCE

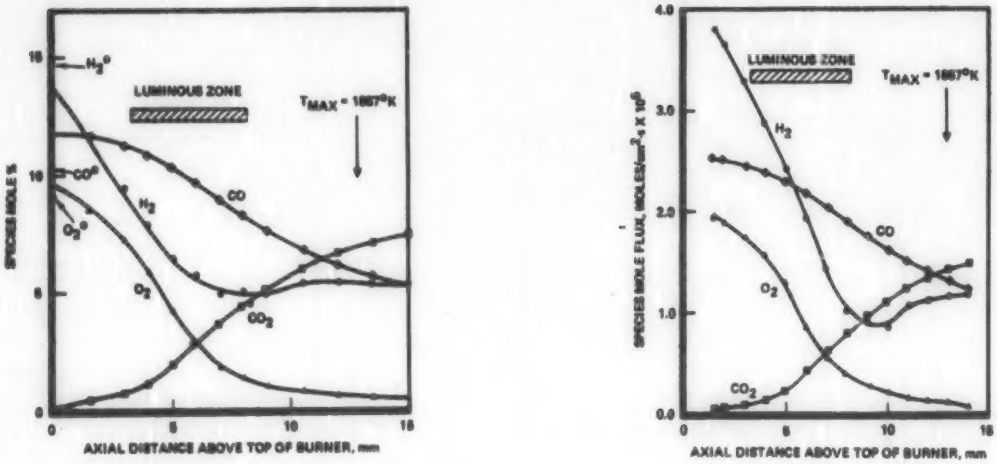

B. MOLE FRACTION PROFILES OF MAJOR SPECIES

C. MOLAR FLUX PROFILES OF MAJOR SPECIES

Figure 11. Fuel-Rich H_2-CO-O_2-Ar Flame (H_2/CO = 1.43, ϕ = 1.4, DR = 1.9, P_T = 50 torr, $\overline{F}_T$ = 8750 cc/min at STP) - Experiment No. 8

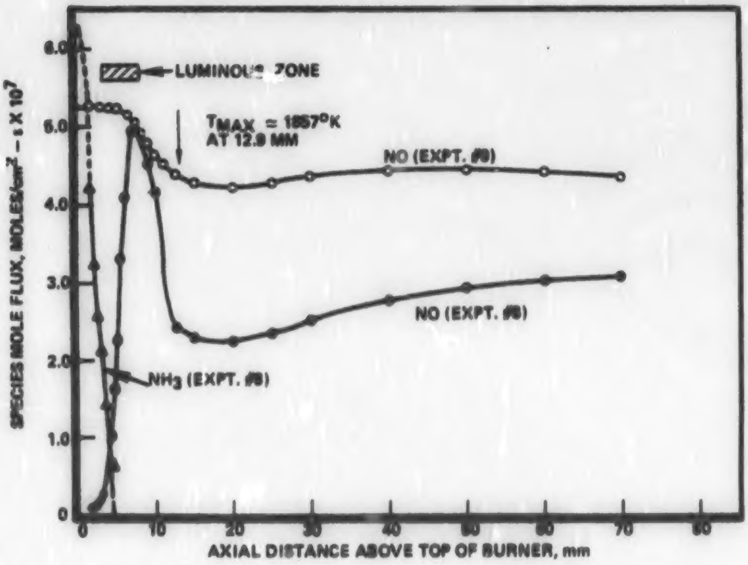

A. NO MOLAR FLUX PROFILES

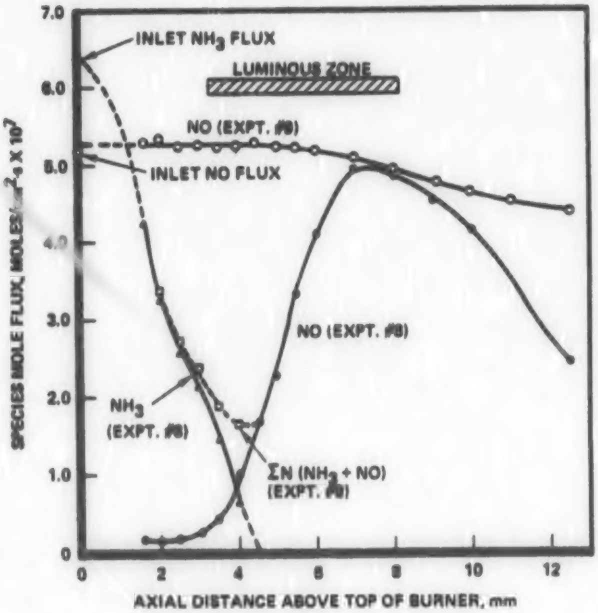

B. N-SPECIES MOLAR FLUX PROFILES
IN LUMINOUS ZONE REGIONS

Figure 12. Fuel NO From and NO Stability in Fuel-Rich H_2-CO-O_2-Ar Flames - Experiments No. 8 and No. 9 (H_2-CO = 1.43, ϕ = 1.4, DR = 1.9, P_T = 50 torr, $\overline{F}_T$ = 8750 cc/min)

FORMATION OF SOOT AND POLYCYCLIC AROMATIC HYDROCARBONS IN COMBUSTION SYSTEMS

Development of a Molecular Beam Mass Spectrometer

By:

J. D. Bittner
Massachusetts Institute of Technology
Cambridge, Massachusetts 02139

Preceding page blank

ABSTRACT

The overall objective of this research program has been to study the production of soot and polycyclic aromatic hydrocarbons (PCAH) in combustion systems. The program has two phases. In one phase the production of soot and PCAH in a turbulent diffusion flame was studied. The results have been reported elsewhere. In the phase to be discussed in this paper, a low pressure flat laminar premixed flame is being used to study the kinetic relationships between soot, PCAH and other hydrocarbon species that may be important as soot nuclei or surface growth species. The molecular beam-mass spectrometer system developed to study the gas phase species will be described. Preliminary mass spectral data on an acetylene-oxygen flame will be reported.

Preceding page blank

INTRODUCTION

The formation of soot in combustion systems has been studied for many years with the objective of attaining a working knowledge of the process to aid in predicting flame emissivities for radiative heat transfer problems. Recently, concern has been expressed that soot and some of the organic compounds associated with incomplete combustion are pollution problems that may have to be controlled. It is known that some polycyclic aromatic hydrocarbons (PCAH) produced in flames and adsorbed on soot particles are carcinogenic. Soot and other organic particulate matter may not be the most abundant particulates emitted, but because the small particles ($<0.2\mu m$) are easily injected deep into the respiratory system, they may be one of the types of particulates most hazardous to human health. The effects of two expected changes in the operation of combustion systems threaten to increase the emissions of particulate organic matter. First, the staged combustion strategy for controlling NO_x requires primary combustion in a fuel rich atmosphere that leads to increased soot and PCAH formation. Second, the planned increased use of coal and coal derived liquids will also lead to increased soot and PCAH formation since aromatic fuels are known to be troublesome in this respect.[1,2] The necessity for learning how to burn low H/C fuels (aromatics) without considerable soot and PCAH formation is especially important for small systems such as gas turbines and internal combustion engines where residence times available for burnout are limited.[3]

The mechanism of soot formation in combustion systems is not well understood. Some of the mechanisms proposed over the years and the confusion surrounding the role of PCAH in the process are illustrated in Figure 1. Since soot particles contain many more carbon atoms and a much lower H/C ratio than the fuel molecules, soot formation must involve processes of

Preceding page blank

aggregation (top to bottom) and dehydrogenation (left to right). The extreme routes, the C_2 route and the saturated polymer route, are unlikely to occur under typical combustion conditions. The C_2 route may be important at temperatures around 3000°K. At lower temperatures, around 700°K, and long reaction times the saturated polymer route may occur. But, in the range 1200-2200°K most mechanisms can be represented by the central portion of Figure 1. From this figure it is seen that PCAH species have been postulated to serve as nuclei for soot growth by surface decomposition of any number of hydrocarbon species (including themselves). They have been postulated to have sufficiently low vapor pressures to physically condense to liquid droplets which then form soot. They have also been postulated to be stable by-products of the soot formation process.

In light of the concern over particulate organic matter as a pollutant and the confusion surrounding soot formation mechanisms and the role of PCAH, the specific objective of this research is to study the chemistry of soot and PCAH formation. Emphasis is on the identification and measurement of relative concentration profiles of the gas phase hydrocarbon species and the measurement of soot particle concentrations, size distributions and total mass of soot at different stages of combustion in a flat premixed flame.

EXPERIMENTAL APPARATUS

DESCRIPTION

The molecular beam mass spectrometer system that has been developed during this project to study premixed low-pressure flat flames is schematically represented in Figure 2. The flame is stabilized on a flat water-cooled drilled copper plate burner that is 7.1 cm in diameter. The burner chamber is pumped by a 60 cfm Stokes mechanical pump. The flame is sampled along the centerline of the burner by moving the burner relative to the rest of the apparatus. The sample is withdrawn supersonically through a quartz nozzle. The nozzle is a hybrid type, as discussed by Biordi et al.[4] The tip has about a 40° outside angle that expands to a 90° angle about 1.5 cm from the tip. The central core of the expanding flame gases passes through the orifice in the tip of the cone-shaped (60° total outside angle) aluminum skimmer. Formation of the molecular beam is completed by collimation with a circular orifice placed between the second and third (mass spectrometer) stages. The beam is modulated by an American Time Products tuning fork chopper placed near the entrance to the ionizer of the Extranuclear quadrupole mass spectrometer. Orifice diameters, separation distances and typical operating pressures are shown in the following table. The partition between the second and third stage is a hollow annulus designed to be filled with liquid nitrogen to provide cryogenic pumping near the ionizer to reduce the amounts of water and other condensible species, especially hydrocarbons, in the background. This recent improvement has been fabricated but not yet tested and the pressures reported in stages two and three are without the benefit of this cryogenic pumping. The system is equipped with an effusive source that can be moved into place to calibrate for mass spectrometer sensitivities and study mass discrimination effects in the beam.

	Orifice diameter, mm	Distance from nozzle, cm	Pressure downstream, flame at 20 torr, torr
nozzle	0.7	-	1.1×10^{-4} (stage 1)
skimmer	0.9	1.8	1.2×10^{-6} (stage 2)
collimator	3.0	∿ 36	1.4×10^{-7} (stage 3)
ionizer	3.0	∿ 40	

For studying the particulate phase the mass spectrometer is removed and the top flange is replaced by a flange that has a mechanism for mounting electron microscope grids and moving them in and out of the beam. The grids are exposed to the beam for a measured time interval with the use of a mechanical shutter. The particles collected on the grid are analyzed by making electron micrographs using either shadowing or transmission procedures. Number densities and size distributions are obtained with the aid of a Zeiss semi-automatic particle counter. Computation techniques developed by Wersborg will be used to calculate profiles of average soot particle size, soot particle number concentration, rates of nucleation, surface growth and coagulation.[5]

A schematic of the mass spectrometer instrumentation is shown in Figure 3.

The molecular beam is chopped by the fixed-frequency tuning fork operating at 220 Hz. The signal from the electron multiplier at any particular mass has a DC component corresponding to ions originating from the background gas molecules and an AC component at 220 Hz corresponding to ions originating from the beam molecules. The signal is amplified with an Extranuclear fast electrometer preamplifier. The amplified signal is DC coupled to an Extranuclear electrometer to obtain a signal corresponding to the background component. A reference signal from the chopper and the AC component of the signal from the preamplifier are introduced into a Princeton Applied Research HR-8 lock-in amplifier to obtain a signal proportional to the beam component. Signals corresponding to beam and background components are then displayed either on a dual-beam storage oscilloscope or a chart recorder.

CALIBRATION

Considerations

Calibration of supersonic molecular beam systems for flame sampling is not a straight forward task due to the many effects that can influence the composition of the beam prior to reaching the mass spectrometer ionizer. Shock formation in front of the skimmer orifice, species condensations, pressure diffusion in the free jet, Mach number focussing downstream of the skimmer, scattering of the beam by the background gas in any or all of the chambers, and effusion of the background gas into the beam are effects that can distort the beam composition and are discussed extensively in a review article by Knuth[6]. Skimmer interference problems can be avoided by proper design of external and internal angles of the skimmer and the selection of the proper distance between the tip and the supporting wall. Species condensations in free jet expansion are not believed to be important at flame temperatures and sub-atmospheric pressures for most flame constituents[6], however little is known about the behavior of the high molecular weight hydrocarbons and care must be taken to look for condensation effects in the interpretation of the data. Pressure diffusion, Mach number focussing and background scattering and effusion are more difficult effects to avoid altogether and all can be functions of source conditions. A study of their importance in this system and techniques for calibration of these effects is now underway. The limited data indicate that background scattering and effusion are negligible under the flame conditions presented here. Pressure diffusion and Mach number focussing are lumped together as "mass discrimination" and can be studied in this system with the aid of the effusive source placed in the second stage upstream of the collimator.

The system for studying mass discrimination is shown schematically in Figure 4. Mixtures of the major stable species are made by metering through critical orifice flow meters and mixing dynamically. These mixtures may be introduced into the mass spectrometer ionizer either as an effusive beam in which no mass discrimination effects occur or as a supersonic beam (through the burner and quartz nozzle) in which high molecular weight species are usually preferentially concentrated relative to low molecular weight species.

To introduce the mixture effusively without mass discrimination, a stainless steel sintered disc with a nominal pore size of 0.5 μm is used to leak into the effusive source in the second stage about 1% of the total gas flow by the disc. The pressure on the high pressure side of the sintered disc is maintained in the range 0.1 to 1 torr. Tubing sizes and pressures are designed to give viscous flow (no mass discrimination) everywhere upstream of the sintered disc and effusive flow through the disc and downstream from it. Under these conditions the flow rate of a component through the disc is inversely proportional to the square root of its molecular weight but its density anywhere downstream of the disc is proportional to its partial pressure upstream. Since the electron impact ionizer is a density detector, ratios of ion signals are proportional to the ratios of partial pressures in the gas mixture upstream of the disc. The effusive source inlet system has been tested with commercially prepared standard gas mixtures and reproduces the suppliers analysis to within 2% on any component.

By comparing signal ratios in the effusive beam to signal ratios in the sonic beam, the mass discrimination between two species in a mixture can be characterized by an enrichment factor, α_{AB}:

$$\alpha_{AB} = \left(\frac{I_A}{I_B}\right)_S / \left(\frac{I_A}{I_B}\right)_S = \left(\frac{X_A}{X_B}\right)_S / \left(\frac{X_A}{X_B}\right)_E$$

where α_{AB} = enrichment factor of species A relative to species B, dimensionless

I_A = beam signal intensity of species A, amperes

I_B = beam signal intensity of species B, amperes

S = sonic introduction

E = effusive introduction

X_A = mole fraction of species A

X_B = mole fraction of species B

The effusive source system is also used to obtain relative mass spectrometer sensitivity factors for stable species, S_{AB}:

$$S_{AB} = \frac{k_B}{k_B}$$

where k_A = sensitivity for species A, amperes/torr

k_B = sensitivity for species B, amperes/torr.

Mass discrimination effects have been studied most extensively by Sharma et al.[7] The enrichment factor may or may not be a function of the source conditions (flame conditions at the sampling point in this case) depending upon how the system geometry and source conditions dictate the point of transition from continuum to free molecular flow. Although the study of these effects in this system is not complete, preliminary experiments at room temperature with a mixture approximating the burned gas composition of the acetylene-oxygen flames studied here indicate that enrichment factors for the major species except that for hydrogen are relatively insensitive to source conditions. An increase in source density by a factor of five resulted in a decrease in $\alpha_{H_2,CO}$ of 23% and changes in all other enrichment factors of less than 12%. Further experimental work to assess the effect of gas composition and source density on the enrichment factors is planned.

The calibration procedures for mass discrimination in the sonic beam and for mass spectrometer sensitivities are carried out at room temperature. The effect of temperature on these two calibration steps must be considered. The mass spectrometer relative sensitivities in some cases might be functions of temperature. In conventional (residual gas analyzer) mass spectrometer ionizers variation with temperature of absolute ionizer sensitivities for total ionization have been found to be due only to the effects of temperature on gas density and the speed of the neutral molecule (which effects ion collection efficiency), implying that actual total ionization cross-sections are not temperature sensitive.[8] In the type of molecular beam ionizer used here the neutral beam molecules are directed along the axis and toward the quadrupoles, therefore the ion collection efficiency might be expected to be high and less sensitive to translational temperatures perpendicular to the beam axis. Although total ionization cross-sections are temperature independent, fragmentation patterns and therefore mass spectrometer sensitivity (when a specific ion is used to follow concentration changes) is highly dependent upon the vibrational energies of the molecule-ion[9]. As temperature increases more fragmentation occurs. With current knowledge of vibrational relaxation processes in supersonic expansions, vibrational energies are impossible to predict and one must if possible avoid the use of high electron energies where fragmentation occurs. The appearance potentials of fragment ions, like heats of reaction, seem to vary but little with temperature.[10] So, if fragmentation does not occur in room temperature calibrations it is not likely to occur in the case of the flame. However, in spite of these arguments, care must be taken in the interpretation of the data and simple experiments must be done to check temperature effects on mass spectrometer sensitivities due to fragmentation effects wherever possible.

The effects of temperature on the mass discrimination enrichment factors must be assessed using the models designed to handle the prediction of enrichment factors for pressure diffusion and Mach number focussing.[5,6] Analysis of these models suggests that these mass discrimination effects depend upon temperature in only the way in which it effects the source density. Therefore enrichment factors from room temperature calibrations carried out at a reduced pressure to reproduce the source density conditions should apply to the higher pressure and temperature conditions in the flame.

Major Stable Species

In accordance with the considerations discussed above, the calibration for most major stable species involves the measurement of enrichment factors and relative mass spectrometer sensitivities. With this calibration information ratios of mole fractions in the flame are calculated from ratios of signal intensities. In the flames studied here 5 mole% argon has been added to the unburned gases as an aid in following density changes in the flame front. Since calibration of this system for water is very uncertain the following relationships are used to calculate mole fractions from ratios of mole fractions in the tail of the flame, where diffusion effects are negligible:

$$X_{O_2} + X_{Ar} + X_{CO} + X_{CO_2} + X_{H_2} + X_{H_2O} + X_{C_2H_2} = 1$$

an oxygen balance

$$\frac{n_I}{n_F}(X_{O_2})_I = X_{O_2} + \frac{X_{CO}}{2} + X_{CO_2} + \frac{X_{H_2O}}{2}$$

an argon balance

$$\frac{n_I}{n_F}(X_{Ar})_I = X_{Ar}$$

and from experimental measurements

$$\frac{X_{H_2}}{X_{Ar}}, \frac{X_{C_2H_2}}{X_{Ar}}, \frac{X_{O_2}}{X_{Ar}}, \frac{X_{CO}}{X_{Ar}}, \frac{X_{CO_2}}{X_{Ar}}$$

where n_I/n_F is the ratio of initial number of moles to final number of moles and $(X_A)_I$ refers to the mole fraction of species A in the unburned gas. Carbon and hydrogen balances can then be used to check the consistency of the data and calibrations. From the calculated ratio $\frac{X_{H_2O}}{X_{Ar}}$ in the tail of the flame and experimental $\frac{I_{H_2O}}{I_{Ar}}$ ratio it is possible to obtain a calibration factor for water:

$$\frac{X_{H_2O}}{X_{Ar}} = C_{H_2O,Ar} \frac{I_{H_2O}}{I_{Ar}}$$

where I_i = signal intensity of species i, amperes

X_i = mole fraction of species i

$C_{H_2O,Ar}$ = calibration factor for water relative to argon.

Now with this additional piece of experimental information the oxygen and argon balances are not needed in the reaction zone where steep gradients require the use of diffusional terms. The assumption is made that $C_{H_2O,Ar}$ is constant throughout the flame (i.e. the enrichment factor is not a function of gas density or composition and mass spectrometer relative sensitivity factors are not functions of flame position.)

Higher Molecular Weight Hydrocarbons

Due to the difficulty of introducing compounds that are liquids of low vapor pressure and solids at room temperature into the system to obtain mass spectrometer sensitivities and mass discrimination enrichment factors, all higher molecular weight hydrocarbon species measurements are made on a relative basis. To account for any changes in mass spectrometer relative sensitivities that might occur, the fragmentation pattern at 20 eV electron energy of perfluorotributylamine is recorded before and after each experiment.

EXPERIMENTAL PROCEDURE

To check out the experimental technique and procedures several fuel-rich acetylene-oxygen flames have been investigated. All flames had a cold gas velocity of 50 cm/sec and burned at a pressure of 20 torr. Five mole percent argon was added to the unburned gas. Four fuel equivalence ratios were investigated, $\phi = 1.5$, $\phi = 2.0$, $\phi = 2.4$ (sooting limit) and $\phi = 3.0$. Complete profiles were made for $\phi = 1.5$, 2.0 and 2.4. Two points near the end of the oxidation zone were sampled in the $\phi = 3.0$ flame.

The mass spectrometer resolution controls were set to give unit resolution from 18 to 502 a.m.u. The electron energy was set at a nominal 20eV which corresponded to an actual electron energy of 17.1eV according to argon ionization potential measurements. At these conditions, room temperature fragmentation of O_2, CO_2, CO and H_2O does not occur. For acetylene, peak 25 is less than 1% of peak 26. Mass spectrometer sensitivity and beam enrichment factor calibrations were made before and after each flame run. Two sweeps across the mass range 0 - 230 a.m.u. were made at each flame position at a speed of $\sim$ 1 a.m.u./sec.

RESULTS AND DISCUSSION

Profiles of signal intensities relative to argon for the $\phi = 2.4$ flame are shown in Figures 5 and 6. The mole fractions of the major stable species in the burned gas, as calculated from the procedure described above, are included in Figure 5.

The experimental points with the most scatter are the hydrogen and water profiles. The characteristics of quadrupole mass spectrometers make it difficult to have a high sensitivity for hydrogen and high molecular weight hydrocarbon species simultaneously. To improve upon this measurement different tuning conditions can be used for the low molecular weight gases and the high molecular weight hydrocarbons. The noise in the water signal is due to a large background peak at 18 a.m.u. The additional cryogenic pumping in the ionizer region should improve this measurement.

The general features of the profiles are in agreement with the measurements on a similar flame by Homann and colleagues.[11,12] About 5.5 mole % of the acetylene is present in the burned gases. The other hydrocarbons in the burned gases are mostly polyacetylenes. They increase through the early part of the oxidation zone and maximize at about 1 cm. Detectable amounts of polyacetylenes up to C_8H_2 are still present in the burned gas. Polyacetylene formation is preceded in the oxidation zone by vinylacetylene (C_4H_4) and a C_6H_6 compound that could be benzene or a straight chain hydrocarbon. These compounds have concentration maxima that are at least an order of magnitude lower than the polyactylene of the same carbon number.

The interaction between the major stable species and the hydrocarbon species throughout the flame is complex and interesting. Oxygen is completely consumed by about 1.4 cm. At this point CO and H_2 have nearly reached their final values. CO_2 and H_2O molefractions peak near 1 cm and decrease slightly into the burned gas. Acetylene continues to decrease until about 2.5 cm above the burner. These basic features can be explained qualitatively by the following scheme of competing reactions early in the oxidation zone:

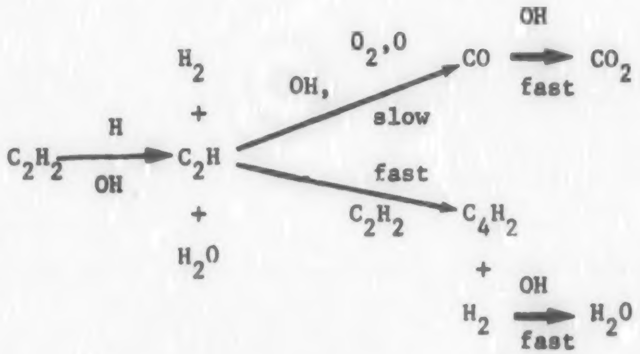

Reactions leading to polyacetylenes and CO_2 and H_2O are faster than reactions involving the same radicals leading to CO and H_2. This ties up oxygen in the form of CO_2 and H_2O and produces super equilibrium amounts of polyacetylenes. Near the end of the oxidation zone where the temperature reaches its maximum, reactions producing OH, CO and H_2 from CO_2 and H_2O:

$$H_2O + H \rightarrow OH + H_2$$

$$CO_2 + H \rightarrow CO + OH$$

become important and the oxidation of polyacetylenes becomes faster than their production.[13] The oxidation rate decreases quickly because of the drop in OH radical concentration leaving some polyacetylenes in the burned gas.[14]

The features of the flame with $\phi = 2.0$ were essentially the same but with lower CO, H_2, acetylene and polyacetylene concentrations as might be expected. At $\phi = 1.5$ no acetylene or polyacetylenes were detectable in the burned gas.

Signals were observed at masses other than those shown in Figures 5 and 6. Table I lists those masses at which positive identifications were not made or contributions from several species were not sorted out. Masses 15, 16 and 17 peak in the middle of the oxidation zone. The most probable contributor to peaks 15 and 16 is methane in this fuel rich flame. Masses 29 and 30 are maximum at the lowest sampling point, 0.17 cm and the contribution of H_2CO to peak 29 has not been determined at these mass spectrometer conditions. Mass 34 appears only at the lowest sampling point. Mass 39 maximizes at 0.62 cm from the burner. Mass 42, probably corresponding to propylene, maximizes at 0.35 cm. Appearance potential measurements along with measurements at lower electron energies to prevent contributions from fragmentation of hydrocarbons must be made to make positive identifications.

Mass spectra were observed at two points near the end of the oxidation zone of a sooting flame of fuel equivalence ratio, $\phi = 3.0$. In addition to the species observed in the $\phi = 2.4$ flame several higher molecular weight aromatic hydrocarbons were observed. Their masses, molecular formula and possible structures are listed in Table II. The sensitivity for higher molecular weight hydrocarbons (100 a.m.u. and above) should be increased by an order of magnitude when the cryogenic pumping in the ionizer region is added since the present sensitivity is limited by noise in the beam spectrum caused by high levels of hydrocarbons in the background.

SUMMARY

A molecular beam mass spectrometer system has been developed for studying sooting flames. Preliminary measurements suggest that molecular beam mass discrimination effects may be relatively insensitive to source conditions and that absolute concentration measurements of major stable species profiles will be possible.

Profiles of relative signal intensities of several non-sooting and barely sooting acetylene-oxygen flames have been made. The results are in agreement with those of previous investigators. Polyacetylenic hydrocarbons up to mass 146 were detected and are the major hydrocarbons present other than the unburned fuel. Maxima in the carbon dioxide and water profiles are supportive of the suggestion that reactions that store oxygen in these species are rapid compared to reactions that lead to CO formation from the fuel in the early part of the flame. At the higher temperatures present at the end of the oxidation zone this oxygen is released in the form of OH that attacks polyacetylenes and unburned fuel.

Under strongly sooting conditions ($\phi = 3.0$) aromatic hydrocarbons have been detected. The addition of cryogenic pumping in the ionizer region is expected to increase the sensitivity for these species by an order of magnitude.

ACKNOWLEDGEMENTS

This work has been done under EPA Grant No. R 803242.

REFERENCES

1. Butze, H.F. and R.C. Ehlers NASA Tech. Mem. NASA JMX-71789. Paper presented at Western States Section of the Combustion Institute, Palo Alto, CA. Oct. 20, 1975.

2. Schirmer, R.M. in "Emissions from Continuous Combustion Systems", W. Cornelius and W.G. Ahnew, ed., p. 189, Plenum Press, N.Y. (1972).

3. Longwell, J.P., "Synthetic Fuels and Combustion" Plenary lecture presented to Sixteenth Symposium (International) on Combustion, Cambridge, Massachusetts, August, 1976.

4. Biordi, J.C., C.P. Lazzara and J.F. Papp, Combust. Flame 23, 73 (1974).

5. Wersborg, B.L., J.B. Howard, and G.C. Williams, Fourteenth International Symposium on Combustion, p. 929, The Combustion Institute (1973).

6. Knuth, E.L., "Direct Sampling Studies of Combustion Processes" in "Engine Emissions, Pollutant Formation and Measurement", G.S. Springer and D.J. Patterson, ed., p. 319, Plenum Press, N.Y. (1973).

7. Sharma, P.K., E.L. Knuth and W.S. Young, J. Chem. Phys. 64, 4345 (1976).

8. Field, F.H. and J.L. Franklin, "Electron Impact Phenomena and the Properties of Gaseous Ions," pp. 202-203, Academic Press, N.Y. (1970).

9. Ibid. pp. 203-204.

10. Ibid., p. 81.

11. Homann, K.H. and H.Gg. Wagner, Berichte der Bunsengesellschaft 69, 20 (1965).

12. Bonne, U., K.H. Homann, and H. Gg. Wagner, Tenth Symposium (International) on Combustion, p. 503, The Combustion Institute (1965).

13. Homann, K.H. Combust. and Flame 11, 265 (1967).

14. Bonne, U., H. Gg. Wagner, Berichte der Bunsengesellschaft 69, 35 (1965).

Table I. MASSES AT WHICH SIGNALS WERE OBSERVED BUT POSITIVE IDENTIFICATIONS WERE NOT MADE. $\phi = 2.4$, P = 20 Torr, $V_o = 50$ cm/s

MASS	POSSIBLE CONTRIBUTING SPECIES
14	CH_2
15	CH_3, CH_4
16	CH_4 (MOST PROBABLE), O
17	OH
25	C_2H, C_2H_2
29	HCO, H_2CO, $C^{13}O$
30	H_2CO, C_2H_6 (UNLIKELY)
34	H_2O_2
38	C_3H_2
39	C_3H_3, $C_3H_3^+$
42	C_3H_6

Table II. ADDITIONAL SPECIES DETECTED NEAR THE END OF THE REACTION ZONE IN A C_2H_2/O_2 FLAME, $\phi = 3.0$, P = 20 Torr, V_o = 50 cm/s

MASS	MOLECULAR FORMULA	POSSIBLE SPECIES	STRUCTURE
92	C_7H_8	TOLUENE	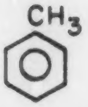
102	C_8H_6	PHENYLACETYLENE	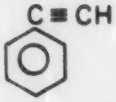
104	C_8H_8	STYRENE	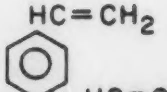
118	C_9H_{10}	METHYL STYRENE	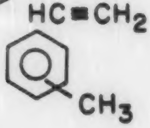
128	$C_{10}H_8$	NAPHTHALENE	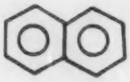
130	$C_{10}H_{10}$	PHENYL BUTADIENE	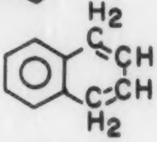
		DIHYDRONAPHTHALENE	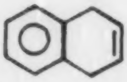
142	$C_{11}H_{10}$	METHYL NAPHTHALENE	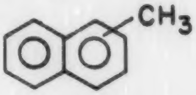
146	$C_{12}H_2$	HEXACETYLENE	$HC\equiv C(-C\equiv C-)_4C\equiv CH$

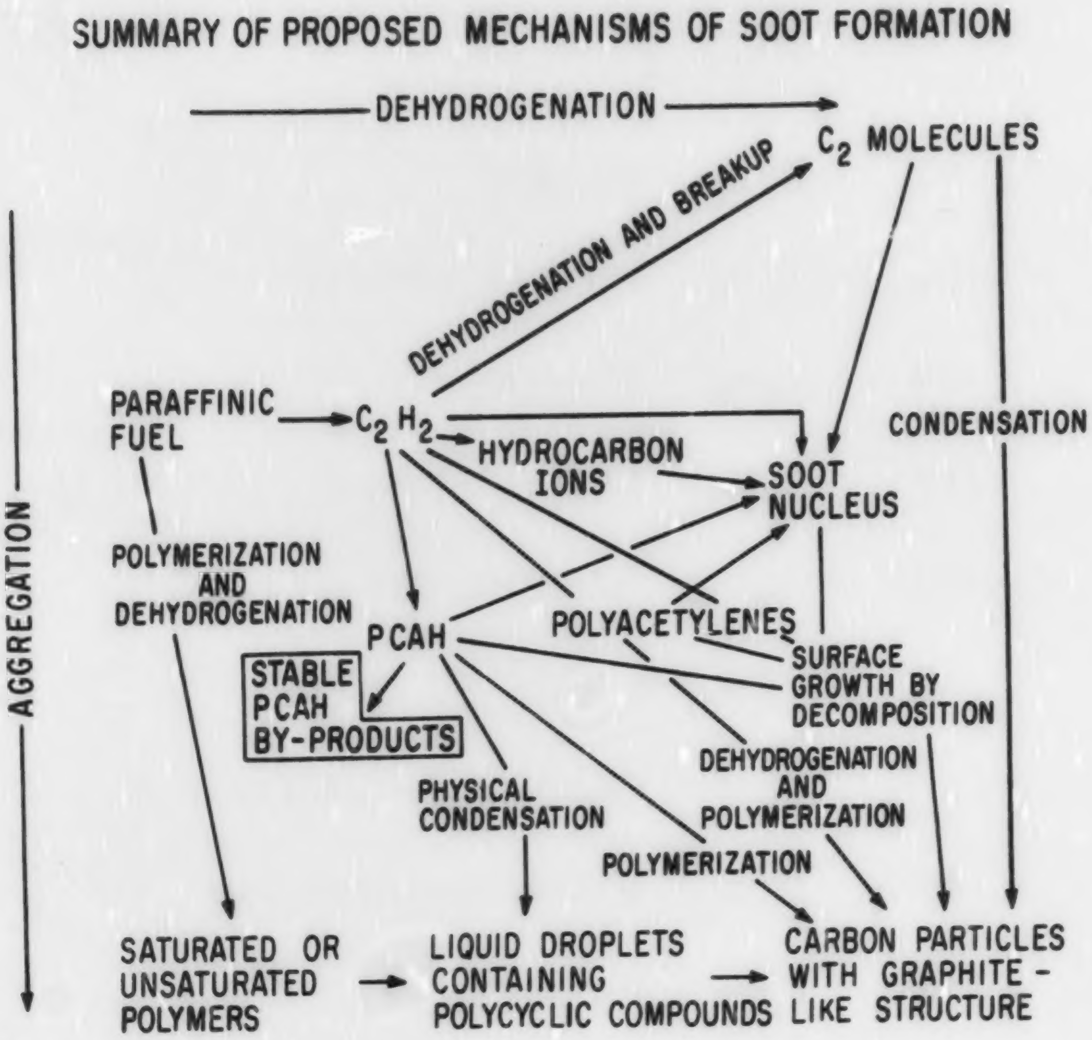
SUMMARY OF PROPOSED MECHANISMS OF SOOT FORMATION
DEHYDROGENATION
C2 MOLECULES
DEHYDROGENATION AND BREAKUP
AGGREGATION
PARAFFINIC FUEL
C2 H2
HYDROCARBON IONS
SOOT NUCLEUS
CONDENSATION
POLYMERIZATION AND DEHYDROGENATION
PCAH
POLYACETYLENES
STABLE PCAH BY-PRODUCTS
SURFACE GROWTH BY DECOMPOSITION
DEHYDROGENATION AND POLYMERIZATION
PHYSICAL CONDENSATION
POLYMERIZATION
SATURATED OR UNSATURATED POLYMERS
LIQUID DROPLETS CONTAINING POLYCYCLIC COMPOUNDS
CARBON PARTICLES WITH GRAPHITE - LIKE STRUCTURE

Figure 1. Summary of proposed mechanisms of soot formation

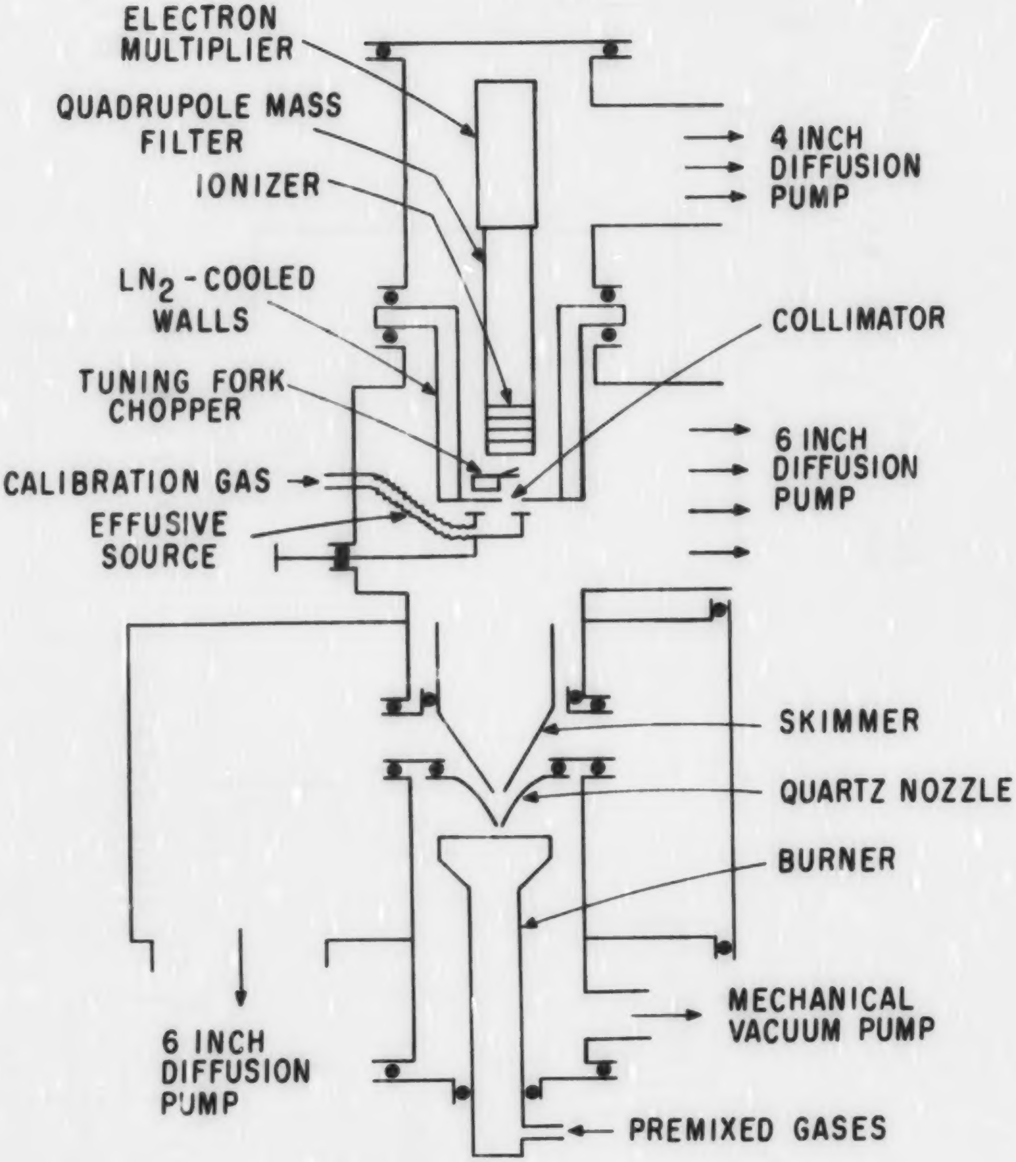
ELECTRON MULTIPLIER
QUADRUPOLE MASS FILTER
IONIZER
LN$_2$-COOLED WALLS
TUNING FORK CHOPPER
CALIBRATION GAS
EFFUSIVE SOURCE
4 INCH DIFFUSION PUMP
COLLIMATOR
6 INCH DIFFUSION PUMP
SKIMMER
QUARTZ NOZZLE
BURNER
MECHANICAL VACUUM PUMP
6 INCH DIFFUSION PUMP
PREMIXED GASES

Figure 2. Molecular beam mass spectrometer system

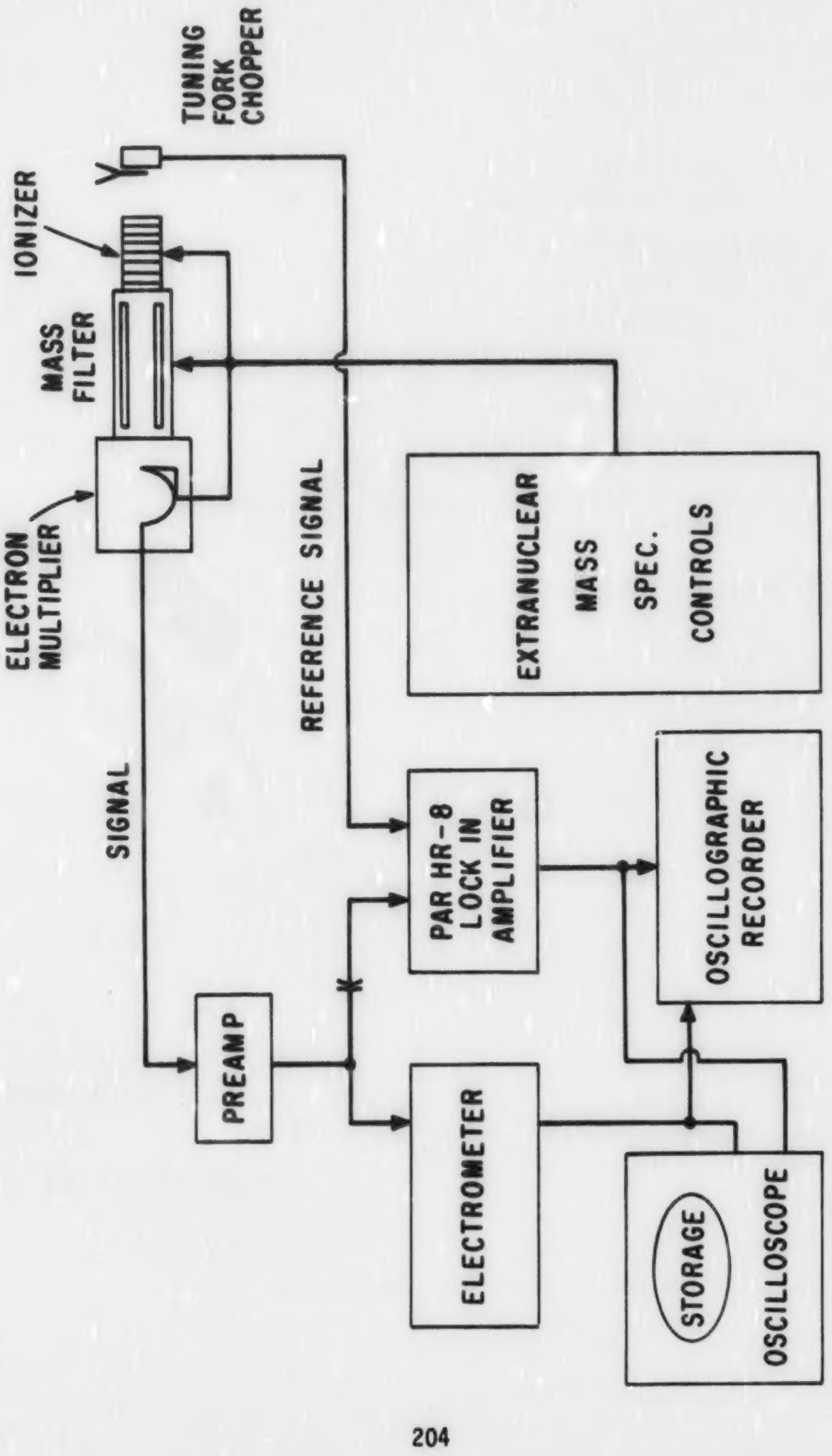
TUNING FORK CHOPPER
IONIZER
MASS FILTER
ELECTRON MULTIPLIER
REFERENCE SIGNAL
SIGNAL
EXTRANUCLEAR MASS SPEC. CONTROLS
PAR HR-8 LOCK IN AMPLIFIER
OSCILLOGRAPHIC RECORDER
PREAMP
ELECTROMETER
STORAGE
OSCILLOSCOPE

Figure 3. Schematic of mass spectrometer instrumentation

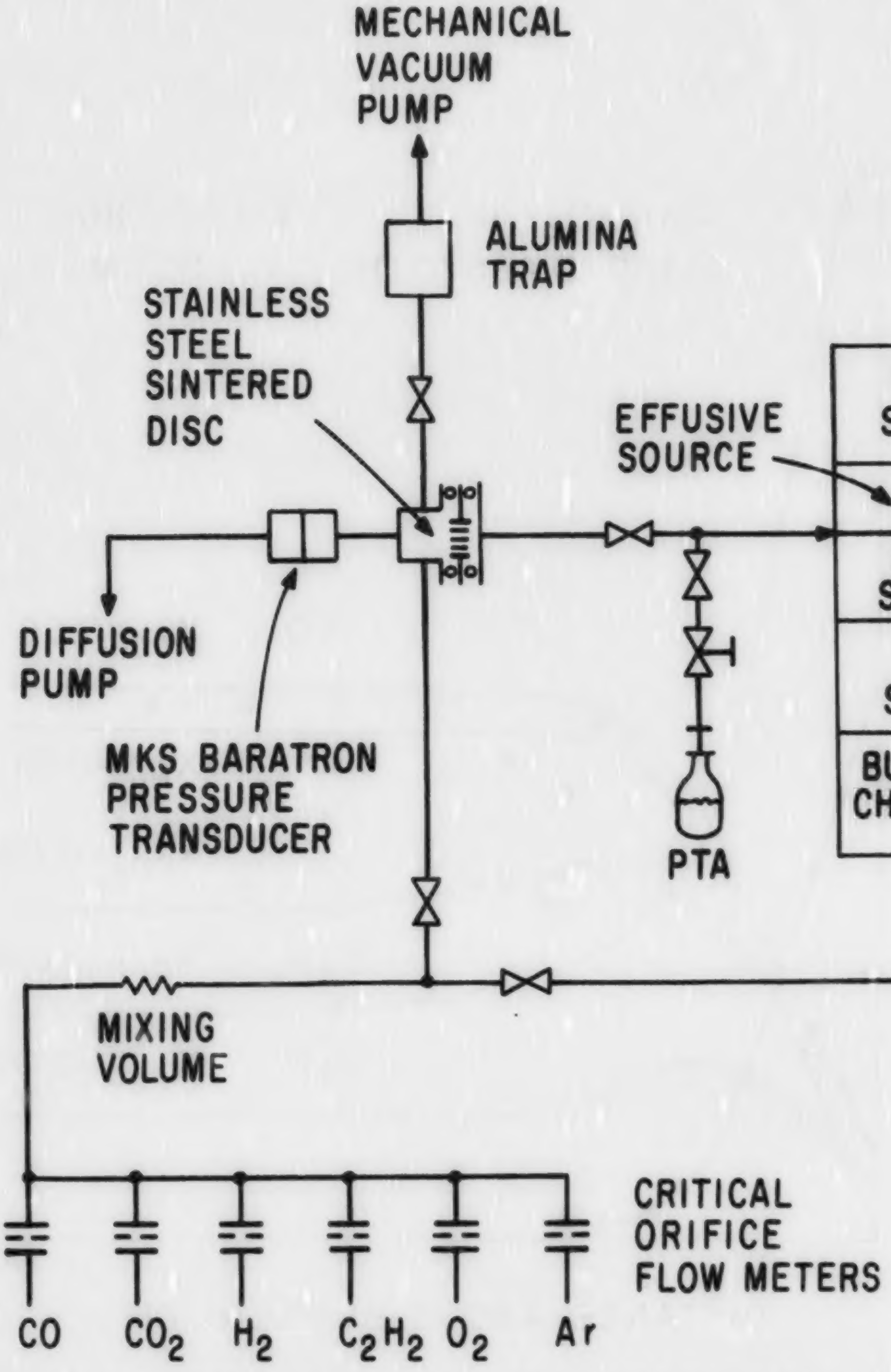
MECHANICAL VACUUM PUMP
ALUMINA TRAP
STAINLESS STEEL SINTERED DISC
EFFUSIVE SOURCE
M.S. STAGE
2 ND STAGE
1 ST STAGE
BURNER CHAMBER
DIFFUSION PUMP
MKS BARATRON PRESSURE TRANSDUCER
PTA
MIXING VOLUME
CRITICAL ORIFICE FLOW METERS
CO
CO_2
H_2
C_2H_2
O_2
Ar

Figure 4. Schematic of gas introduction system for studying mass discrimination

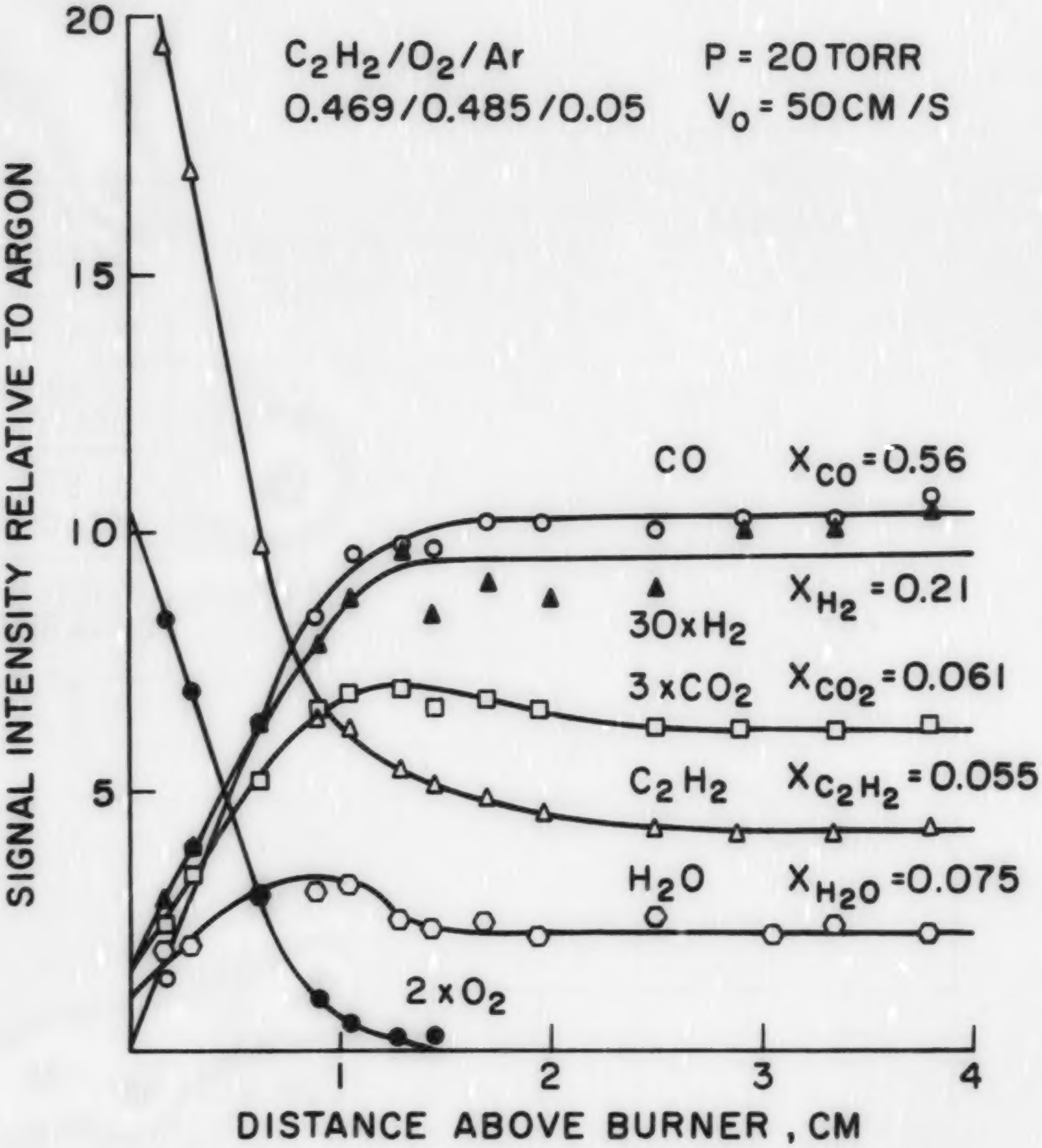

Figure 5. Profiles of signal intensities realtive to argon for major stable species in an acetylene-oxygen flame near the sooting limit. ϕ = 2.4, P = torr, V_o = 50 cm/s, 5m% argon

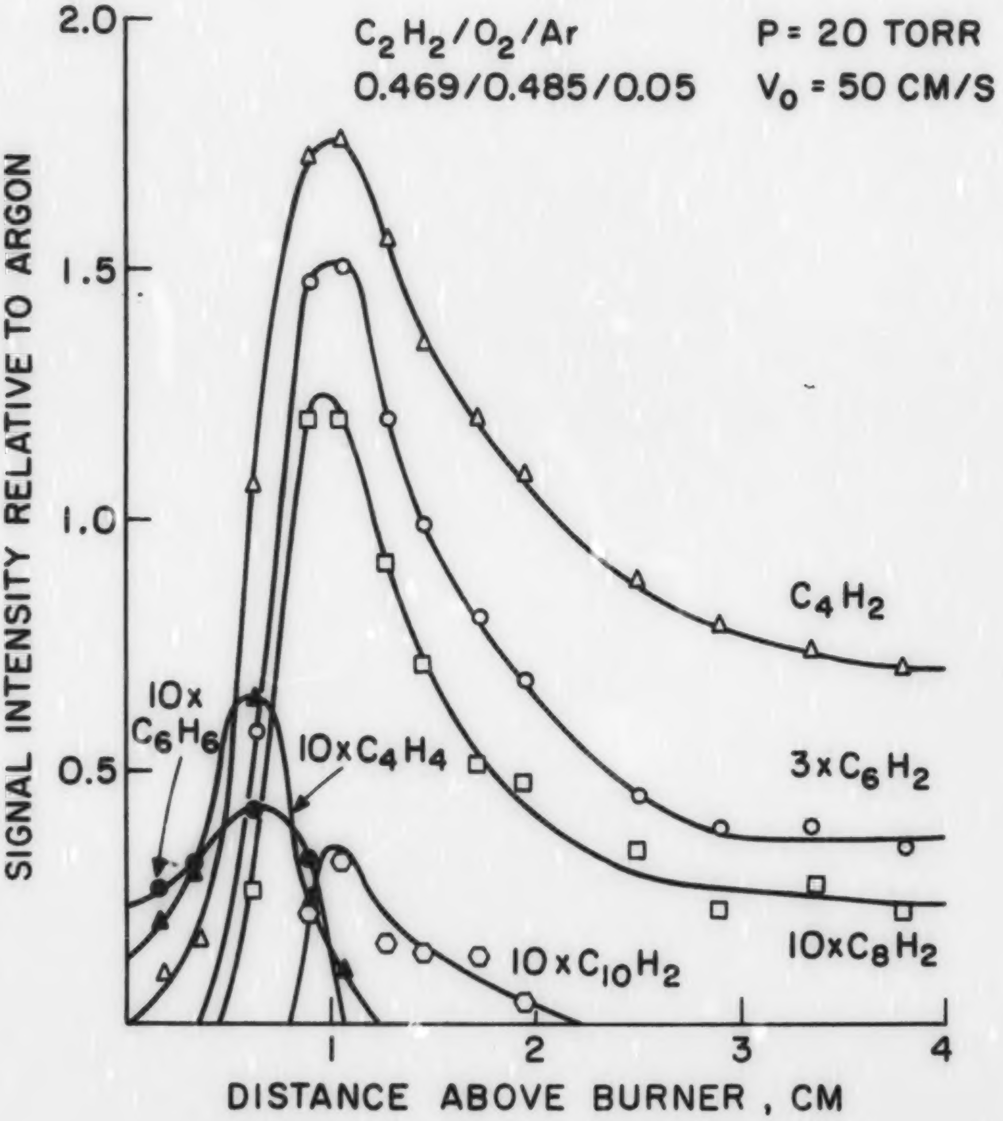

Figure 6. Profiles of signal intensities relative to argon for minor species in an acetylene-oxygen flame near the sooting limit. $\phi = 2.4$, P = 20 torr, V_0 = 50 cm/s, 5m% argon

INVESTIGATION OF NO_x, NITRATE AND SULFATE PRODUCTION IN LABORATORY FLAMES

By:

D. J. Seery, M. F. Zabielski, and L. G. Dodge
United Technologies Research Center
East Hartford, Connecticut 06108

Preceding page blank

SECTION 1

INTRODUCTION

This research program is directed toward an understanding of the chemical kinetics of the formation of NO_x, nitrates and sulfates in laboratory flames. In the first year, efforts will be directed toward elucidating the mechanisms of "prompt" NO formation and NO-NO_2 conversion. As part of the NO-NO_2 conversion study an investigation will be made of the possible perturbation of the NO_2 concentration by chemical reactions in the sampling probes.

The experimental procedure for this program consists of measurements of temperature and composition profiles obtained on a low pressure, flat flame burner and subsequent analysis of these data in terms of chemical mechanisms. Temperature profiles are obtained using miniature thermocouples and gas samples are extracted from the flame for concentration analysis using both a molecular beam sampler and quartz microprobes. The samples extracted by the microprobes will be analyzed by mass spectrometer and chemiluminescent analysis (for NO and NO_x). The molecular beam sampler is combined with a TOF mass spectrometer for analysis of both stable and unstable species. Molecular beam sampling has been selected as a standard for comparison with the microprobe since this technique seemed the one most likely to provide an unperturbed sample of flame gases.

In addition to probe sampling, measurements of NO and OH are being carried out using optical spectroscopy in order to provide an independent check on the accuracy of the concentration measurements of these species.

Preceding page blank

SECTION 2

EXPERIMENTAL

BURNERS AND ACCESSORIES

Two identical flat flame burners are used in the UTRC Flame Laboratory. One burner pictured in Fig. 1 is housed in a 6-inch Pyrex cross and is used for measurements involving optical spectrometry and microprobe sampling. The second burner is housed in a high vacuum chamber which is attached to the molecular beam sampler. A picture of this apparatus is shown in Fig. 2. Both burners have 3-inch diameter, water-cooled, sintered copper surfaces which provide flat flames with negligible radial gradients. The burners can be translated vertically by low-geared motors and the location is measured with a cathetometer to ± .0004". Cooling water to the burners is measured on entering and exiting and the exit temperatures are maintained at 50 ± 5°C. Cooling water to other parts of the burner housing is controlled so as to avoid water condensation.

Gas flow rates are measured by critical flow jewelled orifices. The upstream temperature and pressure are monitored continuously and the mass flow rates can be reset to ± 1%. Both chambers are evacuated through 1.5" lines by a 30 CFM Kinney KD-30 pump. This pump is isolated by a dry ice-acetone trap and provides a two hour run time without water contamination of the pump oil.

Temperatures are measured by means of fine thermocouple probes. For temperatures below 1900°K, 0.003" Pt/Pt-10 percent Rh thermocouples, coated with a mixture of BeO/Y_2O_3 to prevent catalytic reactions (Ref. 1) are used.

Above 1900°K, Ir/Ir-40 percent Rh thermocouples are used. The thermocouple probe is mounted in a flexible bellows housing so that it can be translated both vertically and horizontally. Thermocouple data are rapidly obtained with a Fluke 2100A Digital Thermometer. Both types of thermocouples are flame-welded so that the bead diameter is approximately 0.004". The large radiation correction caused in part by the high emissivity of the coating, poses a serious problem, since the theoretically calculated corrections (Ref. 2) have large uncertainties. Because of this uncertainty the radiation correction factor for these thermocouples is obtained by a detailed comparison with sodium line reversal measurements at several temperatures and extrapolated to other temperatures using the Stephan-Boltzmann relationships. The emissivity of the BeO/Y_2O_3 coating has been measured to be 0.64 ±.02. Using this value radiation corrections were calculated which deviated from the measured correction by up to a factor of two depending on the assumptions used.

An example of the thermocouple measurements is presented in Fig. 3. The data are for a stoichiometric methane air flame burning at a pressure of 76 torr. At two locations in the flame, radial temperature profiles are shown which indicate that the flame does indeed have a flat profile. The dashed line above the temperature data is from a thermocouple with a cracked coating. The increase in temperature is caused by catalytic reactions at the nobel metal surface and is a convenient indication of a coating failure.

Concentration profiles for OH are being measured using the $A^2\pi-X^2\Sigma(0,0)$ band at 3064 A. A water-cooled hollow cathode lamp operating with flowing Ar saturated with water vapor at a total pressure of 2 torr and a current of 100 mA is used as the source of narrow-line OH radiation. The vertical spectrometer slit is rotated by a quartz dove prism to a horizontal image in the flame with a resulting vertical resolution in the flame of better than 1.5 mm. A 0.5 meter spectrometer with a 1200 g/mm grating operated in second order is used to achieve a resolution of better than 0.15 A. The optical system is shown schematically in Fig. 4. Included in the diagram is a multipass system which is required for measurements of NO at low concentrations. Rotational temperature measurements are made to assure rotational equilibrium and that concentration measurements of OH may be made from single spectral line measurements.

A concentration profile for OH as shown in Fig. 5 was determined for the region from 2 mm to 40 mm above the base of the burner by averaging values for the three lines $R_2(3)$, $R_2(4)$, and $R_2(14)$. Data for both temperature and concentration were reduced assuming uniform temperature and concentration profiles across the burner.

MICROPROBE SAMPLING

Microprobe sampling of low pressure flames can be discussed in terms of two problems: (1) perturbation of the flame due to the sampling probe and (2) perturbation of the gas sample by chemical reactions in the probe.

The first problem, perturbation of the flame, can be minimized by working with very fine, uncooled-probes to decrease both the aerodynamic and the thermal disturbance. The design and operation of such probes has been discussed in detail by Fristrom and Westenberg (Ref. 3). It should be pointed out however that even for very small microprobes there is a measurable thermal sink which can have significant effects on the temperature history of the gas sample. Figure 6 presents measurements in a CH_4-Air flame of the gas upstream of a microprobe. The temperature decrease with a water-cooled probe is, of course, larger but in any case this temperature change can and should be measured.

The perturbation of a gas sample by chemical reaction in the probe is a poorly understood phenomena (Ref. 4). Although the initial quench rate in a probe can be readily calculated, because of shock waves and boundary layer effects in the probe the actual aerodynamic conditions are uncertain.

Calculations using the UTRC (Ref. 5) probe deck indicate that for many cases the gas temperature in uncooled probes rapidly returns to the stagnation conditions. Chemical reactions in probes are most important for species present in low concentrations. For example, the concentration of a major product like CO_2 is not likely to be affected by 0.1 % of O atom, whereas the NO or NO_2 concentrations which can be comparable to the O atom can be greatly altered.

The microprobes used in this study are similar to those described in Ref. 3 and by Merryman and Levy (Ref. 10), that is, quartz with 75 to 100 micron orifices both cooled and uncooled. These probes appear to provide reliable gas samples for major constituents based on atom mass balances. The calculated temperature profile shown in Fig. 7 however indicates that the rate of quenching may not be rapid enough to preserve the original concentrations of minor species. The microprobes are attached to a 0.5" diameter, teflon-coated, aluminum line which leads to the specific gas analyzers or a mass spectrometer. Because of the facility's design, sample line lengths can be kept to six feet or less. The sample line is maintained at 125°C to minimize adsorption and condensation of water.

For microprobe measurements, NO and NO_x are determined with a Thermo-Electron Corporation (TECO) Series 10 Chemiluminescent Analyzer. This instrument has a stated minimum detectable concentration of 50 ppb and a linearity of ± 1 percent. Maximum NO concentration is 10,000 ppm. For NO_x measurements, a TECO Model 300 Molybdenum NO_x Converter is used.

MOLECULAR BEAM SAMPLING

A sampling technique that does not have the major disadvantages of microprobes is the molecular beam sampler. Figure 2 is a picture of the molecular beam sampler and Fig. 8 schematically shows the flat flame burner, molecular beam sampler and mass spectrometer ion source. The pressure in the reaction chamber is maintained at 76 torr for all flames. The gases sampled from the flame are supersonically expanded through the nozzle orifice into the nozzle chamber. The mean pressure in this chamber is typically 10^{-3} - 10^{-4} torr. The nozzle is a 120°(40°) "hybrid" (Ref. 6) made of quartz with a .05 cm orifice. Because of the large pressure gradient across the orifice, the hot sampled gases experience a dramatic decrease in temperature that "freezes" most chemical reactions. The central core of this supersonic expansion is then isolated by a skimmer with about a 0.10 cm orifice. This skimmed core constitutes the molecular beam that traverses the chamber. The pressure in the skimmer chamber is maintained at approximately 1×10^{-6} torr. The beam is then collimated and enters the ion source of the mass spectrometer. Typically, the pressure within the mass spectrometer chamber is 5×10^{-7} torr.

The photograph in Fig. 2 shows all of the significant features of the apparatus as presently constituted. Also shown in this photograph are an optical access port (rear port not visible), cooling water thermometers, six-inch diffusion pumps, and associated plumbing. The nozzle and skimmer chambers are separated by a diagonal wall. This is done to insure maximum pumping speed for the nozzle chamber, which handles the bulk of the gas flow. The vacuum line connecting the nozzle chamber to the diffusion pump has a six-inch diameter while the skimmer chamber line has a three-inch diameter line. Nozzle Knudsen numbers of $10^{-1} > K_{no} \geq 2 \times 10^{-3}$ are desired to minimize the boundary layer at the sampling orifice. In the present study the molecular beam has been designed to have $K_{no} = 2 \times 10^{-2}$.

A photograph of a methane-air flame in the beam sampling apparatus is shown in Fig. 9.

MASS SPECTROMETER

The primary analytical instrument used in the low pressure flame investigations is a 1 meter, bipolar 1 KeV, time-of-flight (TOF) mass spectrometer designed and built at UTRC. The instrument has a normal resolving power of 200, and a maximum value of 700. All of the ion sources for this instrument employ electrostatic focusing of the ionizing beam which provides superior low mass sensitivity in comparison with the magnetic focusing found on commercial instruments. This is particularly useful in H and H_2 measurements. Also, the ionizing electron energy can be automatically scanned to further facilitate appearance potential measurements.

The vacuum system is sufficient to limit the residual gas background pressure to about $5\text{-}10 \times 10^{-9}$ torr. Hence, with a source pressure of 1×10^{-3} torr, the interference at a given mass is usually of the order of $1{:}10^6$ or better.

SECTION 3

DATA PROCESSING AND ANALYSIS

In order to facilitate the data reduction and to improve the precision of the data, the mass spectrometer has been coupled with a Northern Scientific NS-575 signal averager. In the measurements that have been made, typically 32 spectra per sampling location have been averaged. This corresponds to an improvement in the signal-to-noise ratio by a factor of 5.7. Using this method, the Ar^{36} and Ar^{38} isotopes in air can be detected. This corresponds to approximately 30 and 4 ppm, respectively, without resorting to ion counting.

The data from the signal averager is recorded on 7-track magnetic tape and then transferred to a Digital Equipment Corporation PDP-6 time-share computing system. A schematic diagram of the burner, sampler, mass spectrometer and data handling equipment is shown in Fig. 10.

Once the data are in the computer, two separate programs are used in the actual reduction. The first program consists of the following sections: (1) a fast Fourier transform (FFT) routine to analyze the noise content of the spectra; (2) Martin-Graham digital filter to smooth the data; (3) a routine for baseline subtraction; (4) a mass marker routine; (5) a peak area and height reading routine, and (6) a deconvolution routine for unfolding overlapping peaks. The deconvolution routine is based on both a Fourier and a modified Gauss-Seidel iterative technique. In addition, the iterative technique has been shown to work in situations where the Fourier techniques fail (Ref. 7); thus, even when small peaks reside on the shoulders of large peaks, quantitative measurements can be made. The second program is used to invert the data matrix generated by the first program. This data matrix can be fairly complex, depending on the range of masses observed and the constituents of the gas being analyzed. Frequently, more than one species contributes to a given mass peak; fortunately, however, the observed peak is the result of the linear superposition of all the ion currents at the particular mass. The overlap of ion currents at a particular mass normally arises from two or more species having the same nominal mass like ethylene, nitrogen and CO at mass 28 and from species that fragment under electron impact such as the ethylene fragment from ethane.

The value of mass spectrometry data obtained from flames is highly dependent on calibration of the experiment and control of minor variables. In the present experiments checks have been made on the effects of variation in chamber pressure, changes in the temperature drop in the water-cooled burner and temperature drop in the flame gases because of the heat sink of the sampling probe. The concentration data are checked for mass balance consistency and, of course, the mass spectrometer sensitivity and the sampling line efficiency are determined for each species to be measured.

The calibration of the microprobe and analytical instrumentation is accomplished by using the critical orifice gas metering system for major species and premixed gas bottles for minor species. Several concentrations representative of the expected flame concentrations are normally chosen. This is required because of the limited dynamic range of the specific gas analyzers and also as a check on the linearity of both the analyzers and the mass spectrometer.

The calibration of the molecular beam is considerably more complicated. First, for the specific range of flame conditions (pressures, temperatures), the optimum nozzle orifice-skimmer orifice distance is determined. If this distance is too small, skimmer interaction with the central core of the free jet expansion occurs. If this distance is too large, then skimming is performed beyond the Mach disk which results in low beam intensity. The optimum location for low pressure flames is usually in the region of translalational freezing point. Once the optimum beam intensity is determined, the burner is removed from the chamber and a quartz chamber and furnace are installed for heating stable species. This high temperature calibration is required because molecular species can be "frozen" in excited states which, consequently, change the ionization potential of the molecule, the appearance potential for certain reactions, and the fragmentation pattern even at 70 eV (Ref. 8). Measurements of the temperature dependence of the methane fragmentation pattern are presented in Fig. 11. For the conditions of the present study the 16/15 ratio for methane does not appear to be dependent on temperature. The net result of this calibration is a set of sensitivity factors and fragmentation patterns that are incorporated into the data reduction program.

A difficulty in analyzing mass spectrometer data is illustrated in Fig. 12, which shows the signal averager data for a methane-air flame in the mass range from 27-31. In (a) the large single peak is at mass 28 and is predominantly attributable to N_2 with only a small contribution from CO. The contribution from CO_2 is negligible for this case. As the sensitivity of the scale is increased, (b) and (c), the peak at mass 29, which is mostly $N^{15}N^{14}$ becomes apparent. Also in (c) the mass 30 peak can be seen, and with increasing sensitivity (d) it can be conveniently measured. The mass 30 peak is composed of contributions from NO, $C^{12}O^{18}$ and $N^{15}N^{15}$ and accurate data is required on the latter two species in order to calculate the NO concentration.

In analyzing concentration data from flames, the diffusion velocity is a major correction and cannot be neglected. A major advantage of low pressure flames is that the concentration gradients are more gradual than in atmospheric flames and thus the diffusion velocity can be calculated with greater accuracy.

The diffusion corrected mass flux data are used to calculate the rates of formation and disappearance of the individual species. Reaction mechanisms and rate constant data can be obtained from this data by the kinds of analysis exemplified in the works of Fristrom and Westenberg (Ref. 3) and Fenimore (Ref. 9), or by matching the data with model calculations.

SECTION 4

REFERENCES

1. Kent, J. H.: Combust. Flame 14, 279 (1970).
2. Kaskan, W. E.: Sixth Symposium (International) on Combustion. Rheinhold, New York, 174 (1975).
3. Fristrom, R. M. and A. A. Westenberg: Flame Structure. McGraw-Hill, New York (1965).
4. Lengelle, G. and C. Verdier: Gas Sampling and Analysis in Combustion Phenomena. AGARDograph No. 168, AGARD, Paris (1973).
5. Cohen, L. S. and R. N. Guile: AIAA Journal 8, 1053 (1970).
6. Biordi, J. C., C. P. Lazzara and J. F. Papp: Combust. Flame 23, 73 (1974).
7. Milne, T. A., J. E. Beachey and F. T. Greene: J. Chem. Phys. 56, 3007 (1972).
8. Zabielski, M. F. and T. M. McHugh: Proceedings of 21st Annual Conference on Mass Spectrometry and Allied Topics, 198 (1973).
9. Fenimore, C. P.: Chemistry in Premixed Flames. MacMillan, New York (1964).
10. Merryman, E. L. and A. Levy: Fifteenth Symposium (International) on Combustion. The Combustion Institute, 1073 (1975).

Fig. 1

FLAT FLAME BURNER

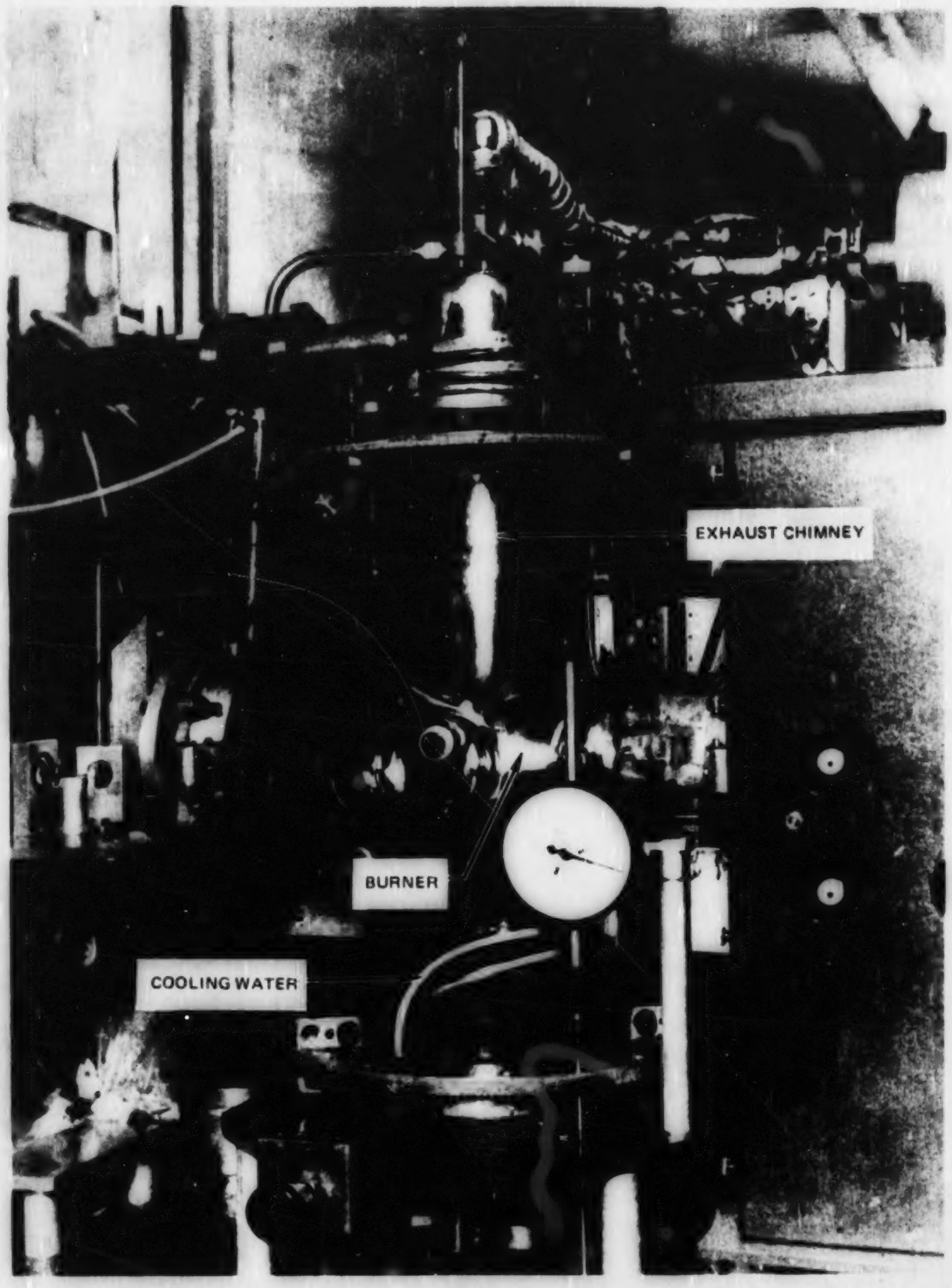
EXHAUST CHIMNEY
BURNER
COOLING WATER

FIG. 2

MOLECULAR BEAM SAMPLER

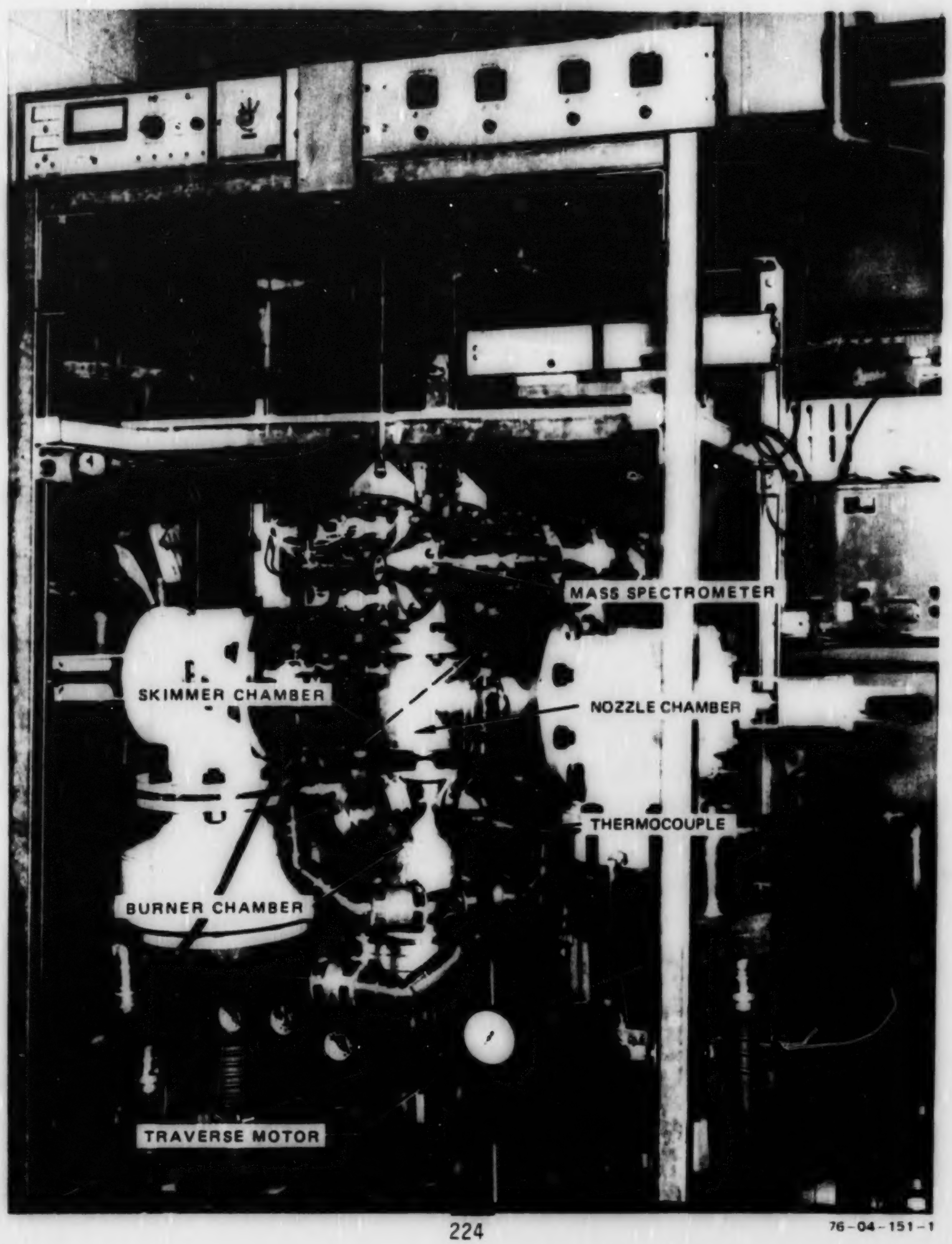
MASS SPECTROMETER
SKIMMER CHAMBER
NOZZLE CHAMBER
THERMOCOUPLE
BURNER CHAMBER
TRAVERSE MOTOR

76-04-151-1

FIG. 3

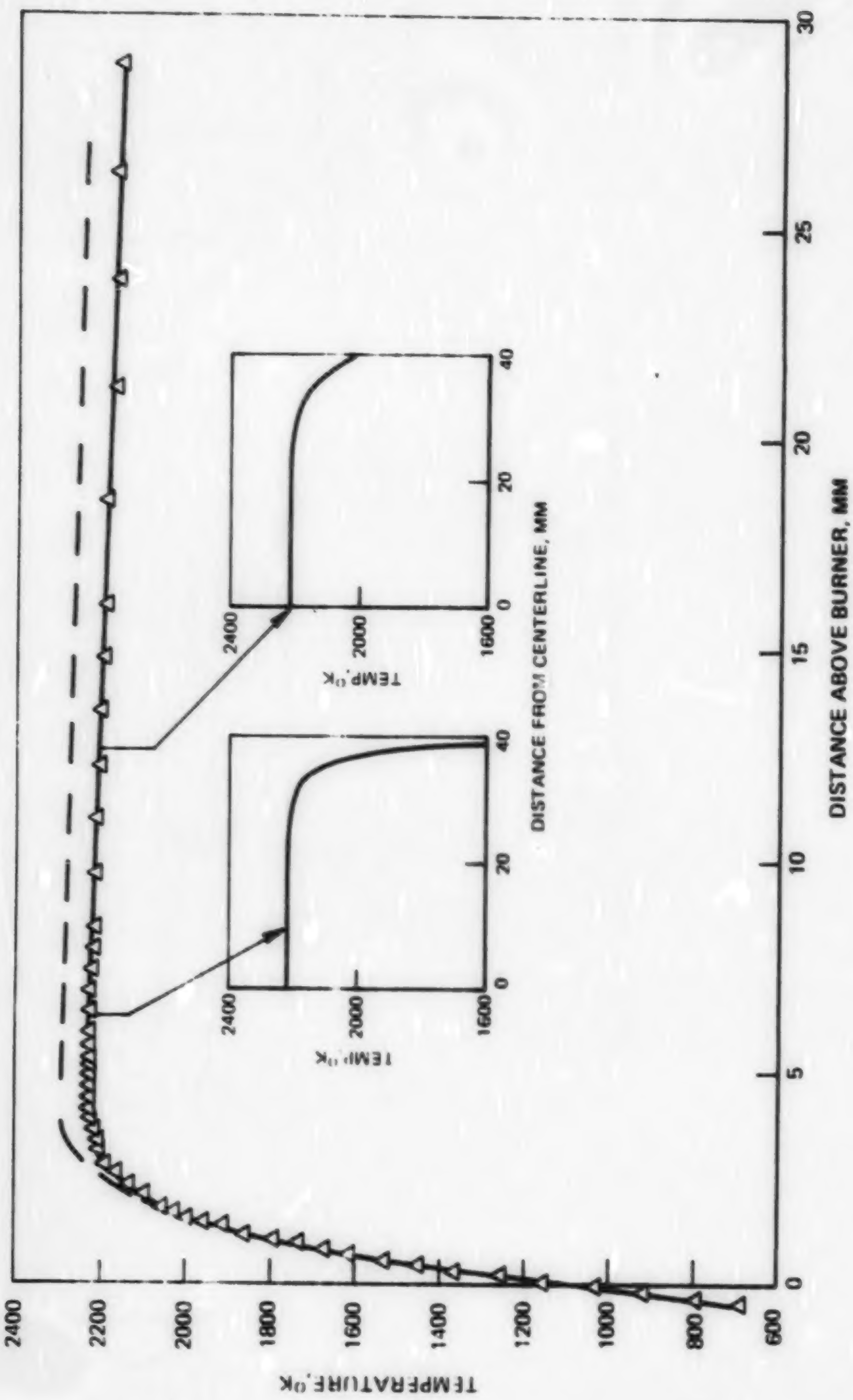

METHANE–AIR FLAME

P-76 TORR   Φ-1.0

77 07 61 3

FIG. 4

OPTICAL SYSTEM FOR MEASUREMENT OF NITRIC OXIDE IN FLAT FLAME BURNER

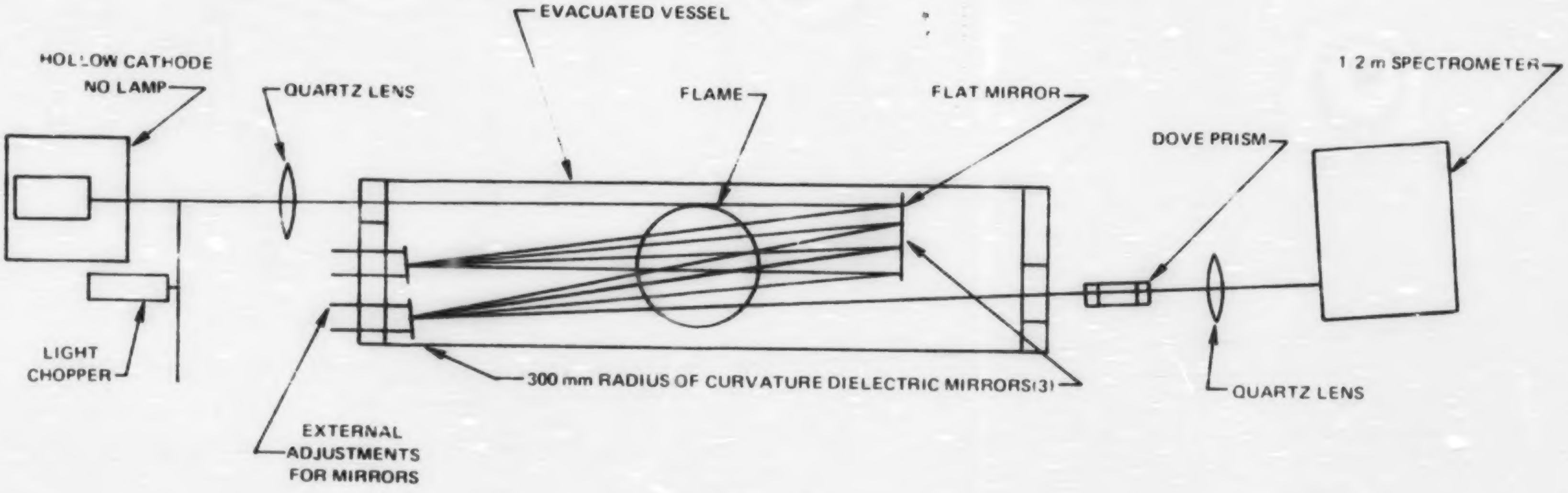
EVACUATED VESSEL
HOLLOW CATHODE NO LAMP
QUARTZ LENS
FLAME
FLAT MIRROR
1 2 m SPECTROMETER
DOVE PRISM
LIGHT CHOPPER
300 mm RADIUS OF CURVATURE DIELECTRIC MIRRORS(3)
QUARTZ LENS
EXTERNAL ADJUSTMENTS FOR MIRRORS

77 07 61 4

FIG. 5

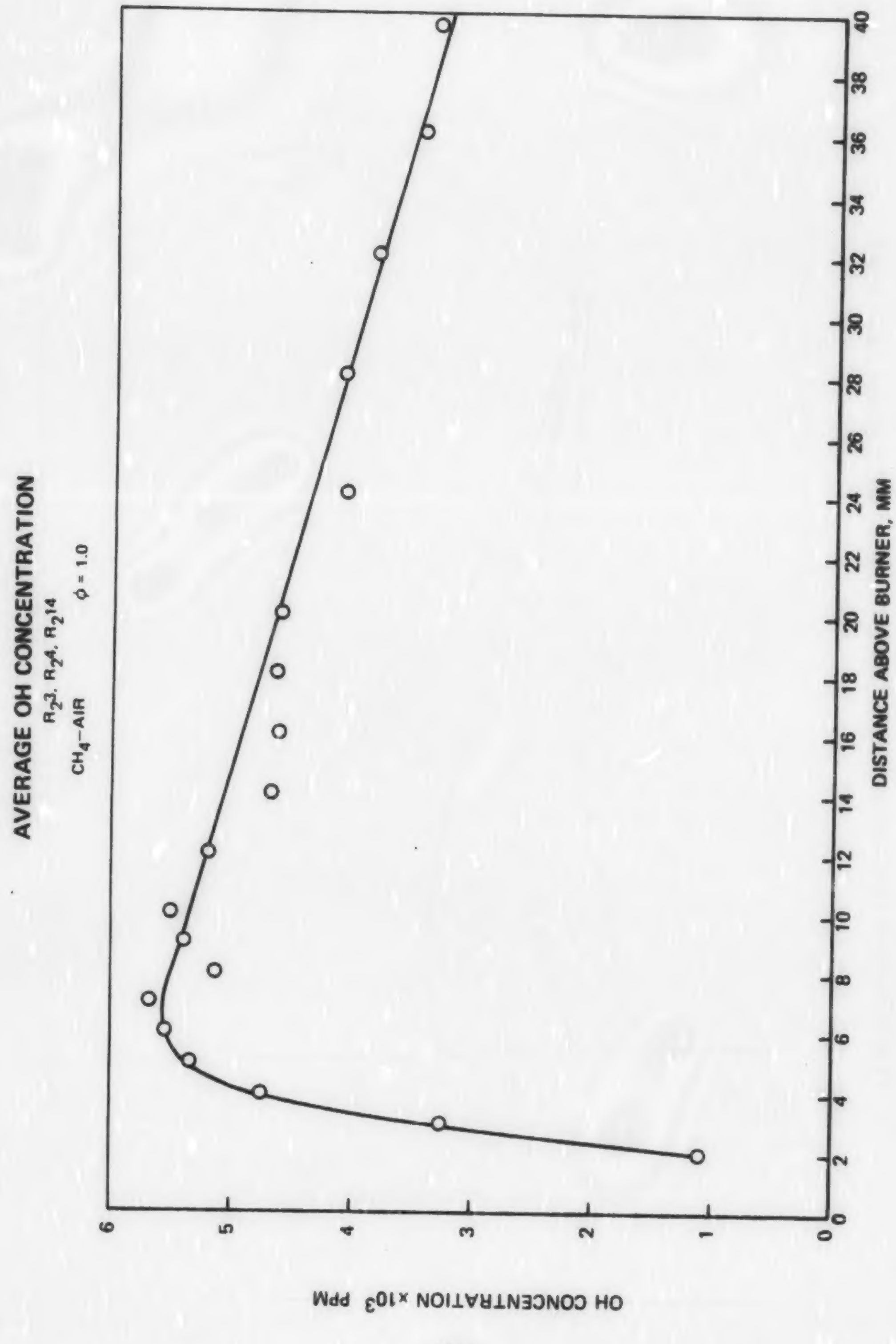

77-07-28-1

FIG. 6

TEMPERATURE PERTURBATION OF UNCOOLED QUARTZ SAMPLING PROBE

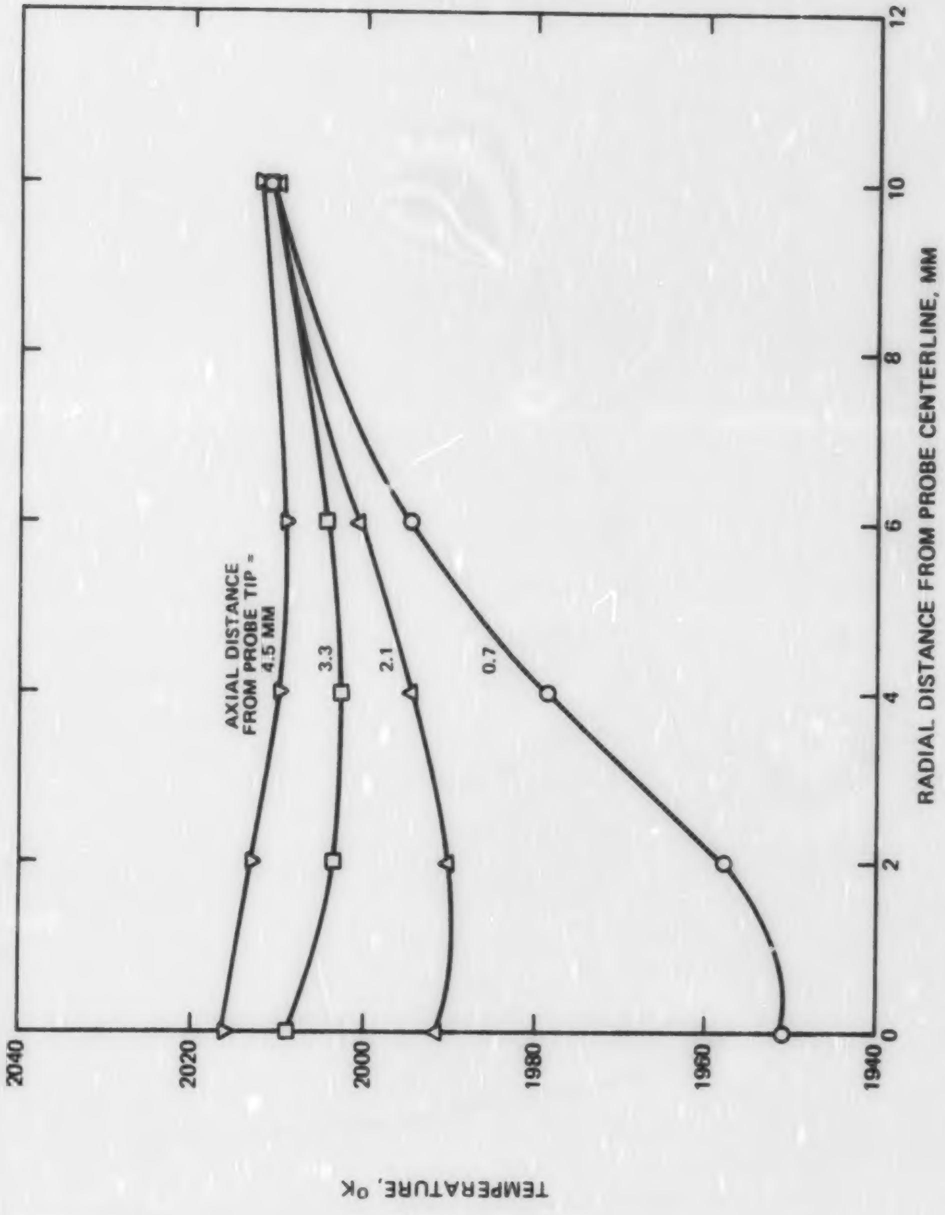

FIG. 7

TEMPERATURE DISTRIBUTION FOR MICROPROBE

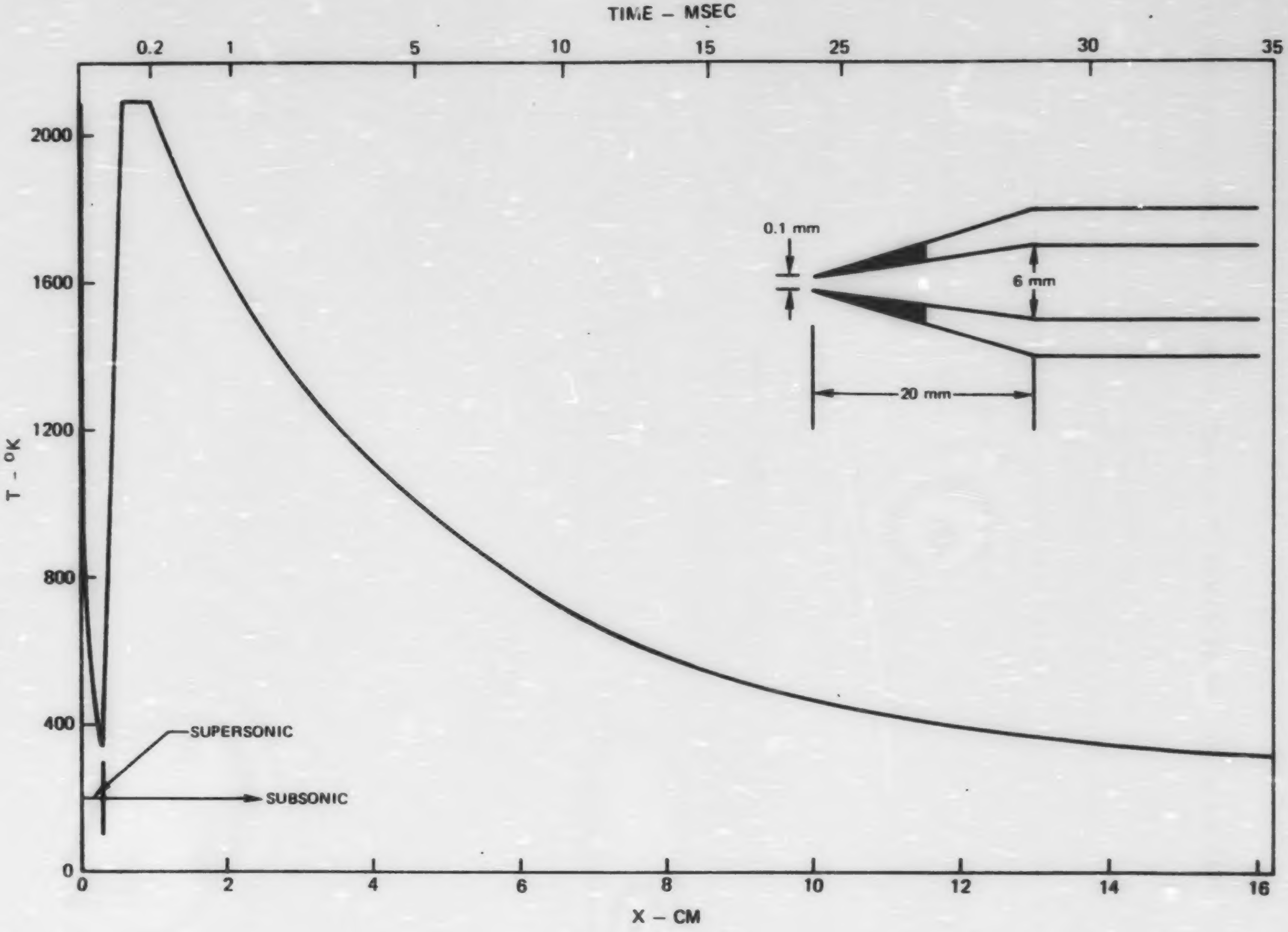

77-07-28 4

FIG. 8

SCHEMATIC REPRESENTATION OF MOLECULAR BEAM MASS SPECTROMETRIC SYSTEM

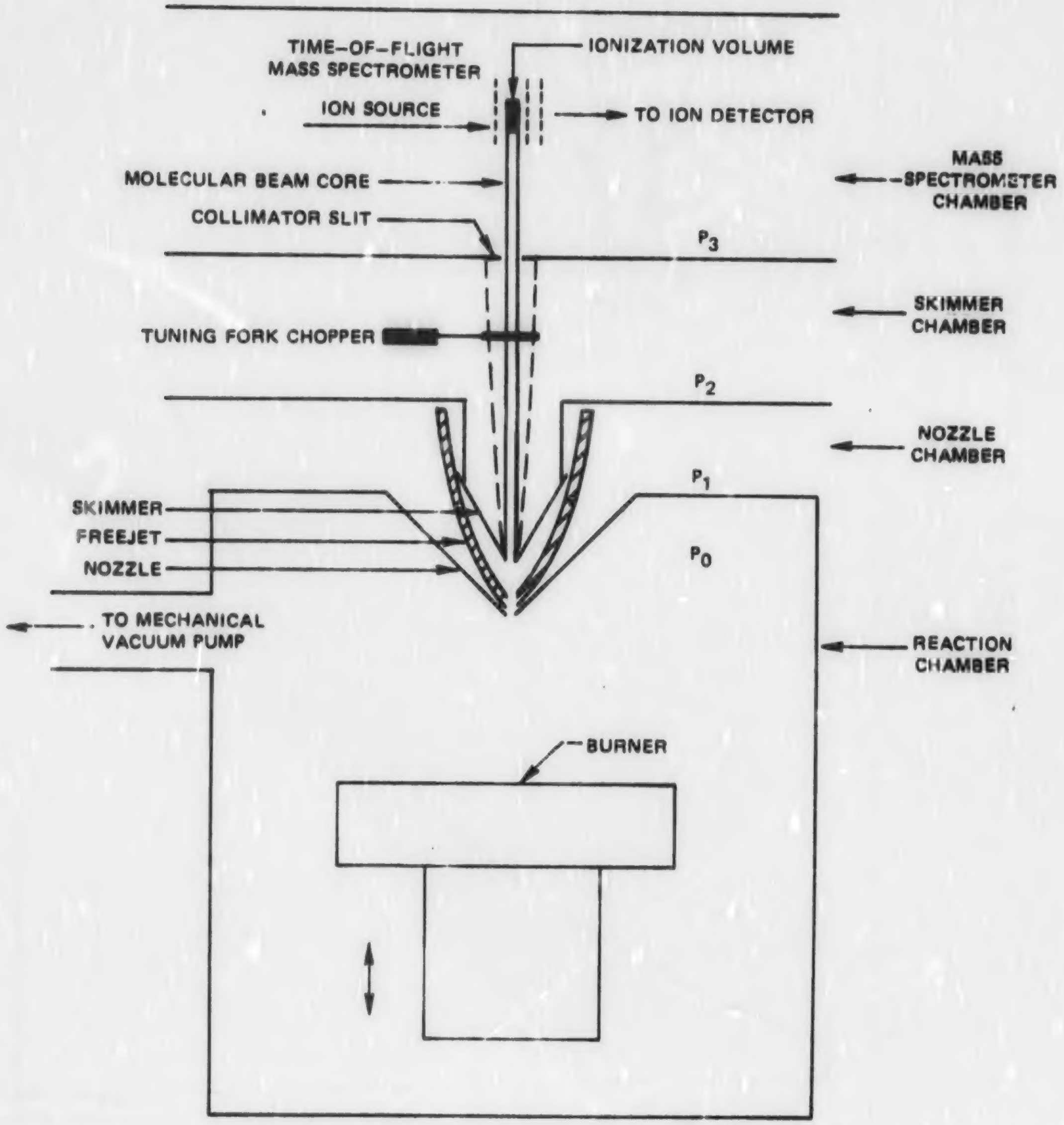
TIME-OF-FLIGHT MASS SPECTROMETER
IONIZATION VOLUME
ION SOURCE
TO ION DETECTOR
MOLECULAR BEAM CORE
MASS SPECTROMETER CHAMBER
COLLIMATOR SLIT
P_3
SKIMMER CHAMBER
TUNING FORK CHOPPER
P_2
NOZZLE CHAMBER
P_1
SKIMMER
FREEJET
NOZZLE
P_0
TO MECHANICAL VACUUM PUMP
REACTION CHAMBER
BURNER

Fig. 9

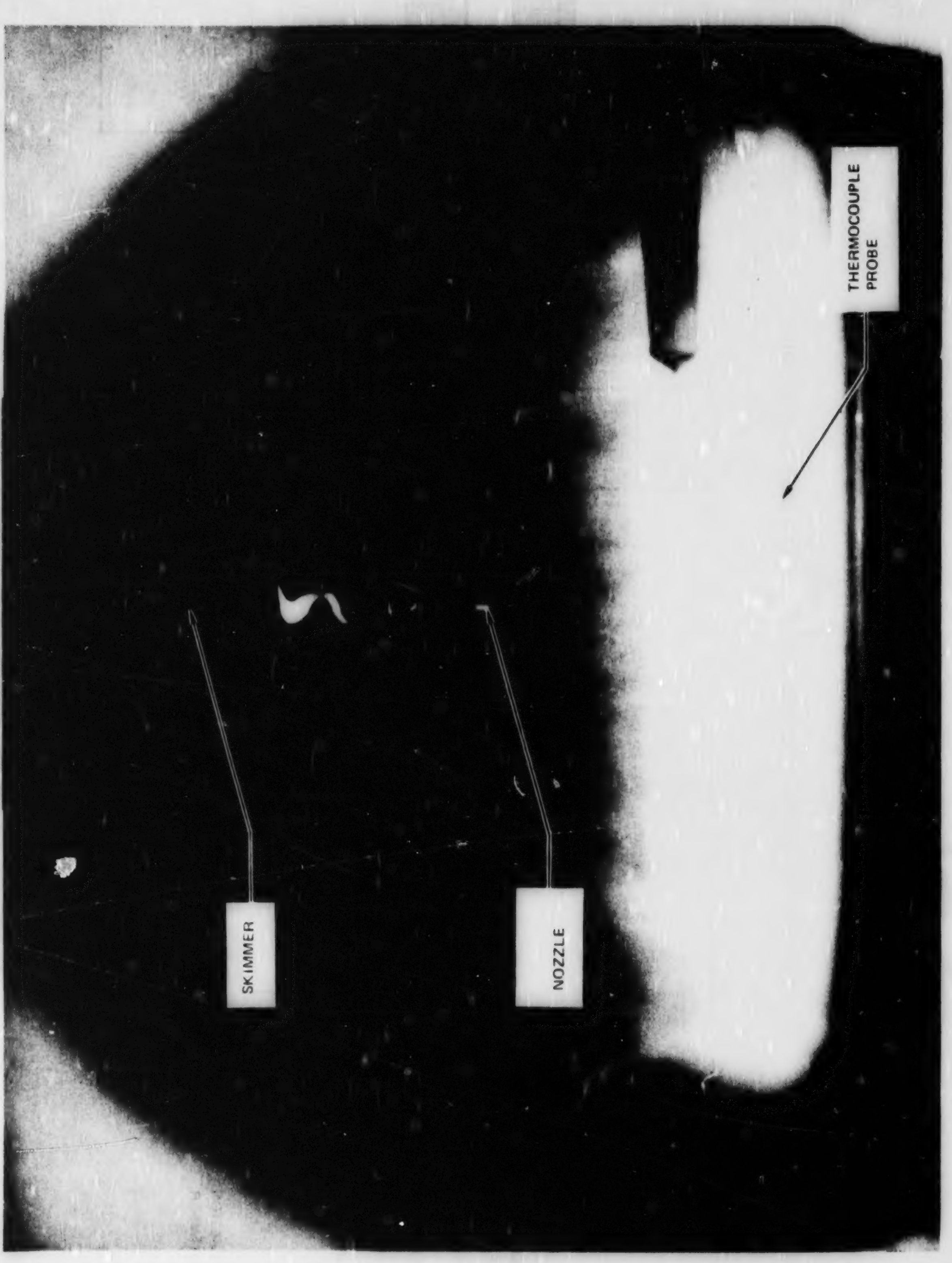
THERMOCOUPLE PROBE
SKIMMER
NOZZLE

MOLECULAR BEAM SAMPLER IN FLAME

SCHEMATIC OF MOLECULAR BEAM SAMPLER AND ACCESSORIES

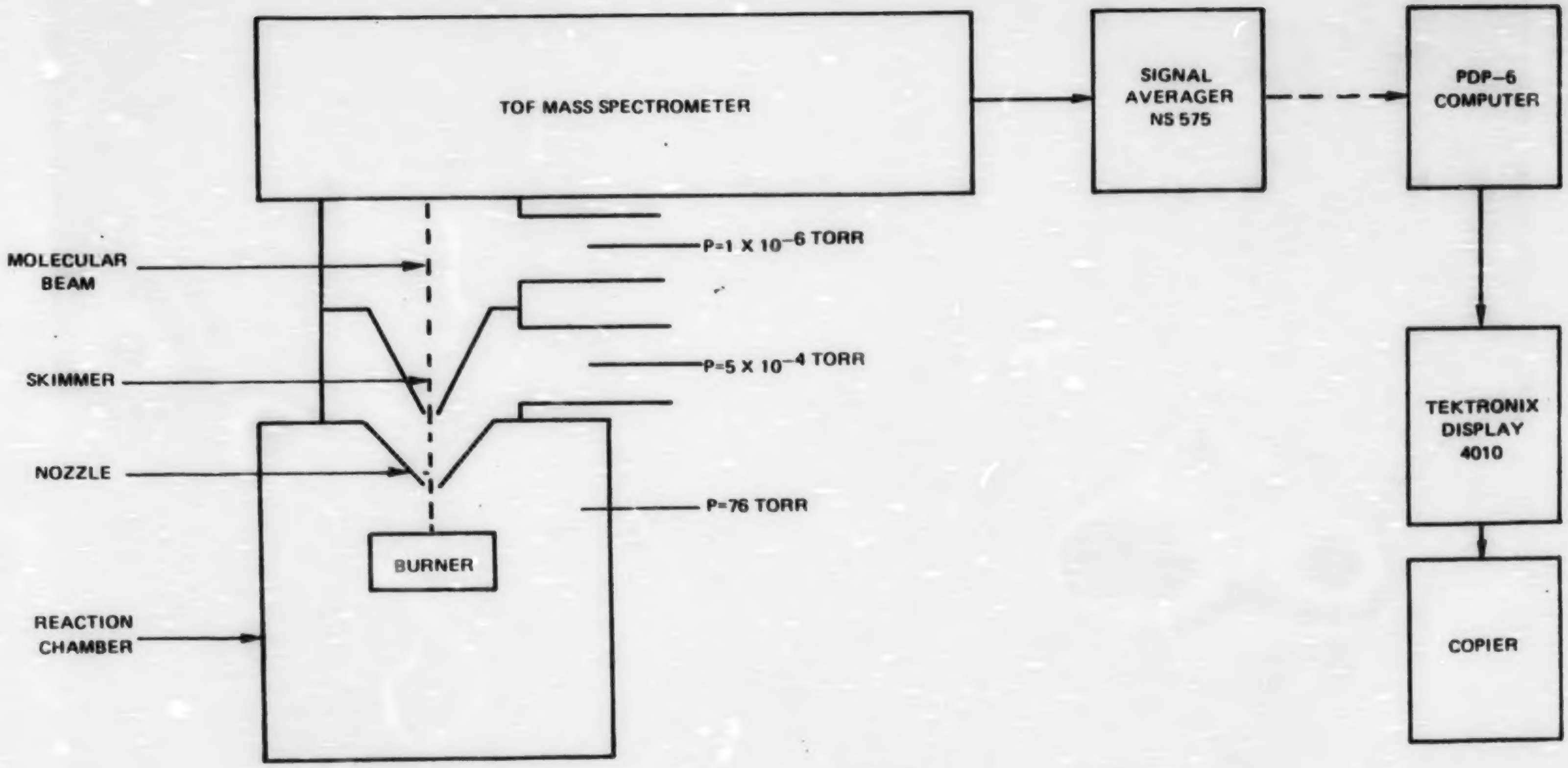
TOF MASS SPECTROMETER
SIGNAL AVERAGER NS 575
PDP–6 COMPUTER
TEKTRONIX DISPLAY 4010
COPIER
MOLECULAR BEAM
SKIMMER
NOZZLE
REACTION CHAMBER
BURNER
P=1 X 10^{-6} TORR
P=5 X 10^{-4} TORR
P=76 TORR

FIG. 10

FIG. 11

TEMPERATURE DEPENDENCE OF METHANE FRAGMENTATION

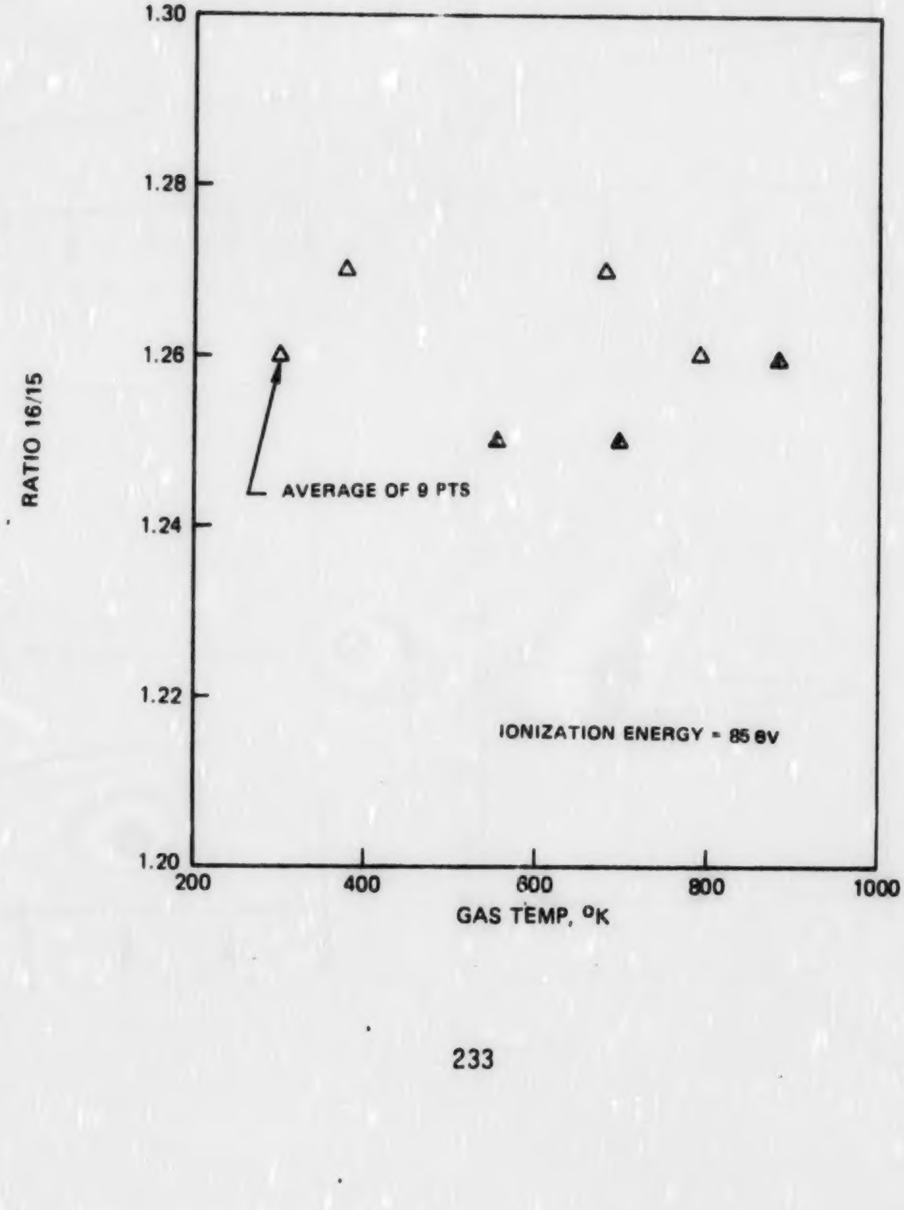

77-07-28-2

FIG. 12

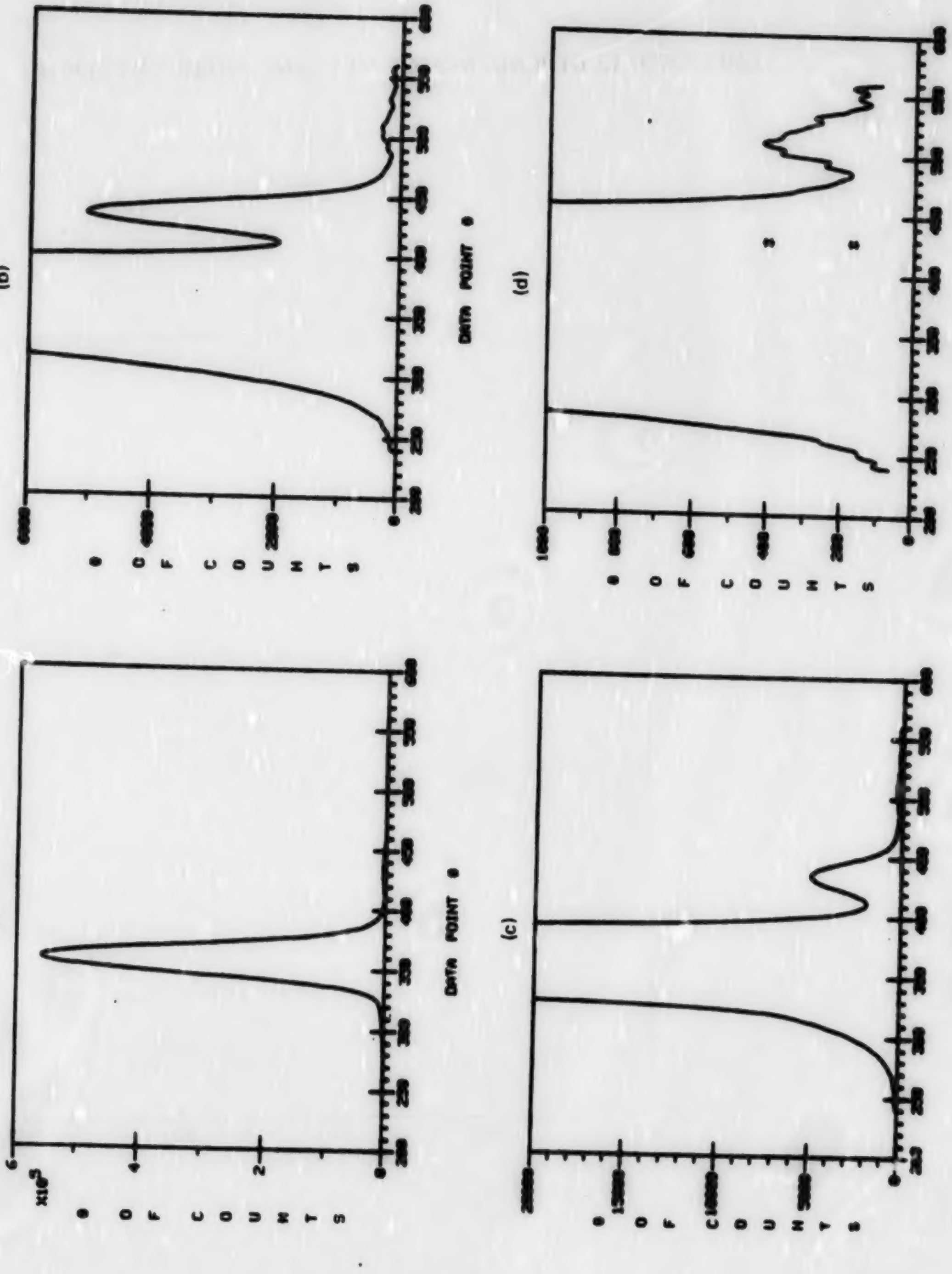

MASS SPECTROMETER DATA

FOR MASSES 27 TO 31

INFLUENCE OF AERODYNAMIC PHENOMENA ON POLLUTANT FORMATION IN COMBUSTION

Phase II -- Liquid Fuels

By:

L. J. Spadaccini, J. B. McVey, J. B. Kennedy, F. K. Owen,
C. T. Bowman, A. Vranos, A. S. Kesten
United Technologies Research Center
East Hartford, Connecticut 06108

ABSTRACT

An experimental investigation of the effects of the interaction between physical and chemical processes on pollutant formation and destruction in a liquid fuel turbulent diffusion flame burner has been carried out. In this investigation, the effects of fuel type, inlet air swirl, inlet air temperature and combustor pressure on the spray characteristics and the time-mean and fluctuating flow field structure have been determined using probing and optical techniques. Changes in the spray and flow field structure have been correlated with changes in pollutant emissions from the burner. The results of this investigation show that variation of these operating parameters produce major changes in spray dynamics and vaporization rates and in the time-averaged fuel/air distribution within the burner which significantly influence energy release rates and pollutant formation and destruction. In addition, it was found that there are significant differences between the mean velocities of the gas and fuel droplets which likely influence droplet vaporization rates and mixing of the vaporized fuel and air.

Preceding page blank

ACKNOWLEDGMENTS

A number of individuals at UTRC made significant contributions to the experimental investigation. Dr. M. F. Zabielski and Mr. G. L. Dodge designed the gas sampling system used in the investigation and developed the calibration procedures employed in the gas sampling portion of the experiments. Mr. T. A. Murrin assisted throughout the experimental program and was responsible for operation of the combustor and for reduction of much of the experimental data.

A special debt of gratitude is owed to Mr. W. S. Lanier, the EPA Project Officer for this contract effort, for asking the critical questions and questioning the critical answers.

Preceding page blank

SECTION 1

INTRODUCTION

A large number of continuous combustion devices, including furnaces and gas turbines, operate on liquid fuels. Investigations of pollutant emissions from these devices indicate that changes in injector design which change the droplet size distribution in the spray and variations in air inlet conditions which alter the interaction between the fuel spray and the surrounding gas stream (1-6) can have a significant effect on pollutant formation and destruction. Norster and Lefebvre (1) found that atomization techniques can affect pollutant emissions, particularly exhaust smoke, in a gas turbine combustor. Grobman (2) reported that improving fuel atomization reduces hydrocarbon and carbon monoxide emissions during idle in a wide range of conventional and experimental gas turbine combustors. Mellor and his co-workers (3,5) and Pompei and Heywood (4) have attributed changes in carbon monoxide and nitric oxide emissions from gas turbine combustion with fuel injection pressures to changes in fuel atomization and vaporization rates. Inlet air temperature and swirl, combustor pressure and combustor reference velocity* significantly influence hydrocarbon, carbon monoxide and nitrogen oxide emissions (1-3,6). Hence, it appears that appropriate modifications of fuel atomization techniques and combustor inlet conditions can result in significant reductions in the emissions of most pollutant species from continuous combustion devices.

*The combustor reference velocity, V_{ref}, is a measure of combustor residence time and is defined by $V_{ref} \equiv \dot{M}_{air}/\rho_{air}A_{max}$ where $\dot{M}_{air}$ = air flow rate, ρ_{air} = inlet air density and A_{max} = maximum combustor cross-sectional area.

The combustion of liquid fuel sprays is a complex process involving simultaneous heat, mass and momentum transfer and chemical reaction which are influenced by the fuel characteristics, the droplet size distribution and number density, the relative velocity between the droplets and surrounding gas and the ambient gas temperature and composition. Although qualitative models and empirical correlations of pollutant emissions from liquid-fueled combustors have been developed (see, for example, 7 and 8), our present understanding of spray burning is insufficient to permit quantitative predictions of the effects of changes in fuel injection techniques and operating conditions on pollutant emissions. Investigations of burning sprays have been hampered by difficulties associated with measuring the characteristics of the spray and with determining the interaction of the spray with the surrounding gas stream. However, recently-developed optical and probing techniques appear to be promising diagnostic tools for measurements on burning sprays.

This paper outlines the results of an experimental investigation, sponsored by EPA under Contract 68-02-1873, of the effects of several operating parameters on the spray characteristics and flow field structure in a liquid-fuel turbulent diffusion flame burner and the subsequent effects on pollutant formation and destruction. This work is documented in more detail in Ref. 9.

SECTION 2

EXPERIMENTAL APPARATUS AND INSTRUMENTATION

The experimental apparatus and approach used in this study are similar to those employed previously to study pollutant formation and energy release in gaseous-fuel turbulent diffusion flames (10). The only significant change in the combustor configuration is the fuel injector modification required for liquid fuel operation. A schematic diagram of the water-cooled combustion system is presented in Figure 1. It consists of an electric resistance-type air heater, a 12.2 cm-dia water-cooled cylindrical combustor section having a centrally located pressure-atomizing fuel injector and an extension section which contained an exhaust probe rake and a water-cooled orifice plate which can be installed to increase the combustor pressure. As in the gaseous fuel study, flame stabilization in the high velocity flows investigated was achieved by producing a recirculation zone in the initial region of the combustor by imparting a swirl component to the airflow. Swirl was imparted by inserting replaceable sets of straight swirl vanes into the annular passage which surrounds the fuel injector. The trailing edges of the swirl vanes are located upstream of the injector exit plane to permit measurement of the airflow characteristics entering the combustor. These measurements permit determination of the inlet conditions which are needed for the analytical modeling effort. The combustor was designed to permit independent variation of each of three operating parameters -- inlet air swirl, combustor pressure and air preheat -- which are known to significantly influence emissions from liquid-fuel combustors.

In the present study, three fuels were investigated -- liquid propane, iso-octane, and No. 2 distillate fuel. These fuels provide an orderly progression in complexity of molecular structure and distillation characteristics and permit an evaluation of the effects of chemical and physical properties of fuels on pollutant formation and energy release. Typical liquid fuel properties and the results of limited quantitative fuel analyses are given in Ref. 9. The injector assembly was water-cooled so that the fuel was not heated by the high-temperature inlet air, and fuel injector design and injection pressure were chosen to ensure liquid injection. A conventional pressure-atomizing swirl-type nozzle which produced a nominal 60 deg hollow-cone spray with a nominal droplet Sauter mean diameter of 100 μm in quiescent air at atmospheric pressure was used for iso-octane and No. 2 distillate fuel. This type of nozzle proved unsuitable for propane since vaporization occurred internally due to expansion in the nozzle swirl chamber. Therefore, a tangential-feed, pressure-atomizing nozzle in which the full pressure drop occurred across the exit orifice was used to maintain the propane liquid to the point of injection. The direction of rotation imparted by the swirlers to both the fuel and the air streams were identical for each of the configurations tested. The fuel injectors, air swirl vane designs, and the fuel injector assembly are shown in Ref. 9.

Measurements in the combusting flow were made through 6.4-cm dia window ports in the combustor sections (Figure 1). A pair of window ports 180 deg apart are present at each location and permit the use of optical measurement techniques (e.g., laser velocimetry and laser holography). The location of a port directly downstream of the injector exit plane allowed an unhindered view of the flame in the vicinity of the fuel injector and permitted acquisition of flow field data close to the injection plane. The combustor probing devices are compatabile with all window ports and may replace a quartz window or water-cooled plug in any given port. In addition, the entry section was designed to permit axial relocation of the fuel injector between tests, thereby increasing the number of axial locations at which radial traverse can be made. A porous-metal disc installed in the air entry section serves to provide a uniform inlet flow, which was verified by laser velocimeter measurements, and the combustor wall temperature was maintained at a constant value (~500°K) along the entire 100 cm length by regulating the coolant flow rates.

The concentration of nitrogen oxides (NO, NO_2), oxygen (O_2), carbon monoxide (CO), carbon dioxide (CO_2), and unburned hydrocarbons (THC) within the combustor were measured using cooled traversing sampling probes coupled to on-line analytical instrumentation. Nondispersive infrared analyzers were used to measure the CO and CO_2 concentrations in the gas sample and a paramagnetic analyzer was used to measure O_2 concentrations. The NO and NO_2 concentrations were measured using a chemiluminescence analyzer. An exhaust probe rake was used to aspirate gas samples from equal annuli for determination of the average concentrations of pollutant species in the exhaust flow. The inlet flow into the gas sampling probes was maintained choked, resulting in aerodynamic cooling of the sample by means of a rapid internal expansion. The combined effects of expansion and wall-cooling served to quench further chemical reactions. A liquid-vapor phase-discriminating sampling probe and a heated flame ionization detector were used to measure the total hydrocarbon (i.e., liquid plus vapor) and gaseous-hydrocarbon concentrations. The flow was sampled isokinetically and phase separation was achieved within the probe by aspirating a portion of the flow into a perpendicularly-oriented vapor-only sampling tube. Temperature distributions at the exhaust plane and within the combustor were obtained using a traversing calibrated-heat-loss thermocouple probe. Although conventional thermocouple materials are limited to temperatures below 2000°K, cooling the exposed junction by conduction extends the range of thermocouple utilization to gas temperatures above the melting point of the material to the 2000-2500°K range. In order to obtain the local stream temperature, the measured stream thermocouple temperature must be corrected for conduction and radiation heat losses; therefore, calibration data were acquired simultaneously with the required temperature measurement. Mean and rms gas and droplet velocities were measured using a dual-beam, frequency-offset laser velocimeter and single-particle time-domain signal processing.

This velocity measurement technique removes directional ambiguity errors which arise in recirculating flows. The laser velocimeter also provided a qualitative measure of droplet number densities in the burning spray which could be used to establish the spray trajectory. Selective seeding of the airstream with micron-sized phenolic resin particles was used to obtain a sufficient signal-to-noise ratio in regions of low fuel droplet number density to permit measurements of the local gas velocity. The number density, trajectory and mean diameter of droplets in nonburning and burning liquid fuel sprays were determined using an off-axis, transmitted-light type laser holography system. Fringe patterns were produced on a holographic plate by the interaction of an object beam, directed through the combustor section, and a reference beam, directed around the combustor section. Reconstruction of the holograms was accomplished with a second optical system and the data were reduced manually using a 12-power loupe. High-speed color motion pictures (500 frames per second) of the flame in the vicinity of the injector were obtained to assist in the interpretation of the test results. Detailed descriptions of the sampling probes and associated instrumentation are given in Ref. 9.

SECTION 3

EXPERIMENTAL RESULTS

DESCRIPTION OF EXPERIMENTS

The principal objective of the experimental program was to investigate the interaction of physical and chemical processes in heterogeneous combustion on pollutant formation and destruction. This was accomplished by (1) determining the effects of combustor operating conditions on pollutant emissions, (2) obtaining detailed maps of the combustor flow field, and information on fuel spray characteristics and liquid-vapor concentration distributions for a range of operating conditions and (3) correlating changes in flow field structure with changes in pollutant formation and energy release. The experimental results will be used to evaluate the combustor flow analysis (CHRISTY code) being developed in the theoretical portion of this program and to assist in assessing the validity of various models for turbulent transport and droplet burning.

The combustor was designed so that it would be amenable to analytical modeling and yet would exhibit many of the essential features of practical burners. Ultimately, it is intended that the information obtained from the experimental and theoretical studies will be utilized for evaluating potential emission control strategies.

The experimental program comprised two different types of tests: (1) input-output tests to establish the relationship of liquid fuel and air input conditions to average exhaust species concentrations, and (2) flow-field mapping tests to obtain radial and axial distributions of temperature, species concentration and mean and rms gas and droplet velocities within the combustor and to evaluate fuel spray characteristics. The matrix of combustor operating conditions for tests conducted using iso-octane, No. 2 fuel oil and propane is presented in Table 1. These conditions were selected to encompass variations in operating parameters which, based on the results of Refs. 10 and 12, are believed to have the greatest influence on pollutant emissions. Tests were conducted at nominal combustor pressures of 1 atm and 3.3 atm, inlet air temperatures of 533K, 644K, and 755K, and for fuel-air equivalence ratios in the range 0.9 to 0.5 (10 to 100 percent excess air). The inlet airflow rate was held constant at a nominal value of 0.137 kg/sec and the swirl number was varied from low (S = 0.3) to moderate (S = 0.6) by interchanging swirl vanes. (Swirl number is defined in Table 1). In the input-output tests, measurements were made at the exit of the combustor extender section (see Fig. 1), while in the mapping experiments detailed measurements were made within the combustor at a minimum of four axial locations. Variations in the average exhaust concentrations with overall fuel-air equivalence ratio and detailed flow field maps describing the effects of inlet air swirl, combustor pressure and air preheat are summarized below.

INPUT-OUTPUT TESTS RESULTS

Emissions data showing the effects of fuel type, inlet air swirl, combustor pressure, and air preheat at equivalence ratio 0.65 are summarized in Table 2. A complete tabulation of all (input-output and mapping) species concentration data is given in Ref. 9. Because neither the Total Hydrocarbon Analyzer nor the sample transfer line were heated to prevent condensation of high molecular weight hydrocarbon species, exhaust THC concentration measurements were obtained only for tests in which propane fuel was used. However, use of the phase-discriminating sampling probe and the discrete-sampling heated hydrocarbon analyzer for the flow-field mapping tests permitted determinations of the total hydrocarbon (i.e., liquid plus vapor) and gaseous hydrocarbon concentrations within the combustor. These measurements are discussed in subsequent sections of the report. The high concentrations of oxygen (compared to equilibrium) measured with the exhaust rake and the low exhaust CO_2 concentrations, particularly for propane and iso-octane, are not indicative of incomplete combustion but rather of a sampling problem. It is likely that the problem was caused in part by the limited number of ports sampling a flow stream with sharp concentration gradients and the potential for blocking of some of these ports by particulates generated during combustion. Significant particulate loading was noted for propane (because of the narrow angle fuel injector employed) and for iso-octane. NO, NO_2 and CO concentrations are presented in Table 2 as measured and also corrected by the ratio of measured oxygen used to equilibrium oxygen used.

Tests conducted at fixed inlet conditions using each of the three fuels resulted in similar trends in exhaust emissions with increasing overall fuel-air equivalence ratio -- NO, CO and CO_2 exhaust concentrations increased while the exhaust concentration of O_2 decreased. These general trends are similar to what would be predicted for gas-phase premixed combustion. Calculated equilibrium exhaust concentrations for premixed, adiabatic combustion are presented in Table 2 for comparison. As would be expected for finite residence times, measured CO levels exceed equilibrium levels and measured NO_x levels are far below equilibrium levels.

Comparison of the emissions data obtained for each of the fuels tested indicates a dependence of exhaust emission on fuel type. These trends reflect in part the different carbon/hydrogen ratios of the fuel but also suggest that differences in the atomization, vaporization and mixing characteristics of the three fuels can affect pollutant formation and destruction. Detailed data describing the influence of fuel spray characteristics on the combustor flow field are discussed in subsequent sections of this report.

The influence of inlet air swirl on exhaust species concentration levels was evaluated using each of the three fuels at a combustion pressure of 1 atm. The emissions data, summarized in Table 2, indicate significant changes in concentration levels as a result of increasing swirl. In addition, variations in the trends of the exhaust composition data were observed for different fuels suggesting that there are differences in the structure of the flow fields which affect the pollutant formation and destruction. These differences were explored in greater detail in the mapping tests discussed in the following sections. Increasing the inlet air swirl from S = 0.3 to S = 0.6 resulted in increased exhaust concentration of NO_x in the liquid propane tests but in decreased NO_x concentrations in the iso-octane and No. 2 fuel oil tests. The trends observed for liquid propane are in agreement with those previously reported for gaseous propane and natural gas and are characteristic of a flow field having high fuel concentrations near the centerline (10 and 12). Visual observations of the combustion process in the vicinity of the injector revealed that liquid propane was being injected in a concentrated stream having a very narrow spreading angle. The opposite trends observed in tests conducted with iso-octane and with No. 2 fuel oil probably are due to differences in the fuel/air distribution in the combustor. The effects of swirl on the combustor flow field are discussed later on in the report.

Input-output tests were also conducted to determine the effect of combustor pressure on exhaust species concentrations. Increasing the combustor pressure while maintaining constant inlet mass flow and temperature results in longer residence times and generally higher temperatures and reaction rates which produce increased NO emissions and decreased hydrocarbon emissions. These trends were found for liquid propane (cf., Tests 11 and 14) and No. 2 fuel oil (cf., Tests 6 and 9). However, the iso-octane tests show opposite trends with combustor pressure (cf., Tests 1 and 4). The measured exhaust NO concentration level decreased significantly and the exhaust CO concentration increased for combustion of iso-octane at 3.3 atm, suggesting a change in the fuel spray characteristics or fuel/air distributions at elevated pressure for this fuel. For the 3.3 atm iso-octane test, the exhaust gas temperature levels decreased and high concentrations of particulate carbon were observed, indicating a reduced combustion efficiency. The effects of pressure on mixing and vaporization are discussed later in the report.

A final series of input-output tests was conducted to determine the effect of inlet air temperature on pollutant emissions. Increased inlet air temperature should result in higher combustion temperatures and more rapid oxidation of fuel and CO and more rapid NO formation. The combustor temperature distributions (discussed in the following section) and the exhaust emissions data presented in Table 2 indicate that an increase in inlet air temperature from 533K to 750K resulted in a significant increase in the exhaust NO concentration and reduced UHC and CO concentrations. Other investigators (13) have reported similar emissions trends with inlet air temperature, and similar increases in NO emissions levels were measured in previous natural gas combustion tests (12).

FLOW FIELD MAPPING RESULTS

Examination of the results of the input-output tests indicates that pollutant emissions levels are particularly sensitive to inlet air swirl, combustor pressure and inlet air temperature. Variations in these parameters produced some experimental trends which cannot be predicted on the basis of thermochemistry alone, suggesting that there is significant coupling between the fluid dynamic and chemical processes in the combustor. Such a coupling was observed in the previous gaseous fuel tests (10). Therefore, detailed maps of the flow field and holograms of the fuel spray were obtained for the six test conditions listed in Table 1. These conditions were selected to encompass variations in combustor operating conditions which have the greatest influence on pollutant emissions, as determined from the input-output tests.

As in the gaseous fuel tests referenced above, the combustor mapping data were reduced to isopleth form to permit visualization of the radial and axial variation of individual flow field parameters and to facilitate comparisons between these parameters for each of the flow configurations investigated. However, since the radial distributions of mean flow properties were determined at a discrete number of axial locations within the combustor, some interpolation between stations was required. Typically a radial traverse consisted of 9 to 15 measurements spaced approximately uniformly across the combustor diameter. A complete tabulation of the experimental data is presented in Ref. 9.

THE EFFECT OF SWIRL ON FLOW FIELD STRUCTURE AND NO FORMATION

When a gaseous fuel is injected axially into a swirling air flow the primary mode of dispersion of the gaseous fuel is turbulent transport and the primary effects of increasing swirl are to increase local mixing rates and to increase radial and axial pressure gradients. Previous tests with natural gas (10) have confirmed that energy release rates increase with increased swirl. However, liquid fuels of low volatility injected with a radial component of velocity may penetrate the airstream primarily as a result of droplet inertia. In this case, swirl would influence relative velocities between fuel droplets and air and would affect droplet vaporization and burning rates.

The input-output tests indicate that the effects of swirl are very different for the three fuels tested. For propane, increasing swirl results in a decrease in CO levels and an increase in NO_x. Here, propane behaves like a gaseous fuel and combustion rates are enhanced by increased turbulent transport rates. However it is found that with iso-octane, CO levels increase and NO_x levels decrease with increased swirl. This result suggests that insufficient vaporization occurs close to the injector to achieve the rapid air/vapor fuel mixing allowed at higher swirl number with an entirely vaporized fuel. In addition the effect of increased swirl is to shift air flow radially outward and increase the radial pressure gradient; this would tend to retard the penetration of small, partially vaporized fuel droplets. Since shear levels decay rapidly with axial distance, vaporized fuel introduced further downstream into the annular airstream does not burn rapidly.

For No. 2 fuel oil, increasing swirl results in a decrease in both CO and NO_x levels. Temperature and composition profiles presented later on in this report indicate that radial droplet penetration was the dominant mode of dispersion of this fuel. Once the fuel is dispersed across the airstream, the droplet combustion rates are probably increased with increasing swirl by higher relative velocities and turbulence levels. More rapid combustion and smaller flame standoff distances in burning droplets or droplet arrays would result in lower levels of both CO and NO_x.

Flow field mapping tests conducted with iso-octane confirm the results of the input-output tests and allow some tentative conclusions to be made about the interactions of swirl with fuels of moderate volatility. The time-mean temperature distributions obtained for iso-octane/air combustion at one atmosphere pressure and for inlet air swirl levels of 0.3 and 0.6, respectively, are presented in Figure 2. An initial examination of the data reveals the similarity of the flow field structure obtained for each of these liquid-fuel test configurations and a general correspondence with the flow fields obtained previously using gaseous fuel (10), i.e., the characteristic shape usually associated with axisymmetric, turbulent diffusion flames. The contours are characterized by peak temperatures occurring off the centerline in an annular region. Variations in liquid fuel and air inlet conditions altered the relative rates at which heat was released within the combustor, and specific trends resulting from these variations are evident with more detailed analysis of the data.

The temperature contours are not symmetric about the combustor centerline, but instead are displaced slightly toward negative values of R/R_0. Since the uniformity of the inlet flow was verified by laser velocimeter measurements and by temperature measurements in the inlet section, the apparatus was eliminated as the source of this asymmetry. Furthermore, the species concentration distributions appear symmetric about the combustor centerline. Therefore, the asymmetry must be the result of blockage introduced into the flow by traversing the comparatively large thermocouple probe (9) from the positive to negative radial direction.

Specific trends resulting from systematic variation of the inlet swirl are evident from the temperature data. For example, increasing the swirl level from 0.3 to 0.6 results in an initial increase in the axial rate of heat release ($X/D < 2$), followed by a gradual decrease in the axial rate of heat release ($X/D > 2$). This initial increase of heat release rate is attributed to more rapid mixing of the vapor fraction. However, insufficient initial penetration of fuel droplets leads to an extended flame as indicated by the radial temperature gradients which remain steeper for a greater axial distance. For the case of 0.3 swirl, the greater part of the available chemical energy was released within an axial distance of approximately six combustor diameters ($X/D = 6$) and the downstream temperature distributions are relatively flat. Isotherms corresponding to $S = 0.6$, on the other hand, indicate a larger flame length, as evidenced by peak temperatures extending the full length of the combustor ($X/D = 14$).

Mean axial gas- and droplet-velocity contours obtained for iso-octane/air combustion at one atmopshere pressure are presented in Figures 3 and 4. Differences between the local gas and droplet velocities are apparent near the injector, as are areas of flow recirculation. Also, some unsteadiness of the flow was indicated by fluctuations in the droplet velocity measurements. Farther downstream ($X/D > 1.0$), droplet sizes and concentrations are reduced by evaporation and combustion and droplets are convected at the local gas velocity. At $S = 0.3$, it was not possible to distinguish between local fuel droplet and gas velocities in the vicinity of the spray near the centerline because of the high droplet concentration. Consequently no gas flow recirculation is shown; however, the existence of a recirculation zone may be inferred from the droplet velocity data, Figure 4A. Gas velocity measurements were possible at $S = 0.6$ and a torroidal-shaped recirculation zone was identified (Figure 3). A primary effect of increasing the inlet air swirl from 0.3 to 0.6 was to shift the regions of droplet recirculation closer to the injector, thereby influencing flame stabilization and energy release in the initial region of the combustor.

The local time-mean axial velocities are somewhat higher at $S = 0.6$ and the diffusion-flame-like flow field structure persists for a greater axial distance. The insensitivity of the fuel droplet axial velocities to the level of inlet air swirl is also apparent from the similar appearance of the droplet velocity distributions in the initial mixing regions; however, at $S = 0.6$, high droplet velocities persist farther downstream. Spray trajectories, as determined from laser velocimetry and laser holography measurements are also shown in Figure 4 and are in good agreement with the nominal spray angle of 60 degrees. The persistence of droplet velocity and the higher gas velocities at S = 0.6 are associated with the increase in recirculation zone size and consequent increase in mass flux density outside the recirculation zone.

Gas composition contours for low (S = 0.3), and moderately (S = 0.6) swirling flows, discussed above, are shown in Figures 5, 6 and 7. These data indicate the tendency of increased swirl to suppress mixing beyond a zone of rapid initial mixing near the injector. Radial concentration gradients are sharper with increased swirl and CO burnout is slower. Further insight into the effect of swirl on iso-octane vaporization and combustion is obtained from comparisons of total hydrocarbon concentration distributions (Figure 8) together with profiles of the percentage of hydrocarbons vaporized (Figure 9). In the upstream section of the combustor, total hydrocarbon concentrations are higher for the lower swirl number (Figure 8) while the concentrations of unvaporized fuel (computed from the product of total hydrocarbon concentration from Fig. 8 and 1 minus the fraction vaporized from Fig. 9) are about the same. In this upstream region increased swirl promotes mixing of vaporized fuel. However, for the higher swirl number, unvaporized fuel persists further downstream and the total hydrocarbon concentrations are greater in the downstream sections even after the fuel has vaporized. It is likely that this is a result of reduced droplet penetration into the airstream with increased swirl and the rapid decay of swirl (shear) induced mixing with axial distance.

NO concentration distributions are shown in Figure 10. The regions of high NO concentration within the combustor are coincident with the regions of locally high temperature. At low swirl, higher concentrations of NO were measured close to the combustor centerline and in the vicinity of the injector. In contrast, at moderate swirl the reaction zone is moved radially outward and closer to the injector, and NO formation occurs in a narrow annular region. The combined effect of low oxygen concentration and low temperature result in a reduced rate of NO formation and, therefore, lower NO exhaust emissions levels at S = 0.6.

The mapping data indicate that, in the present combustor configuration, increasing swirl from 0.3 to 0.6 increases mixing of partially vaporized fuel with air in the initial region of the flow, resulting in increased energy release rates. Hence, increased swirl tends to move the region of flame stabilization closer to the fuel injector. Beyond this initial region, increasing swirl appears to suppress vaporization of the liquid fuel and subsequent mixing of the vaporized fuel with air. At sufficiently high swirl numbers, the radial pressure gradients reduce penetration of partially vaporized droplets into the airstream, resulting in a relatively cold fuel-rich region on the combustor centerline. The reduced vaporization rates result in an extended mixing region. In addition, axial decay of swirl-induced shear levels tends to reduce mixing rates downstream from the injector. Reduced mixing rates result in generally slower fuel oxidation and CO burnout rates and in lower NO formation rates.

EFFECT OF PRESSURE ON FLOW FIELD STRUCTURE AND NO FORMATION

Previous tests (10) with natural gas have demonstrated several effects of pressure on exhaust emissions at constant mass flow rate. Increasing pressure from 1 to 3 atmospheres decreased CO levels and increased exhaust NO levels principally because combustor residence time increases with pressure. However, the local rate of energy release decreased indicating that mixing rate was suppressed at higher pressure. This would be expected since shear levels decrease with decreasing velocity. This conclusion is supported by the fact that at even higher pressure, 7 atm, exhaust hydrocarbon levels increased despite the increased residence time.

For two of the liquid fuels investigated, No. 2 distillate oil and propane, increasing pressure from 1 to 3.3 atmospheres decreased CO levels and increased NO levels. However, when iso-octane was used as a fuel, CO levels increased and NO emission decreased as the pressure was increased from 1 to 3.3 atmospheres. The flow field mapping tests conducted using iso-octane confirm the results of the input-output tests and indicate the effect of pressure on the flow field structure and pollutant formation.

The time-mean temperature distributions, Figure 11, indicate that longer flames are obtained at higher pressure. Furthermore, peak temperatures are lower at higher pressure suggesting lower energy release rates. Examination of the species concentration distributions obtained for iso-octane/air combustion at elevated pressure are consistent with the temperature data. Examination of Figure 12 reveals that at 3.3 atm pressure, the O_2 concentrations near the combustor centerline are lower, indicating a reduced mixing rate. Similarly, initial breakdown of the fuel to CO and oxidation of CO to CO_2 is slower at 3.3 atm. Figure 13 shows that NO is formed in an annular region close to the injector at approximately the same radial location as the peak temperature. There are steep radial gradients and low NO concentration levels at the combustor centerline. Peak NO concentrations at the elevated pressure are much lower than were observed at atmospheric pressure. An increase in pressure from 1.0 atm to 3.3 atm results in a significant decrease in NO emissions which may be attributed in part to lower temperatures.

One possible explanation for the different effect of pressure on flow field structure for iso-octane in comparison with natural gas, propane and No. 2 distillate oil is as follows: The propane rapidly vaporizes on injection into the combustor. Hence, both natural gas and propane may be considered gaseous fuels. In spite of reduced mixing rates resulting from the reduced shear levels associated with the lower air velocities, combustion is enhanced and NO emissions increase due to increased residence time and increased reaction rates. In contrast, No. 2 distillate oil burns largely inhomogeneously since vaporization rates are relatively low due to higher boiling points. Increased droplet penetration at higher pressure partially offsets the effect of reduced mixing due to shear and combustion goes to completion because of increased residence time. Iso-octane is more volatile than No. 2 distillate oil, and droplet vaporization tends to limit droplet penetration. With relatively little penetration of iso-octane liquid, combustion efficiency would be governed largely by droplet vaporization rates. But the droplet vaporization rate is a function of droplet boundary layer thickness, which in turn is a function of the product of gas density and relative velocity between droplets and air. For air moving at a velocity higher than the droplet velocity, as pressure increases the relative velocity might well be reduced far more than the density is increased. This could reduce vaporization rate with increasing pressure. Increasing boiling point with higher pressure would also tend to reduce the heat transfer rate with vaporizing fuel which is proportional to the difference between the ambient temperature and the boiling point temperature. Increased reaction rates due to increased pressure and increased residence time do not compensate for reduced shear levels, poorer penetration and lower vaporization rates and a significant amount of fuel vaporized prior to burning.

EFFECT OF FUEL TYPE ON FLOW FIELD STRUCTURE AND NO FORMATION

Liquid propane, iso-octane and No. 2 fuel oil differ widely in the physical properties which influence the atomization and vaporization (velocity, surface tension, heat capacity, latent heat of vaporization, vapor pressure). The energy added to the airstream by combustion at a given equivalence ratio is of similar magnitude for each of the three fuels; thus little difference in flow field structure or emission levels can be expected on the basis of equilibrium thermodynamic considerations. Also, the amount of fuel-bound nitrogen found in all of the fuels is quite small, and thus this factor is not believed to contribute significantly to the overall level of nitric oxide production. Typical properties of the liquid fuels and the results of limited quantitative fuel analyses are given in Ref. 9.

Significant differences existed between the temperature patterns observed in the burner when using liquid propane as compared to patterns produced when using iso-octane or fuel oil -- see Figure 14. This difference in pattern is due largely to the difference in the fuel distributions achieved when injecting propane. These fuel pattern differences are illustrated in Figure 15 which presents levels of total unburned hydrocarbons within the combustor as determined by use of the phase-discriminating probe. Most of the propane was found to be concentrated near the centerline of the combustor; this fuel distribution is believed to have resulted from flashing of the liquid propane within the injector with the result that a conical spray was not achieved. Because of the initial fuel distribution, combustion was slow and peak temperatures were not achieved in the initial regions of the combustor (Figure 14A). In the case of the iso-octane and fuel oil, spray patterns were similar and fuel penetrated to the outer combustor radii within two test section diameters (9). Temperature patterns produced were also qualitatively similar (Figures 14B and 14C), the most significant difference being the higher temperatures at the outer radii of the combustor in the case of the fuel oil. Combustion appears to be more intense in the case of the iso-octane spray resulting in slightly higher peak temperatures and steeper temperature gradients. The lower volumetric heat release rates in the case of the fuel oil are probably associated with the fuel oil droplet characteristics. The fuel oil droplets were somewhat larger than the iso-octane droplets initially and the fuel oil vaporizes less rapidly than iso-octane. Thus, although the distribution of unburned fuel in the initial region of the combustor is qualitatively similar for the fuel oil and the iso-octane (Figures 15B and 15C), the fuel oil droplets were larger and required greater time, and hence, distance to burn completely. The fact that a greater amount of reaction took place in the outer radii in the case of the fuel oil is confirmed by measurement of the oxygen concentration which shows that lower oxygen concentrations were found in this region (Figure 16).

EFFECT OF AIR PREHEAT ON FLOW FIELD STRUCTURE AND NO FORMATION

An increase in the inlet air temperature will influence flow field characteristics by affecting flow velocities, chemical reaction rates, and heat transfer rates. With all other conditions held constant, an increase in temperature will result in correspondingly higher temperatures throughout the combustor and will create higher flow velocities. These higher flow velocities will have the primary effect of decreasing the residence time of the combustor gases. The diminished time available for completion of the chemical kinetic processes is in most cases more than offset by the strong temperature dependence of individual reaction rates. Decreased time available for the droplet vaporization will be compensated for by the increase heat transfer rate associated with the greater temperature difference between the gas and the droplets.

Examination of the temperature patterns (Figure 17) obtained for the case where the entrance temperature was increased by 220K (a 40 percent increase) shows that the combined effect is primarily to increase the temperature levels -- qualitatively, the temperature pattern did not change significantly. Correspondingly, the inlet temperature change resulted in only small changes in the unburned fuel pattern (Figure 18A and 18B). As would be expected, the fraction of the unburned fuel existing in the vapor state was greater for the increased temperature level case (Figure 18C and 18D).

The rate of formation of nitric oxide is very sensitive to local temperature and accordingly, the increased temperature levels resulted in an approximate doubling of the local NO concentration ratios (Figure 19). This dramatic increase occurred over the complete equivalence ratio range tested in the input-output experiments. Emissions of CO would be expected to decrease with increased preheat level because of the increased rate of CO oxidation and higher temperature levels, and this, indeed, was found to be the case.

In conclusion, the effect of the increased preheat level was primarily to increase the temperature levels throughout the combustor and thereby to increase the production of nitric oxide; temperature patterns and composition patterns remain relatively unchanged.

SECTION 4

REFERENCES

1. Norster, E. R. and A. H. Lefebvre. Effects of Fuel Injection Method on Gas Turbine Combustor Emissions. Emissions from Continuous Combustion Systems, Cornelius, W. and W. G. Agnew (eds.), New York, Plenum Press, pp. 255-278, 1972.
2. Grobman, J. S.. Effect of Operating Variables of Pollutant Emissions from Aircraft Turbine Engine Combustors. Emissions from Continuous Combustion Systems, Cornelius, W. and W. G. Agnew (eds.), New York, Plenum Press, pp. 279-303, 1972.
3. Tuttle, J. H., R. A. Altenkirch and A. M. Mellor. Emissions from and Within an Allison J-33 Combustor. II. The Effect of Inlet Air Temperature. Comb. Sci. Technol. 7: 125-134, 1973.
4. Pompei, F. and J. B. Heywood. The Role of Mixing in Burner-Generated Carbon Monoxide and Nitric Oxide. Comb. Flame 19: 407-418, 1972.
5. Mellor, A. M.. Simplified Physical Model of Spray Combustion in a Gas Turbine Engine. Comb. Sci. Technol. 8: 101-109, 1973.
6. Bowman, C. T. and L. S. Cohen. Influence of Aerodynamic Phenomena on Pollutant Formation in Combustion. Environmental Protection Agency, Research Triangle Park, N. C., Publication Number 650/2-75-061a, p. 159, July 1975.
7. Tuttle, J. H., M. B. Colket, R. W. Bilger and A. M. Mellor. Characteristic Times for Combustion and Pollutant Formation in Spray Combustion. Paper presented at the 16th Symposium (International) on Combustion. Cambridge, Mass., August 1976.

8. Appleton, J. P. and J. B. Heywood. The Effects of Imperfect Fuel-Air Mixing in a Burner on NO Formation from Nitrogen in the Air and the Fuel. Fourteenth Symposium (International) on Combustion. Pittsburgh, PA. The Combustion Institute, pp. 777-786, 1973.

9. Spadaccini, L. J., et.al.. Influence of Aerodynamic Phenomena on Pollutant Formation in Combustion (Phase II - Liquid Fuels). Final Report under Contract 68-02-1873, Environmental Protection Agency, Research Triangle Park, NC, in press.

10. Spadaccini, L. J., F. K. Owen and C. T. Bowman. Influence of Aerodynamic Phenomena on Pollutant Formation in Combustion of Gaseour Fuels. Environmental Protection Agency, Research Triangle Park, NC, Publication Number 600/2-76-247a, September 1976.

11. Kerr, N. M. and D. Fraser. Swirl. Part I: Effect on Axisymmetrical Turbulent Jets. J. Inst. Fuel 38: 519-538, 1965.

12. Bowman, C. T. and L. S. Cohen. Influence of Aerodynamic Phenomena on Pollutant Formation in Combustion. Environmental Protection Agency, Research Triangle Park, NC, Publication Number EPA 650/2-75-061a, July 1975.

13. Tuttle, J. H., R. A. Altenkirch and A. M. Mellor. Emissions from and Within an Allison J-33 Combustor II: The Effect of Inlet Air Temperature. Comb. Sci. Technol. 7: 125-134, 1973.

TABLE 1. NOMINAL TEST CONDITIONS

Fuel	Swirl No.*	Press. (atm)	T_{AIR} (K)	$\dot{M}_{AIR}$ (kg/sec)	Equiv. Ratio	Input-Output	Mapping
Iso-Octane	0.3	1.0	533	0.137	0.5-0.9	x	
	0.3	1.0	533	0.137	0.65	x	x
	0.3	1.0	644	0.137	0.65	x	
	0.3	1.0	750	0.137	0.65	x	
	0.3	3.3	533	0.137	0.65	x	x
	0.6	1.0	533	0.137	0.65	x	x
No. 2 Oil	0.3	1.0	533	0.137	0.5-0.9	x	
	0.3	1.0	533	0.137	0.65	x	x
	0.3	1.0	644	0.137	0.65	x	
	0.3	1.0	750	0.137	0.65	x	x
	0.3	3.3	533	0.137	0.65	x	
	0.6	1.0	533	0.137	0.65	x	
Propane	0.3	1.0	533	0.137	0.5-0.9	x	
	0.3	1.0	533	0.137	0.65	x	x
	0.3	1.0	644	0.137	0.65	x	
	0.3	1.0	750	0.137	0.65	x	
	0.3	3.3	533	0.137	0.65	x	
	0.6	1.0	533	0.137	0.65	x	

---

*As defined in Ref. 11:

$$S = \frac{1}{3}\frac{(1 - Z^3)}{(1 - Z^2)^{1.5}} \tan \eta$$

where Z = hub-to-tip ratio
η = angle of vanes

TABLE 2. EXHAUST SPECIES CONCENTRATIONS*

Test No.	Swirl	Press. (atm)	T_{air} K	Equiv. Ratio	O_2 Mole%	CO_2 Mole%	CO Mole%	$CO_{corr.}$** Mole%	NO ppm	$NO_{corr.}$** ppm	NO_x+ ppm	$NO_{x corr.}$	THC ppm,C	$C_{Balance}$ % deficient at exhaust
							$i\text{-}C_8H_{18}$							
1	0.3	1.0	527	0.65	8.6	8.15	0.22	0.24	58	64	82	90	---	8.6
2	0.3	1.0	637	0.647	9.4	8.0	0.15	0.18	92	107	118	138	---	10.6
3	0.3	1.0	747	0.65	9.4	8.0	0.10	0.12	148	174	185	217	---	11.6
4	0.3	3.3	532	0.652	10.2	7.5	0.25	0.31	39	49	47	59	---	15.6
5	0.6	1.0	530	0.651	10.9	6.67	0.30	0.40	46	62	52	70	---	24.0
	Equil.	1.0	533	0.65	7.5	9.2	0.022		4410				0	
							No. 2 Oil							
6	0.3	1.0	532	0.65	7.7	8.6	0.20	0.20	86	88	87	89	---	10.4
7	0.3	1.0	644	0.655	8.8	-	0.08	0.09	120	135	121	136	---	---
8	0.3	1.0	748	0.644	7.7	8.98	0.041	0.041	166	169	167	170	---	7.3
9	0.3	3.3	533	0.655	6.8	10.4	0.06	0.06	116	112	116	112	---	-5.6
10	0.6	1.0	530	0.655	7.7	8.9	0.0075	0.0078	66	69	72	75	---	9.9
	Equil.	1.0	755	0.65	7.27	9.71	0.014		6883				0	
							C_3H_8							
11	0.3	1.0	533	0.65	11.3	7.3	0.26	0.36	62	87	62	87	461	12.0
12	0.3	1.0	644	0.655	10.9	7.65	0.18	0.24	89	121	89	121	336	9.7
13	0.3	1.0	750	0.655	11.5	7.1	0.08	0.12	110	160	113	164	241	17.3
14	0.3	3.3	533	0.655	8.11	7.3	0.025	0.027	94	100	94	100	186	15.7
15	0.6	1.0	539	0.66	10.9	6.8	0.15	0.20	82	112	82	112	---	20.8
	Equil.	1.0	533	0.65	7.56	8.56	0.028		4322				0	

---

*Expressed as measured on a dry basis

+NO_x = NO + NO_2

**Corrected by the ratio of measured oxygen used to equilibrium oxygen used.

FIG. 1

SCHEMATIC DIAGRAM OF AXISYMMETRIC COMBUSTION FACILITY

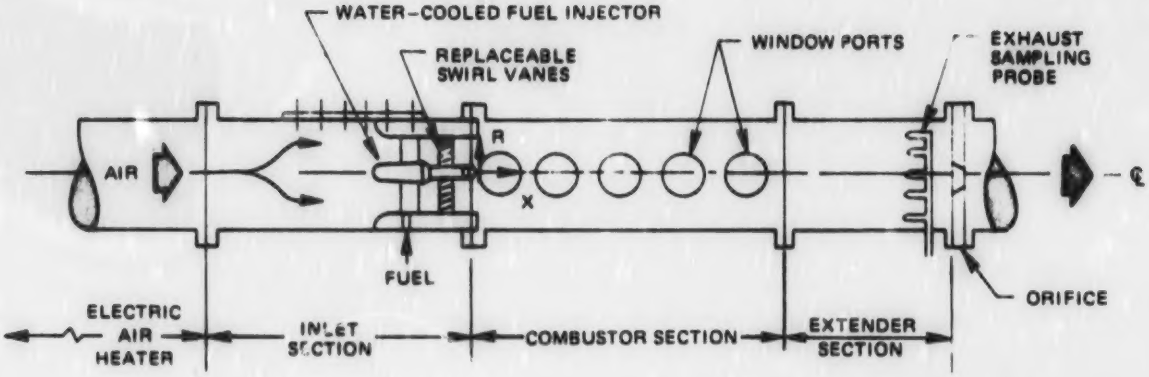
WATER-COOLED FUEL INJECTOR
REPLACEABLE SWIRL VANES
WINDOW PORTS
EXHAUST SAMPLING PROBE
AIR
R
X
℄
FUEL
ORIFICE
ELECTRIC AIR HEATER
INLET SECTION
COMBUSTOR SECTION
EXTENDER SECTION

76 05 198 1

FIG. 2

TIME–AVERAGED TEMPERATURE DISTRIBUTIONS

ISO–OCTANE/AIR, 1 ATM, $T_{AIR} = 533\ ^oK, \phi = 0.65$

(A) SWIRL = 0.3

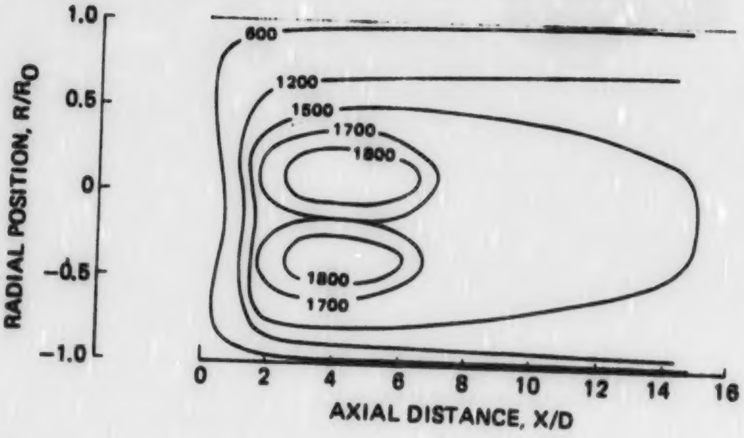

(B) SWIRL = 0.6

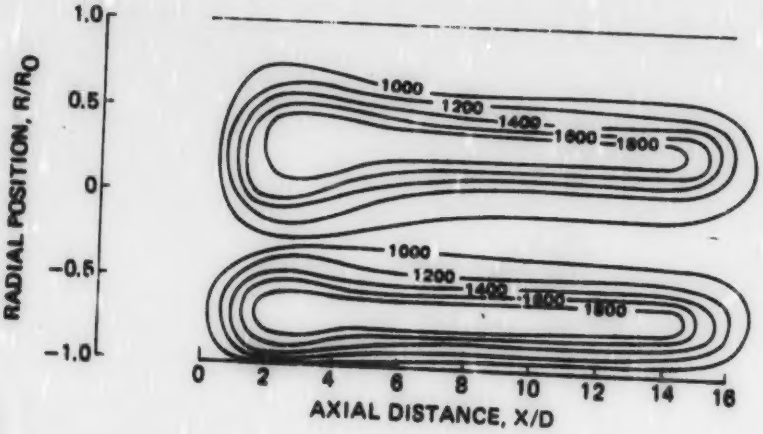

FIG. 3

MEAN AND RMS GAS VELOCITY DISTRIBUTIONS

ISO–OCTANE/AIR, 1 ATM, T_{AIR} = 533°K, ϕ = 0.65

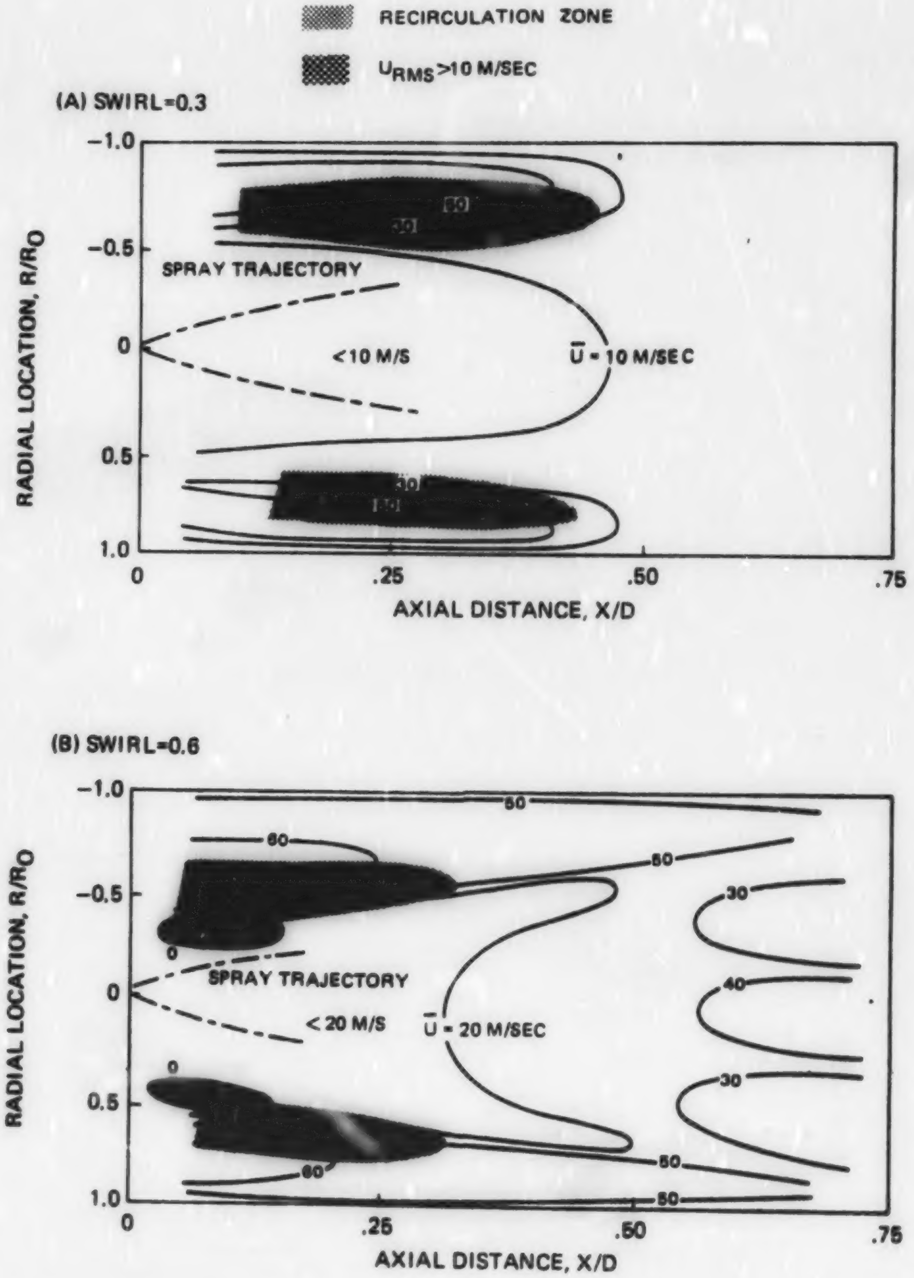

FIG. 4

MEAN AND RMS DROPLET VELOCITY DISTRIBUTIONS

ISO OCTANE/AIR, 1 ATM, T_{AIR} 533°K, ϕ 0.65

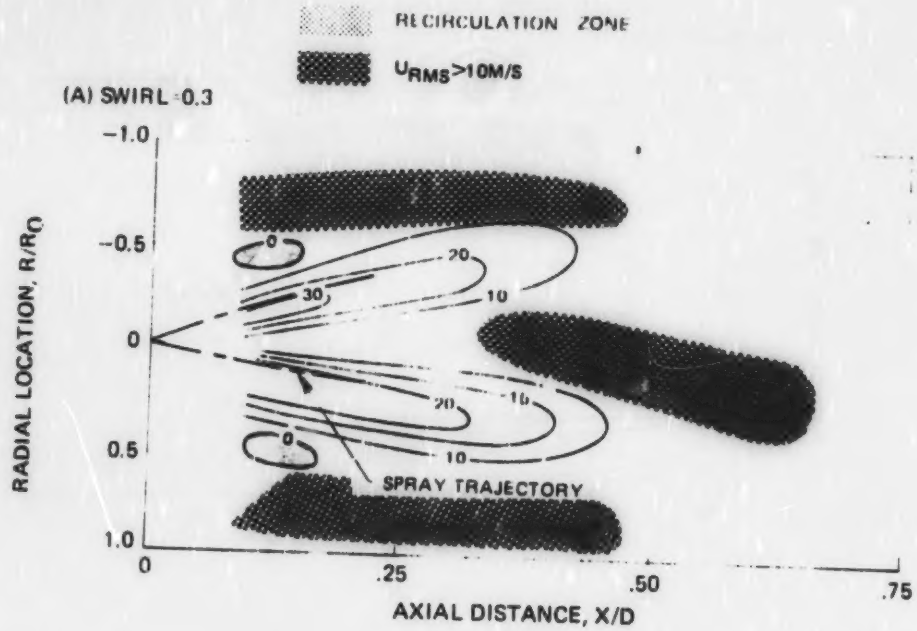

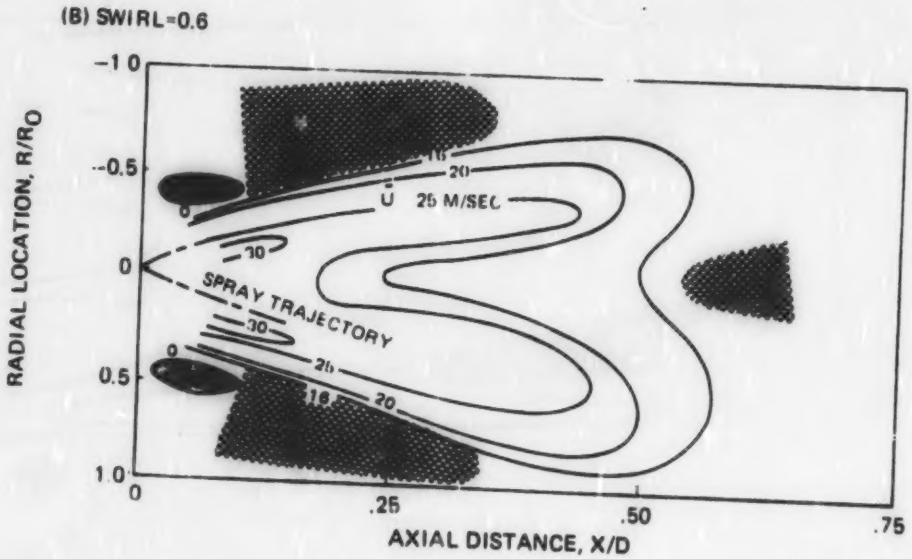

FIG. 5

TIME–AVERAGED O_2 DISTRIBUTIONS

ISO OCTANE AIR, 1ATM, T_{AIR} 533°K, ϕ 0.65

(A) SWIRL=0.3

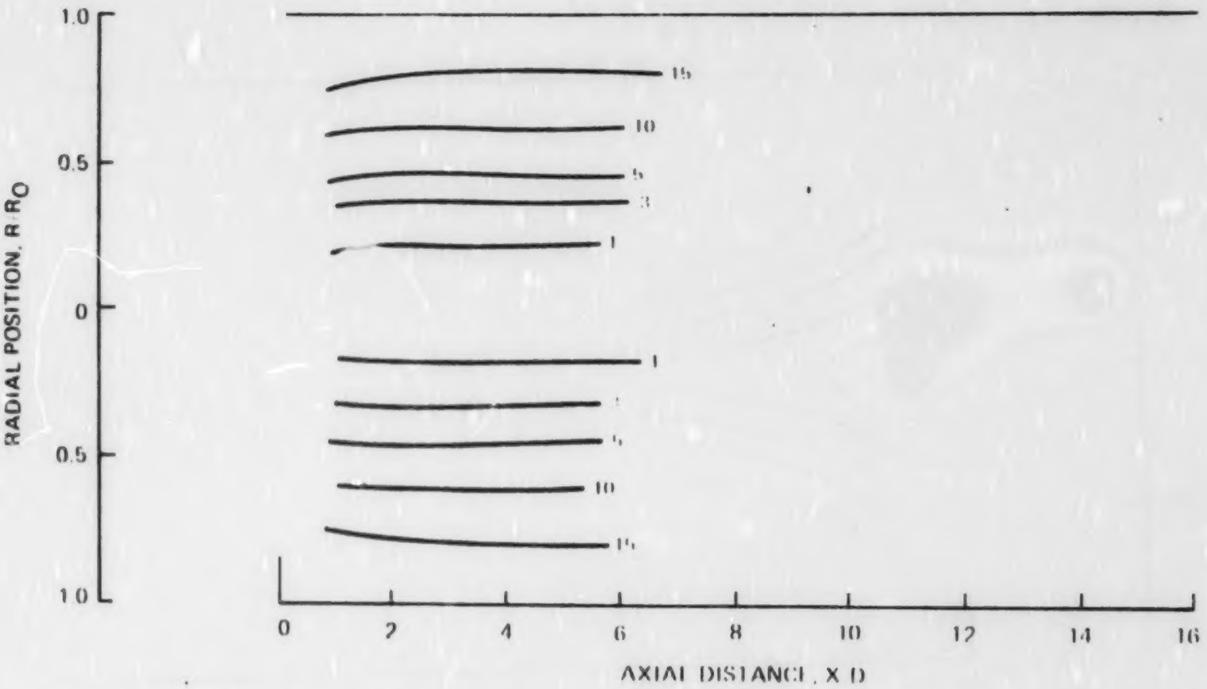

(B) SWIRL=0.6

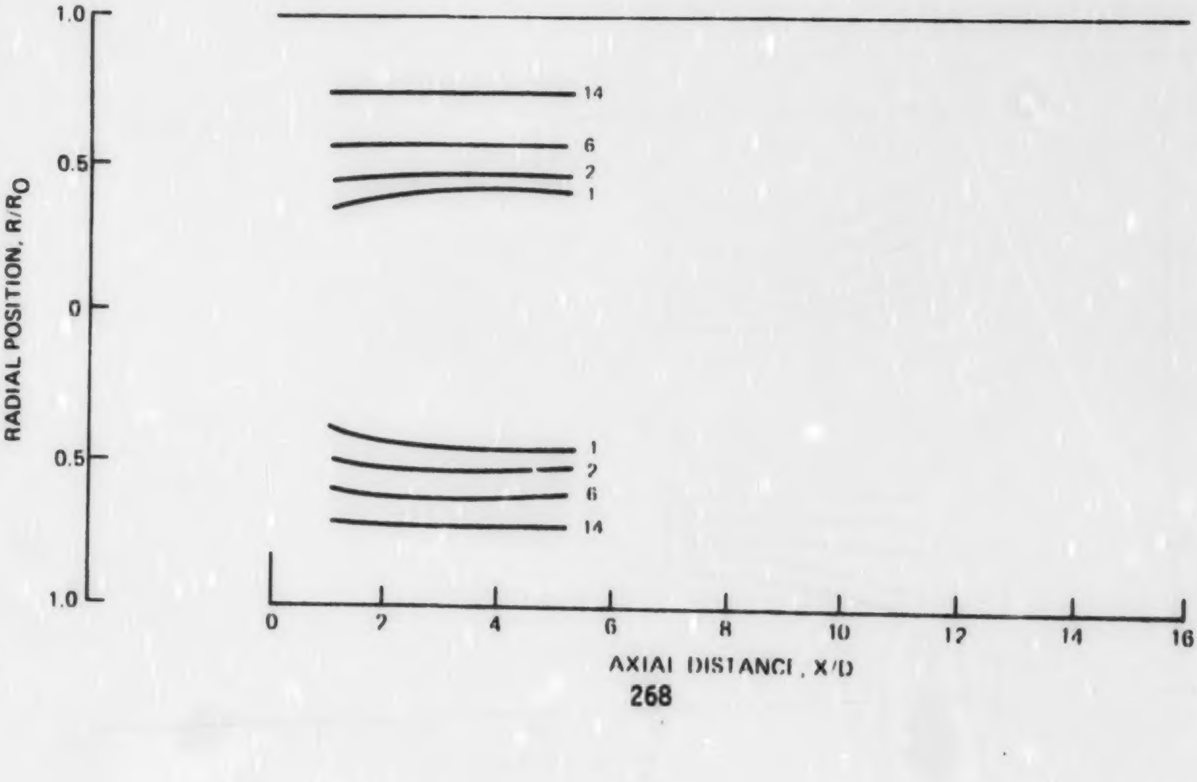

FIG. 6

TIME–AVERAGED CO DISTRIBUTIONS

ISO OCTANE/AIR, 1 ATM, T_{AIR} = 533°K, ϕ = 0.65

(A) SWIRL=0.3

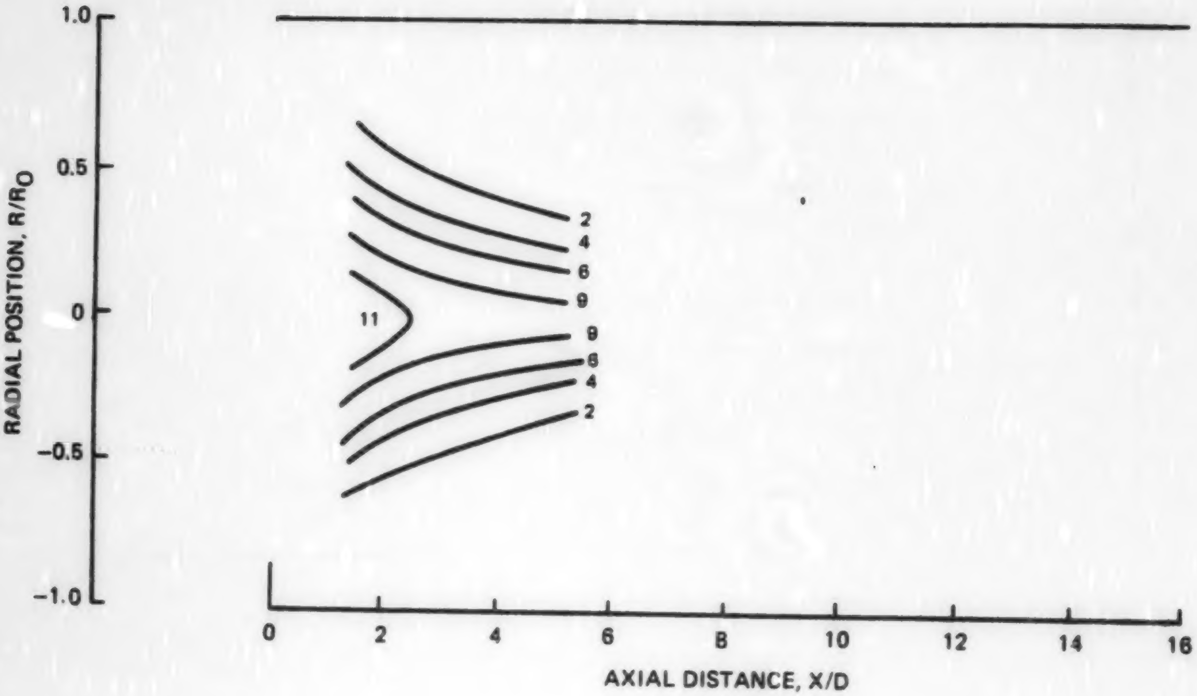

(B) SWIRL=0.6

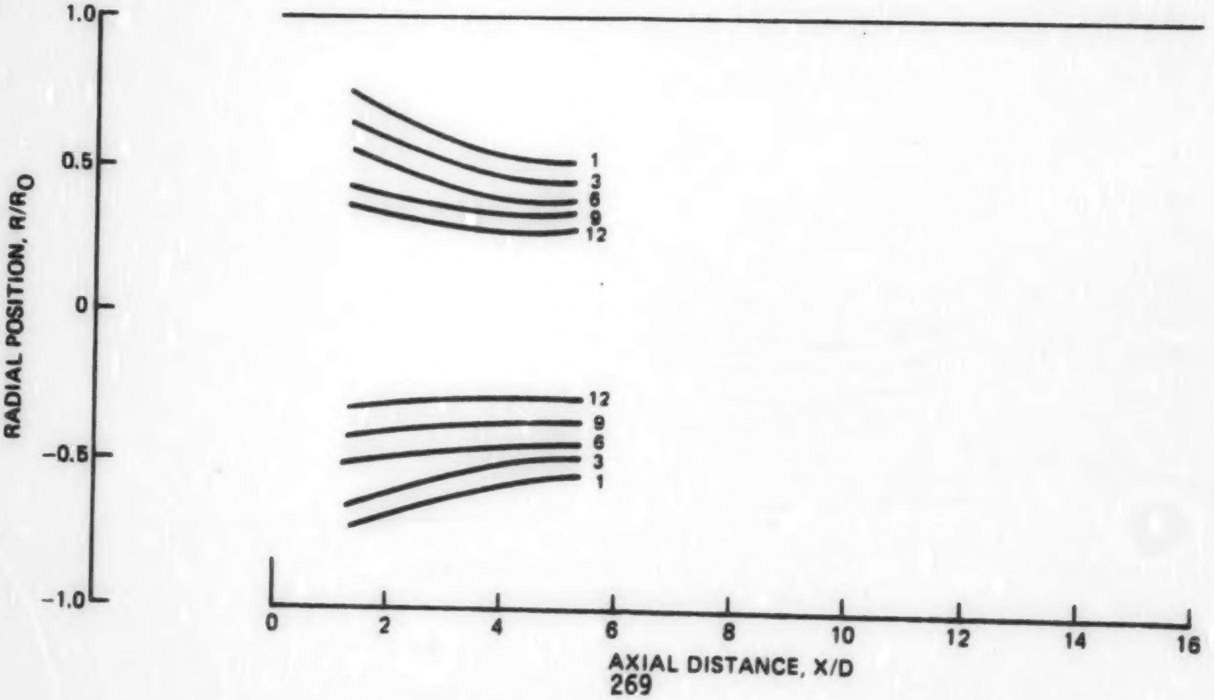

FIG. 7

TIME–AVERAGED CO_2 DISTRIBUTIONS

ISO–OCTANE/AIR, 1 ATM, $T_{AIR} = 533^oK$, $\phi = 0.65$

(A) SWIRL=0.3

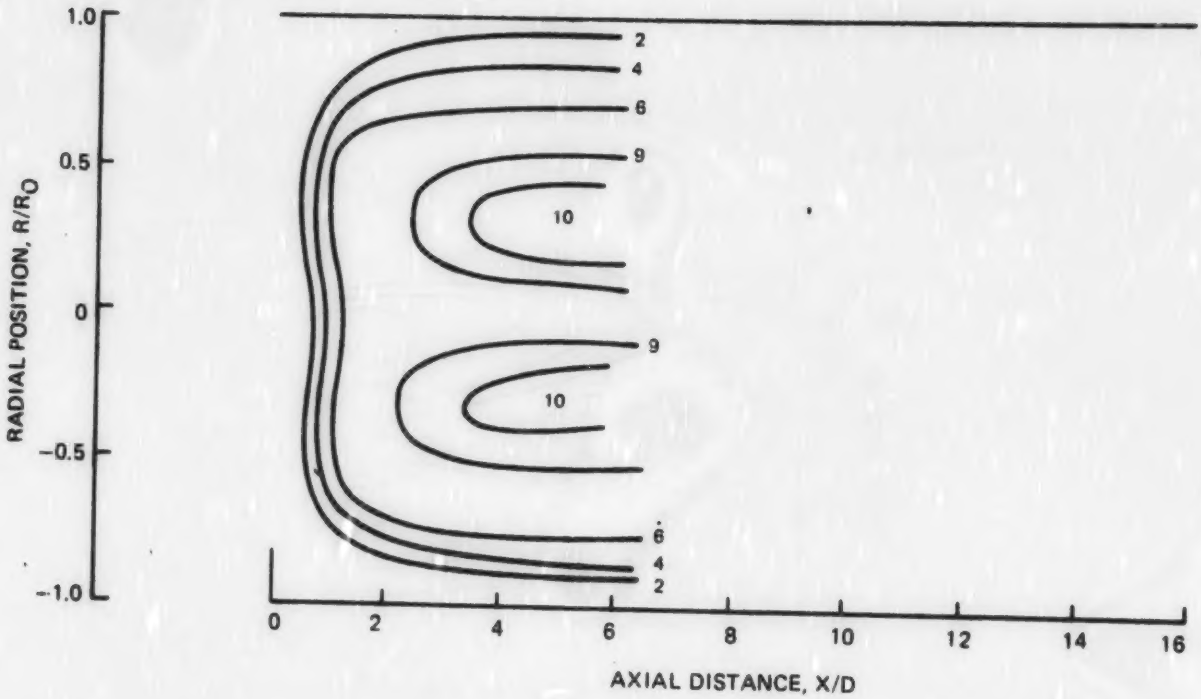

(B) SWIRL=0.6

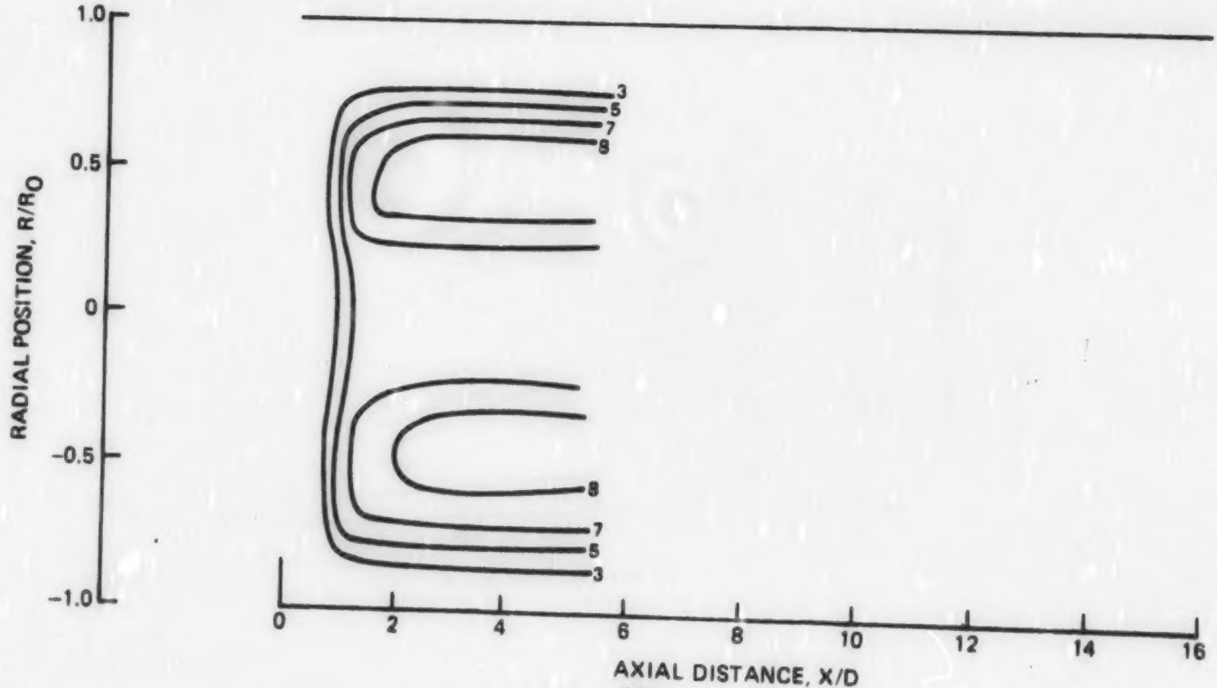

FIG. 8

TIME–AVERAGED DISTRIBUTIONS OF UNBURNED HYDROCARBONS

ISO–OCTANE/AIR, 1 ATM, T_{AIR}=533°K, ϕ =0.65

(A) SWIRL=0.3

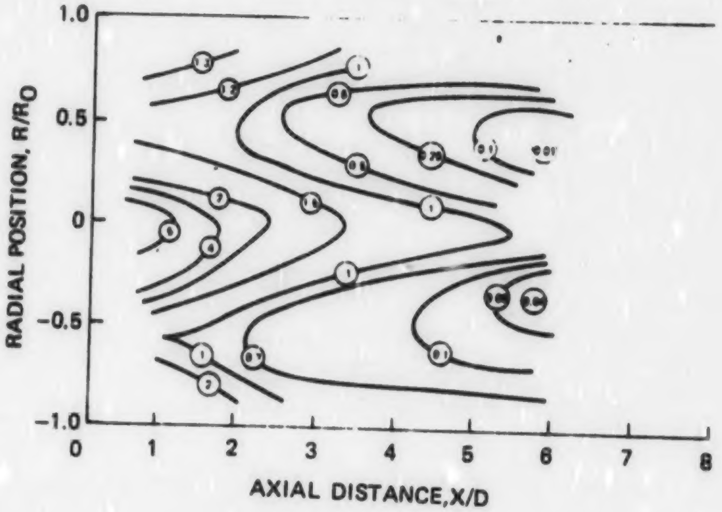

(B) SWIRL=0.6

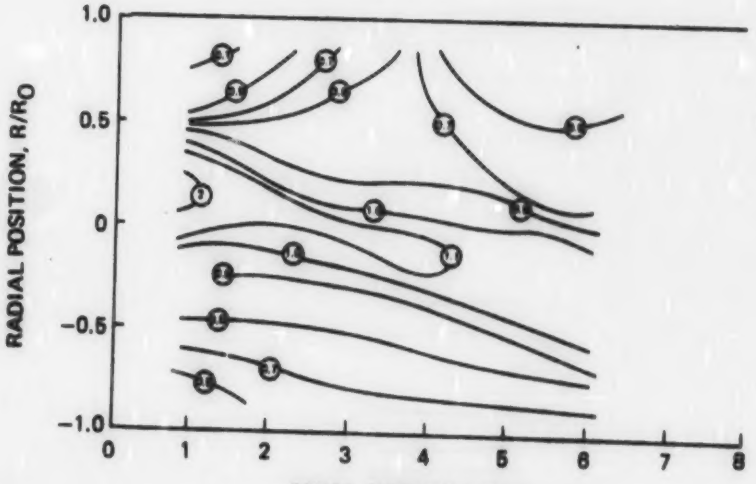

FIG. 9

TIME–AVERAGED PERCENTAGE OF HYDROCARBONS VAPORIZED

ISO–OCTANE/AIR, 1 ATM, T_{AIR}=533°K, ϕ=0.65

(A) SWIRL=0.3

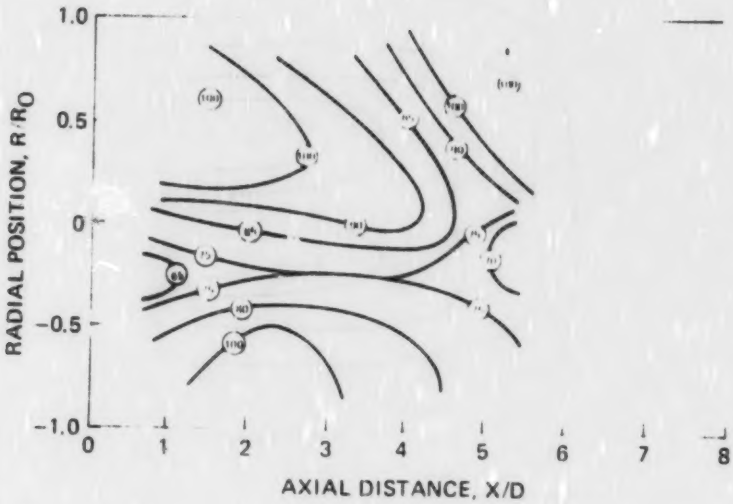

(B) SWIRL=0.6

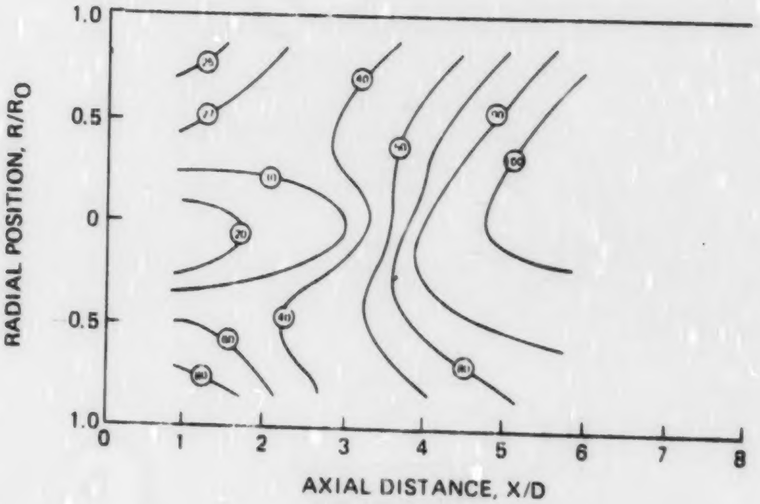

FIG. 10

TIME–AVERAGED NO DISTRIBUTIONS

ISO OCTANE/AIR, 1 ATM, T_{AIR} 533°K, ϕ=0.65

(A) SWIRL=0.3

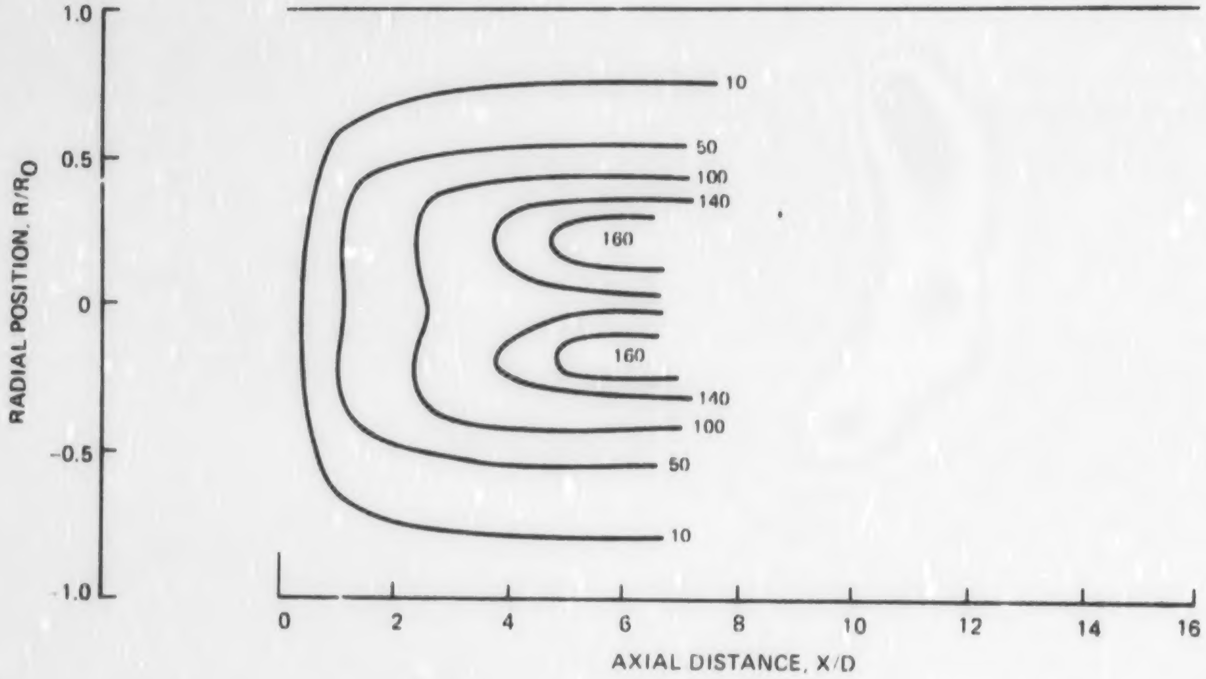

(B) SWIRL=0.6

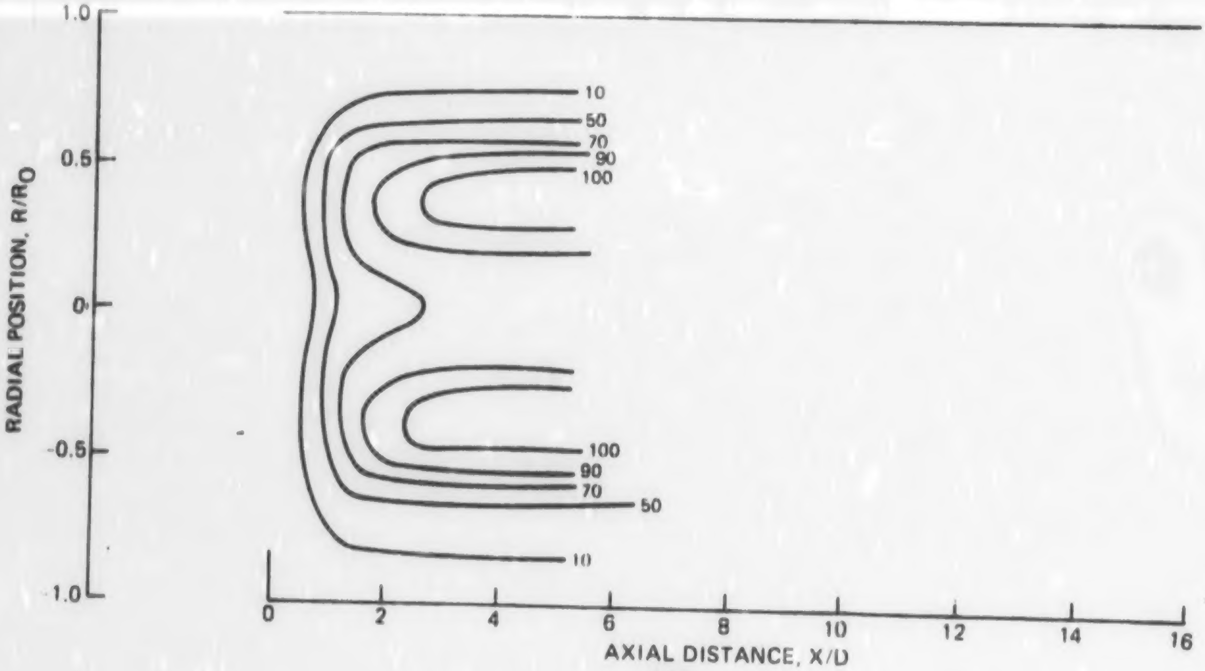

FIG. 11

TIME–AVERAGED TEMPERATURE DISTRIBUTIONS

ISO-OCTANE/AIR, T_{AIR} = 533 °K, ϕ = 0.65

(A) SWIRL = 0.3, 1 ATM

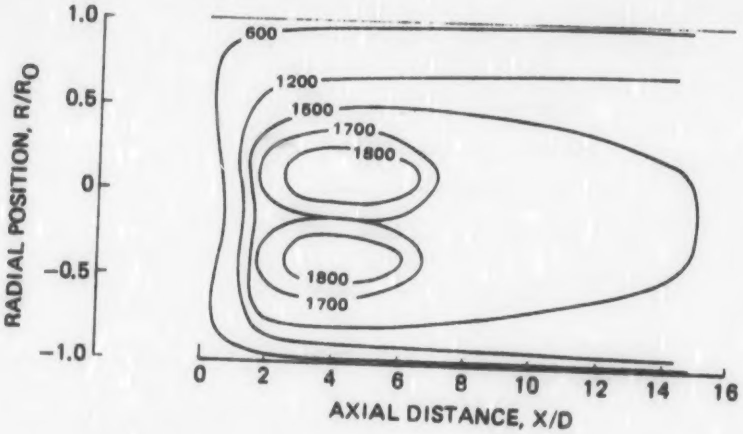

(B) SWIRL = 0.3, 3.3 ATM

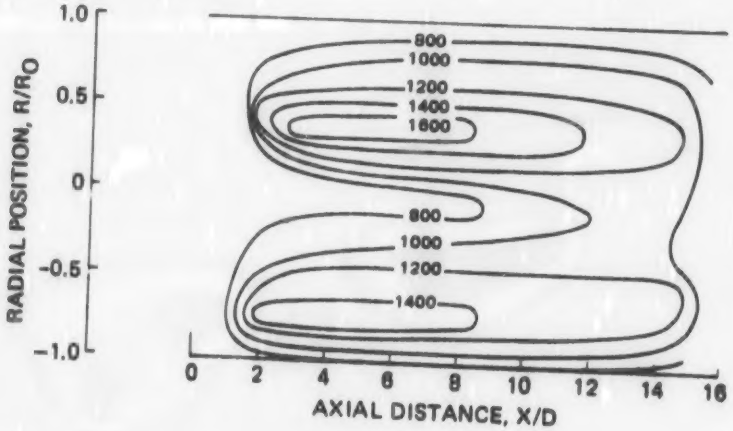

FIG. 12

TIME–AVERAGED O_2 DISTRIBUTIONS

ISO–OCTANE/AIR,1ATM,T_{AIR}=533°K,ϕ=0.65

(A) SWIRL 0.3, 1 ATM

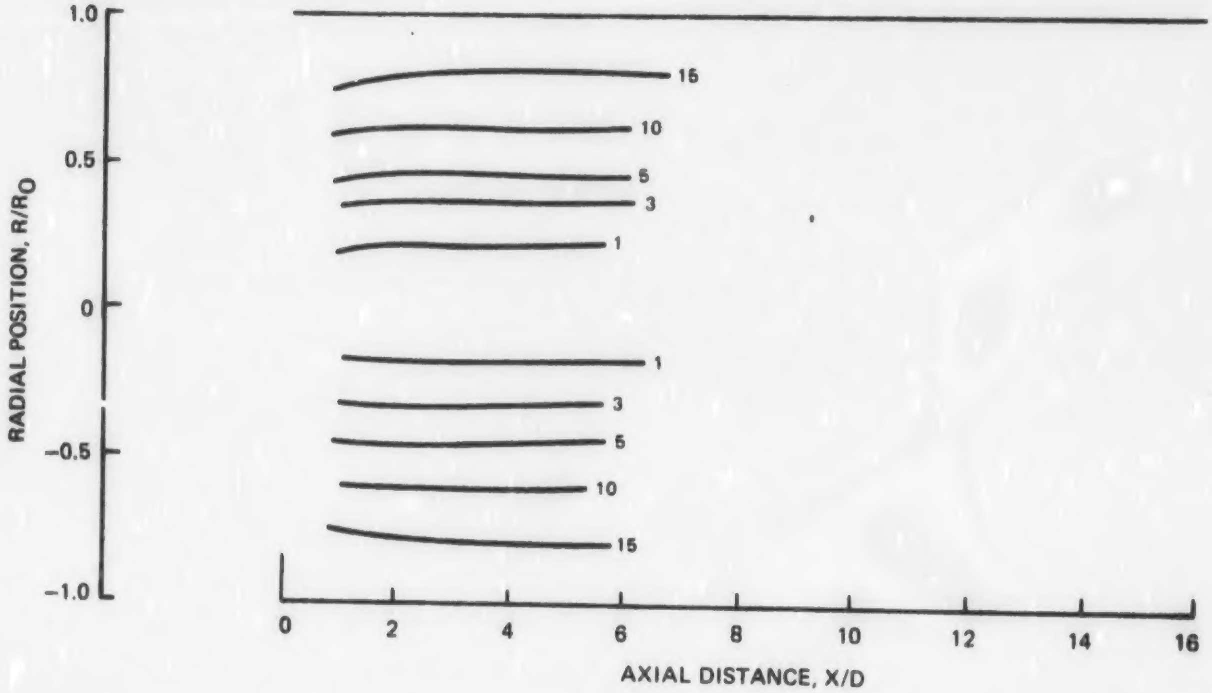

(B) SWIRL=0.3, 3.3 ATM

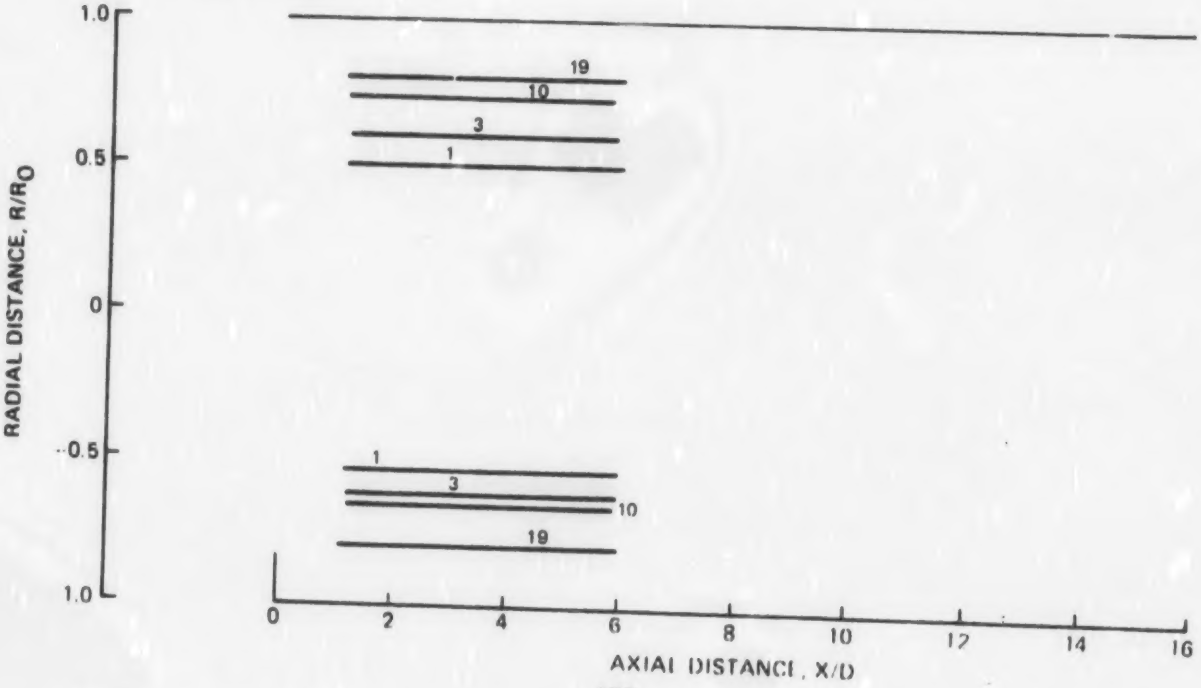

FIG. 13

TIME–AVERAGED NO DISTRIBUTIONS

ISO OCTANE/AIR, T_{AIR} 533°K, ϕ 0.65

(A) SWIRL=0.3,1ATM

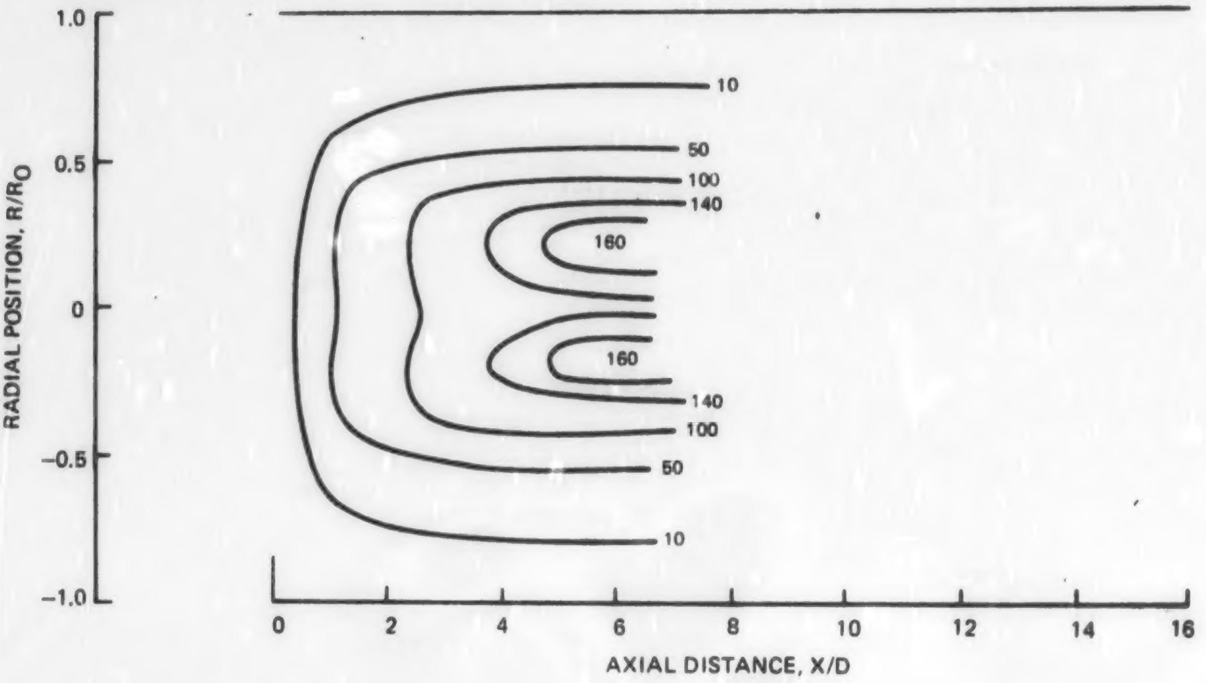

(B) SWIRL=0.3,3.3 ATM

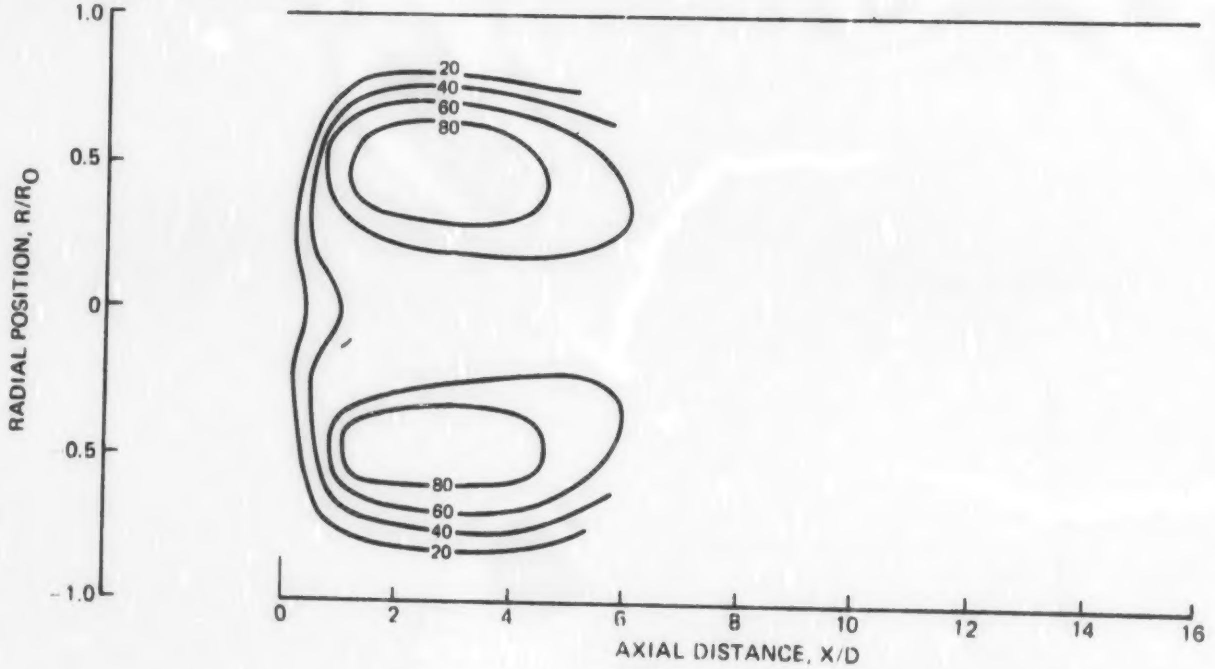

TIME–AVERAGED TEMPERATURE DISTRIBUTIONS

FIG. 14

S =0.3,1 ATM, T_{AIR}=533°K, ϕ=0.65

(A) PROPANE

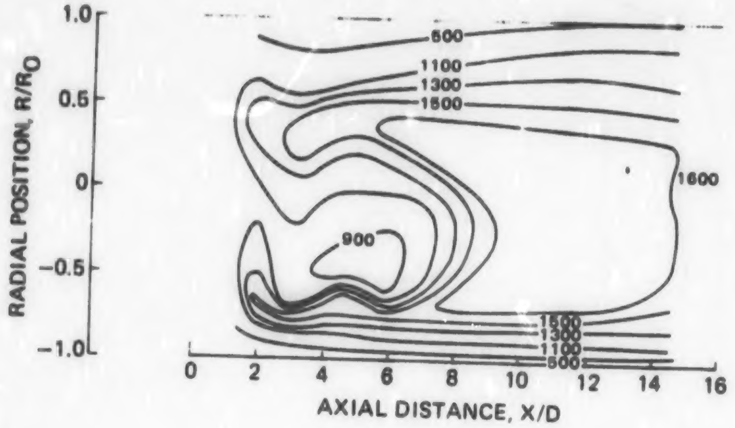

(B) ISO–OCTANE

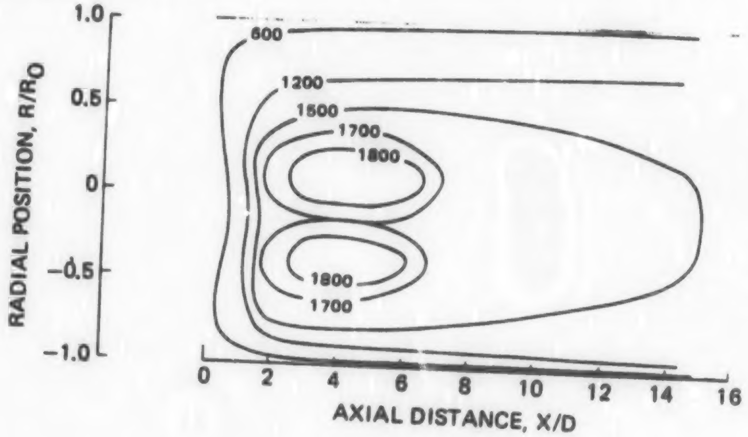

(C) NO.2 FUEL OIL

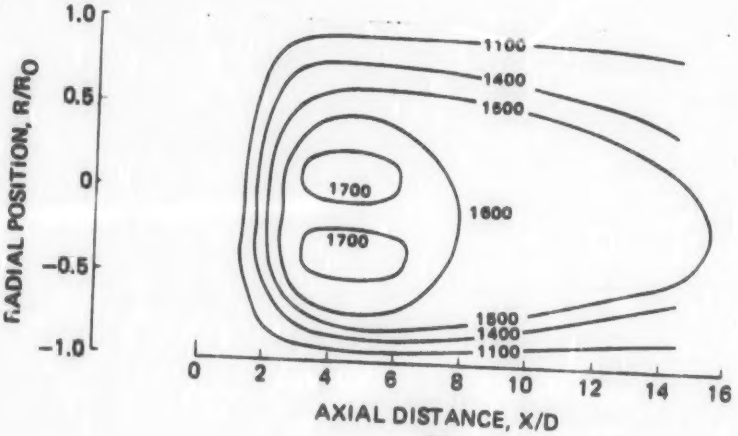

TIME–AVERAGED DISTRIBUTIONS OF TOTAL UNBURNED HYDROCARBONS

S=0.3, 1 ATM, T_{AIR}=533°K, ϕ=0.85

(A) PROPANE

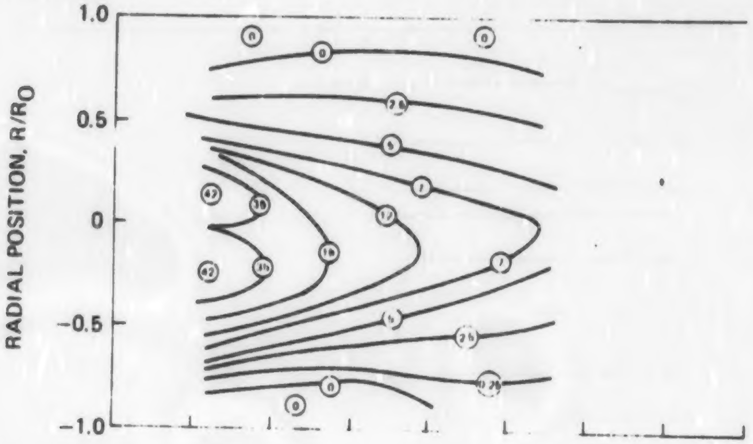

(B) ISO–OCTANE

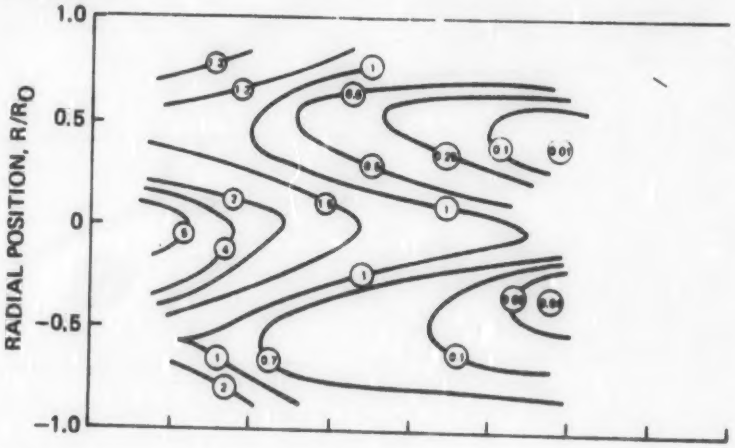

(C) NO.2 FUEL OIL

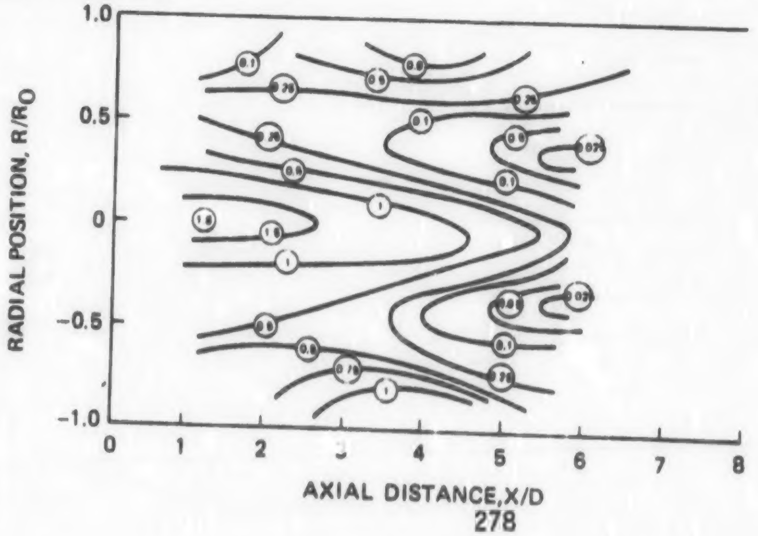

FIG. 16

TIME–AVERAGED O_2 DISTRIBUTIONS

S = 0.3, 1 ATM, T_{AIR} = 533°K, ϕ = 0.65

(A) ISO–OCTANE

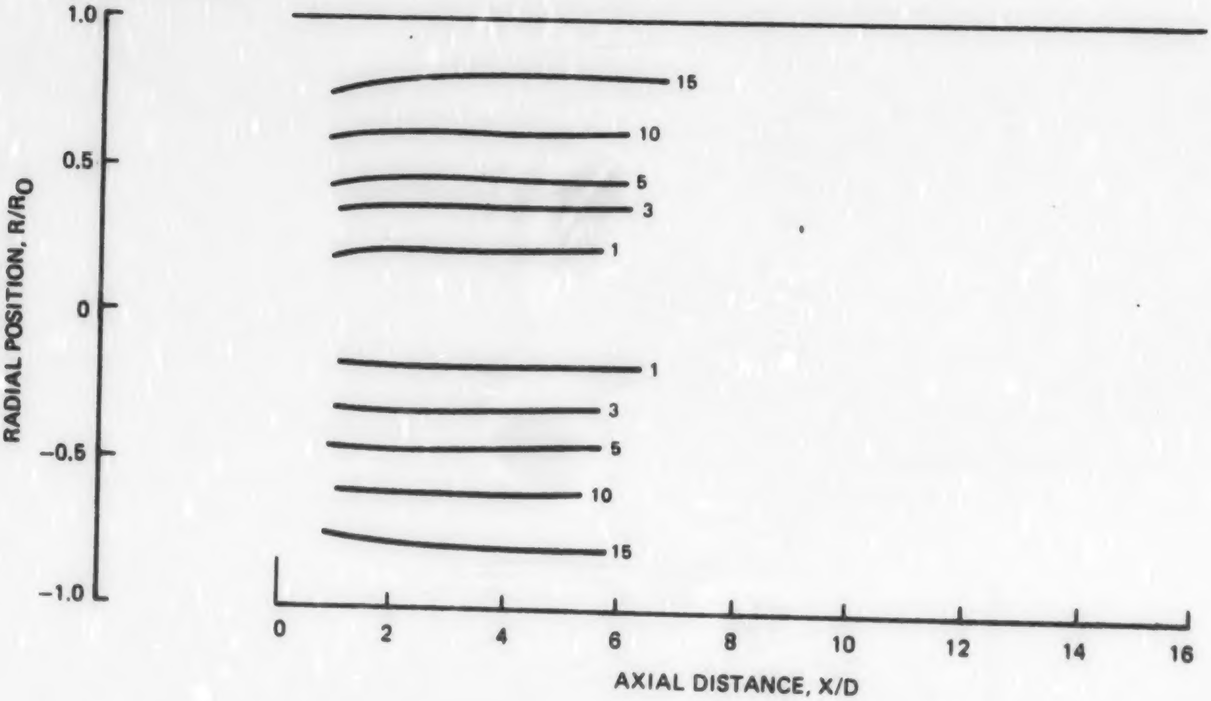

(B) NO.2 FUEL OIL

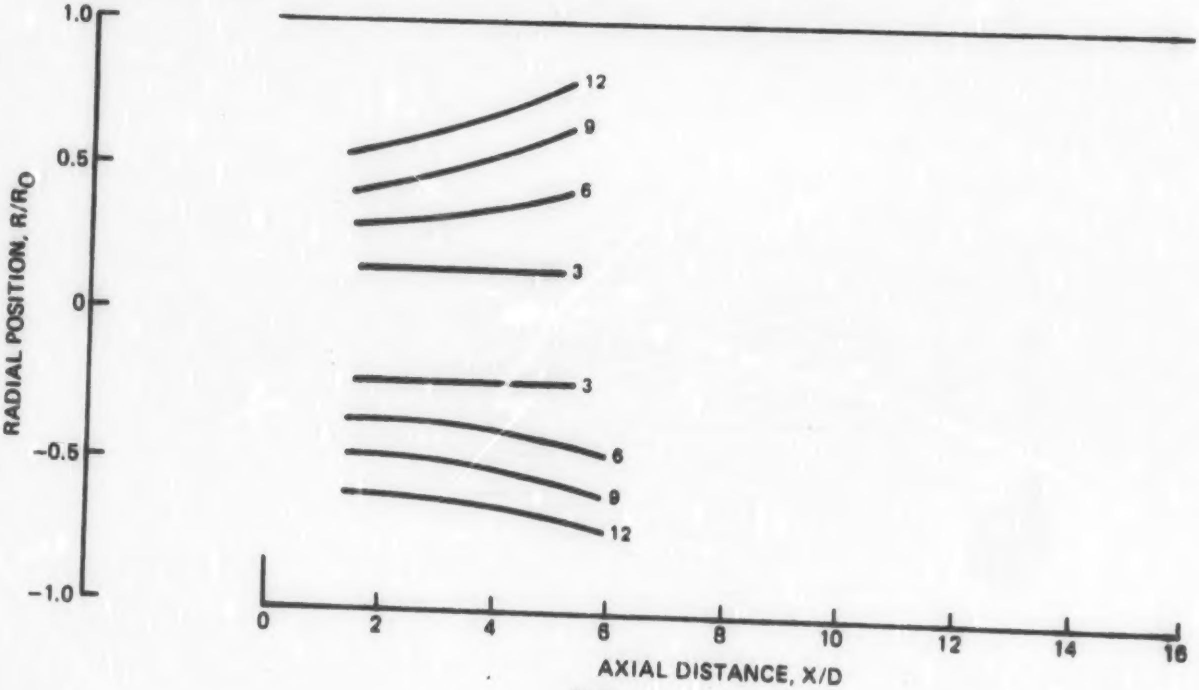

FIG. 17

TIME–AVERAGED TEMPERATURE DISTRIBUTIONS

NO.2 FUEL OIL/AIR, $s = 0.3$, 1 ATM, $\phi = 0.65$

(A) $T_{AIR} = 533\ ^{\circ}K$

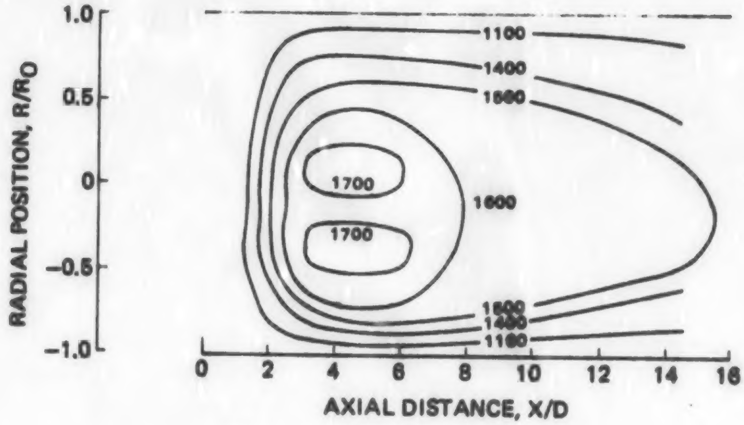

(B) $T_{AIR} = 750\ ^{\circ}K$

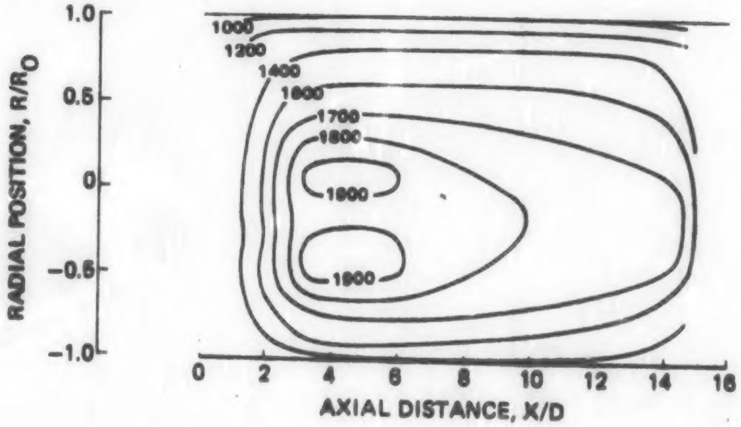

TIME–AVERAGED DISTRIBUTIONS OF UNBURNED HYDROCARBONS

NO.2 FUEL OIL/AIR, 1 ATM, S = 0.3

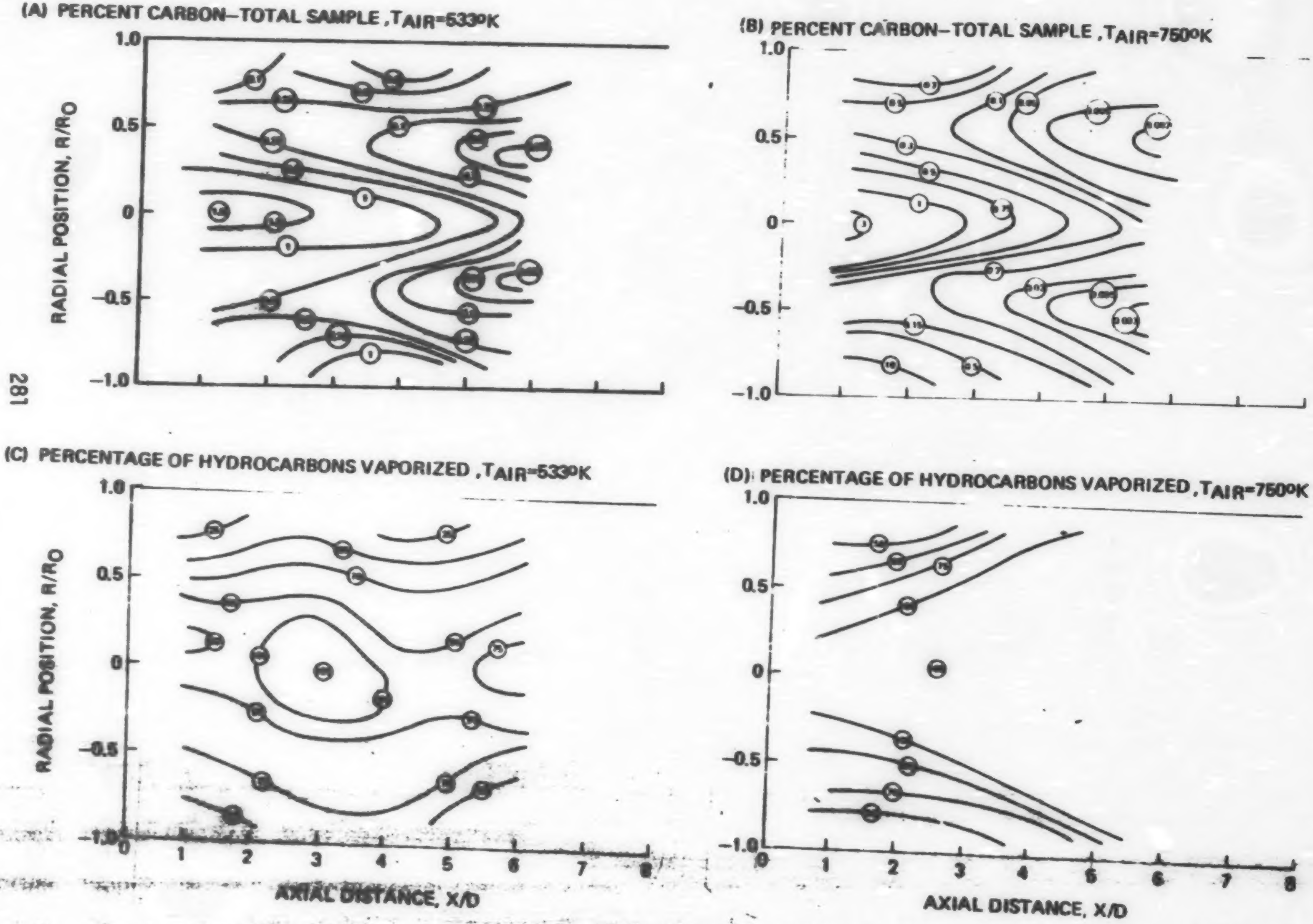

(A) PERCENT CARBON–TOTAL SAMPLE, T_{AIR}=533°K

(B) PERCENT CARBON–TOTAL SAMPLE, T_{AIR}=750°K

(C) PERCENTAGE OF HYDROCARBONS VAPORIZED, T_{AIR}=533°K

(D) PERCENTAGE OF HYDROCARBONS VAPORIZED, T_{AIR}=750°K

FIG. 19

FIG. 19

TIME–AVERAGED NO DISTRIBUTIONS

NO.2 FUEL OIL/AIR, S= 0.3, 1 ATM, ϕ = 0.65

(A) T_{AIR}=533K

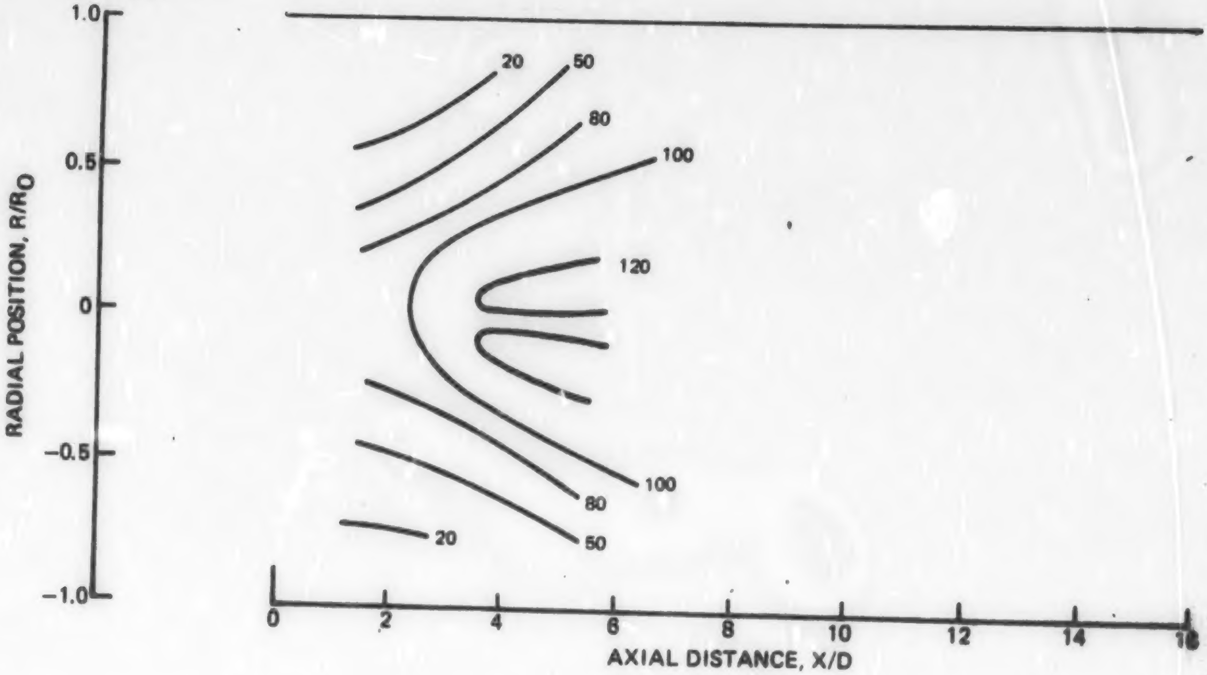

(B) T_{AIR}=750K

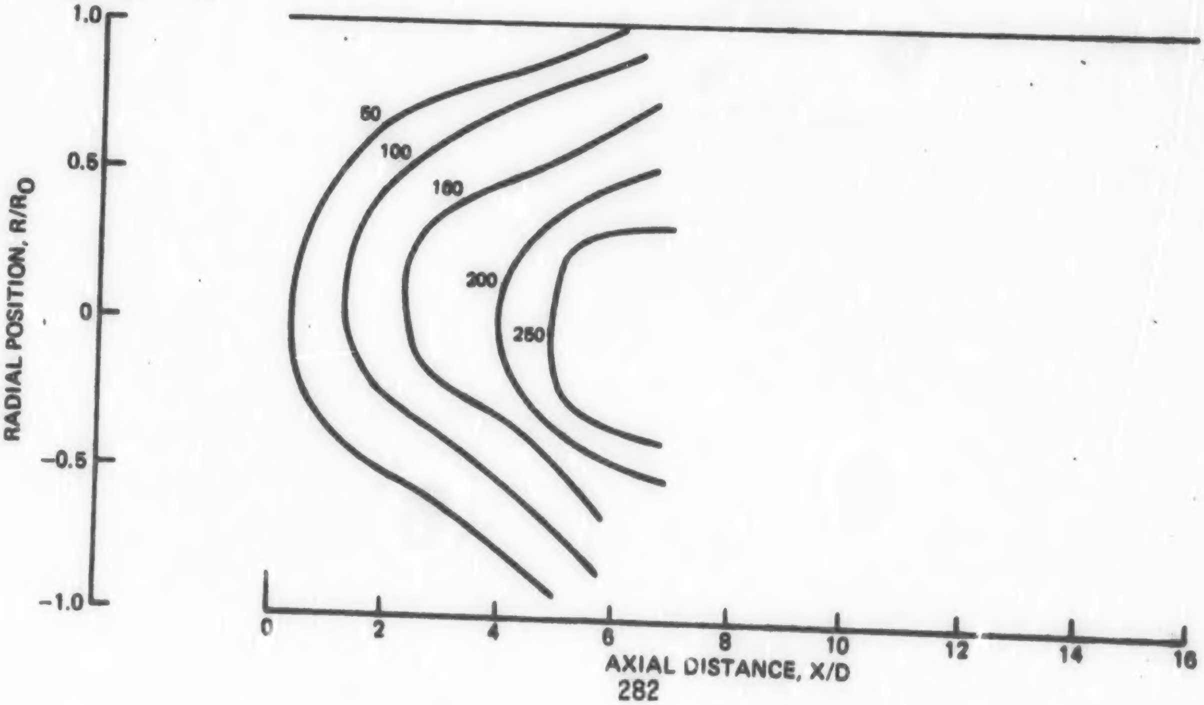

TWO-DIMENSIONAL OR AXIALLY SYMMETRIC MODELING OF COMBUSTING FLOW

By:

H. McDonald
Scientific Research Associates
Glastonbury, Connecticut 06033

and

R. C. Buggeln
United Technologies Research Center
East Hartford, Connecticut 06108

ABSTRACT

A numerical technique has been developed to solve the time-averaged turbulent reacting flow equations in general two-dimensional orthogonal coordinate systems, including the effects of flow recirculation. The numerical procedure utilizes an efficient robust relaxation scheme which solves a finite difference representation of the coupled set of elliptic partial differential equations of conservation of mass, momentum and energy. Physical models representing the effects of turbulent transport, liquid droplets and radiative heat transfer are incorporated into the scheme.

To date the main emphasis of this work has been on obtaining numerical results as free as possible from numerical inaccuracies and truncation error then comparing the experimental results from a methane burner with theoretical predictions. The predictions were made using three versions of two-equation models of turbulence. Results of comparison show good qualitative agreement between the theory and experimental results in regards to the basic flow patterns. For the swirl number equals 0.3 an experimentally observed toroidally shaped recirculation zone was predicted. When the flow passed round the recirculation zone the swirl velocity rapidly accelerated and downstream the swirl velocity profiles filled out and flattened appreciably as was observed experimentally. In addition the theoretical axial velocity profiles exhibited the observed local maximum at the centerline. Quantitatively the predicted axial velocity profiles compare favorably with the experimental data; however, although in qualitative agreement, the comparison of the swirl velocity profiles does not fare quite as well quantitatively. The principle discrepancies in the flow predictions are thought to be mainly due to the difference in the axial location of the theoretically predicted and the measured location of the toroidal recirculation zone. This research was conducted in fulfillment on Contract No. 68-02-1873 by United Technologies Research Center under the sponsorship of the U.S. Environmental Protection Agency. This paper covers the period of April 1975 up to the present.

Preceding page blank

INTRODUCTION

During the last two decades, numerical techniques for the prediction of viscous flows have made significant advances in their ability to represent the flow fields resulting from a wide variety of practical problems. Initially work concentrated on the simplier parabolic version of the viscous flow equations, the so-called boundary layer equations. Considerable success was achieved in making predictions in the boundary layer case where the diffusional effects in the primary flow direction can be neglected and the pressure field determined independently. Because of the parabolic nature of these equations, that is the problem possesses a time-like quality of dependence on initial and boundary conditions, the boundary layer equations lend themself to relatively simple spatial marching integration techniques. However, there is still a considerable practical interest in being able to predict the location of and the detailed features of recirculating flows, which evidently do not possess this time-like quality of the parabolic problem, since in a recirculation zone flow is being convected back against the time-like marching direction. Thus it becomes necessary to consider a more complete set of viscous flow equations which at the very least would not neglect the diffusion in the primary flow direction. For these cases the differential equations are elliptic in nature which is to say that at any point the flow can, in principle, be influenced by all the boundaries and, of course, the spatial marching techniques are no longer applicable except perhaps in some iterative sense. In order to make predictions for these elliptic cases, two basic techniques have become popular for steady state calculations, the time marching and residual relaxation techniques. Both techniques consist of replacing the partial differential equations which describe the elliptic viscous flow phenomena by some form of algebraic analogy. Many investigators have chosen to use a

Preceding page blank

finite difference representation to approximate derivatives; however, other algebraic approximations can and have been used. The time or pseudo time marching technique consists of making an initial guess of the solution at time zero and then integrating a time or pseudo time dependent form of the governing equations out in 'time' until the desired steady state solution is achieved. The residual relaxation technique also relies on making an initial guess of the solution. From this initial guess a measure of the deviation of this guess from the solution is made by inserting the approximate solution in the governing equation and computing the error or residual as it is often called. The error or residual is then used in some manner to make a correction to the guess in an iterative sense until a converged solution is obtained. The time marching technique is more general than the residual technique as it also has the capability of yielding the transient solution as well as the steady state solution, should a steady state indeed exist. In many cases, however, only the steady state solution is of interest, and for these cases the residual relaxation technique can present a competitive and in some senses a superior method for calculating elliptic viscous flow situations since the transient solution does not necessarily have a rapid approach to the steady state. Direct i.e., noniterative techniques have in the past not been competitive with iterative techniques for the desired dense meshes. In recent years there has however been a revived interest in direct techniques but none have reached the point of being able to be applied in the problem of current interest. The numerical basis of the residual relaxation technique used in this investigation, the Field Relaxation Elliptic Procedure (FREP) technique, will not be discussed in this paper as it has been previously described in several other documents (Refs. 1, 2, and 3). Instead this paper will concentrate on four general topics. The first of these general topics will be to discuss the overall objectives and general philosophy followed in applying the FREP numerical technique to combustor problems. Secondly a brief discussion will be made of the history of the development of the numerical scheme and problems encountered during its development. The third topic will discuss the recent and current activities performed under EPA contract 68-02-1873. Finally, some general observations will be given and some recommendations made for what future work should be performed in this particular area of modeling.

Taking the first topic, the overall objective of this combustor modeling effort has always been to develop a numerical procedure that is capable of being able to economically represent the combusting flow and related phenomena associated with a wide range of combustor problems. Consideration has been given to developing a computer code which has the ability of analyzing a large number of geometrical configurations and different fuels. The general approach has been to use "state of the art" physical models of transport and chemistry and insofar as possible the general structure of the code has been developed in such a manner that if the "state of the art" proved inadequate, new technology could relatively easily be incorporated into the code as it became available. Numerical techniques were used which were felt to have the highest probability of success as a general prediction method for the solution of the governing partial differential equations. Consistent with the generality desired, the full Navier-Stokes equations were treated and as few additional approximations as possible were made. These additional approximations occur mainly in the areas of the physical models and in the application of "wall function" boundary conditions, which are approximations designed to make major savings in computer storage and run time with the minimum impact on the overall plausibility.

Developing a combustor analysis comparison of experimental data with computer predictions of combustor flows is a valuable tool for determining the predictive accuracy of the combination of the numerical technique used to solve the differential equations and the physical models used in the computer code. Results of the comparisons are valuable not only in guiding the investigator in his choice of alternate physical models or numerical schemes, but also enables the numerisist to aid the experimentor in his choice of future experiments. For example, in the present study the experimental inlet conditions were essentially unknown. A simple theoretical study using a range of reasonable inlet conditions indicated that the solution downstream of the inlets could be critically affected by these inlet conditions, thus strengthening the motivation of the experimentor to perform the often difficult measurements to map the inlets conditions. Another example from the present study is the observation that the axial velocity profiles are in reasonably good agreement with the experimental data, but the temperature profiles show poor agreement. In view of the close coupling between temperature density and velocity it does not seem likely that the velocities would be predicted correctly unless the temperatures were 'reasonable', and this thought does cast doubt on the temperature measurements since the velocities were measured by a nonintrusive laser velocimeter. To date the indications are that only a limited amount of the theoretical predictions compares reasonably well on a quantitative basis with the experimental combustor data taken under this particular contract. The relatively poor quantitative results (qualitatively the predictions shown remarkable similarities to the observed flow features) may be due to errors arising from the numerical techniques or the physical models used or in part is due to the lack of well defined experimental inlet conditions. Identification of the role of these potential problem areas is in itself a significant conclusion.

BACKGROUND

Insofar as the numerical aspects are concerned the general evolution of the FREP computer code has been that of taking a rather general numerical procedure and gradually adding to it numerous physical models, boundary conditions, additional partial differential equations to consider new effects, and geometric capabilities to consider more complex configurations. At various points in this development process it has also been necessary to modify the numerical procedure in order to both economize on computer time and storage and to generalize the technique to adequately consider the effects of the new physical models and additional differential equations. The first version of the FREP computer code solved the stream function, vorticity, stagnation enthalpy and mass fraction equations. The turbulence model assumed that some global mixing length model was available and the chemistry was an equilibrium model. The above equations were solved in an uncoupled manner; however, it soon became evident that because of the strong coupling of the vorticity to the stream function in many cases of interest it was necessary to solve the stream function and vorticity in a coupled manner. This was done by generalizing the numerical procedure to allow for systems of equations which are solved simultaneously as opposed to the sequential but individual solution of each equation in the system. The formal introduction of the coupling into the system allowed computations at a much higher Reynolds number than had previously been possible as well as of course an increased rate of convergence relative to the uncoupled system. Next came the addition of the swirl equation and elementary radiation equations so that the user could consider the effects of these phenomena. In order to calculate the nitric oxide emission a non-equilibrium (rate) NO equation was added. The assumption was made that the formation of the NO had little effect on the fluid dynamics (little energy release) and hence the NO levels could be calculated after a converged fluid dynamics solution had been obtained. The rate NO equation presented the first exposure to an equation which had a strong nonlinear source term. What could have been a potentially difficult problem turned out to be easily handled by a Newton-Raphson iteration scheme embodied in the FREP procedure.

Work on the second EPA contract (EPA 68-02-1092) falls into four basic areas: (1) basic numerical work, (2) addition of new physical models, (3) added geometrical capabilities and (4) comparison of computer predictions and experimental data for the EPA-UTRC burner. The original version of the FREP computer code used a straightforward upwind differencing on the convection terms. It was found that in some cases as a result of numerical truncation error, mass was not conserved (Ref. 4) to a sufficiently close tolerance. In order to correct this deficiency, central differencing and donor cell differencing of the convective terms, two additional techniques, were incorporated into the computer code. The central differencing and donor cell differencing of the convective terms both conserve mass (and any other term). Central differencing which is second order accurate in space does have the so-called cell Reynolds number problem of wiggles developing in the solution when the cell Reynolds number exceeds two; however, this problem can be minimized by the proper choice of grid spacing and the application of artificial viscosity. Donor cell differencing does not have any stability problems, but it is formerly only first order accurate. At present the technique is to use central differencing whenever possible and to use donor cell differencing for all other cases.

Initially the FREP computer code used a mixing length model to calculate the eddy viscosity and an equilibrium model for the chemistry. It was felt that these models were inadequate for the preliminary evaluation of the code predictions. When this initial evaluation was completed the mixing length model was replaced by a two-equation model of turbulence, the turbulence kinetic energy-dissipation of turbulence kinetic energy model (Ref. 5). The two-equation model of turbulence requires the solution of two addition partial differential equation with nonlinear source terms, but its strength lies in the generality of the flow situation that it can consider. The chemistry model was also improved to account for some of the rate phenomena. Dryer's (Ref. 6) global kinetic methane model was incorporated into the code and it should be mentioned that this implementation required some further approximation. The rate chemistry also required the additional solution of a partial differential equation. The source term of this equation represents the rate of burning of the methane and by assuming that the products are in equilibrium a new chemistry model is evolved. This new model is especially useful for the premixed flows where the equilibrium models predict much too rapid burning which as well as being unrealistic could often lead to numerical instability.

During the initial runs for the comparison of the theoretical results with the experimental (see Figure 1 for a schematic of the experiment), it became evident that effects in the combustor were being felt up in the fuel injector, but of course these effects were prevented from doing so in the calculation by the imposed boundary conditions. In order to account for the phenomenon the computational domain was increased to include the region inside the fuel injector. When the computation was performed with the new domain the results showed that the influence of the main combustion region were indeed felt upstream in the fuel inlet.

Subsequently in performing comparison of computed predictions with the experimental data, it was assumed that the radial velocity was zero at the air inlet plane. It soon became evident that immediately downstream of the air inlet the predicted and measured radial velocity profiles were not in reasonable accord, hence several air inlet profiles of radial velocity were assumed and the resulting downstream characteristics calculated. It was found that the assumed radial velocity profile had a very significant effect on the resulting downstream flow field. The location of the recirculating and in fact the existence of a recirculating zone could be determined by changing the assumed radial velocity profile. Since the air inlet radial velocity profile at the dump plane is rarely measured or otherwise known it then becomes necessary to extend the computational zone up into the air injector where the assumption of zero radial velocity profile is more likely to be a valid approximation. Incorporation of this capability and the numerical problems associated with it will be discussed later.

One of the motivations for going to the more complex Dryer's global kinetic methane scheme was the lack of agreement between the computational and measured temperature profiles. The computational temperature profiles in general had much larger gradients and peak temperatures than the experimental data. It was thought that this was due to the equilibrium assumption and that Dryer's kinetic model as implemented here would tend to diffuse the computational temperature profiles and that the agreement with the data would improve. Unfortunately the present application of Dryer's model was unable to improve the poor predictions. The computational profiles did become slightly more flat, but the agreement with the data was in general not significantly improved.

The computed axial velocity profiles were in general in relatively good agreement with the laser velocimeter measurements of velocity. In the region immediately downstream of the dump plane on the axis of symmetry the computed axial velocity did not exhibit a local maximum, as the experimental data did; however, the profiles further away from the centerline were in good agreement. Farther downstream agreement between theory and experiment was good across the entire combustor. Predictions of swirl velocity were consistently lower than the measured values. Among the possible explanations for this deficiency is that the values of turbulent viscosity used in the swirl equation could be too high.

THE PRESENT EFFORT

Work performed under the present EPA contract has concentrated in four main areas (1) incorporation and evaluation of alternate two-equation turbulence models into the FREP computer code, (2) improve the geometrical capability, (3) improve the generality of the wall function portion of the code and (4) perform further comparisons between theory and experiment for the EPA-UTRC burner. Two alternate two-equation turbulence models were incorporated into the FREP computer code. Both models utilized the turbulence kinetic energy as the first variable. The first model had as the second variable the product of the turbulence kinetic energy and a 'mixing length' (Ref. 7) while the second model had as its second variable a quantity related to the fluctuation of vorticity (Ref. 8). Computations performed with these two alternate two-equation models produced results that differed only slightly from the results produced by the turbulence kinetic energy-dissipation of turbulence kinetic energy equations. It is felt that this is due mainly to the fact that the theoretical basis of the source terms of the second equation of each model are related and hence if the equations are source dominated, similar results should occur. This phenomenon has also been observed by other investigators (Ref. 9), and in part stems from the originator of the particular model ensuring that certain limiting forms of the turbulence model are recovered.

As mentioned in the previous section, there are cases when it is necessary to have as the computational domain regions inside both fuel and air inlets. During the present contract the computer code was modified to allow the computational domain to include the regions inside an arbitrary number of inlets. This required a modification of the basic alternating direction implicit (ADI) scheme to allow for the integration through solid surfaces. This was successfully done by modifying the elements within the ADI matrices in a manner such that the wall boundary conditions were satisfied at each surface. Results performed with this new version of the FREP computer code substantiated the belief that the radial velocity profile on the dump plane of the air injector of the EPA-UTRC burner could not be assumed to be of zero magnitude. In addition a considerable effort was made to generalise the wall function concepts introduced in the previous contract. Wall functions can be viewed as an economical means of approximating the turbulent flow phenomena in the regions of walls. In the regions of walls the derivatives normal to the wall of many variables become very large and hence a large number of grid points is needed in the wall regions to adequately resolve these derivatives. Wall function concepts are based on simplified closed form approximations to the boundary layer profiles of the flow variables in these regions to calculate their derivatives. Under the previous contract it was assumed that the first grid point off the wall was in the well known boundary layer logarithmic velocity profile region. This assumption proved to be invalid in some regions of the flow field where the first grid point actually lay within the viscous sublayer and hence necessitated the need for a more general wall function formulation. The assumption of being in the logarithmic region was replaced by a formulation that allowed for a continuous movement away from the near wall viscous sublayer region through the transition region into the logarithm region. The generalized wall function scheme affects not only the velocity profile near walls, but also the stagnation enthalpy profile for cooled walls, the derivatives of viscosity near walls and the boundary conditions for both equations of the two-equation models of turbulence. Once these improvements were incorporated into the FREP computer code, attempts were made to compare the predictions with the experimental data for the EPA-UTRC burner. However, problems emerged in two areas (1) with the two-equation model of turbulence in the form of the physically impossible negative turbulence kinetic energy and (2) with a lack of overall outer convergence of the system of equations. The predicted negative turbulence kinetic energy occurred in regions of the flow field where the system desired to have a very low level of (positive) turbulence kinetic energy and during the course of the iterative development minor excursions into the domain of negative energy occurred. Once these physically implausible negative values occurred within the solution domain the solutions diverged immediately. Upon close examination of the two turbulence model equations, it was seen that the linearized version of the particular form of the equations in widespread use were in fact singular as the turbulence kinetic energy approached zero. Hence based upon an equivalent but reformulated version of the model equations, a new linearized form which circumvented the singularity problem was developed and incorporated into the FREP computer code. This revision of the form of the turbulence model equations not only helped with the predictions from the turbulence equations, but also speeded the rate of overall outer convergence. However, even at this point the outer convergence of the system of equations could not be obtained to the expected degree, although the general qualitative features of the predicted flow were consistent with the experimentally observed results. For both the swirl number equals 0.3 and 0.6 cases the approximate location of the measured and calculated recirculation zones and the qualitative form of the measured and calculated axial velocity profiles were similar. The predicted axial velocity profiles also exhibited a local maximum on the centerline as was experimentally observed.

In order to improve the degree of outer convergence the form of the swirl equation was reformulated such that the dependent variable was changed from the swirl velocity times the radius to the swirl velocity alone. Some improvement in the swirl velocity predictions were observed but the problem of relatively poor outer convergence still remained. Another problem, previously mentioned and felt to be a possible source for the lack of outer convergence was the very large gradients of temperature, not observed experimentally, that appeared in the predictions and the fact that small physical movements of the flame front could cause locally large residuals. Suspecting that an inadequately assumed value for turbulent effective Prandtl number could be responsible for allowing the large gradients to exist, the turbulent transport of enthalpy was increased by varying the assumed turbulent Prandtl number, but the results indicated that a much larger effect was required to reduce the predicted temperature gradients. With this in mind a simplified radiation effect was included in the stagnation enthalpy equation and with very reasonable emissivity assumptions the large temperature gradients were substantially reduced. Unfortunately this also did not cause the hoped for improvement in the degree of outer convergence.

At this point in the development of the FREP computer code, it is desirable to evaluate the codes performance in the two cases run under the present contract. It appears that the main problem area at the present time is the inability of the code to obtain a satisfactory level of overall outer convergence for these two cases. Further preliminary investigation has indicated that at least some of the difficulty is associated with the slow rate of outer convergence of the two equations associated with the two equation model of turbulence. The "stiffness" of these equations can perhaps be best overcome by still further linearization of these equations or by iterating on the solution of those equations during each outer iteration.

It should be pointed out that the combustor cases generated by the EPA-UTRC combustor are not typical of normal furnaces. The ratio of the velocities in the air and fuel injectors is on the order of 20:1 thus causing the existence of extremely large velocity gradients in the vicinity of the splitter plate. Further adding to the numerical difficulties is the existence of large temperature gradients which are of course typical of diffusion burners. Large gradients with a limited number of grid points to resolve them are always a potential source of numerical difficulties. In addition, further numerical problems can possibly be caused by the thin splitter plate between the fuel and air inlets. Since it was desired to include in the computational domain the regions inside both inlets, it was necessary that the splitter plate be taken to be at least one grid spacing thick. The use of such a small grid spacing in the vicinity of the splitter plate and hence a much larger grid spacing elsewhere is another potential problem area that could only be resolved by the addition of more grid points. Simplier cases (i.e., cases which have smaller gradients of velocity and temperature) involving a premixed fuel and air have been successfully run with the FREP computer code by the present authors (Ref. 10) lending credence to the validity of the overall numerical scheme.

Other investigators have seemingly obtained converged solutions to the various flow equations for combusting flow and in some cases have achieved reasonable agreement between theory and experimental data. In most cases the problems considered have been much less severe and have predominately been premixed or for diffusion burners have been a low ratio of air to fuel

Reproduced from
best available copy.

axial ratio cases. In view of the fact that in the present study it was found that the assumed inlet conditions had a great effect on the downstream flow and that the other investigators did not have inlet information available, it is doubtful if the good agreement between theory and data was obtained without some "experimenting" with the inlet conditions. In some cases it is doubtful if convergence is actually achieved as many of the dependent as well as the derived variables are heavily under-relaxed. This can result in the slowing down of numerical evaluation of the solution and falsely give the impression that the solution has converged. In addition several cases have been reported where extremely coarse grid spacing has been used. This results in the introduction of large amounts of truncation error which in turn causes the large gradients to be smeared out thus resulting in a much less numerical severe case where a converged solution can be obtained. If a much finer mesh had been used, the solution may not have converged. Certainly much work needs to be done on mesh refinement and its effect on both the achievement of a converged solution and on the quality of the converged solution, if it exists.

In spite of what is considered relatively poor outer convergence the following comparisons are presented to indicate the qualitative features of the predictions. It is not expected that the overall flow features will change by an appreciable amount when satisfactory outer convergence is obtained. The overall qualitative features of the predicted flow patterns are in fairly good agreement with the experimentally observed results. The existence of the toroidally shaped central recirculation zone is in approximately the same region as was measured. Figures 2, 3, and 4 compares the predicted and measured axial velocity profiles at three axial locations (X/r_o being the ratio of the distance from the dump plane to the combustor radius). Agreement is in general fairly good especially from a qualitative basis. To be noted is the existence of a local maximum of the axial velocity on the centerline as was experimentally observed. Figures 5 and 6 compare the computed and measured swirl velocity profiles at two axial stations. As can be seen the agreement is poor and appears to become poorer as the flow moves downstream. This is felt to be in part due to incorrect values of effective viscosity used in the swirl equation. Figure 7 shows the isotherms predicted by the FREP computer code. These isotherms when compared with the measured values of temperature have a poor agreement. The predicted temperature profiles in general have much larger radial gradients and exhibit much larger peak temperatures. This lack of agreement, of course, produces a corresponding lack of agreement in NO_X profiles as the predicted NO_X general follows the temperature.

SUGGESTION FOR FUTURE DEVELOPMENT

It is suggested that for the near future that work concentrate both on examining the outer convergence problems and on attempting to compare theoretical predictions with experimental data for cases not as severe as those considered under the present contract, since indeed the cases considered to date are not at all representative of industrial furnaces. Next some basic numerical work should be performed on some simple cases such as the flow in a laminar driven cavity and simple turbulent premixed flows to establish the effect of the grid spacing and mesh refinement on the quality of the solution. In addition further effort should be undertaken to improve the numerical scheme in regards to computational speed and numerical accuracy and robustness, and also to develop a means of eliminating the need to use artificial viscosity when the cell Reynolds number becomes too large. Furthermore, it would be advisable to consider some cases of a diffusion flame where the splitter plate is not of essentially infinitesmal thickness. The consideration of cases which have thicker splitter plates will enable the use of a more approximately equally spaced radial grid spacing and thus eliminate the problems associated with rapid variation of the grid spacing. Since it is felt that the assumed inlet conditions can greatly effect the resultant downstream flow field, it would be desirable to consider experimental cases for which valid inlet data exists or cases where it is reasonable to assume conditions up in the injectors. As a final suggestion, some numerical experimentation could be performed in the area of temperature predictions in combusting flow. Experimental measurement of temperature is difficult in combusting turbulent flow due to the high fluctuation level in both temperature and velocity and because of the angular sensitivity of the measuring apparatus. Some simple hot versus cold flow field comparative studies could be made to determine the effect that combustion has on the development of the flow field. Another potentially valuable study could be performed by setting the temperature field to its experimentally measured values and then letting the velocity field and other variables develop as the numerical solution converged. If the resulting velocity field converged to the experimentally measured one, this would lend credence to the measured temperature field and thus demonstrate the need for further work in the means by which the theoretically calculated temperature fields are predicted.

REFERENCES

1. Anasoulis, R. F. and H. McDonald: A Study of Combustor Flow Computations With Experiment. EPA-65012-73-045, Dec. 1973.
2. Anasoulis, R. F., H. McDonald and R. C. Buggeln: Development of a Combustor Flow Analysis, Part 1: Theoretical Studies. AFAPL-TR-73-98, Jan. 1974.
3. Buggeln, R. C. and H. McDonald: Influence of Aerodynamic Phenomena on Pollutant Formation in Combustion. Environmental Protection Agency, Research Triangle Park, to be published.
4. Roache, P. J.: Computational Fluid Dynamics. Hermosa Publishers, Albuquerque, New Mexico, 1972.
5. Jones, W. P. and B. E. Launder: The Prediction of Laminarization with a Two-Equation Model of Turbulence. Int. J. Heat Mass Transfer, Vol. 15, 1972, pp. 301-314.
6. Dryer, F. L.: High Temperature Oxidation of Carbon Monoxide and Methane in a Turbulent Flow Reactor. AFOSR Report No AFOSR-TR-72-1109, March 1972.
7. Rotta, J.: Recent Attempts to Develop a Generally Applicable Calculation Method for Turbulent Shear Flow Layers. Proceedings of AGARD Conference on Turbulent Shear Flows, 1971.
8. Spalding, D. B.: The Prediction of Two-Dimensional Steady Turbulent Flows. Imperial College, Heat Transfer Section Rep. EF/TN/A/16, 1969.
9. Launder, B. E. and D. B. Spalding: Mathematical Models of Turbulence. Academic Press, New York, 1972.
10. Gibeling, H. J., H. McDonald and W. R. Briley: Development of a Three-Dimensional Combustor Flow Analysis. AFAPL-TR-75-59, Vol. II, Oct. 1976.

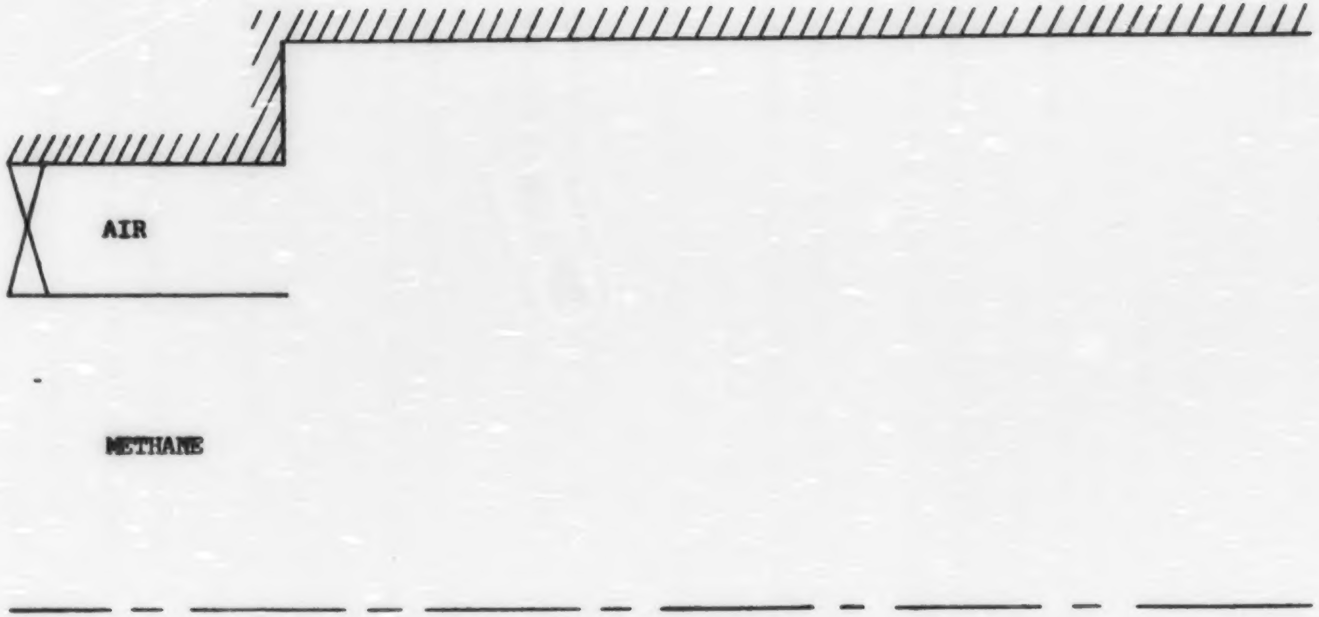
AIR
METHANE

Figure 1. Schematic of the EPA-UTRC Burner

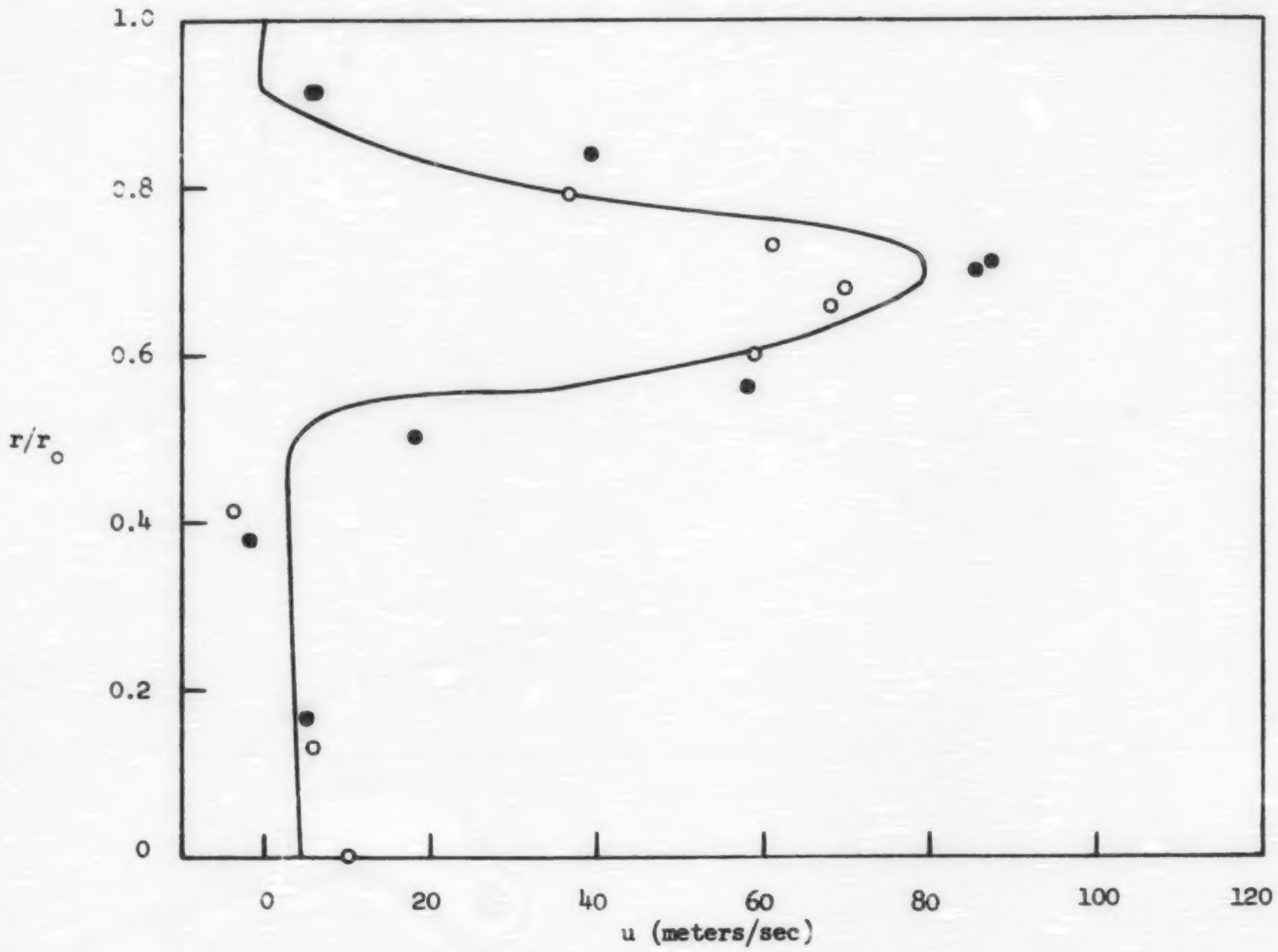

Figure 2. Axial Velocity Profile at Station $x/r_o = 0.10$ for Swirl Number = 0.3

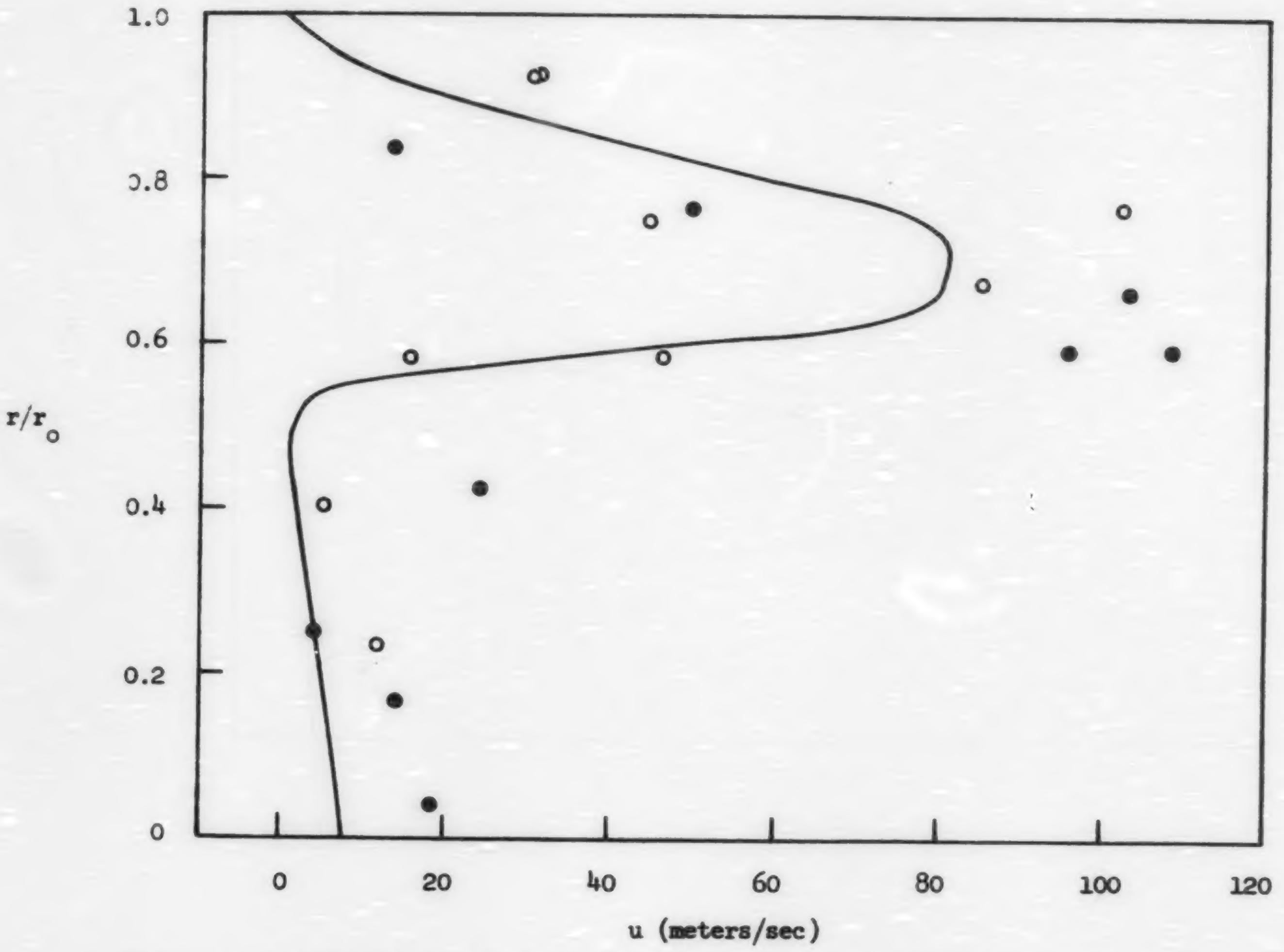

Figure 3. Axial Velocity Profile at Station $x/r_o = 0.26$ for Swirl Number = 0.3

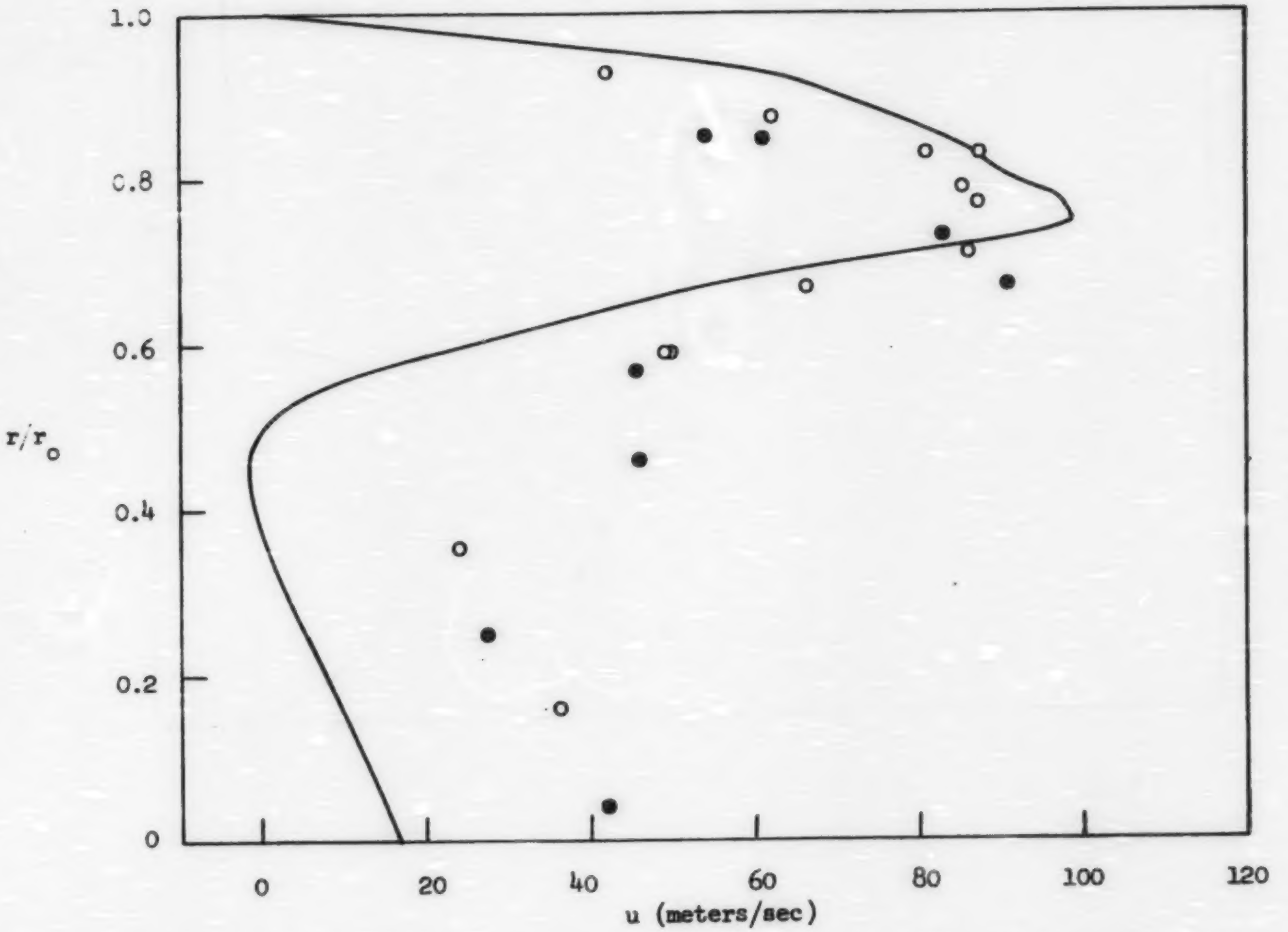

Figure 4. Axial Velocity Profile at Station $x/r_o = 0.97$ for Swirl Number = 0.3

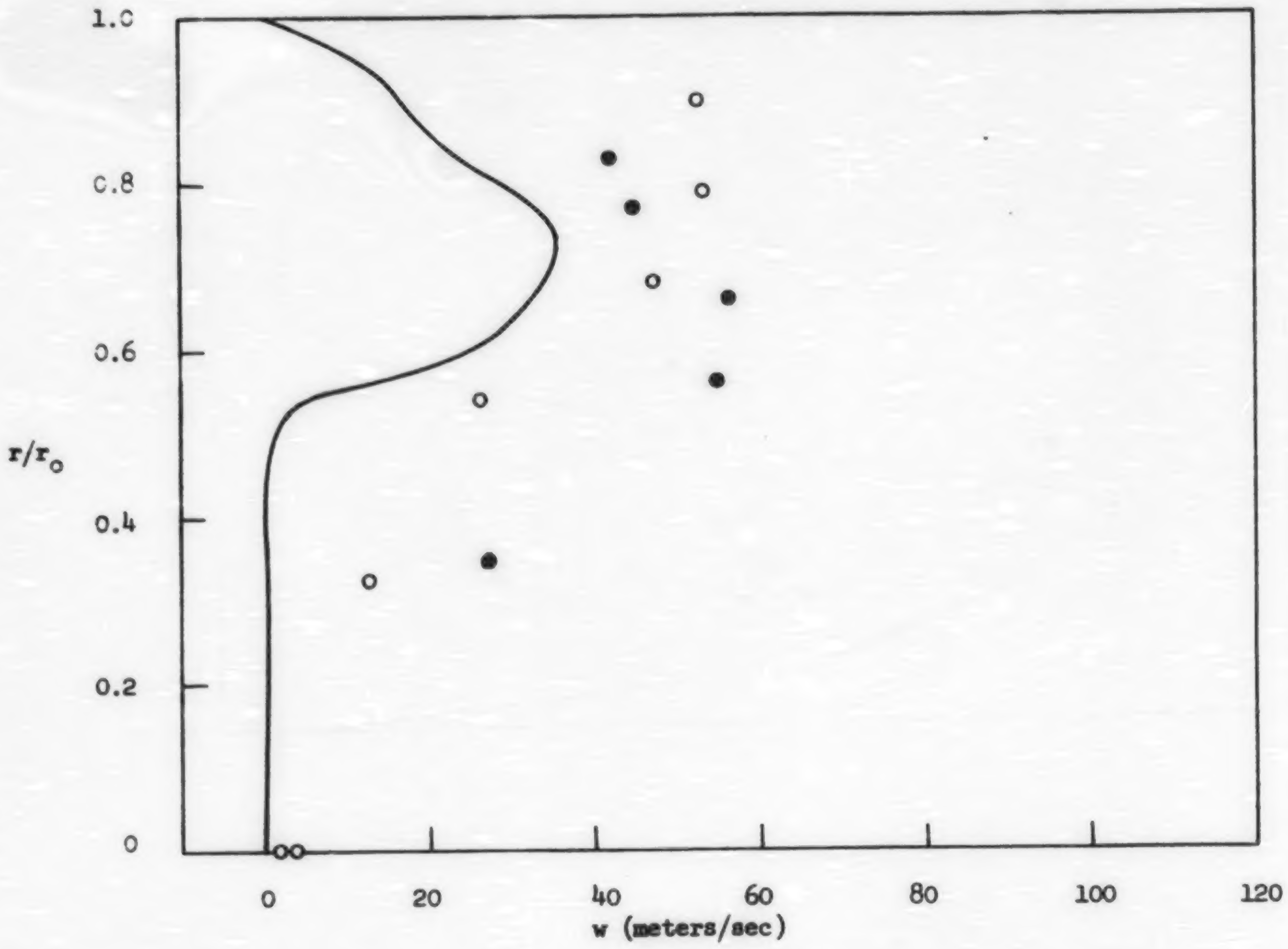

Figure 5. Swirl Velocity Profile at Station $x/r_o = 0.26$ for Swirl Number = 0.3

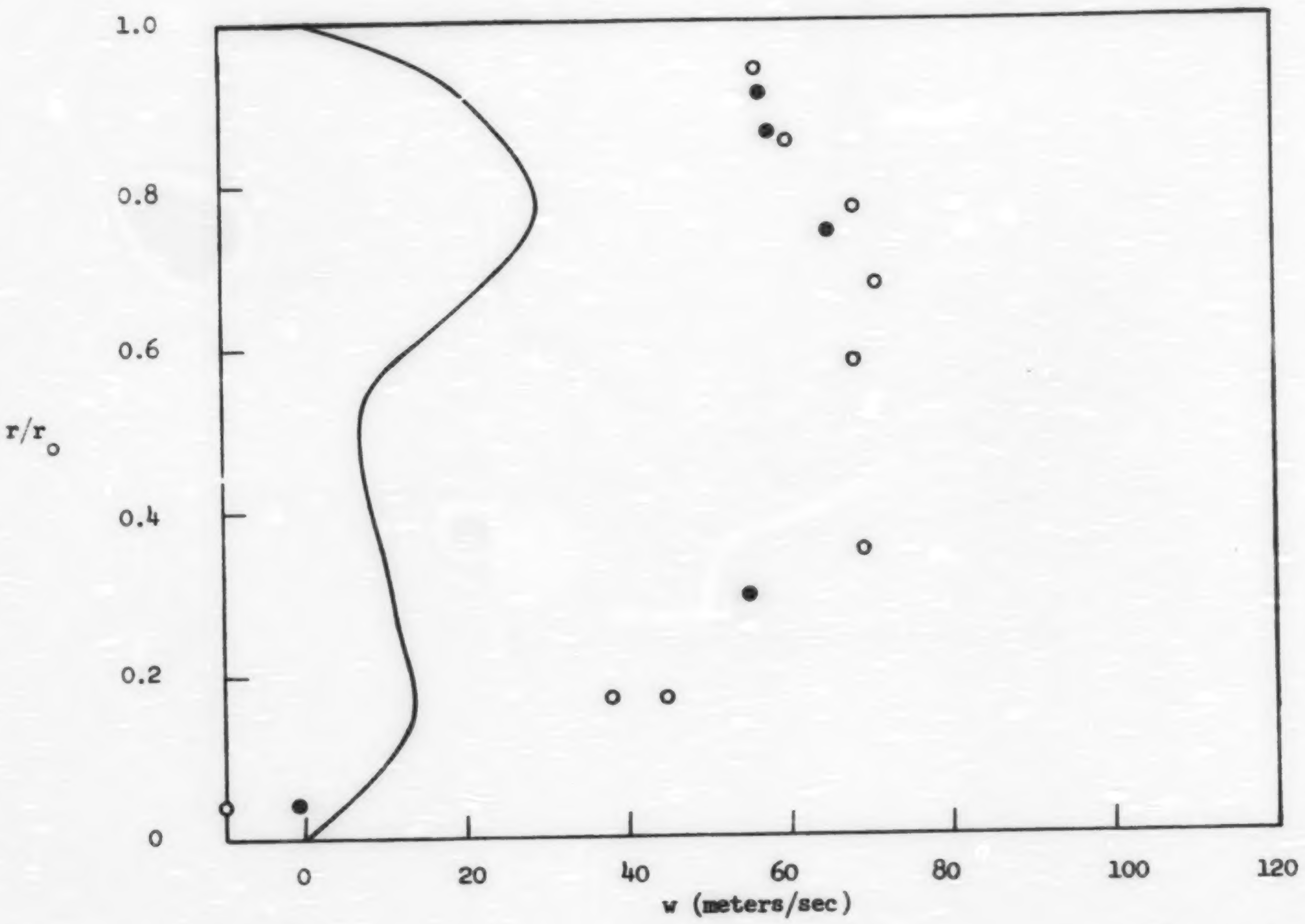

Figure 6. Swirl Velocity Profile at Station x/r_o = 0.97 for Swirl Number = 0.7

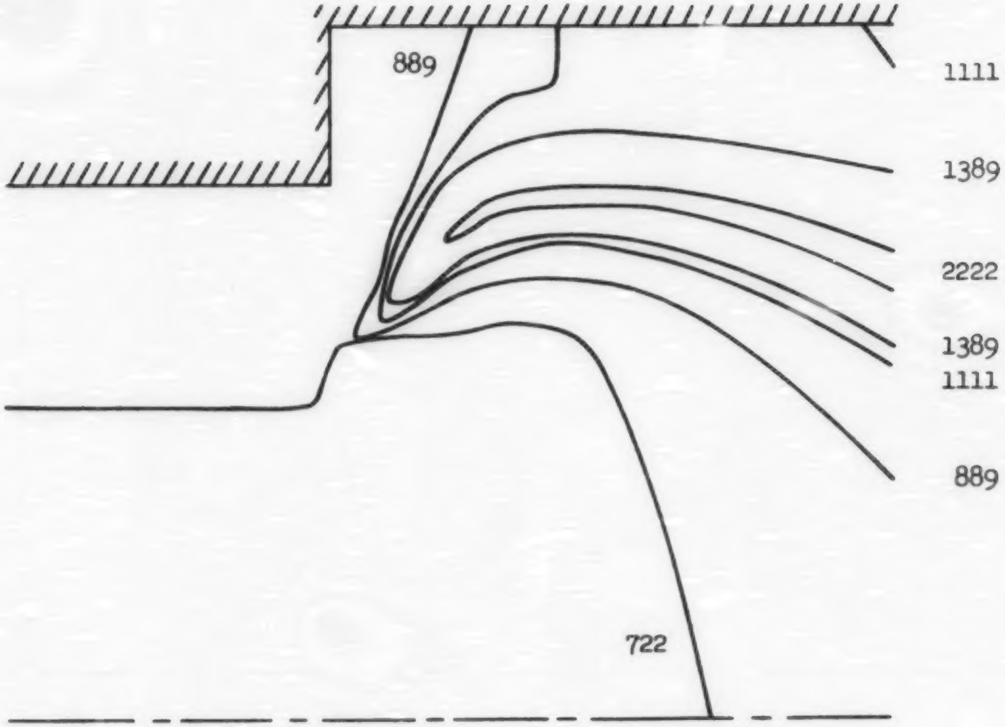

Figure 7. Isotherms °K for the Swirl Number = 0.3 Methane-Air Case

PREMIXED ONE-DIMENSIONAL FLAME (PROF) CODE DEVELOPMENT AND APPLICATION

By:

J. T. Kelly, R. M. Kendall
Acurex Corporation/Aerotherm Division
Mountain View, California 94042

ABSTRACT

The PRemixed One-Dimensional Flame (PROF) code numerically models complex chemistry and diffusion processes in premixed flames. Since the code includes diffusion, realistic solutions of coupled combustion and pollutant formation processes can be obtained in the flame zone, as well as downstream in the post-flame region. Previous experience (Reference 1) has shown that the code can be a valuable aid when analyzing experimentally-found coupled combustion and pollutant formation phenomena such as "PROMPT NO."

The code's accuracy and reliability has now been increased. Also, several models for heat loss to bounding walls have been added to the code to model confined flames, such as those occurring in surface and catalytic combustors. Also, plug and well-stirred reactor options have been added to model combustion and pollutant formation processes in a wide variety of conventional and experimental combustion systems.

Sample calculations are presented to demonstrate the capabilities of the revised PROF code. Also, to illustrate the value of the code in analyzing complex combustion and pollutant formation processes, predictions of NO formation in premixed CH_4/air flames over a wide range of equivalence ratios are presented. These calculations show that the well-known extended Zeldovich mechanism is adequate for stoichiometric and lean conditions, but inadequate under fuel-rich conditions. A possible fuel-rich NO mechanism is then postulated to account for NO formation at equivalence ratios greater than one.

Preceding page blank

INTRODUCTION

Detailed experimental sampling of premixed flat flames have shown that some pollutant formation processes, such as NO formation in fuel-rich hydrocarbon flames, are strongly coupled to combustion processes within the flame zone. The chemical interpretation of data from these flames is usually not clear, since the data is affected by the experimental probe, chemical events are obscured by diffusive processes, and insufficient species concentration data are taken. To help interpret this data, elementary chemical kinetic and diffusion data can be used in comprehensive theoretical flame models to predict species concentrations through flames. These predictions, combined with the experimental data, can provide valuable insights into the complex chemical events taking place within the flame.

The PRemixed One-Dimensional Flame (PROF) code treats combustion and pollutant formation events occuring in premixed flames. Comparing H_2 and CO flame predictions and data (Reference 1) showed that the PROF code is a valuable aid when interpreting and extending flame data. Also, these predictions showed that the PROF code is reliable, quick, and accurate. The need to apply PROF to more complex flames such as CH_4/air with pollutant formation and combustion systems such as catalytic combustors prompted the present study to upgrade and expand the PROF code.

One of the primary objectives in developing the original PROF code was to demonstrate how efficient matrix procedures can be applied to solve flame equations. For this demonstration, the solution procedure was simplified to consider only first order diffusive fluxes, spatially-uniform heat losses, and a mean Lewis number of unity for gas mixtures. Although these simplifying assumptions are acceptable for many flames, in some cases the assumptions give errors. To remedy this situation the PROF code has been upgraded to include:

Preceding page blank

- Higher order species diffusive fluxes
- Flameholder heat losses
- Radiation heat losses
- Nonunity Lewis number effects

Besides the additions, the code has been expanded to model flames with heat losses to reactive or nonreactive bounding walls. Important confined flame problems, such as those in catalytic and surface combustors and tubular reactors can now be treated. In addition, well-stirred and plug flow reactor options have been included in the code so that furnace, gas turbine and other combustion systems can be modeled. With these additions a wide variety of experimental and practical combustion and pollutant formation problems can now be treated with the PROF code.

FORMULATION

The PROF code models the confined flame problem shown schematically below. The code treats both axial and radial transport of heat and mass. The boundary conditions assigned are the state of the gas at the tube wall, the initial bulk species fluxes, and temperature. Given these conditions, the code predicts bulk gas properties along the tube axis.

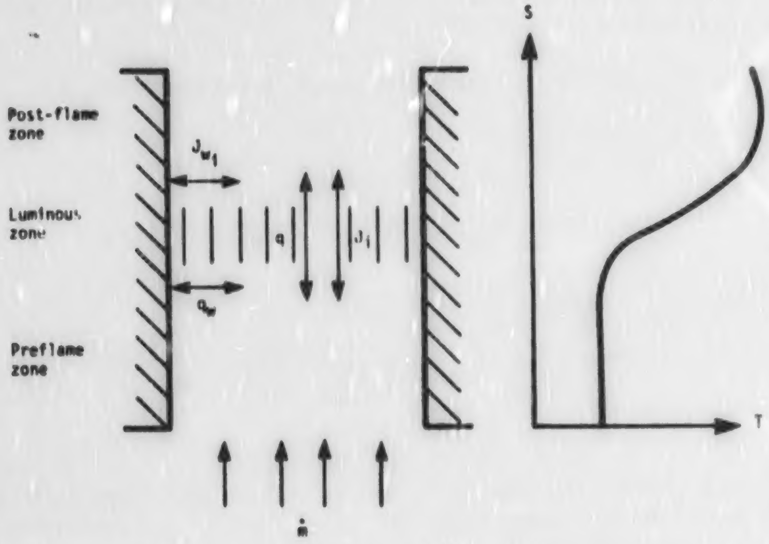

Well-stirred and plug flow reactor problems can also be modeled by the PROF code. These options use the generalized chemistry solution procedure applied in the flame option, but do not consider diffusive species or heat transport between reactor stations.

As described in the following sections, the PROF code solution procedure has been optimized to predict premixed one-dimensional flames. The assumptions and equations used in the development of the PROF code are discussed below. The well stirred and plug flow reactor equations are subsets of the flame equations and will not be discussed herein. The predictor-linearized corrector solution procedure used to solve the flame equations remains essentially unchanged from the original formulation detailed in Reference 1.

FLAME CONSERVATION EQUATIONS

The equations for the flame option are developed by integrating the steady two-dimensional species, mass, and energy equations across a plane perpendicular to the axis. This produces a set of quasi-one-dimensional flame equations in terms of bulk gas properties. These properties vary along the flame axis as a result of fluxes of heat and mass at the radial edge of the flame and chemical reaction and axial diffusive fluxes within the bulk gases. For a large free flame with an initially uniform flow, the edge fluxes are small and the bulk properties are equivalent to local conditions across the flame. For a flame confined in a tube such as in a catalytic combustor, the edge fluxes can be significant. The code treats these fluxes using a transfer coefficient approach in which the fluxes are assumed to be directly proportional to bulk and wall gas states. Using transfer coefficients reduces an essentially two-dimensional problem to one-dimensional form.

The quasi-one-dimensional flame conservation equations can be written as:

Species

$$\dot{m}\frac{dY_i}{ds} = A\,W_i - \frac{d(A\,J_i)}{ds} - C_w J_{w_i} \qquad (1)$$

Energy

$$\dot{m}\frac{dh}{ds} = AQ - \frac{d}{ds}\left(\sum_i AJ_i h_i + Ak\frac{dT}{ds}\right) - C_w q_w \qquad (2)$$

where global continuity has been incorporated into the above equations and the momentum equation has been replaced by assigning a fixed pressure. As shown in Equation (1) the species mass fraction along the flame axis, Y_i, is altered by species bulk gas phase chemical production, W_i; axial diffusive flux, J_i; and wall diffusive flux, J_{w_i}. In the energy equation, the enthalpy, h, along the flame axis is altered by the bulk gas heat loss rate, Q; axial diffusive heat flux, $\sum_i J_i h_i$ + k dT/ds; and wall heat loss, q_w. Expressions for W_i, J_i, J_{w_i}, q, and q_w, and boundary conditions complete the definition of the flame problem.

Species Axial Diffusional Flux

In the PROF code, the simple yet adequate bifuracation approximation for the binary diffusion coefficients is used with the Stefan-Maxwell relations to develop an explicit expression for species flux, J_i. This approximation, developed in Reference 2, assumes that the contributions of species i and j to the diffusion coefficients, $\mathcal{D}_{ij}$, can be separated in the following manner:

$$\mathcal{D}_{ij} = \frac{\bar{D}}{F_i F_j} \tag{3}$$

where $\bar{D}$ is a reference self-diffusion coefficient and F_i and F_j are diffusion factors. The explicit formulation for species flux, J_i, developed using this approximation is:

$$J_i = - \frac{\rho\bar{D}}{\mu_1 F_i}\left(\frac{dY_i}{ds} + \frac{Y_i}{M}\left(\frac{dM}{ds} - F_i \frac{d\mu_2}{ds}\right)\right) \tag{4}$$

where

$$\mu_1 = \sum X_i F_i \quad \text{and} \quad \mu_2 = M \sum Y_i/F_i$$

In Equation (4), $\bar{D}$ is usually taken as the self-diffusion coefficient of a reference species, e.g., O_2. The F_i then are found to be constants independent of temperature and pressure. Computations using this formulation are more efficient than those that use arbitrary expressions for the $\mathcal{D}_{ij}$ and either apply the Stefan-Maxwell implicit equations or develop the concentration-dependent multicomponent diffusion coefficients.

Species Production Terms

Each W_i in the species conservation equation is a summation of contributions from all reactions which include that species. For reactions of the type

$$\sum_i \mu^R_{i_m} B_i \rightleftarrows \sum_i \mu^P_{i_m} B_i$$

where μ are the stoichiometric coefficients on species B_i, W_i can be written as

$$W_i = M_i \sum_m (\mu^P_{i_m} - \mu^R_{i_m}) R_m \tag{5}$$

where

$$R_m = k_{f_m} \left[e^{\Sigma\mu^R_{i_m} \ln p_i} - e^{\Sigma\mu^P_{i_m} \ln p_i - \ln K_{p_m}} \right] \times \sum_i \nu^T_{i_m} p_i \qquad (6)$$

and k_{f_m} has the Arrhenius form

$$k_{f_m} = aT^b \, e^{-(E/RT)} \qquad (7)$$

and $\nu^T_{i_m}$ denotes third body efficiency of species i.

As discussed in Reference 1, solving the species equations, including the above terms, is difficult. In a typical flame problem, reaction rates will range from nearly equilibrated to inactive. A nearly equilibrated reaction will dominate all of the species equations in which it appears, making them very difficult to solve since they are all nearly identical. To solve this set of equations, several species equations must be combined so that the dominating reaction appears in only one equation. This equation is effectively an equilibrium relationship. By rearranging equations, a solution is more easily obtained.

However, even if the equations are rearranged, the iterative Newton-Raphson procedure used to solve them may not work, if the character of the equations has changed significantly. In the PROF kinetics package, a combination of gradual recharacterization of equations and damping has proved highly successful in finding a solution. This is of great importance if an efficient grid-type coupled diffusion/kinetics boundary value solution is to be achieved.

Species Flux at the Wall

The PROF formulation uses an efficient transfer coefficient approach to establish the species flux at the wall. In this approach, the species flux is assumed to be directly proportional to the difference between the bulk and wall gas composition. Since detailed radial distribution of the species concentration need not be known, this formulation remains one-dimensional. For consistency, the wall flux proportionality factor is developed similar to the axial species diffusion, and is written as:

$$J_{w_i} = f \, \frac{\rho\bar{D}}{\mu_l F_i} \, \frac{(Y_i - Y_{w_i})}{r_w} \qquad (8)$$

The scale factor f is included in Equation (8) to bring the effective diffusion coefficient into line with detailed theoretical results for flow in a tube. The value of f depends on the geometry and the state of boundary layer development.

Bulk Gas Volumetric Heat Loss

The term Q in the energy equation is a bulk gas phase volumetric heat source or sink term. If desired, Q can be assigned as a constant or as a function of distance along the flame axis. However, most often Q is the volumetric heat loss due to radiation. The PROF code uses the emission-dominated or optically thin limit approximation to model radiation heat loss. For nonsooting flames of interest, this approximation is reasonable, and is written as:

$$Q = -4K_p \sigma T^4 \tag{9}$$

where K_p is the Planck mean absorption coefficient defined as

$$K_p = \frac{\pi}{\sigma T^4} \int_0^\infty K_\nu B_\nu d\nu \tag{10}$$

The individual Planck mean absorption coefficients, used to construct K_p, are developed from the gas emissivity wide band correlation parameters of Edwards and Balakrishnan (Reference 3). Gas emissivities of the major radiating species, CO_2, H_2O and CO, obtained using this method differ from experimental data by less than 10 percent (Reference 4).

Wall Heat Flux

For nonreactive tube walls, the PROF code formulation treats the wall heat flux by assuming that the heat flux is proportional to the difference between bulk and wall gas temperatures. For the reactive wall, an additional term is included to account for the heat released by chemical reactions which occur between the bulk gas and wall. The general expression for wall heat flux is then:

$$q_w = \frac{f}{r_w} \frac{\rho \bar{D}}{\mu_1} \left[\frac{\tilde{C}_p}{F_T} (T - T_w) + \sum_i \frac{h_{w_i}}{F_i} (Y_i - Y_{w_i}) \right] \tag{11}$$

where f is the same factor as was introduced into the wall species flux expression and F_T is a "mean" Lewis number given by

$$F_T = \frac{\rho \bar{D}}{\mu_1 \frac{k}{\tilde{C}_p}} \tag{12}$$

Specialized Boundary Conditions

For flames in free space, the upstream boundary conditions are the temperature and composition of the unburnt gas and the downstream boundary conditions are negligible diffusion of species and heat. In the laboratory, flames are anchored to their burners with flameholder grids. These grids stabilize the flame by providing a sink for the flame's "excess" heat or reactive species, but they also alter the flame properties. To accurately predict laboratory burner flames, the effects of flameholder processes on flame properties must be included in the code.

One characteristic of flameholders is the absence of heat or reactive species diffusion upstream of the grid. The PROF code now can model this effect by setting the upstream diffusion equal to zero. In addition, the temperature of the gas at the flameholder can be set equal to the measured flameholder temperature. This specification defines the heat loss from the gases to the flameholder surface, and is useful for cases where nonnegligible amounts of heat are lost to a flameholder of known temperature.

Solution of the Finite Difference Form of the Conservation Equations

The species equation (1) is reduced to algebraic form by introducing a normalized distance coordinate, dividing the species concentration equation through by molecular weight, M_i, to obtain concentration per unit mass, α_i, and applying linear finite differencing. The lengthy expression produced is given in Reference 5. The algebraic form of the energy equation can be determined similarly, and is also given in Reference 5. These algebraic equations are solved by a predictor-linearized corrector solution procedure which consists of the following steps:

1. Initial values are selected for α_i, T, h, C_p at all grid points. These may be output from a prior run or may be generated by a linear interpolation between initial and guessed final values.

2. By applying known upstream conditions and the initial guessed values, grid point values for α_i, h, T, etc., are found through matrix solution of the equation set.

3. When the downstream boundary is reached, the no-diffusion boundary condition is applied. (Guessed solution values are not required for this grid point.)

4. Using the derivatives of α_i obtained from chemistry solutions at all grid points, the rate of change of all α_i's with respect to initially guessed α_i's at each grid point are constructed.

5. Assuming the system is linear, corrections to all α_i's are made by applying the derivatives from Step 4.

6. Using the corrected α_i's as new guesses, Steps 2 through 5 are repeated until the guessed α_i equals the corrected α_i.

Although solutions have been found without using Step 5, the corrector step can reduce the number of iterations by factors of 2 to 10. Since Step 5 takes only 10 to 15 percent of the total computation time, it is a very effective method for reducing total computer time. The corrector step also allows the flame speed to be predicted by applying constraints on the grid variables. The flame speed, or mass flow rate, $\dot{m}$, is obtained by assigning a concentration between the inlet and final equilibrium value to a species at a grid point away from the inlet. This value may be assigned to any stable species which monotonically increases or decreases through the flame.

APPLICATIONS

The PROF code can predict confined flames, as shown in the sample calculations of CH_4/air flames in nonreactive and reactive tubes. In addition, the PROF code can be applied to complex coupled combustion and pollutant formation problems, as shown below in predictions of NO pollutant formation in CH_4/air free flames over a wide range of equivalence ratios.

CONFINED FLAME PREDICTIONS

To demonstrate the PROF confined flame predictive capability, calculations of flame quench in nonreactive tubes and flame phenomena in reactive wall catalytic combustors are presented.

Nonreactive Wall Heat Loss

To demonstrate the PROF nonreactive wall heat loss model, stationary CH_4/air flames in small diameter tubes are predicted and compared with experimental data. The flow velocity necessary to maintain stationary CH_4 flames in small diameter tubes is a function of tube diameter. It is commonly believed that the primary process governing flame velocity in tubes is conductive heat loss from the flame to the tube walls. Wall chemical kinetics, radiant heat exchange and buoyancy induced convection effects are secondary to this heat loss for methane flames in small diameter tubes. Therefore, the PROF option for nonreactive wall heat loss is applied to model stationary flames in small diameter tubes. PROF flowrate predictions and methane flame quench and propagation data and natural gas incipient flame flashback data are compared in Figure 1. Predictions and quench data were for a 9.5 percent methane air mixture at 1 atmosphere pressure.

To model CH_4 combustion 15 species (CH_4, O_2, N_2, CH_2, CH_2O, CO, CO_2, H_2O, H_2, CHO, H, HO, O, HO_2, CH) and 37 reactions were specified in the code. (The reactions and their associated rates are given in Table I.) When applied to freely propagating flames this mechanism gives reasonable flame speeds. Figure 1 shows the good agreement between the predicted and measured flame quench diameter (i.e., the zero flowrate tube diameter). Some agreement is also found between the predicted and measured natural gas and methane flame flowrate versus tube diameter values. However, these latter comparisons are not strictly valid since the natural gas mixture is not equivalent to methane in composition. In addition, propagating methane flames are not equivalent (in terms of tube heat loss) to stationary methane flames. However, the predictions and data show the same trends, and the agreement at the quench point shows that the PROF nonreactive wall heat loss model is adequate.

Reactive Wall Heat Loss

Predictions of flame phenomena in catalytic combustors are presented below to demonstrate the PROF reactive wall heat loss or gain model. These predictions also illustrate the importance of "flame" type phenomena in these combustors.

The catalytic combustor used for this prediction consists of a 3.66-inch diameter cylindrical block of ceramic material. Within this cylinder, 2300 circular channels 0.06 inch in diameter have been constructed. The interior surface of these channels are coated with a catalyst material which helps convert fuel and air to product molecules. The rate of this conversion depends on the flowrate of gases through the channels, the surface area of the channels, the reactivity of the catalyst, and the length of the catalytic combustor.

Catalytic combustor experiments have shown that under certain conditions, fuel concentration is rapidly reduced beyond that expected on the basis of wall reactions. These rapid reductions abruptly disappear once the bed flow velocity is increased above a limiting value. The abruptness of the reductions, coupled with the short length over which they occur indicates that a "flame"-type phenomena is responsible for reducing the fuel concentrations.

To demonstrate the "flame" phenomena in catalytic combustors, several PROF calculations were carried out. A 200 percent theoretical air CH_4/air mixture at 540°K was assigned as the initial gas condition. The wall condition was assumed to be the equilibrium composition of the inlet mixture at the adiabatic flame temperature. This condition is reasonable for the low flowrate (3.25 gm/sec) specified. Predictions were made for flows without axial diffusion, but with gas phase chemical reaction; with axial diffusion, but without gas phase chemical reaction; and with both axial diffusion and gas phase chemical reaction.

As the predicted fuel concentration decay rates in Figure 2 show, both axial diffusion and gas phase chemical reaction must be included in the modeling to predict a rapid "flame" like reduction in fuel concentration. If either of these effects is not included, the decay is solely due to wall reactions and a much longer bed length is required to reduce fuel concentrations to very low levels.

The "flame" type phenomena is also shown in Figure 3, where including both axial diffusion and gas phase chemical reaction causes a rapid rise in gas temperature at roughly the 1.5 cm station. Examining the detailed output for the "flame" case shows that surface reactions, prior to the "flame" region, preheat the gases causing a "light off" of the gas phase reactions. This phenomenon is flame-like since it is characterized by a rapid decay in the fuel concentration, a rise in radical (O, H, OH) concentrations, peaks in H_2 and CO concentrations, and decay of CO and H_2 to product molecules, CO_2 and H_2O.

Since the surface reactions are important in preheating the gas to sustain the flame, varying the tube diameter (which alters the wall heat and mass transfer effect) may change the "light off" length. A series of PROF calculations has shown that the "light off" length does change with tube diameter for all other parameters fixed. These results indicate that the tube diameter can be varied to reduce the overall length of the catalytic combustor. Besides determining how "flame" characteristics vary with tube diameter, the PROF code also can be used to assess the impact of initial mixture composition, preheat, and tube geometry on "flame" phenomena.

METHANE FLAME COMBUSTION AND NO POLLUTANT FORMATION CHARACTERISTICS

PROF predictions of low pressure CH_4/O_2 flame species concentrations are compared with detailed measurements to demonstrate that the formulation and the CH_4 chemical combustion mechanism and transport data used in the calculations are adequate. This combustion mechanism and the well-known extended Zeldovich NO mechanism is then applied to atmospheric pressure CH_4/air flames in an attempt to predict NO pollutant formation over a wide range of equivalence ratios. Comparing predictions and data, the Zeldovich mechanism is found to be adequate for lean and stoichiometric flames, but inadequate for fuel-rich flames. An alternate chemical mechanism is then suggested which can account for NO production in fuel-rich CH_4/air flames.

Verification of CH_4 Chemical Combustion Mechanism

Reliable predictions of coupled combustion and pollutant formation processes in CH_4 flames requires specification of adequate chemical combustion mechanisms. For this study, 13 species (CH_4, O_2, CH_2, CHO, CH_2O, CO, O, OH, H, H_2O, CO_2, HO_2, H_2) and 28 reactions were used in PROF to model CH_4/O_2 combustion. The reactions and their associated rates are given in Table II. To verify this mechanism and the transport data input into the code, predictions of low pressure CH_4/O_2 flames employing this mechanism are compared with the extensive data of Peeters and Mahnen (Reference 8).

The data of Peeters and Mahnen is an important basis of comparison, since in this data 12 stable and unstable species concentrations and temperature are available for comparison with predictions as a function of position through the flame. Also, comparison of predictions and this data are straightforward, since the experimental conditions under which the data was taken gives accurate spatial resolution of flame properties and minimal impact of flameholder on flame properties.

PROF predictions are favorably compared with the detailed species and temperature data of Peeters and Mahnen in Figures 4 through 7. The pressure for this flame was 0.053 atmosphere and the initial temperature was 298°K. Initial concentrations of CH_4 and O_2 were 0.095 and 0.905, respectively. The comparisons in Figures 4 through 7 show that temperature and CH_4, CO_2, H_2O, O_2, CO, CH_2O, H_2, OH, O and H concentrations are adequately predicted throughout the flame, but CH_3 and HO_2 predictions are higher than the experimental data. This poor agreement indicates that some uncertainty still remains in the CH_4 combustion mechanism. Nevertheless, considering experimental errors and the uncertainty of rate data, the combustion mechanism is adequate.

The PROF code was then used to predict atmospheric pressure CH_4/air flames as a function of equivalence ratio, and the predicted flame speeds were compared with data (Reference 9) in Figure 8. Agreement of flame speed using this chemical mechanism is good for lean and stoichiometric flames. However, for fuel-rich flames ($\Phi > 1.15$), predicted flame speeds are higher than measured values.

As noted in Reference 10, predicted flame speed varies with the maximum level of radical ([OH], [H]) concentrations in the flame for flames at various pressures and fixed composition, as well as those at fixed pressure and variable composition. Using the predicted flame speeds and maximum radical concentrations ([OH], [H]), from Reference 10, it has been shown in Reference 5 that flame speed is roughly proportional to maximum radical concentrations ([OH], [H]) in the flame. Furthermore, the proportionality of flame speed to maximum H atom concentration has been experimentally observed (Reference 11) and theoretically demonstrated (Reference 1) for fuel-rich H_2/air flames. These results indicate that the CH_4 chemical combustion mechanism given in Table II probably generates excess of H radicals under fuel-rich ($\Phi > 1.15$) conditions.

To check this conjecture, a reaction which depleted H atoms by recombining them with CH_3 was input into the code along with the reaction set given in Table II. Predicted maximum H atom concentrations and flame speed were reduced considerably. Figure 8 compares the flame speeds achieved by the revised mechanism with data at equivalence ratios of 1.05, 1.15 and 1.3. These results demonstrate the relationship between radical concentrations and flame speeds. At an equivalence ratio of 1.3, the baseline chemical mechanism given in Table II will overpredict H atom concentrations by as much as 15 percent. This conclusion will be important in subsequent discussions of NO pollutant formation in fuel-rich flames. At lower equivalence ratios, the mechanism in Table II should be accurate.

NO Pollutant Formation in CH_4 Flames

The formation of NO in combustion systems is typically assumed to occur at a much slower rate than the rate of combustion. Predictions of NO concentrations can be made by applying the Zeldovich mechanism:

$$N_2 + O \rightarrow NO + N$$

$$N + O_2 \rightarrow NO + O$$

where O and O_2 concentrations are determined by assuming all of the combustion products are in equilibrium. For fuel-rich conditions, this NO mechanism is usually augmented by the reaction:

$$N + OH \rightarrow NO + H$$

with OH determined through the assumption of equilibrium combustion products. NO predictions using this approach fall short of measured values for many premixed flame cases, particularly for fuel-rich hydrocarbon/air combustion.

Experimentally, it has been found that within and near the flame zone, the NO formation rate is much greater than downstream measurements and predictions. This rapid NO formation near the flame zone has been termed "PROMPT NO" by Fenimore (Reference 12). This "PROMPT NO" accounts for most of the differences between measurements and predictions. Recently, several studies (References 1, 13, 14, 15, 16) have shown that the extended Zeldovich mechanism can treat flame zone or "PROMPT NO" in many flame systems if actual nonequilibrium concentrations of O, OH and H radicals are used instead of post-flame equilibrium values. NO produced by the Zeldovich mechanism is increased significantly by this "nonequilibrium radical" approach, since radical concentrations are typically far in excess of calculated equilibrium values in the flame zone. These results show that accurate predictions of premixed flame NO concentrations require a coupled approach, which includes both a combustion mechanism to model the radical concentrations and a pollutant formation mechanism to determine NO concentrations.

Several approaches can be used for coupling NO formation and combustion. In Reference 15 a partial equilibrium approach was used to determine the radical concentrations in premixed CH_4/air flames. These radical concentrations were then applied in the Zeldovich NO mechanism to predict NO concentrations in 1 atmosphere, CH_4/air flames at 0.89, 1.05 and 1.15 equivalence ratios.

Good agreement was found between the NO levels predicted and data at equivalence ratios of 0.89 and 1.05. However, at the highest equivalence ratio, 1.15, the measured rates of NO production did not match those predicted. For this case, the data indicated a sharp peak and a rapid fall off in NO production rates through the flame, whereas predictions showed a lower peak and a sustained high rate through the flame. The authors suggested a number of reasons for the lack of agreement. However, it was clear that under fuel-rich conditions, the Zeldovich mechanism may not account for all of the NO formation.

In Reference 16, a straightforward coupled approach, which includes both combustion and pollutant formation chemical kinetic mechanisms, was used to determine NO formation in atmospheric pressure CH_4 combustion.* The detailed CH_4 chemical combustion scheme of Bowman (Reference 13) was combined with the extended Zeldovich mechanism to determine NO formation over a range of equivalence ratios. The predictions qualitatively had the same NO formation behavior as was observed in Reference 15. However, the important flame initiating processes of diffusive heat and mass transport were not treated in these calculations. This necessitated the assignment of arbitrarily and artificially high initial temperatures in the calculations to initiate combustion. Therefore, this approach can only provide qualitative information on flame zone processes where diffusion is significant and most of the "PROMPT NO" is formed.

The uncertainties in partial equilibrium and nondiffusive approaches prevent one from concluding whether the Zeldovich NO formation mechanism is adequate or inadequate for premixed CH_4/air flames. However, using the PROF code, which can treat coupled chemistry as well as diffusion, removes these uncertainties and clearly demonstrates the limitations and range of applicability of the Zeldovich mechanism.

---

*The use of the term flame was avoided in Reference 16 since the important flame processes of diffusion were not included in the calculations.

PROF predictions of atmospheric pressure CH_4/air premixed flames were carried out and compared with data over a wide range of equivalence ratios. The extended Zeldovich NO formation reactions used in the calculations, and their associated rates are:

$$OH + N \rightarrow H + NO \qquad k_f = 4.00 \times 10^{13}\ T^{0.5}$$

$$N + O_2 \rightarrow NO + O \qquad k_f = 6.50 \times 10^{9}\ T\ e^{\frac{-6,300}{RT}}$$

$$O + N_2 \rightarrow N + NO \qquad k_f = 1.4. \times 10^{14}\ e^{\frac{-75,200}{RT}}$$

The combustion mechanism and transport data applied in the NO predictions are identical to those used to calculate low pressure CH_4/O_2 flames. The reactions and their rates are given in Table II. An initial temperature of 298°K was assumed for the reactants and predictions were made for equivalence ratios of 0.7, 0.89, 0.952, 1.05, 1.15 and 1.3. Figure 9 presents NO concentrations for the various equivalence ratios as a function of time through the flame.

These results show that, as the equivalence ratio increases from 0.7 to 0.952, the NO concentration rises from a negligible value to a maximum. Further increases of equivalence ratio decrease NO until at an equivalence ratio of 1.3 very low levels of NO are predicted. For lean and near stoichiometric equivalence ratios, this behavior is in qualitative agreement with the data in Reference 15.

At equivalence ratios of 0.89 and 1.05, peak NO production rates obtained from the detailed computer printout are in good quantitative agreement with peak rates derived from the data in Reference 15. At an equivalence ratio of 1.15, the predicted post-flame zone formation of NO appears to be qualitatively correct. However, the rapid increase of NO within the flame zone, observed in Reference 15 is not found in the predictions.

Comparison of the maximum predicted and measured peak NO formation rates indicates that the Zeldovich mechanism is significantly underpredicting NO formation within the flame zone under fuel-rich conditions. This is clearly demonstrated in Figure 10 where predicted flame zone NO concentrations are compared to "PROMPT NO" values taken from Reference 10. The experimental levels of "PROMPT NO" (equivalent to flame zone NO) were determined by extrapolating post-flame NO concentrations back to the burner face and using the nonzero intercept value. In the predictions, the flame zone was defined as the post-CH_4 depletion and radical peak region. This roughly corresponds with the 2-msec time in Figure 9 for all of the equivalence ratios investigated.

The comparison of predictions and data in Figure 10 shows that "PROMPT NO" is adequately treated by the coupled nonequilibrium radical and Zeldovich NO mechanism for equivalence ratios up to 1.05. Above 1.05, the predictions fall rapidly to zero ($\Phi \approx 1.3$) whereas measurements indicate a rise up to an equivalence ratio of 1.4, followed by a decrease to very low levels at an equivalence ratio of about 1.6.

As discussed previously, considerable care was taken in developing a combustion mechanism which generates accurate levels of radical concentrations through the flame. Comparisons of predictions and flame speed data indicated that radical concentrations were adequately predicted for equivalence ratios up to 1.15. At an equivalence ratio of 1.3, it was estimated that the radical concentration was probably high by 15 percent. Therefore, at equivalence ratios greater than 1.05, the Zeldovich mechanism cannot account for measured "PROMPT NO," even when the correct or even enhanced radical concentrations are used in the NO reactions. For equivalence ratios lower than 1.05, the Zeldovich mechanism can account for "PROMPT NO" if radical concentrations are properly evaluated.

Having shown that the Zeldovich NO mechanism is inadequate in fuel-rich flames, an alternate mechanism was sought to account for "PROMPT NO" in these flames. Fenimore (Reference 12) and Iverach, et al. (Reference 17), experimentally measured hydrocarbon flames, and concluded that the "PROMPT NO" formed under fuel-rich conditions results from energetic hydrocarbon fuel fragment molecules reacting with molecular nitrogen. Reactions such as:

$$CH + N_2 \rightarrow HCN + N$$

$$C + N_2 \rightarrow CN + N$$

were thought to produce N atoms that would react with OH via the extended Zeldovich mechanism to form NO. The unique presence of significant fuel-rich "PROMPT NO" in hydrocarbon flames and the excessively high O atom radical concentration required to produce this NO by the Zeldovich mechanism reinforced the above author's hydrocarbon fragment hypothesis.

Recently, several experimental and theoretical studies have added more evidence to support the hydrocarbon fragment theory. In References 18 through 21, HCN was found in significant quantities (>10 ppm) near the reaction zone of fuel-rich hydrocarbon flames. Also, References 19 through 21 showed that NO rapidly forms within the flame zone as HCN decays. In Reference 19, data indicated that about 90 percent of "PROMPT NO" can be formed by way of HCN. Theoretical studies of CH_4 combustion (Reference 22) in jet-stirred reactors demonstrated that fuel-rich NO can be accounted for if HCN is included as an intermediate in the NO formation mechanism.

The fuel-rich NO mechanism applied in this study consists of:

- CH, CH_2 hydrocarbon fuel fragment attack on molecular nitrogen
- Formation of atomic nitrogen or nitrogen bearing intermediates (HCN, CN, NCO, NH_i)

- Oxidation of atomic nitrogen or nitrogen-bearing intermediates to NO

- Alternate reaction paths for NO back to N_2 or HCN

This mechanism may be schematized as:

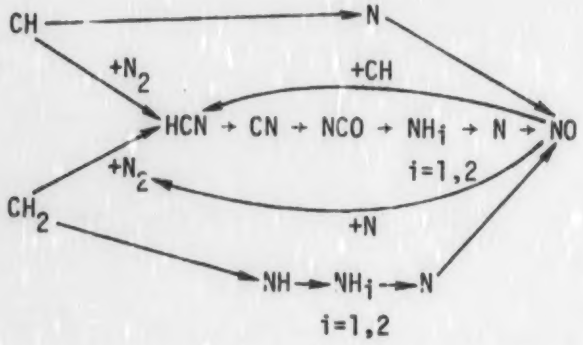

The reactions assumed to take place between these species are listed in Table III. Although additional nitrogen-bearing species and many other reactions can be included in this mechanism, the mechanism is plausible and includes enough reaction steps to account for the observed phenomena. However, considering the limited amount of data and the uncertainty of key reaction rates, other mechanisms, which were not examined in this study, also might be able to account for the data.

Flame speed and "PROMPT NO" levels predicted by the fuel-rich mechanism at 1 atmosphere pressure are compared with experimental data in Figures 8 and 10. As shown in Figure 8, predicted flame speeds and data agree at equivalence ratios greater than or equal to 1.3. Below 1.3 the predictions fall below data. These comparisons show that the chemical combustion mechanism, which includes NO pollutant formation, is reasonable under fuel-rich conditions.

In Figure 10, prompt NO predictions, over a wide range of equivalence ratios, show the same trend as experimental data. Predictions fall somewhat higher than data. However, this lack of agreement is not critical, since there are considerable uncertainties inherent in defining experimental "PROMPT NO." At an equivalence ratio of 1.15, the calculated maximum rate of NO production closely agrees with the experimental value found in Reference 15.

Examining the calculations in detail shows that the fuel-rich mechanism reduces to the Zeldovich mechanism at equivalence ratios less than 1.05. At equivalence ratios above or equal to 1.3:

- Total NO production rate decreases due to the reaction steps

$$N + NO \rightarrow N_2 + O$$

$$NO + CH \rightarrow HCN + O \quad \text{or} \quad CHO + N$$

- The species sets HCN and CN, and NH_2, NH and N become equilibrated through reactions such as

$$HCN + H \rightleftarrows CN + H_2$$

$$NH + H \rightleftarrows N + H_2$$

$$NH_2 + H \rightleftarrows NH + H_2 \quad \text{etc.}$$

- Significant NH_i is produced within the flame and remains downstream of the flame

It is also noted that HCN decays rapidly at equivalence ratios of 1.15 and 1.3, but much slower at equivalence ratios greater than or equal to 1.5. At these higher ratios, significant concentrations (~20 ppm) of HCN remain downstream of the flames.

In summary, the hypothesized fuel-rich mechanism used in this study can account for "PROMPT NO" over a wide range of equivalence ratios, whereas the Zeldovich mechanism by itself is inadequate at ratios equal to or greater than 1.15. However, firm conclusions on the applicability of this mechanism to flames require further comparison between predictions and detailed data at a variety of conditions.

CONCLUSIONS

Predictions of confined flame and plug-flow reactor properties have shown that the upgraded and expanded PROF code is versatile, reliable, quick and accurate. By comparing extensive CH_4/O_2 flame data (Reference 8) and PROF predictions, an adequate chemical combustion model for CH_4 has been developed.

When coupled to a chemical kinetic combustion mechanism, the Zeldovich NO formation mechanism is adequate for predicting CH_4/air flame zone "NO" formation at near-stoichiometric and lean conditions. However, under fuel-rich conditions (Φ >1.05), the Zeldovich mechanism significantly under-predicts CH_4/air flame zone, or "PROMPT NO," formation.

A "hydrocarbon fuel fragment" chemical mechanism can account for "PROMPT NO" in fuel rich CH_4/air flames, as demonstrated by comparing predictions and data. The mechanism considered HCN as an intermediate, with N and NH molecules also being produced. Most of these nitrogen-containing species were then oxidized to NO or converted back into N_2.

LIST OF SYMBOLS

A	cross sectional area
B_ν	monochromatic radiation intensity
C_p	specific heat
C_w	circumference of bounding tube
D_{ij}	binary diffusion coefficient
$\overline{D}$	diffusion constant defined by Equation (3)
E	activation energy for kinetic reaction
f	scale factor on radial heat and mass transport terms
F_i	diffusion factor of species i
h	enthalpy of bulk gas
i	denotes species when used as subscript
J_i	flux of species i in axial direction
J_{w_i}	flux of species i at bounding tube wall
k	thermal conductivity of bulk gas
K_ν	spectral absorption coefficient
K_p	Planck mean absorption coefficient

LIST OF SYMBOLS Continued

K_{p_m}	equilibrium constant for reaction m
$\dot{m}$	mass rate of gas
M	molecular weight
p	pressure
q	axial heat transport
q_w	heat transport at the bounding tube wall
Q	volumetric heat loss
r_w	radius of bounding tube
R	gas constant
S	distance along flame axis
T	temperature
W_i	chemical production rate of species i
X_i	mole fraction of species i
Y_i	mass fraction of species i
α_i	species concentrations in moles per unit mass
$\nu_{i_m}^T$	third body efficiency of species i in reaction m
ρ	density
σ	Stefan-Boltzmann constant

LIST OF SYMBOLS Concluded

Superscripts

P	reaction products
R	reaction reactants

REFERENCES

1. Kendall, R. M. and Kelly, J. T., "Premixed One-Dimensional Flame Code (PROF) — Its Formulation, Manipulation, and Evaluation," Aerotherm Report TR-75-158, July 1975.

2. Bartlett, E. P., Kendall, R. M., and Rindal, R. A., "A Unified Approximation for Mixture Transport Properties for Multicomponent Boundary Layer Applications," Aerotherm Final Report 66-7, Part IV (also NASA CR-1063), March 14, 1967.

3. Edwards, D. K. and Balakrishnan, A., "Thermal Radiation by Combustion Gases," Int. J. Heat and Mass Transfer, Vol. 16, 1973, pp. 221-230.

4. Hottel, H. C. and Sarofim, A. F., Radiative Transfer, McGraw-Hill Book Company, New York, 1967, pp. 229-236.

5. Kelly, J. T. and Kendall, R. M., "Further Development of the Premixed One-Dimensional Flame (PROF) Code," Aerotherm Final Report 76-229, August 1976.

6. Singer, J. M. and von Elbe, G., "Flame Propagation in Cylindrical Tubes Near the Quenching Limit," Sixth Symposium (International) on Combustion, Reinhold Publishing Corporation, New York, 1957, pp. 127-130.

7. Lewis, B. and von Elbe, G., Combustion, Flames and Explosions of Gases, Academic Press, Inc., New York, 1961.

8. Peeters, J. and Mahnen, G., "Reaction Mechanisms and Rate Constants of Elementary Steps in Methane-Oxygen Flames," Fourteenth Symposium (International) on Combustion, The Combustion Institute, Pittsburgh, Pennsylvania, 1973, p. 133.

9. Andrews, G. E. and Bradley, D., "The Burning Velocity of Methane Air Mixtures," Combustion and Flame, Vol. 19, 1972, pp. 275-288.

10. Smoot, L. D., Hecker, W. C., and Williams, G. A., "Prediction of Propagating Methane Air Flames," Combustion and Flame, Vol. 26, No. 3, June 1976, pp. 323-342.

11. Padley, P. J. and Sugden, T. M., "Chemiluminescence and Radical Recombination in Hydrogen Flames," Seventh Symposium (International) on Combustion, Butterworths, London, 1959, p. 235.

12. Fenimore, C. P., "Formation of Nitric Oxide in Premixed Hydrocarbon Flames," Thirteenth Symposium (International) on Combustion, The Combustion Institute, 1971, p. 373.

13. Bowman, C. T., "Kinetics of Nitric Oxide Formation in Combustion Processes," Fourteenth Symposium (International) on Combustion, The Combustion Institute, 1973, p. 729.

14. Homer, J. B. and Sutton, M. W., "Nitric Oxide Formation and Radical Overshoot in Premixed Hydrogen Flames," Combustion and Flame, Vol. 20, 1973, pp. 71-76.

15. Sarofim, A. F. and Pohl, J. H., "Kinetics of Nitric Oxide Formation in Premixed Laminar Flames," Fourteenth Symposium (International) on Combustion, The Combustion Institute, 1973, p. 739.

16. Ay, J. M. and Sichel, M., "Theoretical Analysis of NO Formation Near the Primary Reaction Zone in Methane Combustion," Combustion and Flame, Vol. 26, No. 1, February 1976, pp. 1-17.

17. Iverach, D., Kirov, M. Y., and Haynes, B. S., "The Formation of Nitric Oxide in Fuel-Rich Flames," Combustion, Science and Technology, Vol. 8, 1973, p. 159.

18. Bachmaier, F., Eberius, K. H., and Just, T., "The Formation of Nitric Oxide and the Detection of HCN in Premixed Hydrocarbon-Air Flames at One Atmosphere," Combustion, Science and Technology, Vol. 7, 1973, p. 77.

19. DeSoete, G. G., "Overall Reaction Rates of NO and N_2 Formation From Fuel Nitrogen," Fifteenth Symposium (International) on Combustion, The Combustion Institute, Pittsburgh, Pennsylvania, 1975, p. 1103.

20. Kahn, D., "Low Pressure Flat-Flame Burner Studies," presentation made at U.S. Environmental Protection Agency Contractor's Meeting on Fundamental Combustion Research, Boston, Massachusetts, August 11-13, 1976

21. Haynes, B. S., Iverach, D., and Kirov, N. Y., "The Behavior of Nitrogen Species in Fuel-Rich Hydrocarbon Flames," Fifteenth Symposium (International) on Combustion, The Combustion Institute, 1975, p. 1103.

22. Waldman, C. H., Wilson, R. P., and Maloney, K. L., "Kinetic Mechanism of Methane/Air Combustion with Pollutant Formation," Environmental Protection Technology Series, EPA-650-/2-74-045, June 1974.

TABLE I. CH_4 CHEMICAL COMBUSTION REACTIONS AND RATES

	REACTION					PRE EXP FACTOR	TEMP EXP	ACTIVATION ENERGY
1.	37							
2.	CH4	O		CH3	HO	1.00+10	1.0	8.00
3.	CH4	H		CH3	H2	5.00+10	1.	10.0
4.	CH4	HO		CH3	H2O	3.00+13	0.0	5.00
5.	CH4		M	CH3	H	2.00+17	0.	88.
6.	CH3	HO2		CH4	O2	1.00+11	.5	6.0
7.	CH3	H		CH2	H2	2.00+11	.7	3.0
8.	CH3	HO		CH2	H2O	6.00+10	.7	2.0
9.	CH3	O		CH2O	H	2.00+12	.5	-.30
10.	CH3	O2		CH2O	HO	3.00+13	0.0	30.
11.	CH2O		M	CO	H2	1.00+12	1.0	65.
12.	CH2O	HO		CHO	H2O	3.00+09	1.0	1.0
13.	CH2O	H		CHO	H2	1.25+10	1.0	3.2
14.	CH2O	O		CHO	HO	2.00+11	1.	4.40
15.	CHO	H		CO	H2	3.00+10	1.0	0.0
16.	CHO	O2		CO	HO2	8.00+12	.0	0.0
17.	CHO	CH3		CH2	CH2O	1.50+11	.7	4.0
18.	CHO	CH4		CH2O	CH3	8.00+11	.6	9.0
19.	CHO	HO		CO	H2O	3.00+10	1.	0.00
20.	CHO	O		CO	HO	3.00+11	1.	0.50
21.	CHO		M	CO	H	2.50+20	-1.5	16.8
22.	CH2	O2		CH2O	O	5.00+11	.5	7.0
23.	CO	HO2		CO2	HO	1.00+12	.0	12.
24.	CO2	H2		CO	H2O	1.00+09	.5	15.
25.	CO2		M	CO	O	1.00+15	0.0	100.
26.	CO	HO		CO2	H	4.00+09	.5	.0
27.	H	O2	M	HO2		1.50+15		1.0
28.	H	HO		H2	O	8.00+09	1.	7.00
29.	HO	H2		H	H2O	2.50+13	0.0	5.20
30.	HO	O		H	O2	2.50+13	0.0	0.0
31.	HO	HO		H2O	O	6.00+12	0.0	1.0
32.	H2O		M	HO	H	3.00+15	0.0	105.
33.	H	O	M	HO		8.00+15	0.0	0.0
34.	H	HO2		HO	HO	2.50+14		1.9
35.	HO2	O		HO	O2	5.00+13	0.0	1.0
36.	H	HO2		H2	O2	2.50+13	0.0	.70
37.	O2		M	O	O	2.50+19	-1.	118.7
38.	H2		M	H	H	2.00+14	0.0	96.

TABLE II. CH_4 COMBUSTION CHEMICAL REACTIONS AND RATES.

KINETIC REACTION DATA

NUMBER OF REACTIONS= 28

R	REACTION	PRE EXP FACTOR	TEMP EXP	ACTIVATION ENERGY	INDIVIDUAL THIRD BODY EFFIC.		
1	CH4 +OH + --> CH3 +H2O	.1000+14	.000	6.0000		.000	.000
2	CH4 +H + --> CH3 +H2	.2000+15	.000	11.9000		.000	.000
3	CH4 +O + --> CH3 +OH	.2000+14	.000	6.9000		.000	.000
4	CH3 +O + --> CH2O+H	.3500+14	.000	3.3000		.000	.000
5	CH3 +O2 + --> CH2O+OH	.1000+13	.000	15.0000		.000	.000
6	CH2O+ +M --> CO +H2	.2000+17	.000	35.0000		.000	.000
7	CH2O+OH + --> CHO +H2O	.2500+14	.000	1.0000		.000	.000
8	CH2O+O + --> CHO +OH	.3000+14	.000	.0000		.000	.000
9	CH2O+H + --> CHO +H2	.1700+14	.000	3.0000		.000	.000
10	CHO +O2 + --> CO +HO2	.3000+14	.000	.0000		.000	.000
11	CHO +OH + --> CO +H2O	.1000+15	.000	.0000		.000	.000
12	CHO +O + --> CO +OH	.5400+12	.500	.0000		.000	.000
13	CHO + +M --> CO +H	.2000+13	.500	28.8000		.000	.000
14	CO +OH + --> CO2 +H	.5500+12	.000	1.0800		.000	.000
15	CO +O +M --> CO2 +	.3600+19	-1.000	2.5000		.000	.000
16	HO2 +O + --> O2 +OH	.2500+14	.000	.0000		.000	.000
17	HO2 +OH + --> O2 +H2O	.2500+14	.000	.0000		.000	.000
18	HO2 +H + --> OH +OH	.2500+15	.000	2.0000		.000	.000
19	HO2 +H + --> O2 +H2	.2500+14	.000	.0000		.000	.000
20	H +O2 +M --> HO2 +	.2000+16	.000	.8700	H2O	20.000	.000
21	H +O2 + --> OH +O	.2200+15	.000	16.8000		.000	.000
22	O +H2 + --> OH +H	.1700+14	.000	9.4600		.000	.000
23	OH +H2 + --> H2O +H	.2200+14	.000	5.2000		.000	.000
24	OH +OH + --> H2O +O	.6000+13	.000	.7800		.000	.000
25	H +OH +M --> H2O +	.7000+20	-1.000	.0000		.000	.000
26	O +H +M --> OH +	.4000+19	-1.000	.0000		.000	.000
27	H +H +M --> H2 +	.2000+20	-1.000	.0000		.000	.000
28	O +O +M --> O2 +	.4000+19	-1.000	.0000		.000	.000

TABLE III. FUEL RICH CH_4 COMBUSTION AND NO FORMATION REACTIONS.

NUMBER OF REACTIONS= 58

N	REACTION						PRE EXP FACTOR	TEMP EXP	ACTIVATION ENERGY	INDIVIDUAL THIRD BODY EFFIC.		
1	CH4	+	+M	--=	CH3	+H	.1500+19	.000	100.0000		.000	.000
2	CH4	+HO	+	--=	CH3	+H2O	.1000+14	.000	6.0000		.000	.000
3	CH4	+H	+	--=	CH3	+H2	.2000+15	.000	11.9000		.000	.000
4	CH4	+O	+	--=	CH3	+HO	.2000+14	.000	6.9000		.000	.000
5	CH3	+O	+	--=	CH2O	+H	.3500+14	.000	3.3000		.000	.000
6	CH3	+O2	+	--=	CH2O	+HO	.1000+13	.000	15.0000		.000	.000
7	CH2O	+	+M	--=	CO	+H2	.2000+17	.000	35.0000		.000	.000
8	CH2O	+HO	+	--=	CHO	+H2O	.2500+14	.000	1.0000		.000	.000
9	CH2O	+O	+	--=	CHO	+HO	.3000+14	.000	.0000		.000	.000
10	CH2O	+H	+	--=	CHO	+H2	.1700+14	.000	3.0000		.000	.000
11	CHO	+O2	+	--=	CO	+HO2	.3000+14	.000	.0000		.000	.000
12	CHO	+HO	+	--=	CO	+H2O	.1000+15	.000	.0000		.000	.000
13	CHO	+O	+	--=	CO	+HO	.5000+12	.500	.0000		.000	.000
14	CHO	+	+M	--=	CO	+H	.2000+13	.500	28.0000		.000	.000
15	CO	+HO	+	--=	CO2	+H	.5500+12	.000	1.0800		.000	.000
16	CO	+O	+M	--=	CO2	+	.3600+19	-1.000	2.5000		.000	.000
17	HO2	+O	+	--=	O2	+HO	.2500+14	.000	.0000		.000	.000
18	HO2	+HO	+	--=	O2	+H2O	.2500+14	.000	.0000		.000	.000
19	HO2	+H	+	--=	HO	+HO	.2500+15	.000	2.0000		.000	.000
20	HO2	+H	+	--=	O2	+H2	.2500+14	.000	.0000		.000	.000
21	H	+O2	+M	--=	HO2	+	.2000+16	.000	.0700	H2O	20.000	.000
22	H	+O2	+	--=	HO	+O	.2200+15	.000	16.8000		.000	.000
23	O	+H2	+	--=	HO	+H	.1700+14	.000	9.4600		.000	.000
24	HO	+H2	+	--=	H2O	+H	.2200+14	.000	5.2000		.000	.000
25	HO	+HO	+	--=	H2O	+O	.6000+13	.000	.7800		.000	.000
26	H	+HO	+M	--=	H2O	+	.7000+20	-1.000	.0000		.000	.000
27	O	+H	+M	--=	HO	+	.4000+19	-1.000	.0000		.000	.000
28	H	+H	+M	--=	H2	+	.2300+20	-1.000	.0000		.000	.000
29	O	+O	+M	--=	O2	+	.4000+19	-1.000	.0000		.000	.000
30	CH3	+HO	+	--=	CH2	+H2O	.6000+10	.700	2.0000		.000	.000
31	CH2	+HO	+	--=	CH	+H2O	.5000+12	.500	6.0000		.000	.000
32	CH2	+O2	+	--=	CH2O	+O	.5000+12	.500	7.0000		.000	.000
33	CH	+O2	+	--=	CHO	+O	.5000+12	.500	6.0000		.000	.000
34	CH2	+O	+	--=	CHO	+H	.5000+12	.500	4.0000		.000	.000
35	CH	+HO	+	--=	CHO	+H	.5000+12	.500	10.0000		.000	.000
36	CH	+O	+	--=	CO	+H	.5000+12	.500	4.0000		.000	.000
37	CH2	+H	+	--=	CH	+H2	.3000+12	.700	26.0000		.000	.000
38	HO	+N	+	--=	H	+NO	.6300+12	.500	.0000		.000	.000
39	N	+O2	+	--=	NO	+O	.6500+10	1.000	6.3000		.000	.000
40	O	+N2	+	--=	N	+NO	.1410+15	.000	75.2000		.000	.000
41	CH	+N2	+	--=	CHN	+N	.1500+10	.000	10.0000		.000	.000
42	CH2	+N2	+	--=	CHN	+NH	.2000+11	.000	20.0000		.000	.000
43	CN	+H2	+	--=	CHN	+H	.2000+14	.000	4.0600		.000	.000
44	CN	+H2O	+	--=	CHN	+HO	.1000+14	.000	.0000		.000	.000
45	CN	+CO2	+	--=	NCO	+CO	.3690+13	.000	.0000		.000	.000
46	NCO	+H	+	--=	NH	+CO	.2000+16	.000	.0000		.000	.000
47	NH2	+H	+	--=	NH	+H2	.1390+12	.670	4.3000		.000	.000
48	NH2	+O	+	--=	NH	+HO	.9200+12	.670	.0000		.000	.000
49	NH	+H	+	--=	N	+H2	.2000+13	.680	1.9000		.000	.000
50	NH	+O	+	--=	N	+HO	.1641+14	.700	.1000		.000	.000
51	NH	+HO	+	--=	N	+H2O	.3200+13	.560	1.5000		.000	.000
52	N2	+	+	--=	N	+N	.4000+22	-1.600	225.0000		.000	.000
53	CN	+NO	+	--=	CO	+N2	.1000+15	.000	8.0300		.000	.000
54	CH	+NO	+	--=	CHO	+N	.1500+14	.000	10.0000		.000	.000
55	CH	+NO	+	--=	CHN	+O	.2000+13	.000	.0000		.000	.000
56	CN	+O2	+	--=	CO	+NO	.3200+12	.000	.0000		.000	.000
57	NCO	+H2	+	--=	NH2	+CO	.1000+14	.000	.0000		.000	.000
58	NH2	+NO	+	--=	N2	+H2O	.3500+13	.000	.0000		.000	.000

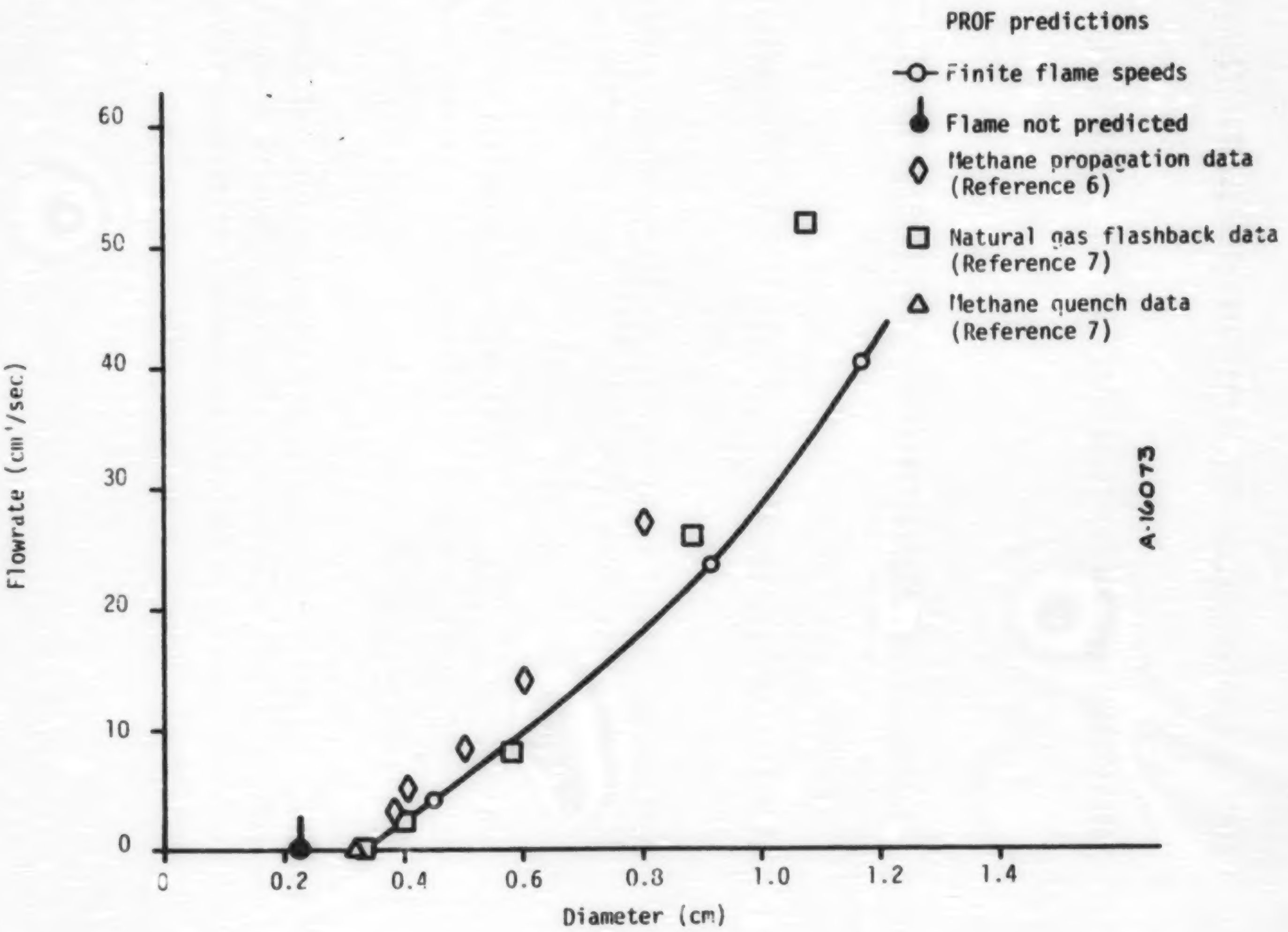

Figure 1. Stationary flame flowrate in small diameter tubes.

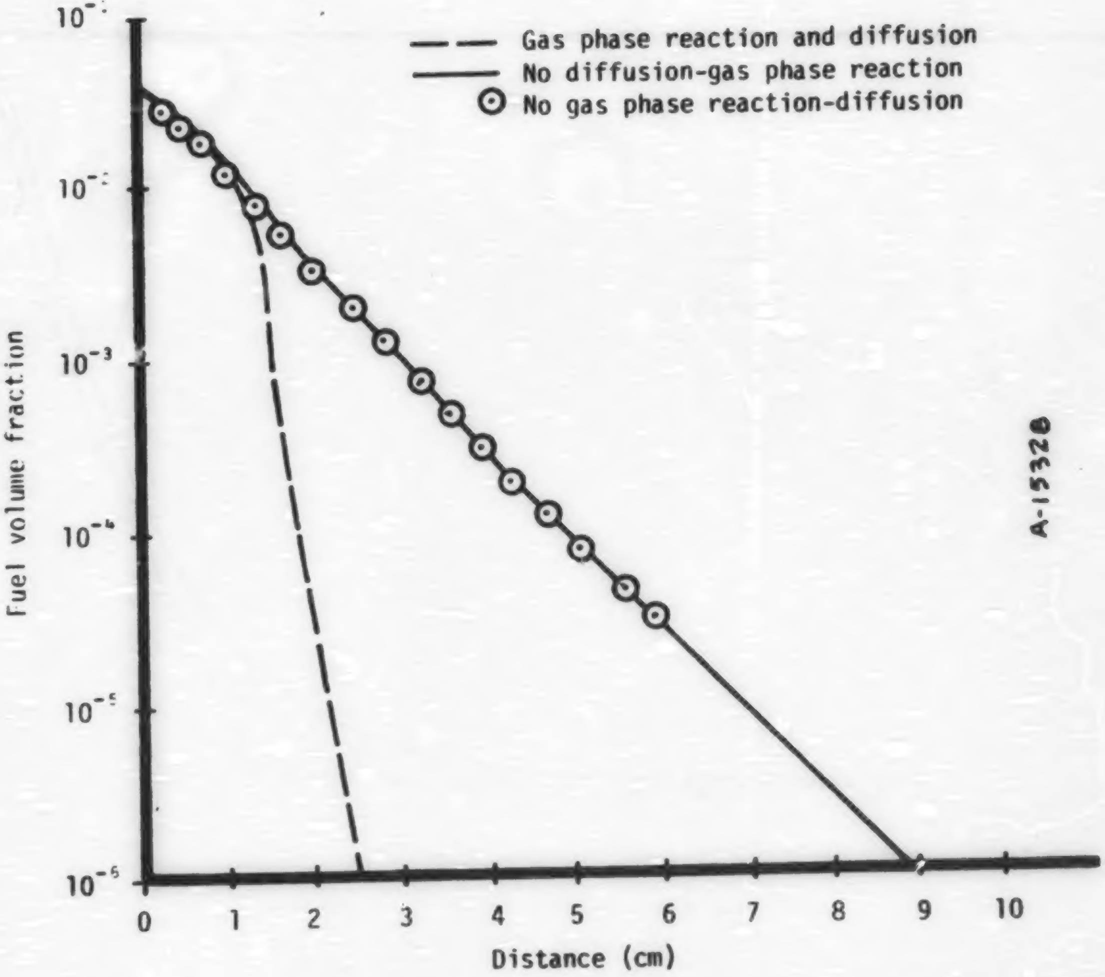

Figure 2. Fuel conversion along a catalytic combustor bed.

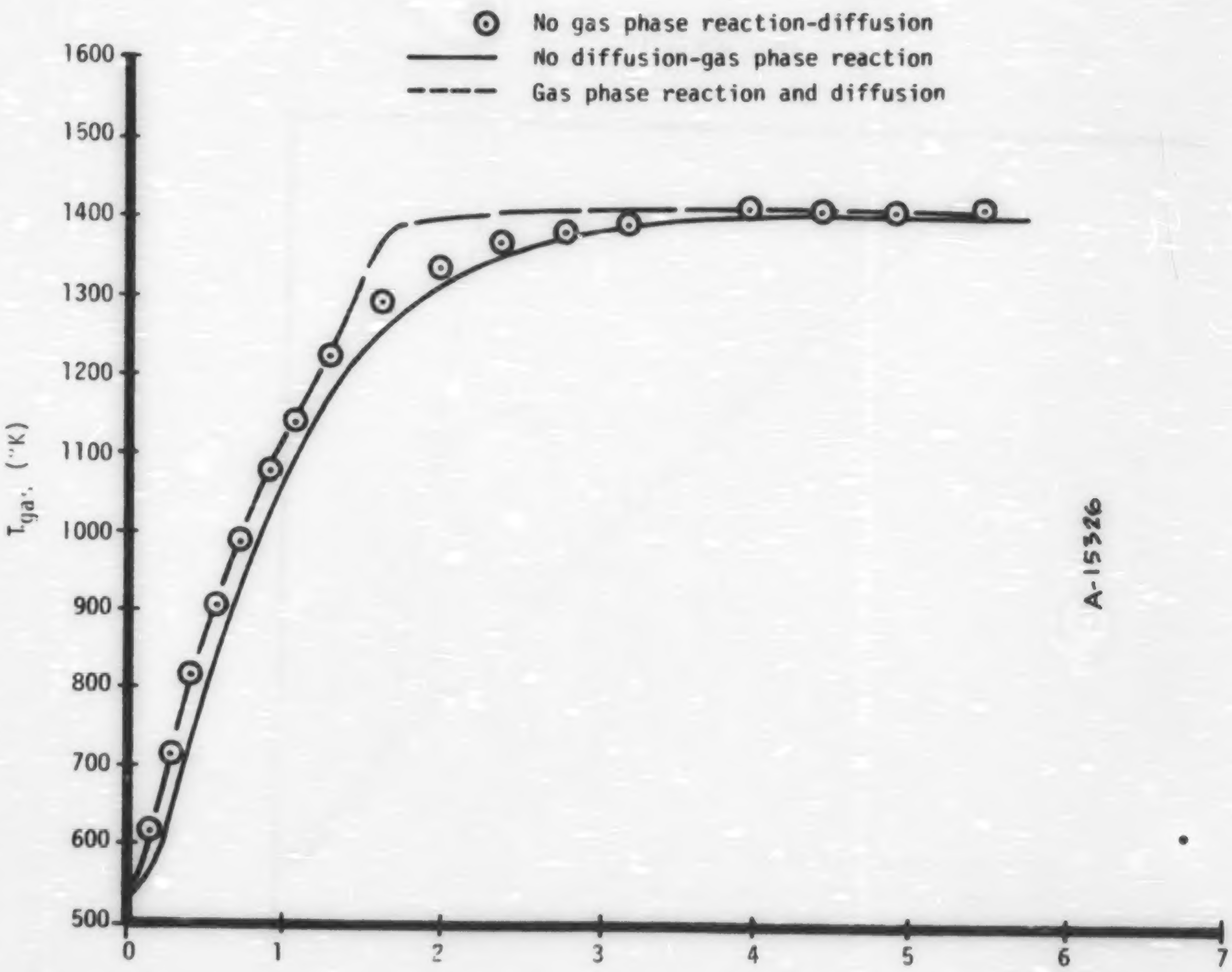

Figure 3. Gas temperature variation along a catalytic combustor bed.

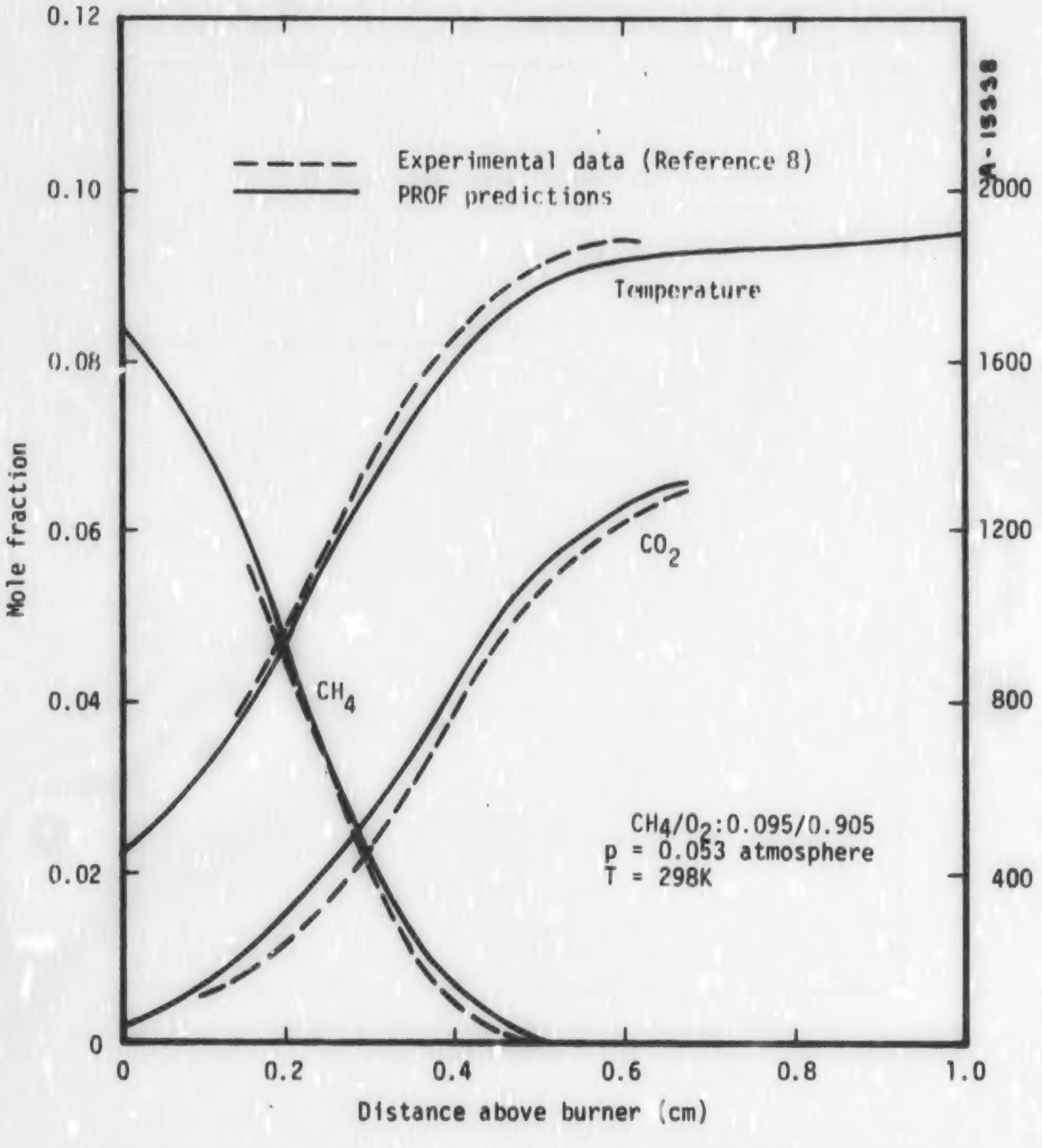

Figure 4. Comparison of predicted and measured low pressure CH_4/O_2 flame species concentrations and temperature.

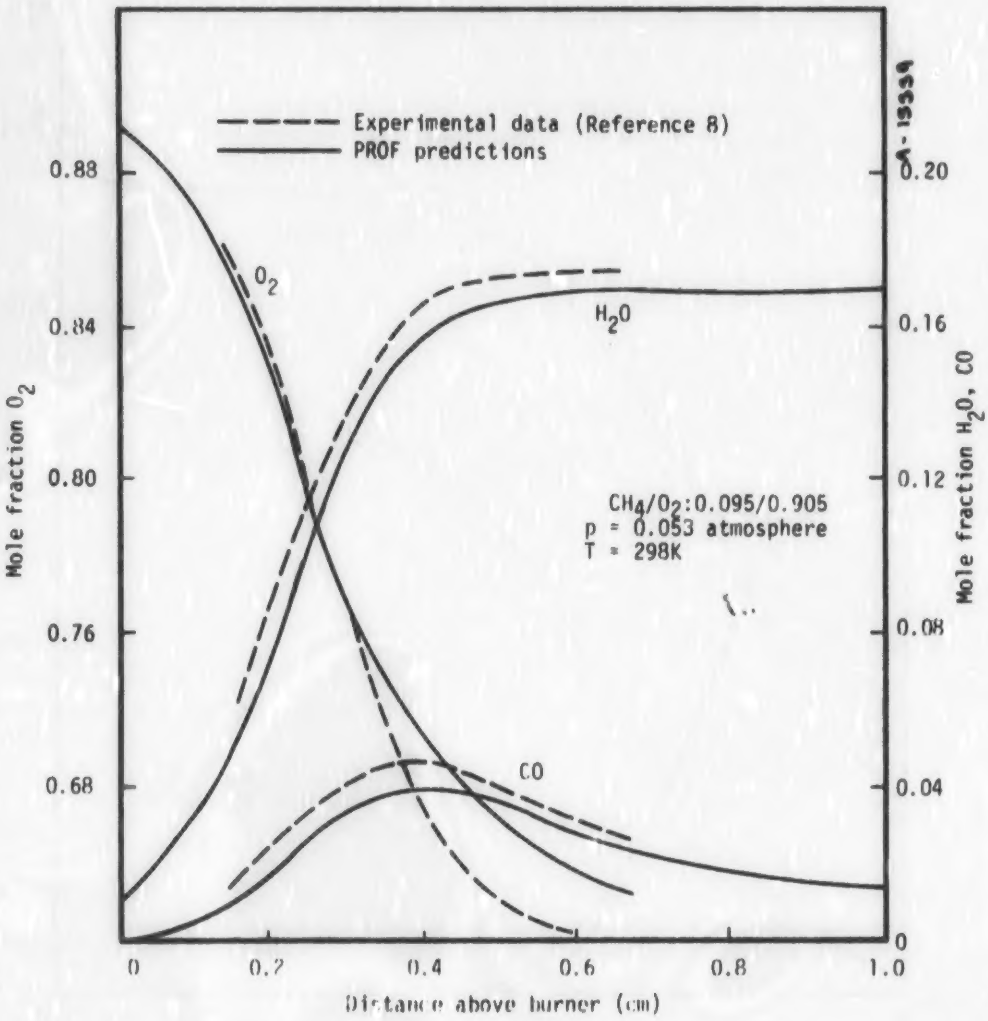

Figure 5. Comparison of predicted and measured low pressure CH_4/O_2 flame species concentrations.

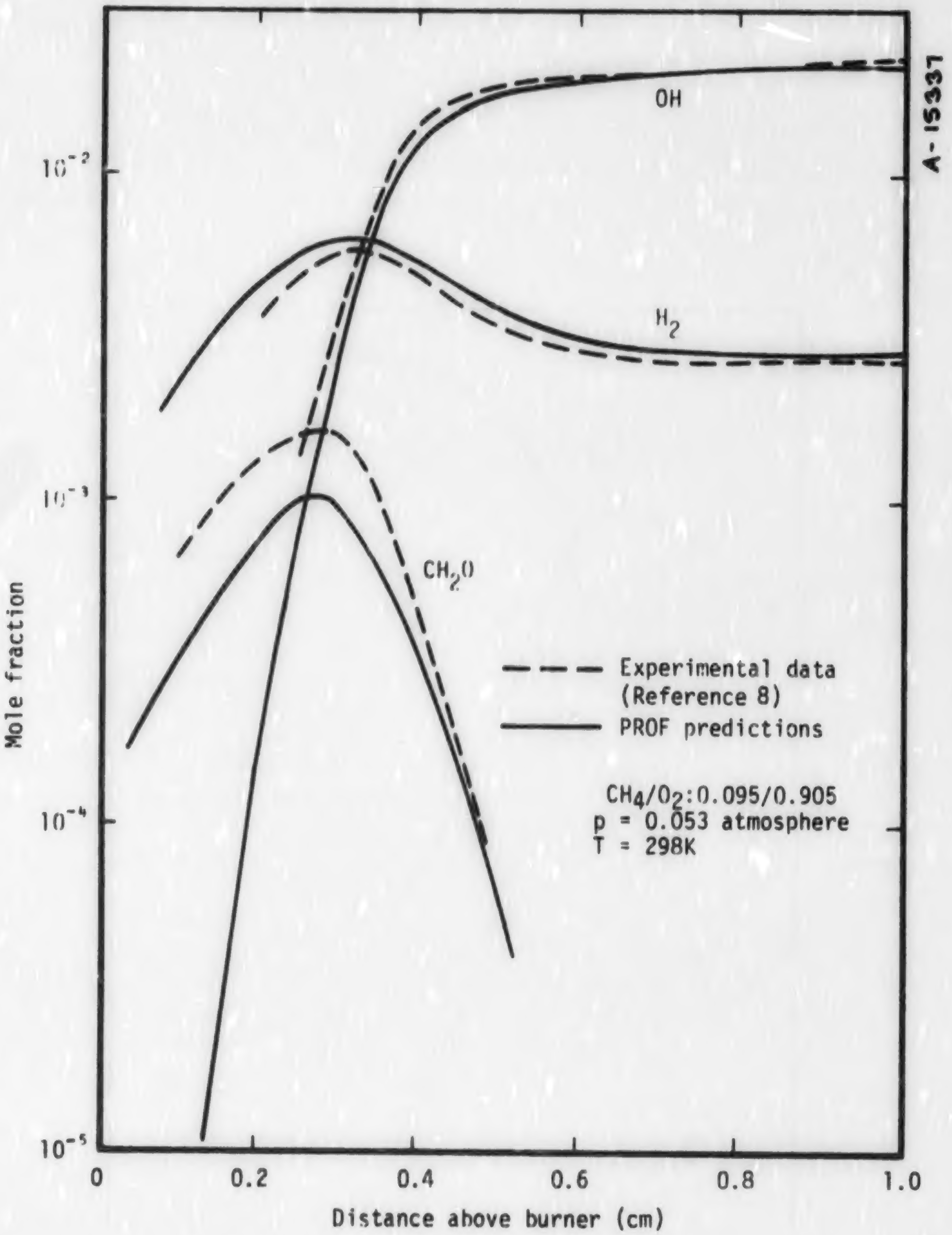

Figure 6. Comparison of predicted and measured low pressure CH_4/O_2 flame species concentrations.

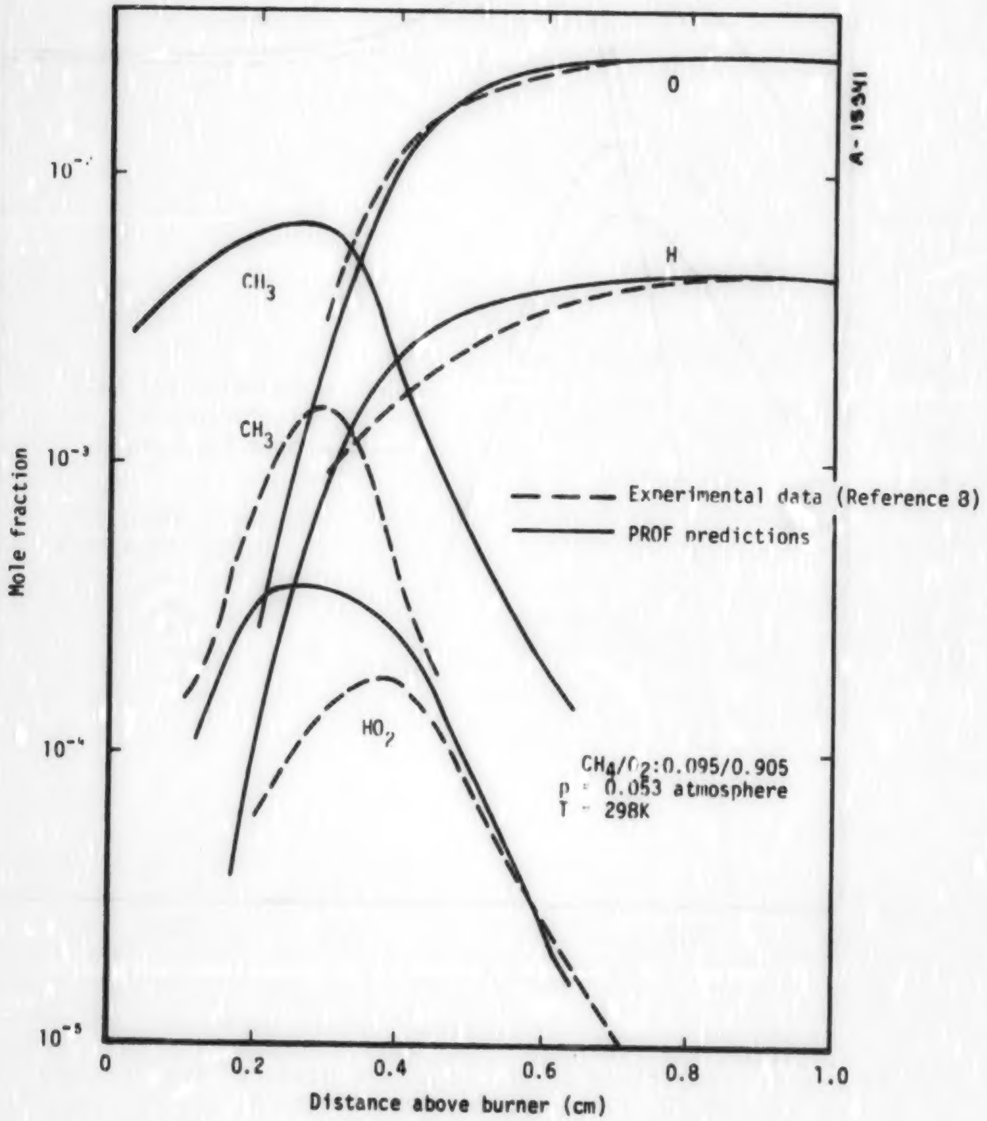

Figure 7. Comparison of predicted and measured low pressure CH_4/O_2 flame species concentrations.

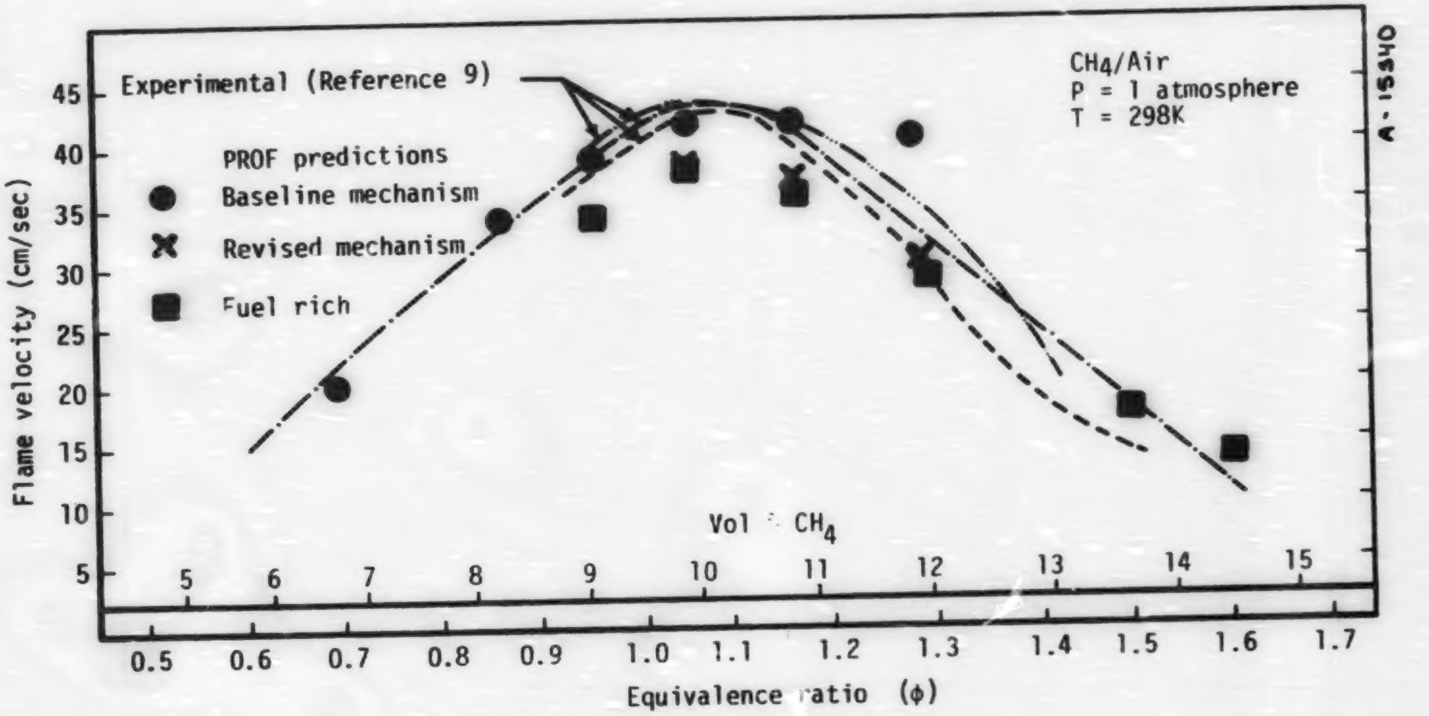

Figure 8. Comparison of predicted and measured atmospheric pressure CH_4/air flame velocity at various equivalence ratios.

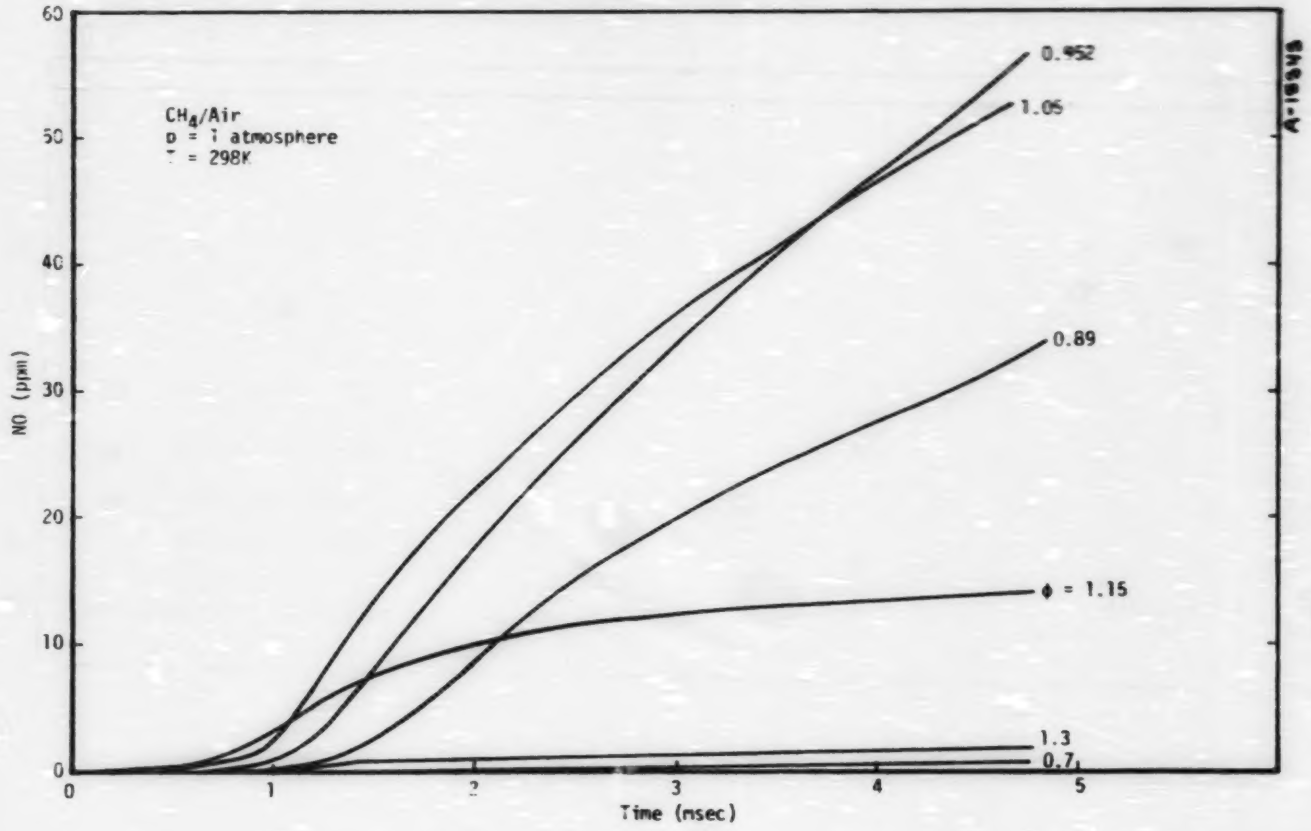

Figure 9. Predictions at various equivalence ratios of Zeldovich generated NO in CH_4/air flames.

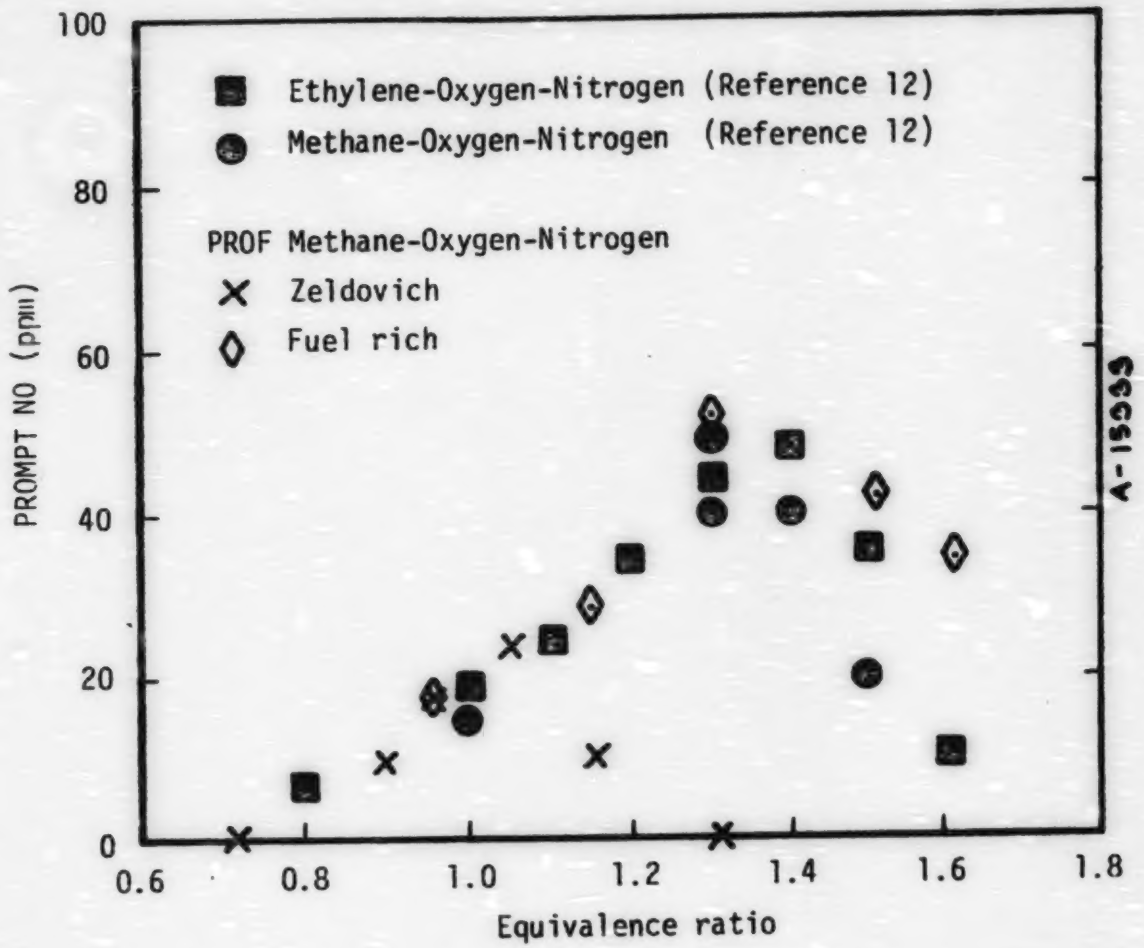

Figure 10. CH_4/air flame PROMPT NO at various equivalence ratios.